CORROSION AND CORROSION INHIBITION STUDIES ON Mg-Al-Zn ALLOY IN AQUEOUS ETHYLENE GLYCOL (30% V/V) MEDIUM

Thesis

Submitted in partial fulfillment of the requirements for the degree of

DOCTOR OF PHILOSOPHY

by

MEDHASHREE H

DEPARTMENT OF CHEMISTRY

NATIONAL INSTITUTE OF TECHNOLOGY KARNATAKA

SURATHKAL, MANGALORE-575025

OCTOBER, 2019

DECLARATION

I hereby *declare* that the Research Thesis entitled "**CORROSION AND CORROSION INHIBITION STUDIES ON Mg-Al-Zn ALLOY IN AQUEOUS ETHYLENE GLYCOL (30% V/V) MEDIUM**" which is being submitted to the National Institute of Technology Karnataka, Surathkal in partial fulfillment of the requirements for the award of the Degree of Doctor of Philosophy in Chemistry is a *bonafide report of the research work carried out by me*. The material contained in this Research Thesis has not been submitted to any University or Institution for the award of any degree.

Medhashree H

Register Number: 138017CY13P02

Department of Chemistry

Place: NITK – Surathkal

Date:

CERTIFICATE

This is to *certify* that the Research Thesis entitled "CORROSION AND CORROSION INHIBITION STUDIES ON Mg-Al-Zn ALLOY IN AQUEOUS ETHYLENE GLYCOL (30% V/V) MEDIUM" submitted by **MEDHASHREE H** (Register Number: 138017CY13P02) as the record of the research work carried out by her, is *accepted as the Research Thesis submission* in partial fulfillment of the requirements for the award of Degree of Doctor of Philosophy.

(Dr. A. Nityananda Shetty)

Research Guide

Chairman - DRPC

ACKNOWLEDGMENT

Research “stands on the shoulders of giants”, at the same time it needs lot of helping hands to make it successful. I take this opportunity to thank all those who made this tough task to be possible.

First and foremost I express my sincere gratitude to my research supervisor Prof. A.Nityananda Shetty, Professor, Department of Chemistry, National Institute of Technology Karnataka, Surathkal, for his precious guidance, continuous support and encouragement during tough times. His sincerity, wisdom and hard work have deeply inspired me to take challenges. I greatly appreciate the freedom he gave to me during this journey of research.

I wish to convey my thanks to Prof. Arun M Isloor, HOD, Department of chemistry, National Institute of Technology Karnataka, Surathkal, for providing all the necessary facilities and support to pursue my research work.

I am thankful to the members of research progress assessment committee (RPAC) Prof. A Chittaranjan Hegde, Professor, Department of Chemistry and Dr. Shashibhushan Arya, Associate Professor, Mettallurgical and Materials Engineering, National Institute of Technology Karnataka, Surathkal for their constructive comments and suggestions during the research progress assessments.

I extend my sincere thanks to National Institute of technology Karnataka for providing Institute fellowship for the first one and half year and for all the necessary facilities to carry out this research work.

For successful completions of any task one needs constructive advices and moral support. Our department faculties, Prof. A Vasudeva Adhikari, Prof. B Ramachandra Bhat, Prof. D Krishna Bhat, Dr. Uday Kumar D, Dr. Darshak R Trivedi, Dr. Sib Sankar Mal, Dr. Beneesh P. B, Dr. Debashree Chakraborty and Dr. Saikat Dutta have given constructive advices and suggestions. I am heartily thankful to all of them.

I am thankful to Department of Metallurgical and Materials Engineering, Department of Chemical Engineering, Department of Physics, National Institute of

Technology Karnataka, Surathkal, University of Mangalore and National Aeronautical Limited, Bangalore for providing necessary facilities.

I am thankful to all the non-teaching staff, Mrs. Shammila, Mrs. Deepa, Mrs. Sharmila, Miss. Vikitha, Mr. Prashanth, Mr. Pradeep, Mr. Santhosh and Mr. Harish for their kind cooperation and help.

I wish to convey my thanks to Dr. Liju Elias and Dr. Sandya Shetty for their help, support and for nice company during conference visits. I am thankful to all the research scholars of the Department of Chemistry for their company and help when I needed.

I extend my gratitude to my fellow research scholars, Dr. Nandini K and Dr. Kshama Shetty, for their guidance and providing peaceful working environment. I deeply extend my thanks to my labmates Dr. Prakashaiah B.G and Mr. Aranganathan V, who helped me a lot during this journey. Thanks to both of them for their support and help.

I am thankful to all the colleagues of Raichur Thermal Power Station, Karnataka Power Corporation Limited, for their co-operation and support during this journey. I convey my heartfelt thanks to Dr. Rajendra H.B, Post-doctoral fellow, Tokiya University, Japan for all the technical support.

Backbone of my energy is my family, without their support I could not have achieved anything. My heartfelt gratitude to my beloved father Sri. Hareesh Bhat and mother Smt. Suvarna for all the support, encouragement, sacrifices, they made for me. The dearest friend of my life is my sister Nadhashree H. I am thankful to her from the bottom of my heart for the advice, love, care, and support in all the testing times of my life. I express my deepest sense of gratitude to my beloved husband Dr. Anila H.A, for his eternal love, support and care. Finally, I extend my heartfelt thanks to my in-laws Sri. Ashok H.T and Smt. Nirmala and also to entire family, for their support and blessings. Last but not the least I thank all those who have helped me directly and indirectly in completing this research work.

Medhashree H

ABSTRACT

Magnesium alloys find applications from automobile industries to medical implant materials because of its enhanced properties in comparison with other light weight alloys. Mg-Al-Zn alloy is one such magnesium alloy, which finds variety of applications in automobile industries. The occurrence of corrosion is beneficial in the medical field of application as it avoids one more surgery for the removal of implants, but is a limitation in automobile industry applications. Therefore, the study of corrosion and its controlling measures have vital role in practical applications.

In this thesis, corrosion of Mg-Al-Zn alloy and its mitigation were studied using electrochemical techniques - potentiodynamic polarization and AC impedance spectroscopy. The surface morphology and surface composition of the corroded alloy surface were examined by SEM and EDX analyses. The aqueous ethylene glycol (30% v/v) solutions, containing chloride and sulfate ions, were chosen as the corrosive media. The corrosion studies were performed at different chloride ion and sulfate ion concentrations, pH and temperature of the medium. The obtained results concluded the trend of higher corrosion rate at higher concentration of chloride and sulfate ions, lower pH and higher temperature.

The synergistic mixtures of sodium dodecyl benzene sulphonate (SDBS) with trisodium phosphate (TSP) and sodium benzoate (SB) were employed as corrosion inhibitors. Similarly morpholine and its two derivatives N-methyl morpholine and dimethyl morpholine were also studied as corrosion inhibitors in the corrosive media. The synergistic mixtures acted as anodic type inhibitors by suppressing anodic reaction. The morpholine and its derivaties acted as mixed type inhibitors. All the inhibitors were more effective at lower temperature and in higher concentration of the corrosive media. The activation and thermodynamic parameters have been calculated and documented. The synergistic mixtures adsorbed on the alloy surface predominantly through physisorption and obeyed Langmuir adsorption isotherm. While the adsorption of morpholine and dimethyl morpholine obeyed Langmuir adsorption isotherm, that of N-methyl morpholine obeyed Temkin adsorption isotherm. The synergistic mixtures of organic-inorganic inhibitors showed higher inhibition efficiency than mixtures of organic-organic inhibitors. The efficiencies of morpholine and its derivatives decrease in the following order: dimethyl morpholine > morpholine > N-methyl morpholine. The possible mechanism of inhibition has been proposed for all the inhibitors.

Keywords: Mg-Al-Zn alloy, synergistic mixture, morpholine derivatives, inhibitor.

CONTENTS

CHAPTER – 1: INTRODUCTION **1**

1.1. CORROSION - A BRIEF HISTORY **1**

1.2. DEFINITION OF CORROSION **2**

1.3. CONSEQUENCES OF CORROSION **2**

1.3.1. Human life, health and safety concern **3**

1.3.2. Economic losses **3**

1.3.3. Effect on conservation of materials **4**

1.4. CLASSIFICATION OF CORROSION **4**

1.4.1. Uniform corrosion **5**

1.4.2. Galvanic corrosion **5**

1.4.3. Crevice corrosion **5**

1.4.4. Pitting corrosion **6**

1.4.5. Intergranular corrosion **6**

1.4.6. Selective leaching **6**

1.4.7. Erosion corrosion **7**

1.4.8. Stress corrosion cracking (SCC) **7**

1.5. FACTORS AFFECTING CORROSION RATE **7**

1.5.1. Metallic factors **8**

1.5.1.1. Metal purity 8

1.5.1.2. Standard electrode potential 8

1.5.1.3. Hydrogen overvoltage 8

1.5.1.4. Nature of the corrosion product 9

1.5.1.5. Ratio of anodic to cathodic area 9

1.5.2. Environmental factors 9

1.5.2.1. Temperature of the medium 9

1.5.2.2. pH of the environment 10

1.5.2.3. Presence of impurities 10

1.5.2.4. Concentration of the medium 10

1.5.2.5. Physical state of the medium 10

1.5.2.6. Conductivity 11

1.5.2.7. Effect of microbes 11

1.5.2.8. Effect of oxygen and oxidizer 11

1.5.2.9. Velocity of the corrosive 11

1.5.2.10. Anodic and cathodic polarization 12

1.5.3. Design factors 12

1.6. ELECTROCHEMICAL THEORY OF CORROSION 12

1.7. THERMODYNAMIC PRINCIPLES OF CORROSION 14

1.7.1. Concept of Free energy and spontaneity 15

1.7.2. Application of thermodynamics to corrosion - Pourbaix diagram 16

1.8. CORROSION KINETICS 18

1.8.1. Electrochemical polarization-departure from equilibrium 19

1.8.1.1. Activation polarization 19

1.8.1.2. Concentration polarization 20

1.8.1.3. Ohmic polarization 21

1.8.2. Exchange current density 21

1.8.3. Mixed potential theory 22

1.9. ELECTROCHEMICAL CORROSION TESTING METHODS 24

1.9.1. DC electrochemical techniques 26

1.9.1.1. Tafel extrapolation technique 27

1.9.1.2. Linear polarization technique 29

1.9.2. AC electrochemical techniques 31

1.9.2.1. Electrochemical impedance spectroscopy (EIS) 31

1.10. CORROSION PREVENTION 34

1.10.1. Materials selection 35

1.10.2. Alteration of environment 35

1.10.3. Design of a structure 35

1.10.4. Cathodic protection 36

1.10.5. Anodic protection 36

1.10.6. Coatings 36

1.11. CORROSION INHIBITORS 37

1.11.1. Classification of inhibitor 38

1.11.1.1. Environment conditioners 39

1.11.1.2. Interfacial inhibitors 40

1.12. FACTORS AFFECTING THE INHIBITOR EFFICIENCY 44

1.12.1. Molecular structure 44

1.12.2. Size of the molecular structure 46

1.12.3. Effect of inhibitor concentration 47

1.12.4. Solubility of the inhibitor 47

1.12.5. Impact of temperature 47

1.12.6. Nature of the metal atom 47

1.12.7. Surface charge on the metal 48

1.12.8. Intermolecular interaction between the adsorbed inhibitor 48

1.12.9. Effect of secondary inhibition 49

1.12.10. Influence of electrical double layer 49

1.12.11. Synergism and antagonism 50

1.13. METHODS FOR INHIBITOR APPLICATION 50

1.14. MECHANISM OF INHIBITION 51

1.14.1. Inhibition by adsorption 51

1.14.2. Inhibition by blocking the active reaction site 53

1.14.3. Inhibition by forming surface film 53

1.14.4. Inhibition by forming chelating complex 53

1.15. INHIBITION IN NEAR-NEUTRAL SOLUTIONS 54

1.16. MAGNESIUM AND MAGNESIUM ALLOYS 54

1.16.1. Application of Magnesium alloys 55

1.16.1.1. Automotive applications 55

1.16.1.2. Aerospace applications 56

1.16.1.3. Medical applications 56

1.16.1.4. Sports applications 57

1.16.1.5. Electronic applications 57

1.16.1.6. Other applications 58

1.16.2. Major alloying elements 58

1.16.2.1. Aluminum 58

1.16.2.2. Zinc 59

1.16.2.3. Zirconium 59

1.16.2.4. Silicon 59

1.16.2.5. Copper 59

1.16.2.6. Iron 59

1.16.2.7. Manganese 60

1.16.2.8. Rare earth metals 60

1.16.3. Classification of magnesium alloys 60

1.17. REVIEW OF LITERATURE 61

1.17.1. Literature review for corrosion of pure magnesium and magnesium alloys 61

1.17.2. Literature review for corrosion inhibitor of magnesium and magnesium alloys 69

1.17.2.1 Synergistic inhibitors for magnesium alloys 79

1.17.2.2 Morpholine and its derivaties as corrosion inhibitors 79

1.18. SCOPE AND OBJECTIVES OF THE WORK 81

1.18.1. Scope of the present work 81

1.18.2. Objectives of the current work 82

1.19. FRAMEWORK OF THE THESIS 83

CHAPTER – 2: MATERIALS AND METHODS 85

2.1. MATERIALS 85

2.2. MEDIA 86

2.2.1. Preparation of chloride media 86

2.2.2. Preparation of sulfate media 86

2.2.3. Preparation of chloride and sulfate media with various pH 86

2.3. INHIBITORS 87

2.3.1. Inhibitor mixture containing sodium dodecyl benzene sulphonate (SDBS) and trisodium phosphate (TSP) 87

2.3.2. Inhibitor mixture containing sodium dodecyl benzene sulphonate (SDBS) and sodium benzoate (SB) 87

2.3.3. Morpholine and its derivatives as inhibitors 87

2.4. METHODS 88

2.4.1. Electrochemical techniques 88

2.4.1.1. Potentiodynamic polarization method 89

2.4.1.2. Electrochemical impedance spectroscopy studies 89

2.4.2. Surface studies 89

2.5. CALCULATIONS 90

2.5.1. Corrosion rate 90

2.5.2. Inhibition efficiency 91

2.5.3. Activation parameters 91

2.5.4. Thermodynamic parameters 92

2.5.5. Synergistic parameters 94

CHAPTER – 3: RESULTS AND DISCUSSIONS 95

3.1. CORROSION BEHAVIOUR OF Mg-Al-Zn ALLOY IN 30% AQUEOUS ETHYLENE GLYCOL CONTAINING CHLORIDE AND SULFATE IONS 95

3.1.1. Potentiodynamic polarization analyses 95

3.1.2. Electrochemical impedance spectroscopy studies 97

3.1.3. Effect of temperature 101

3.1.4. Effect of pH 104

3.1.5. Mechanism of Mg-Al-Zn alloy corrosion 107

3.1.5.1. Microgalvanic corrosion of Mg-Al-Zn alloy 107

3.1.5.2. Anodic magnesium dissolution and negative difference effect 108

3.1.6. Surface analyses 110

3.2. CORROSION INHIBITION OF Mg-Al-Zn ALLOY IN 30% AQUEOUS ETHYLENE GLYCOL CONTAINING AGGRESSIVE IONS BY A MIXTURE OF INHIBITORS, SODIUM DODECYL BENZENE SULPHONATE (SDBS) AND TRISODIUM PHOSPHATE (TSP) 121

3.2.1. Effect of ethylene glycol on the corrosion rate of Mg-Al-Zn alloy 121

3.2.2. Potentiodynamic polarization analyses 122

3.2.3. Electrochemical impedance spectroscopy 124

3.2.4. Effect of temperature 127

3.2.5. Adsorption isotherm 129

3.2.6. Surface analyses 131

3.3. CORROSION INHIBITION OF Mg-Al-Zn ALLOY IN 30% AQUEOUS ETHYLENE GLYCOL CONTAINING CHLORIDE IONS AND SULFATE IONS BY A MIXTURE OF INHIBITORS, SODIUM DODECYL BENZENE SULPHONATE (SDBS) AND SODIUM BENZOATE (SB) 150

3.3.1. Potentiodynamic polarization analyses 150

3.3.2. Electrochemical impedance spectroscopy 151

3.3.3. Effect of temperature 153

3.3.4. Adsorption isotherm 155

3.3.5. Surface analyses 155

3.4. MECHANISM OF CORROSION INHIBITION BY SYNERGISTIC MIXTURES 173

3.4.1. Inhibition mechanism of SDBS 173

3.4.2. Inhibition mechanism of TSP 173

3.4.3. Inhibition mechanism of SB 174

3.4.4. Inhibition mechanism of SDBS and TSP combination 174

3.4.5. Inhibition mechanism of SDBS and SB combination 175

3.4.6. Synergistic effect 176

3.4.7. Effect of medium concentration 177

3.5. CORROSION INHIBITION OF Mg-Al-Zn ALLOY IN 30% AQUEOUS ETHYLENE GLYCOL CONTAINING CHLORIDE IONS AND SULFATE IONS BY MORPHOLINE 178

3.5.1. Potentiodynamic polarization analyses 178

3.5.2. Electrochemical impedance spectroscopy 179

3.5.3. Effect of temperature 181

3.5.4. Adsorption isotherm 183

3.5.5. Surface analyses **184**

3.6. CORROSION INHIBITION OF Mg-Al-Zn ALLOY IN 30% AQUEOUS ETHYLENE GLYCOL CONTAINING CHLORIDE IONS AND SULFATE IONS BY N-METHYL MORPHOLINE **202**

3.6.1. Potentiodynamic polarization analyses **202**

3.6.2. Electrochemical impedance spectroscopy **203**

3.6.3. Effect of temperature **205**

3.6.4. Adsorption isotherm **207**

3.6.5. Surface analyses **208**

3.7. CORROSION INHIBITION OF Mg-Al-Zn ALLOY IN 30% AQUEOUS ETHYLENE GLYCOL CONTAINING CHLORIDE IONS AND SULFATE IONS BY DIMETHYL MORPHOLINE **226**

3.7.1. Potentiodynamic polarization analyses **226**

3.7.2. Electrochemical impedance spectroscopy **227**

3.7.3. Effect of temperature **229**

3.7.4. Adsorption isotherm **231**

3.7.5. Surface analyses **232**

3.8. MECHANISM OF CORROSION INHIBITION BY MORPHOLINE AND ITS DERIVATIES **245**

CHAPTER – 4: SUMMARY AND CONCLUSIONS **249**

4.1. SUMMARY **249**

4.2. CONCLUSIONS **250**

4.3. SCOPE FOR FUTURE WORK **251**

REFERENCES **252**

LIST OF PUBLICATIONS **285**

BIODATA **287**

LIST OF FIGURES

Fig. No.	Contents	Page No.
1.1	Demonstrative diagram of electrochemical reaction occur at the metal surface	14
1.2	Potential-pH diagram for magnesium/water system	17
1.3	Evans diagram for zinc in hydrochloric acid	23
1.4	Schematic diagram of a potentiostat	26
1.5	A hypothetical polarization curve representing Tafel extrapolation	27
1.6	A representative linear polarization plot	30
1.7	Sinusoidal current response in linear system	32
1.8	A representative Nyquist plot	33
1.9	An illustrative Bode plots	34
1.10	A comprehensive categorization of corrosion inhibitors	39
1.11	Evans diagram illustrating the effect of anodic inhibitor addition	41
1.12	Evans diagram depicting the effect of addition of cathodic inhibitor	42
1.13	Evans diagram interpreting the effect of mixed type inhibitor admittance	43
2.1	Mounted alloy sample in epoxy resin	85
2.2	The adopted laboratory instrumentation for electrochemical studies	89
3.1	Potentiodynamic polarization plots for the corrosion of Mg-Al-Zn alloy in 30% aqueous ethylene glycol containing different concentrations of (a) chloride ions at 50 °C and (b) sulfate ions at 50 °C	96

3.2	The Nyquist plots for the corrosion of Mg-Al-Zn alloy in 30% aqueous ethylene glycol containing different concentrations of (a) chloride ions at 50 °C and (b) sulfate ions at 50 °C	98
3.3	Equivalent electrical circuit used for the simulation of experimental impedance data points	100
3.4	Simulation plot for the corrosion of Mg-Al-Zn alloy in 30% aqueous ethylene glycol containing 10 mM chloride ions at 30 °C.	100
3.5	Potentiodynamic polarization plots for the corrosion of Mg-Al-Zn alloy in 30% aqueous ethylene glycol containing (a) 6 mM chloride ions and (b) 6 mM sulfate ions at different temperatures	102
3.6	Nyquist plots for the corrosion of Mg-Al-Zn alloy in 30% aqueous ethylene glycol containing (a) 6 mM chloride ions and (b) 6 mM sulfate ions at different temperatures	102
3.7	Arrhenius plots for the corrosion of Mg-Al-Zn alloy in 30% aqueous ethylene glycol containing different concentrations of (a) chloride ions and (b) sulfate ions	104
3.8	Plots of ln (υ_{corr} /T) vs 1/T for the corrosion of Mg-Al-Zn alloy in 30% aqueous ethylene glycol containing different concentration of (a) chloride ions and (b) sulfate ions	104
3.9	Pourbaix diagram of Mg, Al, Zn	105
3.10	Potentiodynamic polarization curves for the corrosion of Mg-Al-Zn alloy in 30% aqueous ethylene glycol containing (a) 10 mM chloride and (b) 2 mM sulfate ions at different pH and at 30 °C	107
3.11	Nyquist plots for the corrosion of Mg-Al-Zn alloy in 30% aqueous ethylene glycol containing (a) 10 mM chloride and (b) 2 mM sulfate ions at different pH and at 30 °C	107

3.12	(a) SEM image and (b) EDX spectra of freshly polished surface of Mg-Al-Zn alloy	111
3.13	(a) SEM image and (b) optical image of freshly polished Mg-Al-Zn alloy surface after etching in the acetic-picral solution	111
3.14	EDX spectra of (a) intermetallic particle and (b) bare alloy along with the specified region of the SEM images	112
3.15	EDX mapping of Mg-Al-Zn alloy showing the distribution of various elements in the alloy	112
3.16	(a) SEM image of the corroded Mg-Al-Zn alloy surface, after immersing in 30% aqueous ethylene glycol containing 10 mM chloride ions for 24 h (b) corresponding EDX spectra	113
3.17	(a) SEM image (b) EDX spectra of Mg-Al-Zn alloy surface, after immersing in 30% aqueous ethylene glycol containing 10 mM sulfate ions for 24 h	113
3.18	SEM images of Mg-Al-Zn alloy surface after 24 h of immersion in 30% aqueous ethylene glycol containing 10 mM chloride ions with (a) acidic pH of 4, (b) neutral pH of 7 and (c) alkaline pH of 12	114
3.19	SEM images of Mg-Al-Zn alloy surface after 24 h of immersion in 30% aqueous ethylene glycol containing 10 mM sulfate ions with (a) acidic pH of 4, (b) neutral pH of 7 and (c) alkaline pH of 12	115
3.20	(a) Potentiodynamic polarization plots (b) Nyquist plots for the corrosion of Mg-Al-Zn alloy in 10 mM chloride solution, in the presence and in the absence of 30% ethylene glycol at 30 °C	121
3.21	Potentiodynamic polarization plots for the corrosion of Mg-Al-Zn alloy in different concentrations of SDBS in a corrosive medium of (a) 10 mM chloride ions at 30 °C (b) 10 mM sulfate ions at 40 °C	122

3.22 Potentiodynamic polarization plots for the corrosion of Mg-Al-Zn alloy in different concentrations of TSP and 8 mM SDBS in a corrosive medium of (a) 10 mM chloride ions at 30 °C and (b) 2 mM sulfate ions at 50 °C 123

3.23 Nyquist plots for the corrosion of Mg-Al-Zn alloy in different concentrations of SDBS in a corrosive medium of (a) 10 mM chloride ions at 30 °C and (b) 10 mM sulfate ions at 40 °C 125

3.24 Nyquist plots plots for the corrosion of Mg-Al-Zn alloy in different concentrations of TSP and 8 mM SDBS in a corrosive medium of (a) 10 mM chloride ions at 30 °C and (b) 2 mM sulfate ions at 50 °C 125

3.25 Bode magnitude plots for the corrosion of Mg-Al-Zn alloy in different concentrations of TSP and 8 mM SDBS in a corrosive medium of (a) 10 mM chloride ions at 30 °C and (b) 2 mM sulfate ions at 50 °C 127

3.26 Bode phase angle plots for the corrosion of Mg-Al-Zn alloy in different concentrations of TSP and 8 mM SDBS in a corrosive medium of (a) 10 mM chloride ions at 30 °C and (b) 2 mM sulfate ions at 50 °C 127

3.27 Arrhenius plots for the corrosion of Mg-Al-Zn alloy in the presence of 8 mM SDBS and different concentrations of TSP in a corrosive solution of (a) 10 mM chloride ions and (b) 2 mM sulfate ions 128

3.28 Plots of ln (υ_{corr}/T) versus ($1/T$) for the corrosion of Mg-Al-Zn alloy in the presence of 8 mM SDBS and different concentrations of TSP in a corrosive solution of (a) 10 mM chloride ions and (b) 2 mM sulfate ions 129

3.29 Langmuir adsorption isotherms for the adsorption of TSP on Mg-Al-Zn alloy surface at different temperatures in a corrosive medium of (a) 10 mM chloride ions and (b) 2 mM sulfate ions 131

3.30 (a) SEM image of Mg-Al-Zn alloy surface after 24 h of immersion in 132

the corrosive medium of 10 mM chloride solution containing 8 mM SDBS and (b) the corresponding EDX spectra

3.31 (a) SEM image of Mg-Al-Zn alloy surface after 24 h of immersion in the corrosive medium of 10 mM sulfate solution containing 8 mM SDBS and (b) the corresponding EDX spectra 132

3.32 (a) SEM image of Mg-Al-Zn alloy surface after 24 h of immersion in the corrosive medium of 10 mM chloride solution containing 8 mM SDBS and 16 mM TSP and (b) the corresponding EDX spectra 133

3.33 (a) SEM image of Mg-Al-Zn alloy surface after 24 h of immersion in the corrosive medium of 10 mM sulfate solution containing 8 mM SDBS and 16 mM TSP and (b) the corresponding EDX spectra 133

3.34 Potentiodynamic polarization plots for the corrosion of Mg-Al-Zn alloy in the presence of SDBS and different concentrations of SB in (a) 10 mM chloride ions at 35 °C and (b) 2 mM sulfate ions at 40 °C 150

3.35 Nyquist plots for the corrosion of Mg-Al-Zn alloy in the presence of SDBS and different concentrations of SB in (a) 10 mM chloride medium at 35 °C and (b) 2 mM sulfate medium at 40 °C 152

3.36 Bode magnitude plots for the corrosion of Mg-Al-Zn alloy in the presence of SDBS and different concentrations of SB in (a) 10 mM chloride medium at 35 °C and (b) 2 mM sulfate medium at 40 °C 152

3.37 Bode phase angle plots for the corrosion of Mg-Al-Zn alloy in the presence of SDBS and different concentrations of SB in (a) 10 mM chloride medium at 35 °C and (b) 2 mM sulfate medium at 40 °C 153

3.38 Arrhenius plots for the corrosion of Mg-Al-Zn alloy in the presence of 8 mM SDBS and different concentrations of SB in a corrosive solution of (a) 10 mM chloride medium and (b) 2 mM sulfate medium 154

3.39 Plots of ln (υ_{corr}/T) versus ($1/T$) for the corrosion of Mg-Al-Zn alloy in 154

the presence of 8 mM SDBS and different concentrations of SB in a corrosive solution of (a) 10 mM chloride medium and (b) 2 mM sulfate medium

3.40 Langmuir adsorption isotherms for the adsorption of SB on Mg-Al-Zn alloy surface at different temperatures in (a) 10 mM chloride medium and (b) 2 mM sulfate medium 155

3.41 (a) SEM image of Mg-Al-Zn alloy surface after 24 h of immersion in the corrosion medium containing 10 mM chloride ions, 8 mM SDBS and 32 mM SB and (b) corresponding EDX spectra 156

3.42 (a) SEM image of Mg-Al-Zn alloy surface after 24 h of immersion in the corrosion medium containing 10 mM sulfate ions, 8 mM SDBS and 32 mM SB and (b) corresponding EDX spectra 156

3.43 Potentiodynamic polarization plots for the corrosion of Mg-Al-Zn alloy in the presence of different concentrations of morpholine in (a) 6 mM chloride medium at 35 °C and (b) 2 mM sulfate medium at 35 °C 178

3.44 Nyquist plots for the corrosion of Mg-Al-Zn alloy in the presence of different concentrations of morpholine in (a) 6 mM chloride medium at 35 °C and (b) 2 mM sulfate medium at 35 °C 179

3.45 Bode magnitude plots for the corrosion of Mg-Al-Zn alloy in the presence of different concentrations of morpholine in (a) 6 mM chloride medium at 35 °C and (b) 2 mM sulfate medium at 35 °C 181

3.46 Bode phase angle plots for the corrosion of Mg-Al-Zn alloy in the presence of different concentrations of morpholine in (a) 6 mM chloride medium at 35 °C and (b) 2 mM sulfate medium at 35 °C 181

3.47 Arrhenius plots for the corrosion of Mg-Al-Zn alloy in the presence of different concentrations of morpholine in a corrosive solution of (a) 6 mM chloride medium and (b) 2 mM sulfate medium 182

3.48 Plots of ln (υ_{corr}/T) versus ($1/T$) for the corrosion of Mg-Al-Zn alloy in the presence of different concentrations of morpholine in a corrosive solution of (a) 6 mM chloride medium and (b) 2 mM sulfate medium 183

3.49 Langmuir adsorption isotherms for the adsorption of morpholine on Mg-Al-Zn alloy surface at different temperatures in (a) 6 mM chloride medium and (b) 2 mM sulfate medium 184

3.50 (a) SEM image of Mg-Al-Zn alloy surface after 24 h of immersion in the corrosive medium containing 10 mM chloride ions, 800 mM morpholine and (b) corresponding EDX spectra 184

3.51 (a) SEM image of Mg-Al-Zn alloy surface after 24 h of immersion in the corrosive medium containing 10 mM sulfate ions, 800 mM morpholine and (b) corresponding EDX spectra 185

3.52 Potentiodynamic polarization plots for the corrosion of Mg-Al-Zn alloy in the presence of different concentrations of N-methyl morpholine in a) 10 mM chloride medium at 50 °C and (b) 10 mM sulfate medium at 50 °C 202

3.53 Nyquist plots for the corrosion of Mg-Al-Zn alloy in the presence of different concentrations of N-methyl morpholine in (a) 10 mM chloride medium at 50 °C and (b) 10 mM sulfate medium at 50 °C 203

3.54 Bode magnitude plots for the corrosion of Mg-Al-Zn alloy in the presence of different concentrations of N-methyl morpholine in (a) 10 mM chloride medium at 50 °C and (b) 10 mM sulfate medium at 50 °C 204

3.55 Bode phase angle plots for the corrosion of Mg-Al-Zn alloy in the presence of different concentrations of N-methyl morpholine in (a) 10 mM chloride medium at 50 °C and (b) 10 mM sulfate medium at 50 °C 205

3.56 Arrhenius plots for the corrosion of Mg-Al-Zn alloy in the presence of different concentrations of N-methyl morpholine in a corrosive 206

solution of (a) 10 mM chloride medium and (b) 10 mM sulfate medium

3.57 Plots of ln (υ_{corr}/T) versus ($1/T$) for the corrosion of Mg-Al-Zn alloy in the presence of different concentrations of N-methyl morpholine in a corrosive solution of (a) 10 mM chloride medium and (b) 10 mM sulfate medium 206

3.58 Temkin adsorption isotherms for the adsorption of N-methyl morpholine on Mg-Al-Zn alloy surface at different temperatures in (a) 10 mM chloride medium and (b) 10 mM sulfate medium 207

3.59 (a) SEM image of Mg-Al-Zn alloy surface after 24 h of immersion in the corrosive medium containing 10 mM chloride ions, 800 mM N-methyl morpholine and (b) corresponding EDX spectra 208

3.60 (a) SEM image of Mg-Al-Zn alloy surface after 24 h of immersion in the corrosive medium containing 10 mM sulfate ions, 800 mM N-methyl morpholine and (b) corresponding EDX spectra 209

3.61 Potentiodynamic polarization plots for the corrosion of Mg-Al-Zn alloy in the presence of different concentrations of dimethyl morpholine in (a) 2 mM chloride medium at 40 °C and (b) 2 mM sulfate medium at 40 °C 226

3.62 Nyquist plots for the corrosion of Mg-Al-Zn alloy in the presence of different concentrations of dimethyl morpholine in (a) 2 mM chloride medium at 40 °C and (b) 2 mM sulfate medium at 40 °C 227

3.63 Bode magnitude plots for the corrosion of Mg-Al-Zn alloy in the presence of different concentrations of dimethyl morpholine in (a) 2 mM chloride medium at 40 °C and (b) 2 mM sulfate medium at 40 °C 228

3.64 Bode phase angle plots for the corrosion of Mg-Al-Zn alloy in the presence of different concentrations of dimethyl morpholine in (a) 2 mM chloride medium at 40 °C and (b) 2 mM sulfate medium at 40 °C 229

3.65 Arrhenius plots for the corrosion of Mg-Al-Zn alloy in the presence of different concentrations of dimethyl morpholine in a corrosive solution of (a) 2 mM chloride medium and (b) 2 mM sulfate medium 230

3.66 Plots of ln (υ_{corr}/T) versus ($1/T$) for the corrosion of Mg-Al-Zn alloy in the presence of different concentrations of dimethyl morpholine in a corrosive solution of (a) 2 mM chloride medium and (b) 2 mM sulfate medium 230

3.67 Langmuir adsorption isotherms for the adsorption of dimethyl morpholine on Mg-Al-Zn alloy surface at different temperatures in (a) 2 mM chloride medium and (b) 2 mM sulfate medium 231

3.68 (a) SEM image of Mg-Al-Zn alloy surface after 24 h of immersion in the corrosive medium containing 10 mM chloride ions, 800 mM dimethyl morpholine and (b) corresponding EDX spectra 232

3.69 (a) SEM image of Mg-Al-Zn alloy surface after 24 h of immersion in the corrosive medium containing 10 mM sulfate ions, 800 mM dimethyl morpholine and (b) corresponding EDX spectra 232

3.70 Possible interactions between magnesium surface and protonated amine functional group 245

3.71 Possible interactions between magnesium surface and non-protonated amine functional group 246

LIST OF TABLES

Table No.	Contents	Page No.
1.1	Classification of corrosion with examples	4
1.2	Common anchoring groups in the inhibitors	45
1.3	Comparison of physical and mechanical properties of magnesium with natural bone and other implant materials	57
1.4	Alphabets for the major alloying elements	61
1.5	Prominent corrosion inhibitors for magnesium and magnesium alloys in aqueous medium	69
1.6	Eminent corrosion inhibitors for magnesium and magnesium alloy in aqueous organic medium	77
2.1	Elemental composition of Mg-Al-Zn alloy	85
2.2	Structures and concentrations of the studied inhibitor	88
2.3	The n_i, f_i and W_i values of the Mg-Al-Zn alloying elements	90
2.4	List of mathematical forms and verification plots of the common adsorption isotherms	93
3.1	Tafel polarization and electrochemical impedance parameters for the corrosion of Mg-Al-Zn alloy in 30% aqueous ethylene glycol containing different concentrations of chloride ions at different temperatures	116
3.2	Tafel polarization and electrochemical impedance parameters for the corrosion of Mg-Al-Zn alloy in 30% aqueous ethylene glycol containing different concentrations of sulfate ions at different temperatures	117

3.3	Activation parameters for the corrosion of Mg-Al-Zn alloy in 30% aqueous ethylene glycol containing chloride ions	118
3.4	Activation parameters for the corrosion of Mg-Al-Zn alloy in 30% aqueous ethylene glycol containing sulfate ions	118
3.5	Electrochemical parameters for the corrosion of Mg-Al-Zn alloy in 30% aqueous ethylene glycol of different pH, containing different concentrations of chloride ions at 30 °C	119
3.6	Electrochemical parameters for the corrosion of Mg-Al-Zn alloy in 30% aqueous ethylene glycol of different pH, containing different concentrations of sulfate ions at 30 °C	120
3.7 (a)	Potentiodynamic polarization parameters for the corrosion of Mg-Al-Zn alloy in 30% aqueous ethylene glycol containing 2 mM chloride ions, 8 mM SDBS and different concentrations of TSP at different temperatures	134
3.7 (b)	Potentiodynamic polarization parameters for the corrosion of Mg-Al-Zn alloy in 30% aqueous ethylene glycol containing 6 mM chloride ions, 8 mM SDBS and different concentrations of TSP at different temperatures	135
3.7 (c)	Potentiodynamic polarization parameters for the corrosion of Mg-Al-Zn alloy in 30% aqueous ethylene glycol containing 10 mM chloride ions, 8 mM SDBS and different concentrations of TSP at different temperatures	136
3.8 (a)	Potentiodynamic polarization parameters for the corrosion of Mg-Al-Zn alloy in 30% aqueous ethylene glycol containing 2 mM sulfate ions, 8 mM of SDBS and different concentrations of TSP at different temperatures	137
3.8	Potentiodynamic polarization parameters for the corrosion of Mg-Al-	138

(b) Zn alloy in 30% aqueous ethylene glycol containing 6 mM sulfate ions, 8 mM of SDBS and different concentrations of TSP at different temperatures

3.8 (c) Potentiodynamic polarization parameters for the corrosion of Mg-Al-Zn alloy in 30% aqueous ethylene glycol containing 10 mM sulfate ions, 8 mM of SDBS and different concentrations of TSP at different temperatures 139

3.9 (a) Electrochemical impedance parameters for the corrosion of Mg-Al-Zn alloy in 30% aqueous ethylene glycol containing 2 mM chloride ion, 8 mM SDBS and different concentrations of TSP at different temperatures 140

3.9 (b) Electrochemical impedance parameters for the corrosion of Mg-Al-Zn alloy in 30% aqueous ethylene glycol containing 6 mM chloride ion, 8 mM SDBS and different concentrations of TSP at different temperatures 141

3.9 (c) Electrochemical impedance parameters for the corrosion of Mg-Al-Zn alloy in 30% aqueous ethylene glycol containing 10 mM chloride ion, 8 mM SDBS and different concentrations of TSP at different temperatures 142

3.10 (a) Electrochemical impedance parameters for the corrosion of Mg-Al-Zn alloy in 30% aqueous ethylene glycol containing of 2 mM sulfate ions, 8 mM SDBS and different concentrations of TSP at different temperatures 143

3.10 (b) Electrochemical impedance parameters for the corrosion of Mg-Al-Zn alloy in 30% aqueous ethylene glycol containing of 6 mM sulfate ions, 8 mM SDBS and different concentrations of TSP at different temperatures 144

3.10 Electrochemical impedance parameters for the corrosion of Mg-Al- 145

(c) Zn alloy in 30% aqueous ethylene glycol containing of 10 mM sulfate ions, 8 mM SDBS and different concentrations of TSP at different temperatures

3.11 Activation parameters for the corrosion of Mg-Al-Zn alloy in 30% aqueous ethylene glycol containing chloride ions, 8 mM SDBS and different concentrations of TSP 146

3.12 Activation parameters for the corrosion of Mg-Al-Zn alloy in 30% aqueous ethylene glycol containing different concentrations of sulfate ions, 8 mM SDBS and different concentrations of TSP 147

3.13 Thermodynamic parameters for the adsorption of TSP on the surface of Mg-Al-Zn alloy in 30% aqueous ethylene glycol containing chloride ions and 8 mM SDBS 148

3.14 Thermodynamic parameters for the adsorption of TSP on Mg-Al-Zn alloy in 30% aqueous ethylene glycol containing different concentrations of sulfate ions and 8 mM SDBS 149

3.15 (a) Potentiodynamic polarization parameters for the corrosion of Mg-Al-Zn alloy in 30% aqueous ethylene glycol containing 2 mM chloride ions, 8 mM SDBS and different concentrations of SB at different temperatures 157

3.15 (b) Potentiodynamic polarization parameters for the corrosion of Mg-Al-Zn alloy in 30% aqueous ethylene glycol containing 6 mM chloride ions, 8 mM SDBS and different concentrations of SB at different temperatures 158

3.15 (c) Potentiodynamic polarization parameters for the corrosion of Mg-Al-Zn alloy in 30% aqueous ethylene glycol containing 10 mM chloride ions, 8 mM SDBS and different concentrations of SB at different temperatures 159

3.16 Tafel polarization parameters for the corrosion of Mg-Al-Zn alloy in 160

(a) 30% aqueous ethylene glycol containing 2 mM sulfate ions, 8 mM SDBS and different concentrations of SB at different temperatures

3.16 (b) Tafel polarization parameters for the corrosion of Mg-Al-Zn alloy in 30% aqueous ethylene glycol containing 6 mM sulfate ions, 8 mM SDBS and different concentrations of SB at different temperatures 161

3.16 (c) Tafel polarization parameters for the corrosion of Mg-Al-Zn alloy in 30% aqueous ethylene glycol containing 10 mM sulfate ions, 8 mM SDBS and different concentrations of SB at different temperatures 162

3.17 (a) Electrochemical impedance parameters for the corrosion of Mg-Al-Zn alloy in 30% aqueous ethylene glycol, containing 2 mM chloride ions, 8 mM SDBS and different concentrations of SB at different temperatures 163

3.17 (b) Electrochemical impedance parameters for the corrosion of Mg-Al-Zn alloy in 30% aqueous ethylene glycol, containing 6 mM chloride ions, 8 mM SDBS and different concentrations of SB at different temperatures 164

3.17 (c) Electrochemical impedance parameters for the corrosion of Mg-Al-Zn alloy in 30% aqueous ethylene glycol, containing 10 mM chloride ions, 8 mM SDBS and different concentrations of SB at different temperatures 165

3.18 (a) Electrochemical impedance parameters for the corrosion of Mg-Al-Zn alloy in 30% aqueous ethylene glycol containing 2 mM sulfate ions, 8 mM SDBS and different concentrations of SB at different temperatures 166

3.18 (b) Electrochemical impedance parameters for the corrosion of Mg-Al-Zn alloy in 30% aqueous ethylene glycol containing 6 mM sulfate ions, 8 mM SDBS and different concentrations of SB at different temperatures 167

3.18 (c)	Electrochemical impedance parameters for the corrosion of Mg-Al-Zn alloy in 30% aqueous ethylene glycol containing 10 mM sulfate ions, 10 mM SDBS and different concentrations of SB at different temperatures	168
3.19	Activation parameters for the corrosion of Mg-Al-Zn alloy in 30% aqueous ethylene glycol containing chloride ions, 8 mM SDBS and different concentrations of SB	169
3.20	Activation parameters for the corrosion of Mg-Al-Zn alloy in 30% aqueous ethylene glycol containing different concentrations of sulfate ions, 8 mM SDBS and different concentrations of SB	170
3.21	Thermodynamic parameters for the adsorption of SB on Mg-Al-Zn alloy surface in 30% aqueous ethylene glycol containing chloride ions and 8 mM SDBS	171
3.22	Thermodynamic parameters for the adsorption of SB on Mg-Al-Zn alloy in 30% aqueous ethylene glycol containing different concentrations of sulfate ions, 8 mM SDBS and different concentrations of SB	172
3.23 (a)	Synergistic parameters for the interaction of SDBS with TSP and SB on the alloy surface in 30% aqueous ethylene glycol containing 10 mM chloride ions	176
3.23 (b)	Synergistic parameters for the interaction of SDBS with TSP and SB on the alloy surface in 30% aqueous ethylene glycol containing 10 mM sulfate ions	177
3.24 (a)	Tafel polarization parameters for the corrosion of Mg-Al-Zn alloy in a corrosive solution containing 2 mM chloride ions and different concentrations of morpholine at different temperatures	186
3.24	Tafel polarization parameters for the corrosion of Mg-Al-Zn alloy in	187

(b) a corrosive solution containing 6 mM chloride ions and different concentrations of morpholine at different temperatures

3.24 (c) Tafel polarization parameters for the corrosion of Mg-Al-Zn alloy in a corrosive solution containing 10 mM chloride ions and different concentrations of morpholine at different temperatures 188

3.25 (a) Tafel polarization parameters for the corrosion of Mg-Al-Zn alloy in a corrosive solution containing 2 mM sulfate ions and different concentrations of morpholine at different temperatures 189

3.25 (b) Tafel polarization parameters for the corrosion of Mg-Al-Zn alloy in a corrosive solution containing 6 mM sulfate ions and different concentrations of morpholine at different temperatures 190

3.25 (c) Tafel polarization parameters for the corrosion of Mg-Al-Zn alloy in a corrosive solution containing 10 mM sulfate ions and different concentrations of morpholine at different temperatures 191

3.26 (a) Electrochemical impedance parameters for the corrosion of Mg-Al-Zn alloy in a corrosive solution containing 2 mM chloride ions and different concentrations of morpholine at different temperatures 192

3.26 (b) Electrochemical impedance parameters for the corrosion of Mg-Al-Zn alloy in a corrosive solution containing 6 mM chloride ions and different concentrations of morpholine at different temperatures 193

3.26 (c) Electrochemical impedance parameters for the corrosion of Mg-Al-Zn alloy in a corrosive solution containing 10 mM chloride ions and different concentrations of morpholine at different temperatures 194

3.27 (a) Electrochemical impedance parameters for the corrosion of Mg-Al-Zn alloy in a corrosive solution containing 2 mM sulfate ions and different concentrations of morpholine at different temperatures 195

3.27 Electrochemical impedance parameters for the corrosion of Mg-Al- 196

(b) Zn alloy in a corrosive solution containing 6 mM sulfate ions and different concentrations of morpholine at different temperatures

3.27 (c) Electrochemical impedance parameters for the corrosion of Mg-Al-Zn alloy in a corrosive solution containing 10 mM sulfate ions and different concentrations of morpholine at different temperatures 197

3.28 Activation parameters for the corrosion of Mg-Al-Zn alloy in 30% aqueous ethylene glycol containing chloride ions and different concentrations of morpholine 198

3.29 Activation parameters for the corrosion of Mg-Al-Zn alloy in 30% aqueous ethylene glycol containing sulfate ions and different concentrations of morpholine 199

3.30 Thermodynamic parameters for the adsorption of morpholine on Mg-Al-Zn alloy in 30% aqueous ethylene glycol containing different concentrations of chloride ions and different concentrations of morpholine 200

3.31 Thermodynamic parameters for the adsorption of morpholine on Mg-Al-Zn alloy in 30% aqueous ethylene glycol containing different concentrations of sulfate ions and different concentrations of morpholine 201

3.32 (a) Tafel polarization parameters for the corrosion of Mg-Al-Zn alloy in a corrosive solution containing 2 mM chloride ions and different concentrations of N-methyl morpholine at different temperatures 210

3.32 (b) Tafel polarization parameters for the corrosion of Mg-Al-Zn alloy in a corrosive solution containing 6 mM chloride ions and different concentrations of N-methyl morpholine at different temperatures 211

3.32 (c) Tafel polarization parameters for the corrosion of Mg-Al-Zn alloy in a corrosive solution containing 10 mM chloride ions and different concentrations of N-methyl morpholine at different temperatures 212

3.33 (a)	Tafel polarization parameters for the corrosion of Mg-Al-Zn alloy in a corrosive solution containing 2 mM sulfate ions and different concentrations of N-methyl morpholine at different temperatures	213
3.33 (b)	Tafel polarization parameters for the corrosion of Mg-Al-Zn alloy in a corrosive solution containing 6 mM sulfate ions and different concentrations of N-methyl morpholine at different temperatures	214
3.33 (c)	Tafel polarization parameters for the corrosion of Mg-Al-Zn alloy in a corrosive solution containing 10 mM sulfate ions and different concentrations of N-methyl morpholine at different temperatures	215
3.34 (a)	Electrochemical impedance parameters for the corrosion of Mg-Al-Zn alloy in a corrosive solution containing 2 mM chloride ions and different concentrations N-methyl morpholine at different temperatures	216
3.34 (b)	Electrochemical impedance parameters for the corrosion of Mg-Al-Zn alloy in a corrosive solution containing 6 mM chloride ions and different concentrations of N-methyl morpholine at different temperatures	217
3.34 (c)	Electrochemical impedance parameters for the corrosion of Mg-Al-Zn alloy in a corrosive solution containing 10 mM chloride ions and different concentrations of N-methyl morpholine at different temperatures	218
3.35 (a)	Electrochemical impedance parameters for the corrosion of Mg-Al-Zn alloy in a corrosive solution containing 2 mM sulfate ions and different concentrations of N-methyl morpholine at different temperatures	219
3.35 (b)	Electrochemical impedance parameters for the corrosion of Mg-Al-Zn alloy in a corrosive solution containing 6 mM sulfate ions and different concentrations of N-methyl morpholine at different	220

temperatures

3.35 (c) Electrochemical impedance parameters for the corrosion of Mg-Al-Zn alloy in a corrosive solution containing 10 mM sulfate ions and different concentrations of N-methyl morpholine at different temperatures 221

3.36 Activation parameters for the corrosion of Mg-Al-Zn alloy in a corrosive solution containing different concentrations of chloride ions and N-methyl morpholine 222

3.37 Activation parameters for the corrosion of Mg-Al-Zn alloy in a corrosive solution containing different concentrations of sulfate ions and N-methyl morpholine 223

3.38 Thermodynamic parameters for the adsorption of N-methyl morpholine on Mg-Al-Zn alloy in a corrosive solution containing different concentrations of chloride ions at different temperature 224

3.39 Thermodynamic parameters for the adsorption of N-methyl morpholine on Mg-Al-Zn alloy in a corrosive solution containing different concentrations of sulfate ions at different temperature 225

3.40 (a) Tafel polarization parameters for the corrosion of Mg-Al-Zn alloy in a corrosive solution containing 2 mM chloride ions and different concentrations of dimethyl morpholine at different temperatures 234

3.40 (b) Tafel polarization parameters for the corrosion of Mg-Al-Zn alloy in a corrosive solution containing 10 mM chloride ions and different concentrations of dimethyl morpholine at different temperatures 235

3.41 (a) Tafel polarization parameters for the corrosion of Mg-Al-Zn alloy in a corrosive solution containing 2 mM sulfate ions and different concentrations of dimethyl morpholine at different temperatures 236

3.41 Tafel polarization parameters for the corrosion of Mg-Al-Zn alloy in 237

(b) a corrosive solution containing 10 mM sulfate ions and different concentrations of dimethyl morpholine at different temperatures

3.42 (a) Electrochemical impedance parameters for the corrosion of Mg-Al-Zn alloy in a corrosive solution containing 2 mM chloride ions and different concentrations of dimethyl morpholine at different temperatures 238

3.42 (b) Electrochemical impedance parameters for the corrosion of Mg-Al-Zn alloy in a corrosive solution containing 10 mM chloride ions and different concentrations of dimethyl morpholine at different temperatures 239

3.43 (a) Electrochemical impedance parameters for the corrosion of Mg-Al-Zn alloy in a corrosive solution containing 2 mM sulfate ions and different concentrations of dimethyl morpholine at different temperatures 240

3.43 (b) Electrochemical impedance parameters for the corrosion of Mg-Al-Zn alloy in a corrosive solution containing 10 mM sulfate ions and different concentrations of dimethyl morpholine at different temperatures. 241

3.44 Activation parameters for the corrosion of Mg-Al-Zn alloy in 30% aqueous ethylene glycol containing chloride ions and different concentrations of dimethyl morpholine 242

3.45 Activation parameters for the corrosion of Mg-Al-Zn alloy in 30% aqueous ethylene glycol containing sulfate ions and different concentrations of dimethyl morpholine 242

3.46 Thermodynamic parameters for the adsorption of dimethyl morpholine on Mg-Al-Zn alloy in a corrosive solution containing different concentrations of chloride ions at different temperature 243

3.47 Thermodynamic parameters for the adsorption of dimethyl 244

morpholine on Mg-Al-Zn alloy in a corrosive solution containing different concentrations of sulfate ions at different temperature

NOMENCLATURE

AC	Alternating current
ASTM	American Society for Testing and Materials
CPE	Constant phase element
DC	Direct current
EDX	Electron dispersive x-ray analysis
EIS	Electrochemical impedance spectroscopy
EW	Equivalent weight of the corroding material
GDP	Gross domestic product
HSAB	Hard and soft acid base
IMPACT	International Measures of Prevention, Application and Economics of Corrosion Technology
NACE	National Association of Corrosion Engineers
NDE	Negative difference effect
OCP	Open circuit potential
SB	Sodium benzoate
SCC	Stress corrosion cracking
SCE	Saturated calomel electrode
SDBS	Sodium dodecylbenzenesulphonate
SKPFM	Scanning kelvin probe force microscopy
SEM	Scanning electron microscopy
TEM	Transmission electron microscopy
TSP	Trisodium phosphate
VPI	Vapor phase inhibitors
8HQ	8-hydroxyquinoline

LIST OF SYMBOLS

E_a	Activation energy
n_i	Alloying element Valence
ω	Angular frequency
β_a	Anodic tafel constant
i_a	Anodic current density
$\Delta H^{\#}$	Apparent enthalpy of activation
$\Delta S^{\#}$	Apparent entropy of activation
W_i	Atomic weight of alloying element
N	Avogadro's number
C_{dl}	Capacitance of electrical double layer
C_{dif}	Capacitance of the diffusion
C_f	Capacitance of surface film
b_c	Cathodic slope
β_c	Cathodic tafel constant
i_b	Cathodic current density
R_{ct}	Charge transfer resistance
C_{inh}	Concentration of inhibitor
Q_{dif}	Constant phase element corresponding to electrolyte diffusion
Q	Constant phase element constant
Q_{dl}	Constant phase element associated with double layer
Q_f	Constant phase element associated with surface film
i_{corr}	Corrosion current density
$i_{corr\ (inh)}$	Corrosion current density in the presence of the inhibitor
E_{corr}	Corrosion potential
υ_{corr}	Corrosion rate
I_t	Current at time t
ρ	Density of the corroding alloy
i_o	Exchange current density
F	Faraday's constant
R_f	Film resistance

ΔG	Free energy
ω_{max}	Frequency at which the imaginary part of the impedance has a maximum
A	Geometric surface area
Z''	Imaginary impedance
Z	Impedance
Z_{mod}	Impedance modulus
η	Inhibition efficiency
R^2	Linear regression coefficient
n	Number of electrons involved in a reaction
χ	Number of water molecules replaced per molecule of adsorbed inhibitor
r_{oxid}	Oxidation rate at equilibrium
$\varepsilon°$	Permittivity of the air
θ_{max}	Phase maximum
Φ	Phase shift
h	Planck's constant
R_p	Polarization resistance
E_{pzc}	Potential of zero charge
E	Potential difference or emf
E_t	Potential at time t
r_{red}	Reduction rate at equilibrium
Z'	Real impedance
R_{dif}	Resistanace due to electrolyte diffusion
E_o	Rest potential
R_s	Solution Resistance
$\Delta H°_{ads}$	Standard enthalpy of adsorption
$\Delta S°_{ads}$	Standard entropy of adsorption
$\Delta G°_{ads}$	Standard free energy of adsorption
$E°$	Standard reduction potential
θ	Surface coverage
S	Synergistic parameter
T	Temperature

d	Thickness of the electrical double layer
t	Time
R	Universal gas constant
f_i	Weight fraction of alloying element

CHAPTER – 1: INTRODUCTION

1.1. CORROSION - A BRIEF HISTORY

Metallic corrosion has been existed from the day where the common metals such as iron, copper, etc., were first put into use. This undesirable phenomenon was commonly known by ancient as rust, which bankrupts the luster of the metal and shorten its life span. The term corrosion has emanated from a Latin term *corrodere* and has the meaning 'gnawing to pieces' (Sastri et al. 2007). Some historical perspectives of corrosion mentioned in ancient time are (Ahmad 2006):

- Pliny (AD 23-79), a Roman philosopher mentioned about the corrosion of iron in his article as 'Ferrum Corrumpitar'.
- The production of metal from its ore was a well-established in the fourth century AD in India.
- In fifth century BC, Herodotus advised the use of tin for shielding the iron from corrosion.
- In 1675, Robert Boyle published two articles which account for the causes of corrosion.
- In 1788, alkalinity of neutral water by the reaction with iron was noticed by Austin.
- In 1819, Louis Jacques Thenard proposed that metallic corrosion is an electrochemical process.
- In 1824, Davy discovered the sacrificial anode method for the protection of iron.
- In 1829, Hall investigated that oxygen is essential element for the occurrence of rusting of iron.
- Michael Faraday (1834-1840), described the relationship between chemical reaction and generation of electric currents. Today, the first and second laws of Faraday are the base for the estimation of the rate of metallic corrosion.

- In 1903, Whitney found the electrochemical observation for the prevention of corrosion.
- In 1923, Evans put forward his classical electrochemical theory for understanding the causes and the prohibition of metallic corrosion.
- Ulick R. Evans, Herbert H. Uhlig and Mars G. Fontana are the pioneers in current understanding of corrosion.

1.2. DEFINITION OF CORROSION

In general, corrosion is an exterior destruction of a metal or non-metal such as ceramics, plastics, rubber, composites, etc., in an aggressive environment (Fontana 2005). It can be defined for metals as, a chemical or an electrochemical process in which metal transfers its valence electron to the surrounding environment like gas, liquid or hybrid soil-liquid and endure a valence change from zero to a real value (Perez 2004).

The inevitable phenomenon, corrosion is an inverse process of extraction of metals. Extractive metallurgy involves, forcing the metal from its energetically stable state to a higher unstable state by various refining process. The extracted metal attains lower energy by spontaneously reacting with its environment. This tendency of a metal to acquire lower energy state by forming the oxidized product is the driving force for the occurrence of corrosion (Fontana 2005).

1.3. CONSEQUENCES OF CORROSION

The modern civilizations exist on a metal based society. All the metals in the periodic table undergo corrosion to different extent and at distinct rates. Metallic corrosion, although ostensibly innocuous, indeed, has an influence on human life, health and safety, national economy and conservation of materials. The main consequences of metal deterioration on society are as follows (McCafferty 2010):

1.3.1. Human life, health and safety concern

An unexpected corrosion failure leads to collapse of bridges and constructions, the explosion of boilers and pressure vessels, discharge of nuclear wastes, toxic gases, hazardous chemicals and flammable materials to the environment, premature mixing of fuel and oxidizer in missiles and thus causing accidents, personal injury and annihilation. Corrosion of containers and tanks may lead to the contamination of food products, pharmaceuticals, dyes, chemicals, potable drinking water, etc. Metal degradation in biological system decrease the structural integrity of the orthopedic implant and the release of corrosion product may elicit an adverse effect in the host (Jacobs et al. 1998).

1.3.2. Economic losses

The economic losses due to corrosion are classified into direct and indirect losses. Direct losses include replacement and remediation maintenance of the corroded equipments in petroleum, chemical, petrochemical, construction material, pulp and paper manufacturing and transportation industries as well as in domestic metallic equipments. Indirect losses refer to loss in production profit due to unexpected plant shutdown and contamination of product, loss of valuable product due to leakage, loss of efficiency as a result of deposition of the corrosion product in the heat exchanging system, expenditures for the purpose of improving aesthetic value and facial integrity, use of corrosion resistance coating, corrosion inhibitor and corrosion resistance alloy, etc.

International Measures of Prevention, Application and Economics of Corrosion Technology (IMPACT) reported in 2016, that the annual global cost of corrosion was US$ 2.5 trillion which is nearly equal to 3.4% of the world Gross Domestic Product (GDP). Implementation of corrosion mitigation methods could save 15-35% of global corrosion damage cost (NACE 2016).

1.3.3. Effect on conservation of materials

Metals play a significant role on the advancement of any nation. Loss of precious metal by corrosion puts a considerable constraint on non-renewable natural resources, as recycling of corroded metal is not economically fruitful. This ravage of corrosion out-weighs the discovery of contemporary resources which may induce a future metal crisis. Metal corrosion takes its toll on significant historical artifacts, works of art and national monuments which reflects on the national history. To preserve and restore these valuable resources one has to understand the mechanism of destruction by corrosion and its protection by applying different corrosion protection techniques.

1.4. CLASSIFICATION OF CORROSION

Corrosion can be classified in many different ways, depending on the internal and external influence for its occurrence, apparent morphology of the surface and its mechanism. Some important examples for each classification are given below (Sastri et al. 2007).

Table 1.1 Classification of corrosion with examples.

Classification	Examples
General corrosion	Uniform, non-uniform, quasi uniform corrosion, galvanic or two metals corrosion.
Localized corrosion	Pitting, crevice and filiform corrosion.
Metallurgically influenced corrosion	Sensitization, exfoliation, dealloying and intergranular corrosion.
Microbiologically induced corrosion	Microbial corrosion.
Mechanically assisted corrosion	Corrosion fatigue, wear and erosion corrosion.
Environmentally induced cracking	Stress-corrosion cracking, hydrogen damage, embrittlement, hydrogen-induced blistering, high-temperature hydrogen attack, hot cracking, liquid metal embrittlement and solid metal-induced embrittlement.

Fontana has conveniently classified the different types of corrosion into eight forms based on the appearance of the corroded surface by visual examination. The eight types of corrosion are explained as follows (Fontana 2005):

1.4.1. Uniform corrosion

As the name suggests, here the chemical or electrochemical reactions which are taking place over the entire uncovered surface area are uniform. For uniform corrosion to occur the corrosive environment must be uniformly accessible to the entire exposed area and exposed metal should be metallurgically and compositionally homogeneous (Jones 1996). As a result of uniform corrosion, metal equipments eventually fail due to subsequent thinning of metal. Even though, uniform corrosion represents significant loss of metal on a tonnage basis, it can be accurately estimated to prevent possible abrupt failures.

1.4.2. Galvanic corrosion

Galvanic corrosion is also called as two metal corrosion or differential metal corrosion. When potentially differing two dissimilar metals are coupled in a conductive solution, the less corrosion resistant metal is preferentially corroded and the more resistant metal is protected. The potential developed across two dissimilar metals is the driving force for the occurrence of galvanic corrosion. The non-uniform microstructure of the alloy, the position of the metal and alloy in a galvanic series, the nature of the environment, area and distance of the associated metals, etc., decide the extent of galvanic corrosion.

1.4.3. Crevice corrosion

Crevice corrosion is also termed as cavernous corrosion or corrosion under deposit. A localized type of corrosion that occurs under shielded area where corrosive access is restricted is called crevice corrosion. The geometric shape forms a crevice, which is oxygen starved, acts as an anode with respect to the rest, exposed to electrolyte having abundant oxygen. This discrepancy in the concentration of oxygen

leads to a cell of two different potential for localized corrosion. The degree of crevice corrosion depends on the type of crevice, geometry of the crevice, bulk electrolyte, concentration of oxygen, mass transmission in and out of crevice, etc.

1.4.4. Pitting corrosion

Pitting is the most detrimental and insidious type of awfully localized attack in which small area of the surface corrodes preferentially resulting in the formation of cavities or pits. Pitting corrosion is an autocatalytic process where rapid metal dissolution occurs within the pit and oxygen reduction crop up on adjoining metal surfaces. Practically detection of pits is an arduous task because pits are small in size, having various depths and often concealed with corrosion products. The number of pits and its depth that produced under alike condition are different which makes difficulty in predicting pitting corrosion by simple laboratory tests. This misguides in the quantitative measurement of pits and in the forecast of the structural failure.

1.4.5. Intergranular corrosion

During the casting of a metal, crystal mismatch forms an energetically high and chemically active grain boundary region. Intergranular corrosion is the localized corrosion at and adjacent to these grain boundary regions, resulting in deficit of strength and ductility of a metal. In intergranular attack grain boundary serves as an anode to the large cathodic grain area with comparably little corrosion effect. It can occur due to the presence of impurities at the grain boundaries and enrichment or depletion of single alloying element in the grain boundary regions.

1.4.6. Selective leaching

Selective leaching or dealloying or parting corrosion is a selective removal of one or more active metals from an alloy matrix leaving a porous weak residue of the remaining nobler metals (Sastri et al. 2007). Selective removal of zinc from brass and dealloying of gray iron are the classic cases for selective leaching and are called dezincification and graphitic corrosion, respectively. Dezincification turns yellow

brass into copper colored alloy having porous and weak layer of cathodic metal copper and its oxide. Whereas in graphitic corrosion iron is preferentially removed leaving a weak porous network of graphite. The corroded alloy losses its tensile strength and ductility but it may appear undamaged and may retain its original architecture.

1.4.7. Erosion corrosion

The appearance of directional pattern deterioration on the metal surface because of relative movement of corrosive fluid is called erosion corrosion. The directional pattern may be grooves, trenches, valleys and wavy appearance, etc. The nature and properties of the surface film, velocity and nature of the corrosive liquid, effect of impingement, galvanic effect, composition of the metal or alloy, etc., are the important factors which are directly pertinent to the rate of erosion corrosion.

1.4.8. Stress corrosion cracking (SCC)

The part of the metallic material under stress is at higher energy state than the stress free region and susceptible for corrosion attack. The failure of a metal due to the combined action of tensile stress and corrosive environment which creates cracks on the surface is called stress corrosion cracking. The formed cracks may be intergranular or transgranular depending on the direction of crack growth along or across the grain boundaries, respectively. Stress corrosion cracking depends on the amount of stress, composition of the corrosive and its temperature, metal structure and composition.

1.5. FACTORS AFFECTING CORROSION RATE

The rate of corrosion is decided by large number of influencing factors. These can be categorized into three main groups: Metallic factors, environmental factors and design and fabrication factors. The detailed description of these three categories is as follows (Fontana 2005, Ahmad 2006, Uhlig and Revie 2008, Gadag and Shetty 2010).

1.5.1. Metallic factors

Irrespective of corrosive medium, the nature and composition of a metal or an alloy plays a significant role on the magnitude of corrosion rate. The inherent properties of the metal which have remarkable effects on the mechanism as well as on the degree of corrosion are summarized below.

1.5.1.1. Metal purity

Pure metal is less corrosion susceptible than its adulterant. But low strength and cost are the hurdles for its complete applications. To increase its strength and properties metals are subjected to different metallurgical processes. During this, formation of inclusion, deposition of mill scale, formation of different crystallographic orientation, formation of grain and grain boundaries, formation of different phases, localized stress, scratches, etc., will takes place which will initiate and stimulate the rate of corrosion.

1.5.1.2. Standard electrode potential

The potential difference between any two metals is the driving force for the occurrence of corrosion and hence electrode potential of the metal decides its tendency to undergo corrosion. The metal with lower value of standard electrode potential is less corrosion resistance than noble metal with higher standard electrode potential. Coupling of two metals with less difference in its standard electrode potential will have minimum risk of corrosion.

1.5.1.3. Hydrogen overvoltage

In general hydrogen over potential is the measure of difficulty in the evolution of hydrogen gas from the surface of the metal. For most of the corrosion process hydrogen evolution is the common cathodic reaction in aqueous medium, metal with lower hydrogen potential is with lower corrosion resistance and vice versa. Lower hydrogen potential makes cathodic reaction rate faster and thus accelerate the overall deterioration process.

1.5.1.4. Nature of the corrosion product

The growing rate of corrosion upon its initiation is chiefly dependent on the nature of the corrosion product formed. If the corrosion product is thin, stable, uniform, nonporous, continuous and adherent then it acts as a barrier between the metal and the corrosive medium and thus retards the rate of corrosion. The protective efficacy of the corrosion product is decided by Pilling-Bedworth ratio. According to this ratio, the corrosion product is protective only when the volume of the corrosion product is greater than the volume of the parent metal from which the product is formed.

1.5.1.5. Ratio of anodic to cathodic area

During corrosion anodically generated electrons are consumed by the cathodic reactions. If smaller anodic area is in contact with a large cathodic area then electrons are withdrawn in a faster rate in order to balance the half-cell reaction rate and thus accelerate the overall corrosion rate. Therefore smaller the ratio of anodic to cathodic area, more severe will be the metallic corrosion.

1.5.2. Environmental factors

The environment surrounding the corroding specimen has equally responsible as inherent metallic properties. Some environmental factors which have a profound effect on the rate of the corrosion are described below.

1.5.2.1. Temperature of the medium

The rate of any chemical reaction increases with the increase in temperature of the medium. Since corrosion is also an electrochemical process, increase in temperature definitely hastens the rate of corrosion by increasing the ionic mobility and surface film dissolution. But the effect of temperature for steel above 80 °C differs in open and closed system. In an open system above 80 °C, dissolved oxygen will get away from the medium which will not occur in closed system. Therefore in an

open system corrosion rate decreases above 80°C whereas it increases like other chemical reaction in a closed system (Jones 1996).

1.5.2.2. pH of the environment

At lower pH corrosion rate increases due to the availability of H^+ ion for cathodic reduction reactions. Whereas at higher pH formed passive film decreases the corrosion rate for most of the metal except amphoteric metals such as aluminium, copper, lead and zinc.

1.5.2.3. Presence of impurities

Acids are produced in the environment by the combination of atmospheric pollutants or impurities with moisture. The so formed acids enhance the corrosion rate in metals. Formation of sulphuric acid from sulphur dioxide and moisture is the good example for the increased corrosiveness by atmospheric impurities.

1.5.2.4. Concentration of the medium

Increase in the concentration of the medium intensifies the rate of corrosion as it represents the corrosive ion quantity. Omitting weak acids, majority of the media show this behavior. However, at very high medium concentration corrosion rate declines due to the reduced ionization. But passive metals have subtle effect for the wide change in concentration of the medium.

1.5.2.5. Physical state of the medium

Physical state of the corrosive agent plays a pronounced effect on the corrosion rate. For example, a wet soil is more corrosive than dry soil where the former dissolves salts and increase the conductivity of the medium. Dry environment reduces the corrosion current by offering high resistance. Therefore boilers are dry preserved to solve many corrosion problems.

1.5.2.6. Conductivity

Highly conducting medium accelerates the motion of the ions in between anodic and cathodic sites. As a result, the overall electrochemical reaction increases and thus increased conductivity of the medium will amplify the rate of corrosion.

1.5.2.7. Effect of microbes

Presence of microbes like bacteria, algae, yeasts and molds in aquatic system promotes the corrosivity of the medium. For instance, hydrogen sulfide, serious steel corrodant is produced from sulfide reducing bacteria.

1.5.2.8. Effect of oxygen and oxidizer

Since oxygen and oxidizer are the common reactants for cathodic reduction reaction, existence of oxygen and oxidizer in the medium boosts up the rate of metal degradation. Noble metals such as gold, silver, platinum, etc., undergo corrosion in the presence of powerful oxidizers. The metal which demonstrates the active-passive transition can be easily passivated by the addition of moderate oxidizers. To resolve corrosion problems chemical oxygen scavenger like hydrazine is often used in power plants to remove the dissolved oxygen.

1.5.2.9. Velocity of the corrosive

The dependency of the corrosion rate on the velocity of the medium is complex and depends on the nature of the metal and its environment. Activation controlled corrosion processes are free from corrosive velocity. Whereas diffusion controlled corrosion process increases on agitation. On increasing the velocity of the corrosive medium, easily passivating metals become more corrosion resistant. But for the metals which form protective films, increased medium velocity will mechanically damage or detach the surface film and accelerate the corrosion rate.

1.5.2.10. Anodic and cathodic polarization

The phenomenon of polarization is an inactivation of the reaction. The electrode polarization significantly diminishes the rate of corrosion. The electrochemical reaction rate is restricted by various chemical, physical and environmental factors. In an electrochemical reaction rate of electron movement has always surpassed the rate of ionic conduction. Hence the anodic reactions in the proximity of anode build up the metal ion and polarize the anode. In addition to this, metallic passivity also produces anodic polarization. Activation polarization controls the cathodic reaction sequence occurring at metal electrolyte interface. Cathodic reaction is also hampered by concentration polarization due to the decelerated diffusion of cathodic reactants.

1.5.3. Design factors

Design of a structure always demands good mechanical and strength characteristics along with corrosion resistance property. Some designing factors which have a significant effect on the corrosion rate are mentioned below:

- Riveted joints cause more crevice corrosion than welded joints.
- Dissimilar material contact leads to galvanic corrosion.
- Sharp bends facilitate erosion corrosion than blunt bends.
- Improper material selection for different corrosive environment causes structural failure.
- Erroneous drainage structure in tanks causes stagnation of corrosive liquids.
- Non homogeneous surfaces are more corrosive than homogeneous surfaces.
- Frequently failing components of the vast structure are constructed separately than in subservient structure for their easy replacement.

1.6. ELECTROCHEMICAL THEORY OF CORROSION

The phenomenon of metallic corrosion is an electrochemical reaction. Generally corrosion takes place through a series of coupled half-cell reactions. In an

electrochemical half-cell reaction the electrons are present in one side of the reaction. In a reaction if electrons are at the right hand side or electrons are product of a reaction then such a half cell reaction is termed as oxidation half-cell reaction, whereas on the other hand if electrons are at the left-hand side or the reactant of the reaction, is named as reduction half-cell reaction. The region of the metal surface where oxidation and reduction reaction takes place are, respectively called as anode and cathode, and corresponding reactions are called as anodic and cathodic reactions (McCafferty 2010).

The anodic and cathodic half-cell reactions with equations are explained below:

Anodic half-cell reaction: In all the corrosion reactions, the common anodic reaction is the simple metal dissolution with single or multiple oxidation reactions. Here the number of electron produced denotes the valence of the corresponding metal. The anodically generated electrons are responsible for corrosion current.

$$M \rightarrow M^{n+} + ne^{-} \quad (1.1)$$

Cathodic half-cell reactions: The cathodic reduction reactions are complicated compared to anodic oxidation reaction. The most common reduction reactions are listed as follows (Ahmad 2006):

- **Hydrogen evolution:** The frequently encountered cathodic reaction in acidic medium is the formation of molecule of hydrogen gas from hydrogen ions. In neutral medium reduction of water to form hydroxyl ion takes place.

$$2H^{+} + 2e^{-} \rightarrow H_2 \quad (1.2)$$

$$2H_2O + 2e^{-} \rightarrow H_2 + 2OH^{-} \quad (1.3)$$

- **Oxygen reduction:** In aerated aqueous solution having acidic pH oxygen reduction reaction produces water, whereas in alkaline or neutral solution production of hydroxyl ion is favored.

$$4H^{+} + O_2 + 4e^{-} \rightarrow 2H_2O \quad (1.4)$$

$$2H_2O + O_2 + 4e^{-} \rightarrow 4OH^{-} \quad (1.5)$$

- **Metal ion reduction:** This is the intermittent reaction found in chemical processing units.

$$M^{3+} + e^{-} \rightarrow M^{2+} \quad (1.6)$$

- **Metal deposition:** Reduction of secondary metal ions and its deposition at cathode as follows:

$$M^{2+} + 2e^{-} \rightarrow M \quad (1.7)$$

- **Sulfate reduction:** Bacterial reduction of sulfate takes place by the following reaction.

$$SO_4^{2-} + 8H^{+} + 8e^{-} \rightarrow S^{-} + 4H_2O \quad (1.8)$$

From the above reactions it is clear that, cathode acts as 'electron sinks' by consuming electrons generated at the anode at a same rate as they are produced and thus maintain electro-neutrality. The anodic product and anion of the cathodic product diffuse in electrolyte and forms corrosion product in between anode and cathode (Fontana 2005). The formation of electrochemical cell and corrosion product on the metal surface is demonstrated in the Fig. 1.1.

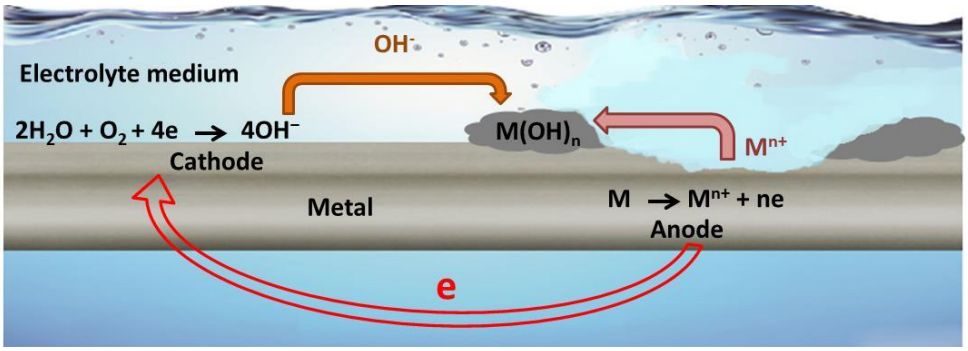

Fig. 1.1 Demonstrative diagram of electrochemical reaction occur at the metal surface.

1.7. THERMODYNAMIC PRINCIPLES OF CORROSION

Thermodynamics is the scientific study of change in energy of the system. In aqueous solution corrosion is the charge transfer reaction and its rate is greatly affected by the change in electrochemical potential of a metal surface. Corrosion

thermodynamics gives the understanding of changes in energy of an electrochemical corrosion reaction. The change in energy gives the driving force for the occurrence and also it control the spontaneity of the chemical reaction. Therefore, thermodynamics is very much useful in adjusting the condition to make corrosion impossible. But when corrosion is possible, it will not predict the rate of a reaction (Jones 1996). The principles of thermodynamics applicable to corrosion process are discussed below:

1.7.1. Concept of Free energy and spontaneity

The accessibility of maximum electric energy or the work capacity of a system corresponds to its free energy. It is well known that electrochemical corrosion reaction produces electrical energy. For electrical and electrochemical reactions, the work done by the system is equal to the amount of electrical energy generated, which is the product of quantity of the electricity involved and the potential difference between the half cells. By using Faraday's law the work done by the system is expressed in terms of change in free energy (ΔG) as follows (Ahmad 2006):

$$\Delta G = -nFE \qquad (1.9)$$

where n is the number of electrons taking part in the cell reaction, F is Faraday's constant, E is the potential difference or emf.

The negative change in the free energy of the system in transition from one state to another state, indicates the decrease in free energy of the system as well as the direction of spontaneous reaction (Fontana 2005). From the above equation it is clear that for any electrochemical process to be spontaneous its potential should be positive and hence negative is its free energy change. By considering the hydrogen evolution on the common cathodic reaction in the process of corrosion, the above equation of free energy change can be expressed as in the following equation:

$$\Delta G = -nF[E_{(H^+/\,H_2)} - E_{(M^{n+}/\,M)}] \qquad (1.10)$$

It follows from the above equation that the metal will corrode only when the standard electrode potential ($E°$) of the metal is more negative than the cathodic process (Sastri

et al. 2007). Finally from thermodynamics the criterion for corrosion is stated as corrosion is impossible unless the metal oxidation reaction is spontaneous.

1.7.2. Application of thermodynamics to corrosion - Pourbaix diagram

The major application of thermodynamics to the field of corrosion is the construction of potential-pH plots. A Belgium electrochemist and corrosion scientist Professor Marcel Pourbaix, in the year 1963 correlated the stability of a metal as a function of potential and pH. These potential-pH diagrams are also called as Pourbaix diagrams in respect of Dr. M. Pourbaix, who pioneered its construction and use in many applications such as fuel cells, hydrometallurgy, water treatment, batteries, electrolysis and electroplating technology. Pourbaix diagrams are constructed by using the calculations based on Nernst equations and solubility data for metal and its species. In this diagram, vertical axis represents the redox potential of the corroding system and horizontal axis shows pH scale. Horizontal lines in the Pourbaix diagram represent electron transfer reactions which are pH independent and potential dependent; whereas vertical lines are potential independent but pH dependent. The slanted straight lines which pertain to reactions involving both the redox potential of a solution and also its pH. These diagrams are computed for the equilibrium conditions at 25 °C. The potential-pH plots are subdivided into region of immunity, corrosion and passivation and the corresponding metal behaviors are listed in the following:

- **Immune region**: In this region corrosion is thermodynamically impossible.
- **Corrosion region**: Here soluble corrosion products are formed and metal undergoes a spontaneous corrosion process.
- **Passive region:** In passive region the metals remains passive. The formed insoluble corrosion product hinders the corrosion rate. Passivity depends on the impervious and adherent properties of the formed corrosion product.

The stability of the magnesium in aqueous environment at 25 °C can be theoretically predicted by Pourbaix diagram as shown in the Fig. 1.2 (Pourbaix 1974). Pourbaix diagram for pure magnesium-water system consists of a large corrosion domain, a

narrow region of immunity and a passive region at a condition of high alkalinity. The large corrosion domain at positive potential than its standard reduction potential (–2.37 V) and pH below 10.5, indicates the spontaneous corrosion process. A narrow corrosion immune region is at a condition of more negative potential than standard electrode potential of magnesium and a passive region at high alkaline (pH > 10.5) zone which favors the formation of magnesium hydroxide ($Mg(OH)_2$) precipitation. Pourbaix diagram predicts that the formed $Mg(OH)_2$ surface film passivate the underlying metal.

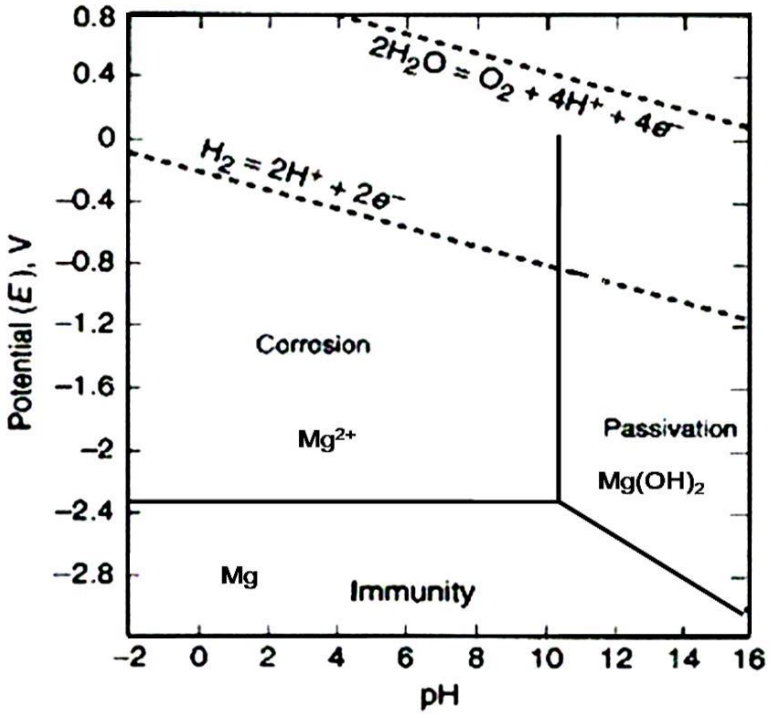

Fig. 1.2 Potential-pH diagram for magnesium/water system (Pourbaix 1974).

Advantages of Pourbaix diagrams are:

- It offers huge thermodynamic information in an efficient and compact manner.
- It predicts the thermodynamic stability or corrosion tendency of a metal in water.
- Explains the stability and composition of the corrosion product.

- These data can be used in corrosion control process like cathodic protection and altering the environment to prevent the thermodynamic probability of corrosion.

Some limitations of Pourbaix diagrams are:

- The data given in the Pourbaix diagram are only based on thermodynamical aspects but no information regarding the kinetic aspects like actual corrosion rates are conveyed.
- The equilibrium condition is assumed, but in all cases the practical conditions may be far from equilibrium.
- Pourbaix diagram explains the condition for the formation of diffusion-barrier film but the protective performances such as porosity, thickness, adherence to metal, etc., remains obscure.
- Pourbaix diagram does not explain the effect of chemical composition, temperature and velocity of the electrolyte on corrosion behaviour.
- Conventional Pourbaix diagram gives the idea of corrosion domain for pure metal which are not of much practical applications (Ahmad 2006).

1.8. CORROSION KINETICS

The tendency of an electrode to undergo corrosion is explained by the aspects of thermodynamics, whereas the rate of the reaction is addressed by the kinetics. The rate of corrosion in the given environment is a crucial factor in deciding the lifetime of a metal or an alloy in structural and electronic applications. The kinetics of an electrochemical reaction on electrode surface is dependent on the electrode potential. Hence the rate of a reaction is strongly depends on the rate of electron flow in metal electrolyte interface (Perez 2004). The rate study of the reaction at the interface between an electrode and electrolyte is called electrode kinetics. The concepts of electrode kinetics have made possible many advances in understanding corrosion and its practical rate measurements. Some concepts of kinetics are discussed as follows (Uhlig and Revie 2008):

1.8.1. Electrochemical polarization-departure from equilibrium

At equilibrium, partial current for the forward reaction and reverse reaction are precisely equal and opposite. The deviation of the potential from their equilibrium value upon the application of an external current is called polarization. Various physical and chemical factors tend to retard the rate of electrochemical reactions (Ahmad 2006). The electrochemical polarization is said to be either anodic or cathodic. Anodic polarization is the acceleration of anodic process by displacing the electrode potential in the noble direction and hence electrode acts more anodic. Whereas cathodic polarization accelerates the cathodic process by moving the potential in the active direction (Roberge 2008). The magnitude of polarization is termed as overvoltage or overpotential and is given by the following equation:

$$\text{Overvoltage} = E - E_o \tag{1.11}$$

where E and E_o are the electrode potentials for some condition of current flow and electrode potential for zero current flow, respectively. Electrode potential for zero current flow is also called as open-circuit potential or corrosion potential or rest potential. The electrochemical polarization can be divided into three types and the total polarization across an electrode is the summation of all individual polarization. The three types of polarization are explained as follows (McCafferty 2010):

1.8.1.1. Activation polarization

When the rate of the reaction is controlled by the slowest step of the reaction sequence occurring at the metal-electrolyte interface, the reaction is said to be under activation polarization. Such a slowest step in order to commence requires activation energy in the form of potential. Activation polarization depends on the current density, type of the material, surface roughness, temperature, pressure, pH, agitation and adsorption of ions.

Activation polarization can be illustrated by considering the hydrogen evolution reaction at the metal-electrolyte interface. Hydrogen evolution involves reduction

reaction of hydrogen ion followed by their combination according to the following reactions:

$$H^+ + e^- \longrightarrow H_{ads} \text{ (reduction reaction)} \quad (1.12)$$

$$2H_{ads} \longrightarrow H_2 \text{ (combination)} \quad (1.13)$$

If electrons are supplied to the electrode at a faster rate than they can react to form H atom, then electrons build-up at the metal side of the metal-electrolyte interface and thus shifts the electrode potential to the negative direction. As a result electrode acts more cathodic due to activation polarization.

At the anode, the process becomes evident when the metal oxidation is slow. Due to this phenomenon electron concentration decreases at the metal side of the interface and electrode potential becomes more positive.

$$M \longrightarrow M^{n+} + ne^- \text{ (metal oxidation)} \quad (1.14)$$

1.8.1.2. Concentration polarization

Concentration polarization in an electrochemical reaction refers to a polarization where change in concentration of the electrode active species near the electrode surface occurs due to diffusion. Concentration polarization is said to be cathodic, when the electrons accumulation at the cathodic interface takes place due to the slow diffusion of the reducing species from bulk electrolyte towards the cathodic surface. As a result of cathodic concentration polarization the potential of the electrode becomes more negative.

Whereas anodic concentration polarization arises due to the slow diffusion of metal ion from anodic interface into the bulk electrolyte. As a consequence, the electrode potential becomes more positive due to the metal ion gathering at the interface. The magnitude of concentration polarization is strongly affected by the following factors:

- Agitation: It increases the rate of ion diffusion by removing the concentration gradient between the corroding metal and bulk electrolyte.

- Temperature: The thickness of the diffusion layer decreases at increased temperature.
- Velocity: A very high velocity of the electrolyte nullifies the driving force for the occurrence of concentration polarization, where the process is totally controlled by activation polarization.
- Ionic concentration: Higher ionic concentration causes greater concentration polarization.
- Geometry: Geometry of the fluid flow and design of the electrochemical cell also affect the magnitude of concentration polarization.

1.8.1.3. Ohmic polarization

The potential drop or IR drop due to the resistance of the electrolyte is referred as ohmic polarization. Even high-conductivity solutions also offer some degree of resistance to the flow of electrons, but it is negligible in comparison with low conductivity media like organic solutions and some soils. Apart from solution resistance, various surface films such as oxides, hydroxides, coatings, also induce ohmic polarization. Practically IR drop can be minimized using Luggin-Haber capillary in electrochemical measurements. This decreases the distance between reference and working electrode by keeping the reference electrode as close to the surface of the working electrode as experimentally possible.

1.8.2. Exchange current density

The current density at an electrode equilibrium where the rate of oxidation and rate of reduction are equal is called the exchange current density. Practically the exchange current density is a misnomer as there is no net current flow at equilibrium. The reaction rate and exchange current density are related by Faraday's law as follows:

$$r_{oxid} = r_{red} = i_o/nF \qquad (1.15)$$

where r_{oxid} and r_{red} are, respectively, oxidation and reduction rate at equilibrium and i_o correspond to the exchange current density in A cm^{-2}.

The exchange current density should be determined experimentally as there is no precise theoretical way for its measurement. The magnitude of experimentally determined exchange current density influenced by some factors listed below (Fontana 2005):

- Exchange current density is estimated on the basis of apparent surface area. Surface roughness offers greater exchange current density as roughened surface contributes more surface area. Therefore platinized platinum electrode has greater i_o for hydrogen reduction reaction than bright platinum. Former has the higher actual geometric surface area than the later.
- Exchange current density for H^+-H_2 system is greatly decreased in the presence of trace catalytic poisons such as arsenic, sulfur, antimony.
- It depends on the ratio of oxidized and reduced species presence.
- Temperature of the system affects the exchange current density.

1.8.3. Mixed potential theory

The basic principle of mixed potential theory says that at steady state the total rate of anodic reaction must equal to the total rate of cathodic reaction. The point where the total rate of anodic reaction equals to the total rate of cathodic reaction is the mixed potential of the system. Although the ideas utilized in the mixed potential theory were known in the 19th century, for the first time in the year 1938, Wagner and Traud formally presented the concepts of this theory. The mixed potential theory resides on the following two postulates.

- Electrochemical reaction is composed of two or more partial oxidation and reduction reactions.
- There can be no net spontaneous build-up of electric charge during an electrochemical process.

Mixed potential theory can be explained by considering the mixed electrode system. Mixed electrode in an electrochemical reaction is the electrode which is in contact with two or more redox systems. Mixed potential theory can be illustrated by

considering the corrosion of zinc in hydrochloric acid. Fig. 1.3 shows the graphical variation of electrode potential and current density for electrode kinetic behavior of zinc in hydrochloric acid solution. This type of graphical representation of variation in electrode potential and current density is known as Evans diagram. In Fig. 1.3, the anodic curve represents the sum of all the partial oxidation reactions whereas sum of all the reduction reactions are represented in the reduction curve. The convergent point in the system represents the total rates of zinc oxidation is equal to rate of hydrogen reduction reaction. The two electrons released per single zinc oxidation reaction are utilized in the formation of single hydrogen molecule. Hence conservation of electric charge is maintained at this intersection point. The corresponding current density and potential at this point is called corrosion current density (i_{corr}) and corrosion potential (E_{corr}), respectively. By using corrosion current density in Faraday's law, corrosion rate can be calculated. Mixed potential theory explains the effect of oxidizer, probability of coupling the two metals, effect of galvanic coupling and effect of area ratio, on the rate of corrosion (Fontana 2005).

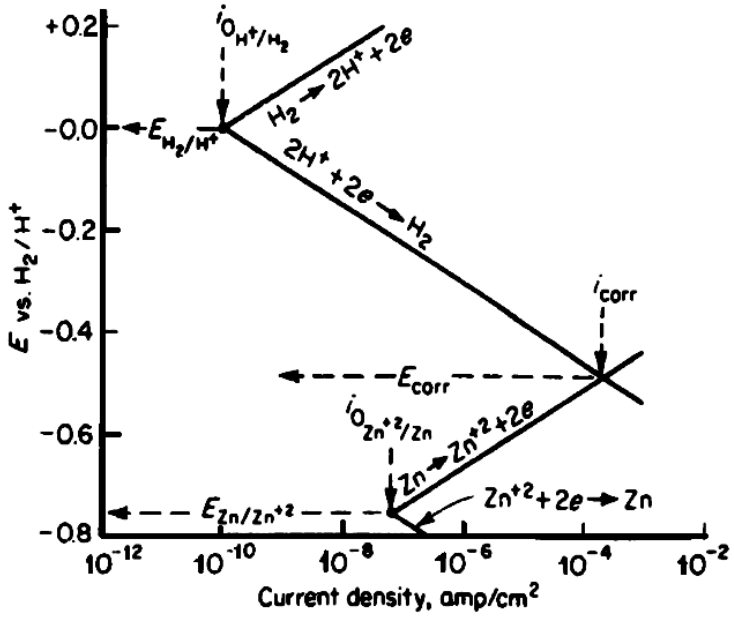

Fig. 1.3 Evans diagram for zinc in hydrochloric acid (Fontana 2005).

1.9. ELECTROCHEMICAL CORROSION TESTING METHODS

Corrosion testing is a significant step in the materials selection process. It is essential to perform the corrosion tests on materials of interest in the anticipated corrosive environments. The key objectives of corrosion testing are listed as follows (Sastri et al. 2007):

- Corrosion testing method is crucial in evaluation and selection of materials for the opted application.
- To evaluate new materials for the given corrosive environments and to determine suitable environment.
- To improve the corrosion resistance property of the material and to control the corrosivity of the environment.
- To study the mechanism of corrosion.

National Association of Corrosion Engineers (NACE) and American Society for Testing and Materials (ASTM) have developed many corrosion testing methods such as weight loss method, weight gain method, inert marker method, gasometric methods, chemical analysis of solution, thickness measurements, electrical resistance method, electrochemical techniques, etc., for measuring the rate of corrosion. A suitable corrosion testing method is followed based on the type of the metal and the form of corrosion (McCafferty 2010). For instance, the weight loss method of corrosion testing is best and most reliable method of testing when uniform corrosion is concerned. But it is slow and time consuming in comparison with electrochemical techniques. The advancement of microprocessor based measurement system for the study of corrosion has made possible corrosion scientist and engineers to acquire experimental data with enhanced accuracy and speed (Ahmad 2006).

Each of the corrosion testing methods mentioned above has an application either in laboratory or in field. Except electrochemical methods none of the above corrosion testing methods can provide insights into the mechanism of corrosion. In addition to this, the electrochemical methods offer the feasibility of mitigating

corrosion by controlling the electrode potential (McCafferty 2010). And also corrosion is electrochemical in its nature and hence electrochemical corrosion testing methods are precise in determining its rate. Electrochemical techniques are broadly classified into two types in determining the rate of corrosion. They are:

- Direct current (DC) electrochemical techniques
- Alternating current (AC) electrochemical techniques

Both these electrochemical methods often use three electrode systems. The cell components and functions of three electrode system are described as follows:

- **Working electrode**: The specimen under study is made as the working electrode. By using an auxiliary electrode current is supplied to the working electrode.
- **Reference electrode**: It has a fixed and known value of potential and measure the potential change across the working electrode. Reference electrode is placed as close as possible to the working electrode to minimize the error caused by ohmic resistance through electrolyte. Saturated calomel electrode, silver-silver chloride electrode, saturated copper-copper sulfate electrode are the common reference electrodes used for electrochemical measurements.
- **Auxiliary electrode:** A counter or an auxiliary electrode is used to complete the path of the current flow. Generally counter electrodes are made from inert material like platinum, gold and graphite. Platinum electrode is the common counter electrode in most of the electrochemical techniques.

For measuring the potential and current density, a programmable instrument called potentiostat is used. The schematic representation of the potentiostat is as shown in Fig.1.4.

Potentiostat consist of electrometer, logarithmic converter and data acquisition unit which provide a continuous sweep over a desired potential range. This instrument automatically provides the desired potential between the study specimen and the reference electrode by passing the suitable current between the study specimen and

the auxiliary electrode. This programmable device works based on ohm's law and controls the current between the study specimen and the auxiliary electrode and measures the potential of the specimen with respect to the reference electrode. The change in potential is measured by using high impedance voltmeter and the applied current is recorded by a low resistance ammeter.

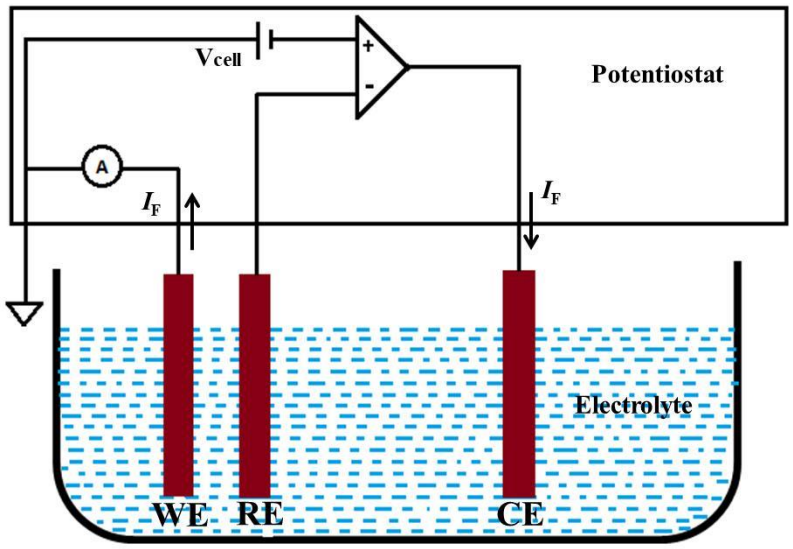

Fig. 1.4 Schematic diagram of a potentiostat.

1.9.1. DC electrochemical techniques

Mixed potential theory gives the basis for the two DC electrochemical corrosion testing techniques: Tafel extrapolation and linear polarization methods. In both the techniques the working electrode is polarized by dragging its potential away from the steady state potential. This polarization induces the electrochemical reactions and thus causes electrochemical changes at the working electrode. The magnitude of the generated current is controlled by the kinetics of the reactions and diffusion rates of the electroactive species. The generated current with respect to applied potential is recorded as a function of time or potential (Thompson and Payer 1998).

1.9.1.1. Tafel extrapolation technique

Wagner and Traud used Tafel extrapolation of corrosion rate determination method to verify the mixed potential theory. In this technique initially the test specimen is allowed to attend a steady state, where the electrochemical reactions attain a constant rate. This steady state electrode potential is called open circuit potential (OCP). After the attainment of OCP the electrode is polarized both anodically and cathodically with respect to OCP. Tafel plots are obtained on plotting logarithm of current density verses applied potential as shown in the Fig. 1.5. The obtained anodic and cathodic branches of Tafel plots are nonlinear near to OCP and linear at a potential away from OCP. The region of linearity of the polarization curve is referred as Tafel region. To determine the corrosion rate from Tafel plots, the Tafel region is extrapolated back to meet the OCP. The point of intersection of the extrapolation gives E_{corr} and i_{corr}, respectively, at its potential and current axis. At corrosion potential, the rate of anodic reaction is equal to the rate of cathodic reaction and the point of intersection corresponds to the corrosion rate of the metal expressed in terms of current density.

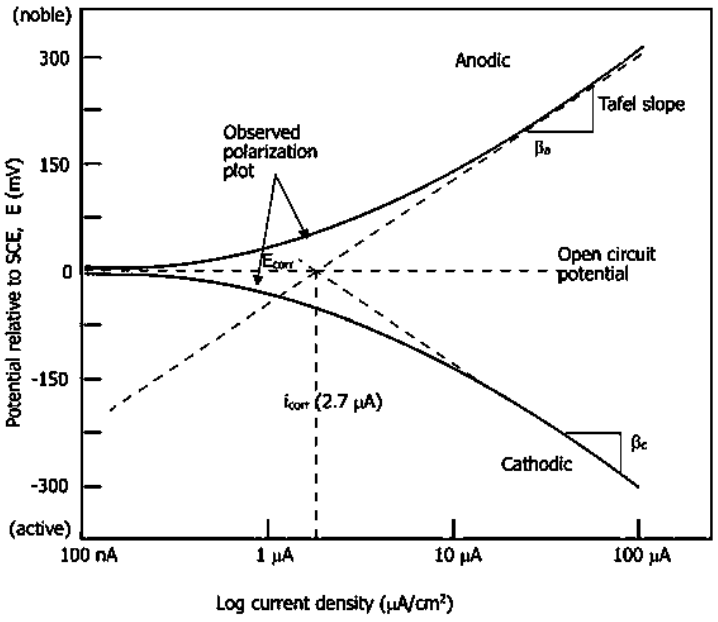

Fig. 1.5 A hypothetical polarization curve representing Tafel extrapolation.

The corrosion rate (υ_{corr}) of the metal is calculated by using corrosion current density from the following equation.

$$\upsilon_{corr} = \frac{K \times i_{corr} \times EW}{\rho} \quad (1.16)$$

where *K* is a constant. The unit of corrosion rate is defined by the value of *K*. For the given value of υ_{corr} in mpy (mills per year), μm year^{-1} and mm year^{-1}, the value of *K* is 0.129, 3.27 and 0.00327, respectively. i_{corr} is the corrosion current density in μA cm^{-2}, ρ is the density of the corroding metal expressed in g cm^{-3}, *EW* is the equivalent weight of the corroding metal.

The Tafel equation for the kinetically controlled electrochemical half-cell reaction is as shown below:

$$i = i_o e^{[2.303\ (E-E_o)/\beta]} \quad (1.17)$$

where *i* and i_o are the current density and exchange current density, *E* and E_o are the electrode potential and equilibrium potential, respectively, β is the Tafel slope have the units of volts/current density decade. The Tafel equation for the combination of anodic and cathodic reactions of a corroding system yields the following Butler-Volmer equation:

$$i = i_a + i_c = i_{corr}[e^{[2.303(E-E_o)/\beta_a]} - e^{[-2.303(E-E_o)/\beta_c]}] \quad (1.18)$$

where i_a and i_c are the cathodic and anodic current density, β_a and β_c are the anodic and cathodic Tafel constant, respectively. These Tafel constants are related to resistance polarization (R_p) as given by the Stern-Geary equation as follows:

$$R_p = \frac{\beta_a \times \beta_c}{2.303\ i_{corr}\ (\beta_a + \beta_c)} \quad (1.19)$$

Merits of Tafel extrapolation methods are:

- It requires only a few minutes to determine the corrosion rate whereas conventional weight loss methods need several days or more.
- This technique allows to measure extremely low corrosion rate with high accuracy.

- With this technique it is possible to measure the continuous corrosion rate like in process plants which needs high purity of the product.

Tafel extrapolation has following demerits:

- The specimen under study is liable to be damaged at higher current rates.
- Tafel extrapolation method is applicable to the system with single reduction process whereas for multiple reduction process the Tafel region is distorted and hence this method will not be applicable for such systems.
- In most of the practical systems Tafel region is often obscured because of concentration polarization or in the presence of more than one activation polarization or because of other extraneous effects. In such situation Tafel region may not spread over a current range of at least one order of magnitude in order to achieve substantial accuracy.

1.9.1.2. Linear polarization technique

The demerits of Tafel polarization technique are largely overcome by the linear polarization analysis. In this technique the working electrode is scanned through a potential of 25 mV above and below the corrosion potential and the resulting current density is plotted against potential as shown in the Fig. 1.6 (Sastri et al. 2007). This technique depends on the fact that the obtained current density is a linear function of the applied potential around the corrosion potential.

In Fig. 1.6 the plot is linear in a region of within ± 20 mV more noble or more active than the corrosion potential. The slope of the plot has the units of resistance; this technique is also called as 'polarization resistance' technique. The kinetic parameters of the system and linear polarization curve are related by the following equation:

$$\frac{\Delta E}{\Delta i} = \frac{\beta_a \times \beta_c}{2.303\, i_{corr}\, (\beta_a + \beta_c)} \tag{1.20}$$

where $\Delta E/\Delta i$ is the slope of the linear portion of the polarization curve, β_a and β_c are the Tafel constants for anodic and cathodic slopes and i_{corr} is the corrosion

current density. From linear polarization method corrosion rate can be calculated by finding the corrosion current density on substituting the experimentally determined values of slope and Tafel constants in the equation 1.20.

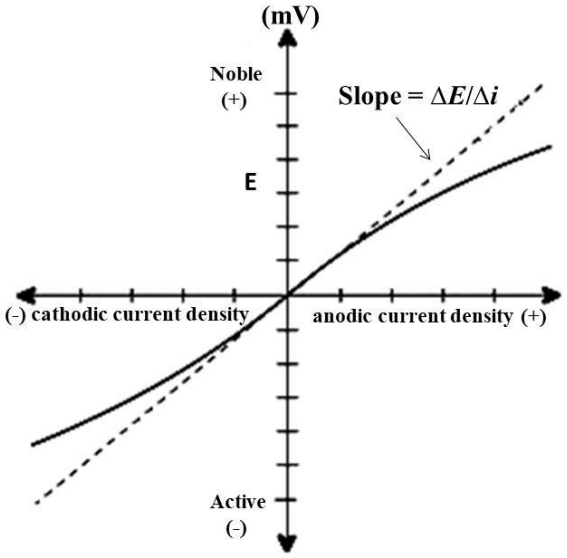

Fig. 1.6 A representative linear polarization plot.

Linear polarization method has the following advantages (Sastri et al. 2007):

- In this technique the applied potential on the metal being small, any changes in the electrode surface due to polarization are minimal. Hence electrode can be re-used repetitively to calculate the corrosion rate at different immersion time.
- As Tafel method, linear polarization method is rapid, accurate and can be used for the continuous corrosion rate measurement.

Limitations of linear polarization method are (Tait 1994):

- This method is susceptible to errors caused by uncompensated solution resistance.
- The Tafel slope values are deduced from Tafel extrapolation method and hence this method is partially dependent on Tafel extrapolation method.

1.9.2. AC electrochemical techniques

An AC voltage has variable magnitude and both anodic as well as cathodic polarity in each polarization cycle. Earlier AC measurements were done with a Schering bridge which needs manual balancing to null the bridge to determine the equivalent parallel resistance and capacitance. But this method of estimation is tedious and sluggish. With the improvement in advanced technique under computer control and acquisition, AC impedance spectroscopy has become an important tool of making electrochemical measurements. This versatile technique has been used to study the various corrosion related issues such as metal-solution interface, corrosion mechanism, effects of oxide film, inhibitor and different surface coatings on metals (McCafferty 2010). The electrochemical metal-solution interfaces are understood well when viewed from an impedance standpoint. Apart from corrosion, impedance finds applications in biosensors, battery and fuel cell development sectors. The detailed description of electrochemical impedance spectroscopy is in the following subsection.

1.9.2.1. Electrochemical impedance spectroscopy (EIS)

Impedance is the proportionality factor between voltage and current in an alternating current or in other words it is an AC equivalent of DC resistance. In simple way it is the opposition for the flow of electrons in an AC circuit and this effect is provided by capacitors and inductors in AC circuits. In impedance measurements a sinusoidal perturbation (either potential or current) is applied to a corroding electrode, centered around the suitable DC condition of interest. The employed sinusoidal perturbation must be of small amplitude about the free corrosion potential and which circumscribes a wide range of frequencies. Such wide frequency stimulation facilitates the computation of electrode capacitance and rate of different electrochemical reactions. Sufficiently small amplitude perturbation is applied so as to get a linear response of the input function (Fontana 2005). The output response for the sinusoidal alternating potential input will be a sinusoidal current at the same frequency with shifted phase as shown in the Fig. 1.7.

By using Ohm's law, the time dependent current response to a sinusoidal alternating potential excitation of an electrode is expressed as a frequency dependent impedance as given in equation 1.21.

$$Z = \frac{E_t}{I_t} = \frac{E_o \sin(\omega t)}{I_o \sin(\omega t + \varphi)} = Z_o \frac{\sin(\omega t)}{\sin(\omega t + \varphi)} \quad (1.21)$$

where Z is the impedance, E_t and I_t are the potential and current at time t, E_o and I_o are the amplitude of potential and current signals, φ is the phase shift, ω is the angular frequency and Z_o is the magnitude of the impedance (Perez 2004).

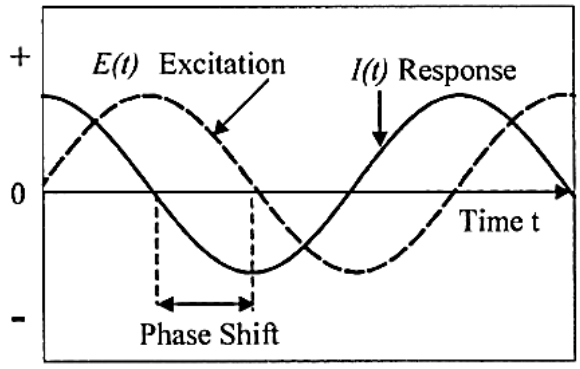

Fig. 1.7 Sinusoidal current response in linear system.

Since impedance is a complex number, it can be expressed in terms of real and imaginary components as follows:

$$Z = Z' + jZ'' \quad (1.22)$$

where Z' is the real component, Z'' is the imaginary component. The mathematical convention for separating the real and imaginary components is to multiply the magnitude of the imaginary component by j (=√-1) and report the real and imaginary values as a complex number (Ahmad 2006).

In electrochemical analysis Nyquist and Bode plots are commonly developed to interpret impedance data. Nyquist plot is also called as complex-plane plot, Argand diagram or Cole-Cole plot. This plot is obtained by plotting Z' along x-axis and Z''

along y-axis. In Nyquist plot, impedance is represented as a vector quantity having both magnitude and direction. The length of the vector corresponds to magnitude of Z_o and φ is the angle with which the vector remains inclined to x-axis. A representative Nyquist plot is as shown in Fig. 1.8. But Nyquist plot does not explain the frequency specific impedance nature of the corroding system. In order to overcome this drawback of Nyquist plot, Bode plots are constructed which display the exact frequency of all the data points.

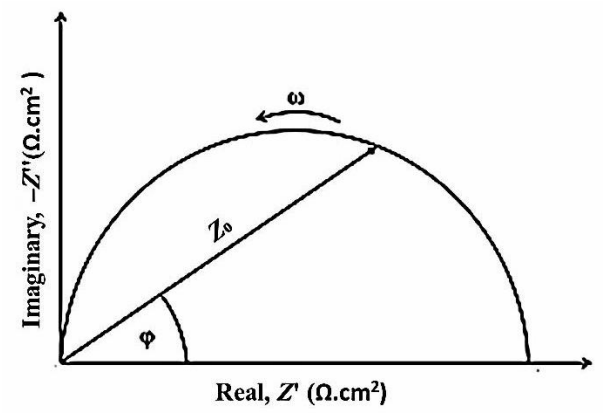

Fig. 1.8 A representative Nyquist plot.

A plot of log (frequency) (frequency in hertz) along x-axis and log (Z_o) along y-axis generates Bode magnitude plot, whereas Bode phase angle plot is acquired by plotting φ along y-axis verses log (frequency) along x-axis. The schematic diagrams of Bode plots are as shown in Fig. 1.9.

Interpretation of AC impedance can be done by simulating the experimental behavior with theoretical equivalent circuit model. These equivalent circuits composed of various combinations of common electrical elements such as resistors, capacitors and inductors. The chosen equivalent electrical circuit should fit to the obtained impedance data to explain the experimental corroding behavior with theoretical elements.

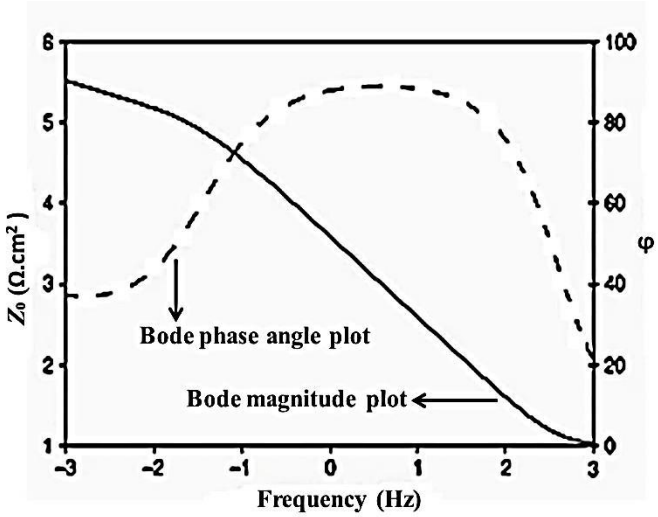

Fig. 1.9 An illustrative Bode plots.

EIS has some advantages over DC technique as listed here under (Fontana 2005):

- EIS has proved to be a very effective technique in analyzing corrosion of reinforcements in concrete, soil and organic solution.
- A sensitive technique that allows the estimation of very low corrosion rate and can provide mechanistic information of the corroding metal.
- Porosity of the insulating coating can be estimated by EIS technique.

Some impediments in EIS measurements are:

- EIS is expensive compared to other electrochemical methods.
- Interpretation of impedance data is ambiguous and complicated.

1.10. CORROSION PREVENTION

As corrosion manifests in several forms its prevention is indeed an arduous task. The mechanism and condition of occurrence are so distinct that single corrosion prevention method cannot be applicable. A suitable corrosion prevention technique is adopted based on the type of material and its design, nature of the environment and

the form of corrosion. Various forms of corrosion can be controlled by the following methods (Jones 1996, Fontana 2005):

1.10.1. Materials selection

Selection of proper metals and alloys for a particular corrosive environment is the foremost method in corrosion prevention. Selection criteria should meet mechanical property, fabricability, availability, cost and corrosion resistance property for a particular application. In general whenever practicable the more corrosion resistance pure metals and nonmetallics such as rubber and plastics or high temperature resistance ceramics or electric and heat conducting carbon and graphite or wood can be chosen. For example, pure aluminum of 99.5% is more useful in handling hydrogen peroxide than its counter alloy form. Presence of other impurity elements in the latter case may lead to the decomposition of hydrogen peroxide by catalytic effect.

1.10.2. Alteration of environment

Environmental factors are the key elements in causing material corrosion. Altering the corrosive environment provides a versatile and unique way to reduce material degradation. In this regard lowering the medium temperature, decreasing the fluid velocity, eliminating oxygen and oxidizers from the corrosive atmosphere and changing the corrosive concentration, etc., open the door to subside corrosion. Use of corrosion retarding catalysts, called inhibitors, also comes under the category of environmental alteration scheme. The detailed description of corrosion inhibitor is presented in the following subsection 1.11.

1.10.3. Design of a structure

The structural design is as important as selection of materials for construction. The improper material design may end up with initiation and acceleration of corrosion phenomenon. Design of a structure should meet mechanical and strength obligations together with an allowance for corrosion. Therefore it is necessary to follow some

design rules such as, weld joints in tanks and containers, increased wall thickness of the pipes, tanks and avoiding heterogeneity, mechanical stresses, contact of dissimilar metals, sharp edges in structures.

1.10.4. Cathodic protection

Cathodic protection is the oldest method of corrosion prevention technique which was used in 18^{th} century by Humphrey Davy to protect British naval ship. In cathodic protection, electrons are supplied to the metal surface to make it intrinsically resistant cathode material. Cathodic protection can be accomplished either by impressed current method or by galvanic coupling with more active metal. In an impressed current method negative terminal of the external power supply is connected to the metal to be protected and positive terminal to the inert anode material. Required amount of current is passed to the metallic structure to maintain it as a cathode with respect to an inert anode. Whereas in galvanic coupling more active metal such as magnesium or zinc is coupled to act as a sacrificial anode.

1.10.5. Anodic protection

Anodic protection of corrosion prevention method is relatively new in contrast to cathodic protection and was first proposed by Edeleanu in 1954. This technique is applicable to the metal and alloys which show active passive transition and can be passivated by applying external anodic current using potentiostat. The potentiostat keeps the metal at a constant potential where passivity prevails. In operation, optimum protection potential is obtained by electrochemical measurements. The preliminary advantages of anodic protection over cathodic protection are its low current requirement and its applicability in strong corrosive environments.

1.10.6. Coatings

Coating can afford an adequate barrier between the metal and the corrosive environment. Depending on the suitability metallic, inorganic as well as organic coatings are opted. Metallic coating are applied by electrodeposition or electroplating

techniques, flame spraying or metallizing procedures, cladding skills, hot dipping and vapor deposition modes. Whereas inorganic coatings are applied by spraying schemes, diffusion methods and chemical conversion processes. Irrespective of the method followed coating must be non-porous, even, chemically resistant to corrosive and impervious to give long shelf life.

1.11. CORROSION INHIBITORS

An inhibitor is a retarding catalyst which will suppress the rate of corrosion on minute amount of its addition to the corrosive environment. Since the addition of inhibitor decreases the corrosivity of the environment, this method of corrosion control comes under the heading of environment alteration technique. Use of inhibitor in corrosion mitigation is a more convenient and easy approach in comparison with other mode of corrosion control. Because the addition of inhibitor is very simple and easy technique, it does not require special equipment for implementation, it will not disrupt the ongoing process, it needs in small quantity and thus economically feasible (Guo et al. 2013). Inhibitor finds its major application in the field of petroleum refineries, oil and gas production units where they are contemplated as the first line of defense in facing the corrosion. Inhibitors are added in water cooling systems, feedwater and boiler section of the power plant, water systems which need protection of circulating pipelines and heating systems. The inhibitors are also used in safeguarding the reinforced steel components in construction industries, in the production and transportation of machinery and equipment and in metal extraction enginery. From many years inhibitors have been employed in acid pickling (cleaning) solutions, chemical manufacturing industries, engine coolants of automobiles (Sastri 1998, Gräfen et al. 2000, McCafferty 2010). Nowadays the growing interest in the field of corrosion inhibitor is illustrated in its incorporation with paints and coatings to improve corrosion resistance property of the metal and alloys (Zheludkevich et al. 2007, Armelin et al. 2008, El-Fattah et al. 2017, Mirzakhanzadeh et al. 2018). Selection of the inhibitor for various applications considers the following criteria (Ahmad 2006):

- The magnitude of suppression in the corrosive environment to dreadful forms of corrosion.
- Duration of effectiveness.
- Solubility and dispersibility in the corrosive medium.
- Effect on the other metals joined to the main metal system (bimetallic coupling).
- Stability of the inhibitor for different temperatures and corrosive concentrations.
- Toxicity and pollution on environment.
- Consequence of inhibiting compound on heat transfer characteristics.
- Economic and technical competition with the existing inhibitors.

But the use of inhibitor is not advisable in the following conditions:

- Equipment and component of the machine which are subjected to turbulent flow.
- System operating at very high velocity, temperature, etc., which are above the stability limits of corrosion inhibitor.

1.11.1. Classification of inhibitor

There are numerous types of inhibitors which reduce metallic corrosion in different ways. The classifications of inhibitor are made on the basis of mechanism and composition. The most suitable classifications of corrosion inhibitors are shown in Fig. 1.10. This broad classification covers the mode of action, chemical nature, inhibitor nature and filed of application (Flick 1993, Schweitzer 2009, Papavinasam 2011, Sastri 2012). Corrosion inhibitors are mainly classified into interfacial inhibitors and environment modifiers. Interfacial inhibitors interact with metal surface and as a result impede the ongoing metal corrosion. On the other hand environment modifiers modify the corrosive surrounding into a less corrosive or noncorrosive environment by interacting with corrosive species. The detailed descriptions of each class of inhibitors are in the following subsections.

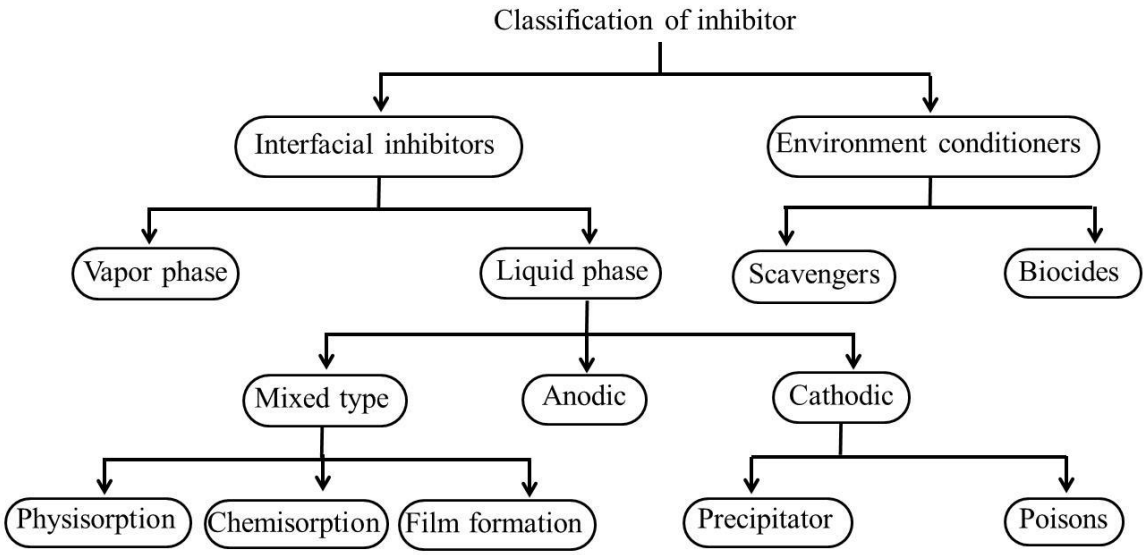

Fig. 1.10 A comprehensive categorization of corrosion inhibitors.

1.11.1.1. Environment conditioners

These inhibitors interact with the aggressive species of the corrosive environment and thus reduce its attack on the metal surface. The further groupings of environment conditioners are briefed in the following.

a) Scavengers: Presence of trace amount of oxygen in the closed system such as boilers, condensing systems, feedwater lines and economizers imparts corrosiveness to the medium. Therefore oxygen must be eliminated from the closed system to protect the metal from corrosion. The chemicals which are added to eliminate the oxygen from the system are named as scavengers. In near neutral solution oxygen reduction is the predominant cathodic reaction and elimination of oxygen is bound to diminish the rate of cathodic reaction, which subsequently cut down the rate of corrosion. Sodium sulfite and hydrazine are the common examples for scavengers which remove the oxygen as in the equations shown below.

$$Na_2SO_3 + ½\ O_2 \rightarrow Na_2SO_4 \qquad (1.23)$$

$$N_2H_4 + O_2 \rightarrow N_2 + 2H_2O \quad (1.24)$$

b) Biocides: Microbial corrosion causes intense damage and severe corrosion problem in cooling towers and filters. The growth of the bacteria is controlled by employing bacteriostats or bacteriocides. Bacteriostats put the bacteria, algae, yeast, sulfate reducers, molds and slime formers in a dormant condition, whereas bactericides kill the bacteria. Bacteriostats and bacteriocides are collectively called as biocides. The main objective of biocides is to control bacterial counts and curtail their deleterious effect on material degradation. Cocoamine acetate, benzalkonium chloride, acrolein and chlorine dioxide are the widely employed biocides in industries.

1.11.1.2. Interfacial inhibitors

Interfacial inhibitors are also referred to as adsorption inhibitors. These inhibitors bring about corrosion inhibition by adsorbing along the metal/electrolyte interface. Most of the corrosion inhibitors are interfacial in their action. The further classification of interfacial inhibitors are into vapor phase inhibitors and liquid phase inhibitors.

a) Vapor phase inhibitors (VPI): Vapor phase inhibitors or volatile corrosion inhibitors are by definition, are volatile in nature and can be transported to the desired location by volatizing the low vapor pressure compounds. The vapor of the low vapor pressure compounds exhibit corrosion inhibiting property. The mechanism of vapor phase inhibitor is not well established, but it is assumed that the undissociated inhibitor molecule migrates to the metal surface and undergoes hydrolysis in the presence of moisture. Solid or liquid forms of vapor phase inhibitors are used depending on its application. Liquid vapor phase inhibitors are impregnated in wrapping papers or polymeric films and used to pack the components to be protected. Whereas solid vapor phase inhibitors are accommodated in porous bags or sachets to provide sufficiently high concentration of the inhibitor in the confined spaces. Vapor phase inhibitors are useful in long period storage of equipment and transportation of

machinery and components. They also have been used to safeguard the electronic materials like circuit boards.

b) Liquid phase inhibitors: These inhibitors interact with metal surface in a solubilized form. Liquid phase inhibitors are further classified into anodic, cathodic and mixed-type inhibitors depending on the half-cell reaction retardation by inhibitor molecule.

Anodic inhibitors: These inhibitors selectively act on the anodic metal dissolution reaction. Oxyanions like chromates, molybdates and tungstates are the common examples for anodic inhibitors. They react with the metal ions at the anodic region. Generally metal salts of these inhibitors are sparingly soluble and hence precipitate over the metal surface as films. These films acts as barriers and passivate the underlying metal when they are impervious and continuous. The added oxyanions play a role of repairing the defective surface film when metal is inherently passive. But the major disadvantage of anodic inhibitors is that good protection is rendered with the addition of sufficient amount of inhibitors whereas on the other hand corrosion will be accelerated with inadequate amount of inhibitors. The result of anodic inhibitor addition on the polarization curve is illustrated in the Fig. 1.11. The anodic polarization curve alone shifts to more positive corrosion potential region. This brings down the current density and rate of anodic reaction or in general increase the inhibition of corrosion.

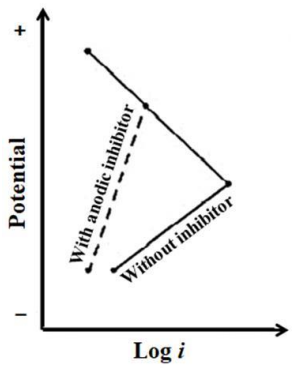

Fig. 1.11 Evans diagram illustrating the effect of anodic inhibitor addition.

Cathodic inhibitors: These inhibitors inhibit the hydrogen evolution or oxygen reduction reaction in acidic and neutral or alkaline solutions, respectively. These can be cathodic poisons or precipitators which selectively hinder the cathodic reactions of corrosion.

Cathodic poisons: The compounds which readily undergo reduction and consequently deposit on the cathode as adherent metallic films to poison hydrogen evolution are called cathodic poisons. Compounds with high hydrogen overpotential in acidic media and those can give insoluble product in alkaline media constitutes the effective cathodic poisons. The oxides of arsenic, antimony, bismuth, salts like sodium meta-arsenite have been used as promising cathodic poisons.

Cathodic precipitators: These inhibitors selectively precipitate upon the cathodic site to form impermeable films. The formed film will hinder the reduction of cathodic reactants from getting reduced at the cathode. The film formed from urea, thiourea and mercaptants will selectively block the path of hydrogen ion and hydroxide of zinc sulfate and magnesium sulfate will resist the diffusion of oxygen. The shift in the corrosion potential to the more negative region and decrease in the current density value upon the addition of cathodic inhibitors is shown in the Fig.1.12.

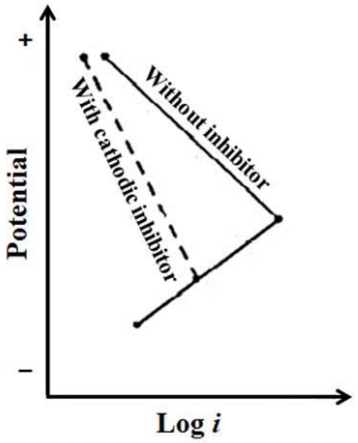

Fig. 1.12 Evans diagram depicting the effect of addition of cathodic inhibitor.

Mixed-type inhibitors: This class of compounds minimizes the rate of both half-cell corrosion reactions to different extent. Most of the organic compounds show this feature. The electron density distribution in the mixed type inhibitors favors the adsorption at cathodic as well as at anodic reaction sites. The predominant changes in the polarization curves on the addition of mixed-type inhibitors are as represented in the Fig. 1.13.

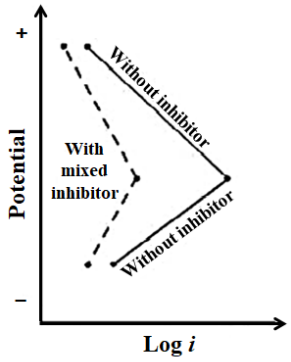

Fig. 1.13 Evans diagram interpreting the effect of mixed type inhibitor admittance.

On the addition of mixed-type inhibitor both the polarization curve shift to lower current density region with insignificant change in corrosion potential. The mixed type inhibitors inhibit the metallic surface by one or more of the following mechanism of inhibition.

a) Chemical adsorption
b) Physical adsorption
c) Film formation

a) Chemisorption type of inhibitors: In chemisorption, charge transfer interaction between the inhibitor molecules and metal surface establishes a strong coordinate chemical bond. The coordinate chemical bond is preferred between the vacant, lower energy orbital of the metal with inhibitor having lone pair of electrons. The formed coordinate chemical bond strengthens with time and rise in temperature and hence

chemisorbed inhibitors operates more efficiently at higher temperatures. The main features of chemisorption are large heat of adsorption, specificity and persistence. In addition to coordinate bond the hydrocarbon tail of the inhibitor molecules orient towards the electrolyte, make the cluster of hydrophobic hydrocarbon tails and thus give further protection by keeping the water molecules and other aggressive ions away from the metal surface. The effectiveness of the chemisorbed inhibitor depends on the electron donor ability, size and solubility of the inhibitor molecule.

b) Physisorption type of inhibitors: The physical adsorption takes place through the weak electrostatic force of interaction between the inhibitor molecules and the metal surface. The metal spontaneously develops a charged interface in the electrolyte. The negatively charged metal surface attracts the positively charged inhibitor molecules and vice versa. The instantaneous physisorption necessitates less activation energy and vulnerable to desorb at higher temperature and at increased velocity. Therefore, the process of physisorption is reversible in nature.

c) Film forming inhibitors: Some surface adsorbed inhibitor initiate reaction which leads the formation of surface films. The phenomenon of film formation is complex and the efficiency of the surface film depends on the thickness, solubility and composition of the film. The adherent, insoluble and impervious films are highly efficient and promising as protective barrier against corrosion.

1.12. FACTORS AFFECTING THE INHIBITOR EFFICIENCY

The efficiency of any inhibitor depends on the specified metal and its environment. Therefore the selection of inhibitor for a particular metal and its surroundings always consider the following influential factors.

1.12.1. Molecular structure

The molecular structure of the inhibitor will have profound effect on the efficiency of the inhibitor. The structure of the inhibitor is composed of an anchoring group, a backbone and a substituent group. The effect of these three moieties will

decides the electron donor ability of the molecule and hence the overall efficiency of any inhibitor.

a) Anchoring group: On the basis of the electron donor-accepter interaction, inhibitors are considered as Lewis bases and functional groups of the inhibitor operate as anchoring groups. The interaction strength between the metal and inhibitor is decided by the electron density and the polarizability of the anchoring group. For substantial interaction anchoring group should bear either pi-bonds or hetero atoms having lone pair of electrons or both. The loosely bounded electrons of the pi-bond and lone pair electrons of the hetero atom can transfer charge efficiently. For a given homologous series of organic compounds which differ only in terms of heteroatom the order of inhibition efficiency follows: P > S > N > O (Papavinasam 2011). Common anchoring groups in the inhibitor are as given in Table 1.2 (Sastri et al. 2007).

Table 1.2 Common anchoring groups in the inhibitors.

Structure	Name	Structure	Name
-OH	hydroxy	$-CONH_2$	amide
-C≡C-	-yne	-SH	thiol
-C-O-C-	epoxy	-S-	sulfide
-COOH	carboxy	-S=O	Sulfoxide
-C-N-C-	amine	-C=S-	thio
$-NH_2$	amino	-P=O	phosphonium
-NH	imino	-P-	phospho
$-NO_2$	nitro	-As-	Arsano
-N=N-N-	triazole	-Se-	Seleno

b) Backbone: The backbone of the inhibitor refers to the basic structural unit which bears functional and substituent groups. For organic molecules, aromatic rings with

delocalized pi-electron and long chain aliphatic hydrocarbons are considered as backbones. These backbones amplify the electron density of the anchoring group. In particular, aliphatic hydrocarbon chains lower the solubility and hence encourage precipitation of inhibitor and formation of surface films. Such surface films induce hydrophobicity to control corrosion in aqueous media.

c) Substituent groups: The structural units other than anchoring groups attached to the backbone are substituent groups. These substituent groups boost the electron density of the anchoring group for giving superior inhibition efficiency. But, the substituent group steric effect may hinder the efficiency of the inhibitor. Therefore, for outstanding inhibition efficiency the substituent groups should be positioned in such a way that the steric hindrance is lessened and electron density of the anchoring groups is augmented.

Theoretically by using Hammett equation the electronic effect of the substituent groups can be calculated (Sastri et al. 2007). Plenty of researchers have studied the correlation between the molecular structure and its inhibition efficiency. They have considered both practical and theoretical quantum chemical studies to investigate the impact of molecular structure on inhibition efficiency (Lukovits et al. 2001, Fang and Li 2002, Khaled 2008, Kara et al. 2012, Aouniti et al. 2013, John and Joseph 2013, Debab et al. 2018, Singh et al. 2018).

1.12.2. Size of the molecular structure

Basically inhibitor with larger molecular area gives the better inhibition efficiency. However, with bigger molecular structures like polymers, steric problem appears. Because of steric problem large molecules cannot fit on to a surface which is partially occupied by previously adsorbed molecules. In such cases complete surface coverage by inhibitor may be obscure and hence gives lower inhibition (McCafferty 2010).

1.12.3. Effect of inhibitor concentration

Initially with the increase in the concentration of the inhibitor, the rate of corrosion decreases because of the adsorption of the inhibitor. But for chemisorption type inhibitors, after the surface of the alloy is covered by the adsorption monolayer, further increase in inhibitor concentration will not produce decrease in the corrosion rate (McCafferty 2010).

1.12.4. Solubility of the inhibitor

Solubility of the inhibitor decides its efficiency to cover the surface area. Generally less soluble molecules will have a greater tendency to adsorb than more soluble inhibitors.

1.12.5. Impact of temperature

The impacts of temperature rely upon the type of interaction between the metal and inhibitor. Physical adsorption processes are relatively weak and need low activation energy. At higher temperature there is a chance of desorption of physisorbed molecule. But the phenomenon of chemisorption is relatively slow, which involves the coordinate type of bond between the metal and the inhibitor. Therefore chemisorption requires higher activation energy and shows higher inhibition efficiency up to certain increment in temperature. But at elevated temperature decomposition of the organic inhibitor molecule contributes to the reduced efficiency, irrespective of the type of metal inhibitor interactions (Revie 2011).

1.12.6. Nature of the metal atom

According to Sastri et al. metal atoms, metal ions and bulk metals are classified into hard acids, soft acids and borderline acids. Similarly inhibitors are also classified into hard inhibitors, soft inhibitors and borderline inhibitors. The principle of hard and soft acid base (HSAB) says that hard acids tend to form complexes with hard bases, soft acids form complexes with soft bases and borderline acids forms

complexes with either soft or hard bases. By using HSAB principle one can rationalize the probable efficiency of the corrosion inhibitor (Sastri et al. 2007).

1.12.7. Surface charge on the metal

The charge on the metal surface plays a crucial role in deciding the extent of physisorption. The metal surface of the metal/solution interface can have abundance of electron or deficiency of the electron, and accordingly metal surface has negative or positive charge, respectively. This electrically charged surface attracts the opposite charges towards itself. The potential at which the surface has zero charge is called potential of zero charge (E_{pzc}). The value of E_{pzc} varies from metal to metal and also with the surrounding electrolyte (McCafferty 2010). The difference between the corrosion potential (E_{corr}) and E_{pzc} decides the charge on a metal surface according to the following equation:

$$E_{surf} = E_{corr} - E_{pzc} \tag{1.25}$$

The appropriate inhibitor for a given type of metal can be predicted by knowing the values of E_{corr} and E_{pzc} of the metal (McCafferty 2010). When $E_{corr} > E_{pzc}$, metal is positively charged and attracts anionic inhibitors where as in other case, $E_{corr} < E_{pzc}$ results in negatively charged metal surface and hence captivates cationic inhibitor (Papavinasam 2000).

1.12.8. Intermolecular interaction between the adsorbed inhibitor

At increased surface coverage, the intermolecular interaction between the adsorbed inhibitor molecules becomes more prominent. The attractive lateral interaction between the adsorbed molecules leads to the enhanced surface coverage and hence gives the superior inhibition. For instance, inhibitor with long chain aliphatic hydrocarbons gives higher inhibition due to the attractive van der Waals forces between the hydrocarbon chains. On the other hand if the lateral interactions are repulsive then imperfect surface coverage induces the impoverish inhibition.

1.12.9. Effect of secondary inhibition

The inhibition brought about by the addition of native form of the inhibitor molecules is called primary inhibition. The nature of the original inhibitor molecule present in the electrolyte may change with time as a result of chemical reactions such as reduction, polymerization or precipitation. The inhibition shown by such reaction products is named as secondary inhibition. The effectiveness of the secondary inhibition depends on the nature of the reaction products. For instance, diphenyl sulfide is the electrochemical reaction product of diphenyl sulfoxide on the metal surface. The former is more effective inhibitor than its precursor. Conversely the reduction product of thiourea and its alkyl derivatives gives the bisulfide anion (HS^-), which is corrosive and accelerates the rate of corrosion (Revie 2011). Similarly the surface active agents called surfactants produce metal precipitation upon its adsorption on metal, which forms the hydrophobic surface layer and hence controls the aqueous corrosion (Schweitzer 2009).

1.12.10. Influence of electrical double layer

Immersion of an electrode into an electrolyte creates charged electrode/electrolyte interface by adsorbing charged species of the electrolyte. The array of charged species at the electrode/electrolyte interface is called the electrical double layer. The electrode side of the interface can be positive or negative according to the withdrawal or supply of electrons. This surface charge of the electrode is balanced by the ions of the electrolyte interface. The electrical double layer plays an important role in the adsorption of inhibitor molecules. When an organic molecule adsorbs on the metal surface, first it must enters into the electrical double layer. This intrusion of organic molecule increases the thickness and decrease the effective dielectric constant of the electrical double layer. The thickness and dielectric constant of the electrical double layer are related to the capacitance by the following relation.

$$C_{\mathrm{dl}} = \frac{\varepsilon}{d} \tag{1.26}$$

where C_{dl} is the capacitance of the electrical double layer, ε is dielectric constant and d is the thickness of the double layer. Increase in the value of C_{dl} with the addition of inhibitor indicates the efficiency of the inhibition process. The value of C_{dl} can be determined by using single current pulse technique or AC impedance methods (McCafferty 2010).

1.12.11. Synergism and antagonism

The performance of the combination of two or more inhibitors depends on the lateral interaction between the inhibitors. If the resulting lateral interaction is attractive then the inhibition efficiency of the combination will be greater than the sum of the individual efficiencies. This phenomenon is called synergistic effect. The mixture of formaldehyde and furfuralimine is the good example for this effect. In contrast to synergistic effect, combination of narcotine and thiourea gives lower efficiency compared to that exists when narcotine and thiourea are used separately. This repulsive interaction between the mixtures of inhibitors is named as antagonistic effect (Revie 2011).

1.13. METHODS FOR INHIBITOR APPLICATION

The best performing inhibitor will also fail if it is applied improperly. The application of inhibitor to the corroding object follows three well know methods.

a) Continuous injection
b) Batch treatment
c) Squeeze treatment

a) Continuous injection: In this process inhibitors are continuously injected to the structure by using chemical pumps to achieve the objective of the inhibition. In order to obtain uniform distribution, electric or gas driven pumps will inject the inhibitor to the point of turbulence. In this technique a constant supply of inhibitor is provided at a controlled rate. This method is cost effective and widely used in the oil industries, cooling and municipal water treatment systems to avoid scaling as well as corrosion.

b) Batch treatment: This technique is also called as slug treatment and is applicable to the area where continuous injection is practically impossible. In this periodic treatment bulk chemicals are added for an extended period of time. In batch treatment the tube displacement technique is followed. Several barrels of chemicals are pumped from the top of the tubing. This chemical is displaced to the bottom with the help of fluids in the oil well and well is closed for certain time before operation. Batch treatment is mainly used to treat the water with biocides. Since large quantities of biocides are wasted in this technique, it is not economical and also corrosion is not controlled during shutdown time.

c) Squeeze treatment: This method is employed to continuously treat the oil well with inhibitors. Here, the liquid inhibitor is transformed to the oil forming geological formation which works as a chemical reserve. The inhibitor is mixed with large quantity of water and fed into the well before pumping the over-flush fluid. Over the time the adsorbed inhibitor in the formation slowly escapes and inhibits the corrosive fluid. This method is not cost effective but continuous and deliberate addition of inhibitor is achieved by this technique.

1.14. MECHANISM OF INHIBITION

Although some of the principles are same in the inhibition of chemical compounds, there is no overall theory which will explain the mechanism of the inhibiting performance of chemical compounds. Inhibiting mechanisms are complex and often involve more than a simple barrier between the metal and medium. Different compounds inhibit the process of corrosion at different stages and act as inhibitors. Some commonly observed mechanisms of inhibition are presented in the following sections.

1.14.1. Inhibition by adsorption

The electrostatic interaction between the surface charge of the metal and dipole or ionic charge of the inhibitor molecule induce the adsorption of inhibitor on the metal surface. The charge on the inhibitor is decided by the presence of lone pairs

of electrons, π-electrons, aromatic systems and elements of the functional group. The stronger adsorption needs greater charge on the anchoring group and the substituent which intensify the charge density on the anchoring group.

The phenomenon of adsorption takes place by the following mechanism:

The surface of the metal is always adsorbed with the water molecules in aqueous phase. The adsorption of inhibitor on the surface of the metal replaces the previously adsorbed water molecules according to the following reaction.

$$(\text{Inhibitor})_{\text{solution}} + (\chi\, H_2O)_{\text{adsorbed}} \rightleftharpoons (\text{Inhibitor})_{\text{adsorbed}} + (\chi\, H_2O)_{\text{solution}} \qquad (1.27)$$

where, $(\text{Inhibitor})_{\text{solution}}$ and $(\text{Inhibitor})_{\text{adsorbed}}$ are the free inhibitor molecule in the electrolyte and the adsorbed inhibitor molecule on the metal surface, respectively. $(H_2O)_{\text{adsorbed}}$ is the water molecules adsorbed on the metal surface before the adsorption of inhibitor and χ is the size ratio which corresponds to the number of water molecules ejected during the adsorption of single inhibitor molecule. The electrostatic interaction between the metal and the inhibitor judge the ability of the inhibitor to replace the adsorbed water molecules and also it depends on the size and orientation of the inhibitor. The very first interaction between the inhibitor and surface of the metal is always nonspecific and requires low activation energy. This rapid and reversible process is called physical adsorption. Under favorable circumstance, the interaction of the adsorbed molecule with the surface of metal forms the chemical bond. This type of chemical interaction is called chemisorption, which is specific and irreversible process. In any case, ultimately the adsorption of inhibitors impedes anodic and/or cathodic reactions that depend upon the electrode on which the adsorption of inhibitor is favorable. The strength of the adsorption is determined from the adsorption isotherm, which demonstrates the equilibrium relation between the surface adsorbed inhibitor and its concentration in the bulk electrolyte (Revie 2011).

1.14.2. Inhibition by blocking the active reaction site

The adsorbed inhibitor layer on the metal surface possibly covers the active reaction sites. Some inhibitor molecules block the cathodic reaction rate more than the rate of anodic reaction, or vice versa. But the adsorption of inhibitor on the metal surface appears to be general over the surface instead specific at anodic or cathodic reaction sites. The anode or cathode active site blocking hinders the rate of corresponding electrochemical reactions. Such inhibitors will not participate in the electrode reactions nor do they change mechanism of corrosion. Therefore addition of such inhibitor to the corrosive solution will not greatly alter the corrosion potential, but it appreciably reduces the rate of corrosion. This action of inhibitor can be identified from the parallel shift in the Tafel polarization curves with negligible change in their slope values (Uhlig and Revie 2008).

1.14.3. Inhibition by forming surface film

Some surface adsorbed inhibitor precipitates as sparingly soluble salts and thus forms surface films. This surface film insulates the metal and hence prevents the attack of corrosive species. To be efficient as a physical barrier, the film should be non-porous, adequately thick and continuous over the surface with considerable stability and adherence (Revie 2011).

1.14.4. Inhibition by forming chelating complex

During inhibition some organic compounds having minimum two polar functional groups will form a closed ring structure with metal cation. Such compounds which can form a ring structure with metal cation are called chelating compounds. Initially chelating compounds react with the metal ions present in the oxide film or they may interact with metal cations produced by metallic dissolution. Latter, a high molecular weight low solubility complex will precipitate near the surface and barrier film will form on the metal surface. Like in bulk solution, surface chelates having five membered ring structures are more stable with more steric requirements than in bulk solution. The chelates having high surface activity and low

solubility in the corrosive solution are effective corrosion inhibitors, if not they may provoke the rate of corrosion (McCafferty 2010, Revie 2011).

1.15. INHIBITION IN NEAR-NEUTRAL SOLUTIONS

The metal corrosion and its inhibition are pH dependent. The metallic corrosion in neutral solution is different than in acidic solution. Because in acidic solution the metal surface is free from oxide layer as strong acid dissolves it. Secondly, the main cathodic reaction in acid solution is hydrogen evolution whereas in neutral solution saturated with air, oxygen reduction represents the one. Therefore in acidic solutions inhibitor adsorption occurs over an oxide-free surface, but in neutral solution the adsorption is on the surface film, which is formed by the sparingly soluble corrosion product. The surface films in neutral solution offer some degree of protection to the underlying metal. Therefore in order to protect the metal in neutral solution inhibitors are expected to adsorb over the pre-existent surface film (Schweitzer 2009, McCafferty 2010).

Inorganic anions such as phosphates, carbonates and silicates have been reported as efficient inhibitors in near neutral solution (Aramaki 2002, Dunn et al. 2004, Valcarce and Vázquez 2010, Yohai et al. 2011). Oxidizing ions like chromates and nitrates are also known to be corrosion inhibitors in near neutral media (Pokhmurskii et al. 2011, Lee et al. 2012, Ortíz et al. 2013). The salts of organic acids such as benzoate, cinnamate, salicylate also inhibit the metallic corrosion in near neutral solution (Forsyth et al. 2002, Rammelt et al. 2008, Shi et al. 2011). Some chelating agents have also been explored as corrosion inhibitors in neutral media such as derivatives of sarcosine, oximes and quinolone (Frignani et al. 1996, Ebenso et al. 2010, Senthilkumar et al. 2011), etc.

1.16. MAGNESIUM AND MAGNESIUM ALLOYS

The geochemical assessment confirms magnesium as the eighth most abundant element constituting 2.5% of the earth's crust. It was first discovered by Joseph Black in the year 1755 and first isolated by Sir Humphrey Davy in 1808. Pure

magnesium is highly active and hence it is available in the earth's crust as magnesium compounds. The most common magnesium ores are magnesite ($MgCO_3$), dolomite ($MgCO_3.CaCO_3$), brucite ($Mg(OH)_2$) and carnallite ($KCl.MgCl_2.6H_2O$), etc. Magnesium is also available in sea water as dissolved mineral. As a matter of fact magnesium is the third most dissolved mineral in the sea water. The metallic magnesium is produced from metallic extraction of its ores and also by the electrolysis of molten magnesium chloride derived from seawater (Gupta and Sharon 2011).

Magnesium is the lightest metal of all known structural metals for applications (Fekry and Fatayerji 2009). It has a density of 1.74 g cm^{-3}, which is nearly one-fourth that of steel. But Standard electrode potential of Mg is –2.363 V, which indicates its high susceptibility to corrosion (Fontana 2005). To enhance corrosion resistance and strength, magnesium is alloyed with several other elements such as aluminium, zinc, lithium, rhenium, thorium, silver and minor addition of cerium, manganese and zirconium. These alloys have excellent properties like low density, good mechanical properties, excellent castability, high strength, great damping capability, good electric shielding effect, acceptable recyclability, non-toxic to human body, biocompatibility, non-magnetic, have relatively high thermal and electrical conductivity, good vibration and shock adsorption ability, etc. These properties find number of applications in various streams (Froes et al. 1998, Agnew 2004, Gupta and Sharon 2011).

1.16.1. Application of Magnesium alloys

The magnesium alloys have great demand in structural applications, particularly in weight-critical applications. Some notable applications are explained as follows (Gupta and Sharon 2011).

1.16.1.1. Automotive applications

In 1920s magnesium parts are first used in the racing cars. Later in the year 1930s, it was utilized in commercial vehicles. Over the past decade, the enhanced

environmental and legislative pressure on the automobile industries to produce light-weight, fuel efficient and high performance vehicles have aroused in the surge in the use of magnesium. Leading automobile makers such as Audi, Volkswagen, DaimlerChrysler (Mercedes-Benz), Toyota, Ford, BMW, Jaguar, Fiat, Hyundai, and Kia Motors corporation have used magnesium-based materials in wheel assembly, gearbox housing, steering wheels, fuel tank cover, seat frame, steering column housing, driver's air bag housing and lock body, etc (Luo 2002, Blawert et al. 2004, Rosen et al. 2005, Cole 2007, Logan 2007).

1.16.1.2. Aerospace applications

In aerospace industry, high strength to weight ratio is the critical objective due to the increasing need for emission reduction and fuel efficiency. The extensive use of magnesium in spacecraft and missiles are due to the demand for lightweight materials to cut-down the lift-off weight. Magnesium alloys have the capability to withstand elevated temperatures, exposure to ozone, bombardment of high energy particles and small meteorites. Magnesium based materials are extensively used in both civil and military aircrafts as thrust reverser, gearbox, engines and helicopter transmission casings, etc (Wendt 2005).

1.16.1.3. Medical applications

Magnesium alloys were first explored as orthopedic biomaterials in the first half of the last century. Compared to other implant materials it has lighter density, greater fracture toughness, elastic modulus and compressive yield strength values. The comparison of magnesium with other implant materials and natural bone is given in the Table 1.3. Magnesium also assists in many human metabolic reactions and is nontoxic to the human body. Since magnesium has good biocompatibility and biodegradable property in body fluid, it eliminates the need for another operation to remove the implant materials (Gu and Zheng 2010). These features make magnesium based material a promising implant material in medical applications.

Table 1.3 Comparison of physical and mechanical properties of magnesium with natural bone and other implant materials.

Materials	**Density ($g\ cm^{-3}$)**	**Fracture toughness ($MPa\ m^{1/2}$)**	**Elastic modulus (GPa)**	**Compressive yield strength (MPa)**
Natural bone	1.8-2.1	3-6	3-20	130-180
Ti alloy	4.4-4.5	55-115	110-117	758-1117
Co-Cr alloy	8.3-9.2	-	230	450-1000
Stainless steel	7.9-8.1	50-200	189-205	170-310
Hydroxyapatite	3.1	0.7	73-117	600
Magnesium	1.74-2.0	15-40	41-45	65-100

1.16.1.4. Sports applications

The excellent specific strength and ability of magnesium alloys to form intricate shapes resulted in number of applications in sporting industry. Magnesium based materials are used in the preparation of handles of archery bows, tennis rackets and golf clubs. The lightweight and excellent damping property of the magnesium alloys made them a popular material choice in bicycle frames and the chassis of in-line skates. The shock and vibration absorbing property of the magnesium materials allows rider to exert less energy and more comfortable ride.

1.16.1.5. Electronic applications

Electronic equipment industry needs lightweight and durable materials. Magnesium based materials meet the necessary requirements such as light as plastic, great strength, heat transfer and ability to shield electromagnetic interference and radio frequency interference. All these properties are made use in housings of cell phones, computers, laptops, portable media players, heat sinks and the arms of the hard drive reader, housings of cameras and digital image projection systems, etc.

1.16.1.6. Other applications

Magnesium materials are used to make the frame of the eye wear, rifle scopes and binoculars. Most of the hand-held working tools such as magnesium chain saw housing, magnesium housing and cylinder of pneumatic nail gun, housings of gear and engine of hand-held tools, handle of hand shears, housing of hand drills are made from magnesium alloys.

1.16.2. Major alloying elements

The incorporation of alloying elements to the pure magnesium enhances its physical and chemical properties. The chemically active magnesium can easily react with the alloying element to form intermetallic compounds. The formed intermetallic compounds influence the microstructure of the magnesium alloy and thus its mechanical properties. The influences of addition of major alloying elements are discussed in the following sections (Gupta and Sharon 2011).

1.16.2.1. Aluminum

Magnesium alloy containing 2-10% Al with minor addition of zinc and manganese is most widely used Mg-Al alloy. Aluminum is generally regarded as a beneficial element in improving corrosion resistance. Addition of aluminum into a single α-phase introduces secondary phase β-$Mg_{17}Al_{12}$ into a magnesium alloy. Solid solution of aluminum in the matrix phase plays an important role in the corrosion resistance of this alloy (Song 2005). The aluminum is partly in solid solution and partly precipitated in the form of $Mg_{17}Al_{12}$ along the grain boundaries as a continuous phase as well as part of a lamellar structure. Aluminum alters the composition of hydroxide film which is formed on the surface of the magnesium and thus reduces the corrosion rate. Concentration of aluminum up to 4% in the magnesium alloy increases the corrosion resistance, whereas additions up to 9% gives only modest further improvements. Aluminum addition reduces the iron tolerance limit from 170 wt-ppm to 20 wt-ppm. The tolerance limit of iron decreases almost linearly with increasing aluminum content (Song and Atrens 1999).

1.16.2.2. Zinc

Zinc can increase the tolerance limits and decreases the effect of impurities. It increases the tolerance limit of Fe, Cu and Ni, but its amount is limited to 1-3%. The tolerance limit of Fe increases to 30 wt-ppm by the addition of 3% zinc and it greatly reduces the corrosion rate for iron concentration of up to 180 wt-ppm for the Mg-Al-Mn alloy. In the case of Mg-Al-Mn-Ni alloys addition of 3% zinc increases the tolerance limit of Ni from 10 to 20 wt-ppm.

1.16.2.3. Zirconium

Addition of zirconium increases the corrosion resistance property of the magnesium alloy. Zirconium forms a stable compound with aluminum and manganese, and it can be an excellent grain refiner when incorporated into alloys containing zinc, thorium, rare earths or a combination of these elements.

1.16.2.4. Silicon

Fluidity of molten alloy increases by the addition of the silicon. Corrosion resistance can be compromised by using along with the iron.

1.16.2.5. Copper

Copper has limited solubility in magnesium alloy. It forms Mg_2Cu intermetallic by reacting with magnesium. Copper increases the room temperature and high temperature strength of the magnesium alloy.

1.16.2.6. Iron

Addition of iron decreases the corrosion resistance property of the magnesium alloy. A total of 0.005% of iron content is the upper limit allowed for the best protection of an alloy.

1.16.2.7. Manganese

The saltwater corrosion resistance property of Mg-Al and Mg-Al-Zn alloy can be enhanced by the addition of manganese. But low solubility of manganese in magnesium alloy limits the amount of manganese addition.

1.16.2.8. Rare earth metals

The high temperature strength, creep resistance and corrosion resistance property of the magnesium alloy increases by the addition of the rare earth metals. The presence of rare earth metals decreases the freezing range of the alloys which will results in decreased casting porosity and weld cracking.

1.16.3. Classification of magnesium alloys

Magnesium alloys are classified into two major alloying systems:

1. Alloys containing aluminum (2-10%) with minor addition of zinc and manganese. These alloys find application in the temperature range of 95-125 °C.
2. Alloys containing various elements such as rare earths, zinc, thorium and silver but not aluminum. Zirconium provides grain refinement and improved mechanical properties. These alloys have improved elevated temperature properties compared to the alloys which contain aluminum as a major alloying element.

According to American Society for Testing and Materials (ASTM) system for designating magnesium alloys, principle elements in the alloy are indicated by first two alphabets followed by numbers. Alphabets for the major alloying element are listed in the following Table 1.4. The first letter indicates the greater concentration alloying element, followed by the next higher concentration. If alloying elements are in equal concentration, then it is listed alphabetically. Numbers indicate the nominal compositions of alloying elements, rounded off to the nearest whole number. For example, AZ91 magnesium alloy which contains 9% aluminum and 1% zinc as major alloying constituents. In addition, letters that are sometimes appended to the alloy

designation are assigned chronologically and usually indicate alloy improvements in purity (Uhlig and Revie 2008).

Table 1.4 Alphabets for the major alloying elements.

Alloying Element	Alphabet
Aluminum	A
Rare earths	E
Thorium	H
Zirconium	K
Manganese	M
Silver	Q
Zinc	Z

1.17. REVIEW OF LITERATURE

1.17.1. Literature review for corrosion of pure magnesium and magnesium alloys

The susceptibility of magnesium and its alloys towards corrosion in different corrosive media, has been well entrenched. Magnesium has been delineated as a moderately passive metal in natural circumstances, but tends to corrode when exposed to pitting assistant like chloride ions in non-oxidizing surroundings (Tunold et al. 1977). Tunold et al. also proposed that the breakdown of the passive film results in unusual feature of magnesium metal known as negative difference effect (NDE). Different models have been proposed in literature to explain the strange phenomenon of magnesium metal. Some important models of mechanism are (1) Univalent magnesium ion (Mg^{+}) model, according to this model Mg^{+} is assumed to exist as a reactive intermediate (Greenblatt 1956, Natta 2001, Song and Atrens 2003, Atrens and Dietzel 2007, Thomaz et al. 2010, Qiao et al. 2012, Shi et al. 2012, Frankel et al. 2013), (2) partially protective film model, predicts the presence of partly protective film of corrosion product (Song 2005), (3) particle undermining model, demonstrates

the NDE in the concept of undermining and falling away of cathodic secondary phase particles due to micro-galvanic corrosion (Makar and Kruger 1990), (4) magnesium hydride (MgH_2) model, explains the formation of unstable MgH_2 during magnesium corrosion process (Perrault 1970, Gulbrandsen 1992). Cao et al. suggested the new mechanism for hydride dissolution by studying the corrosion of ultra-pure magnesium in 3.5% NaCl saturated with $Mg(OH)_2$. They reported the difference between the corrosion rates measured by hydrogen evolution and weight loss studies and demonstrated the dissolution of formed MgH_2 to form corrosion product (Cao et al. 2013). Song et al. combined partially protective film model and univalent magnesium ion model to propose a new mechanism for NDE. According to this model the surface film free area increases with increasing the applied electrode potential and production of monovalent magnesium ion and subsequent formation of hydrogen takes place in these film free areas (Song et al. 1997a). Out of the entire four models partially protective surface film model is most accepted mechanism and is demonstrated in many studies. Pebere et al. investigated the electrochemical behavior of magnesium in the presence of aerated sodium sulfate solution by using electrochemical impedance spectroscopy method (Pebere et al. 1990). The low value of capacitance and increased protection with the increase in immersion time gave evidence for the existence of $Mg(OH)_2$ and/or MgO protective layer on the surface. Gulbrandsen et al. demonstrated the transform of $Mg(OH)_2$ into MgF_2 in the presence of alkaline fluoride solution (Gulbrandsen et al. 1993). An electrochemical investigation of pure magnesium in NaCl solution at different pH demonstrated by Song et al. showed the breakdown of partially protective surface film at higher anodic overvoltage and acceleration of magnesium dissolution (Song et al. 1997b). The morphology and structure of the oxide film on pure magnesium in humid air and water have been explored by Nordlien et al. using transmission electron microscopy (TEM) (Nordlien et al. 1997). The formed surface film is composed of three layers; inner cellular layer of MgO-$Mg(OH)_2$, an intermediate thin, dense and amorphous film of MgO and outer thick layer of $Mg(OH)_2$, which is porous and having platelet structure. Baril and Pebere studied the corrosion behavior of pure magnesium in aerated and deaerated

sodium sulfate solution by means of polarization and impedance techniques (Baril and Pebere 2001). This study stated that the presence of CO_2 inducing the faster corrosion rate in aerated solution because of the breakdown of $Mg(OH)_2$ film by reaction product of CO_2 in water. Cain et al. explained the role of surface film and its dissolution in different solution by using NDE and examined the effect of chloride ions on surface film (Cain et al. 2017).

Plenty of magnesium alloys have been evolved to meet the current demand in exclusive fields of applications. The followings are the prominent work which have been laid to discern the consequence of the alloying elements and the microstructure of the alloys on the corrosion features of magnesium.

The effect of addition of Y and Nd on the corrosion behavior of magnesium alloy WE43 has been documented by Zucchi et al. The result of the study stated that presence of Y and Nd augmented the passivation of magnesium even in strong corrosive solution (Zucchi et al. 2006). The beneficial effect of rare earth element Ce inclusion to AZ91D magnesium alloy has been explored by Fan et al. Addition of Ce improved the corrosion resistance property of the AZ91D alloy along with its microstructure and mechanical properties (Fan et al. 2006). Several studies reported the beneficial outcome on the addition of rare earth elements into magnesium alloys (Wu et al. 2005, Rosalbino et al. 2006, Takenaka et al. 2007, Song et al. 2007, Niu et al. 2008, Birbilis et al. 2009, Liu et al. 2009;2017, Südholz et al. 2009, Nakatsugawa et al. 2011, Sudholz et al. 2011, Zhang et al. 2011a, Arrabal et al. 2012, Rokhlin 2014, Mingo et al. 2017, Leleu et al. 2018, Sadeghi et al. 2018, Wang et al. 2018, Chen et al. 2019).

The grain refinery element zirconium is beneficial when it is present in optimal concentration in magnesium alloy (Qian et al. 2003, Peng et al. 2005, Prasad et al. 2012). Song and StJohn found the result of zirconium grain refinement on the corrosion strategy of rare earth containing magnesium alloy MEZ. The addition of zirconium stabilized the solid solution in MEZ alloy and thus reduced the rate of

anodic dissolution process, increased the grain boundary phase, reduced the hydrogen evolution, modified the grain size of the grain boundary phase to increase the barrier effect (Song and StJohn 2002). The optimum concentration of 0.42% zirconium for Mg-Gd-Y alloy where it was shown a best corrosion resistance and mechanical property was discovered by Sun et al (Sun et al. 2009). In this study size and distribution of zirconium-rich particles have been considered as the major influencing factor in deciding the corrosion resistance and mechanical property. Gandel et al. examined sixteen different binary Mg-Zr alloys and four commercial zirconium containing magnesium alloys to study the effect of concentration and distribution of zirconium on magnesium alloy corrosion (Gandel et al. 2014). The deleterious effect of zirconium both in solid solution and metallic particle were studied on the corrosion rate of magnesium and they suggested to cut down this effect by the addition of multiple alloying elements to Mg-alloy. Simanjuntak et al. prepared 71 custom magnesium alloys to test the effect of addition of zirconium along with iron and manganese (Simanjuntak et al. 2014). They empirically explored the tolerance limit ratio of aluminum free magnesium alloy by using artificial neutral network model. Various studies investigated the effect of zirconium addition on the corrosion behavior, microstructure and mechanical properties of magnesium alloy (Xia et al. 2015, Jafari and Amiryavari 2016, Li et al. 2017b, AbdelGawad et al. 2018, Jafari and Hassanizadeh 2018, Jeong et al. 2018, Shrestha et al. 2018, Shubo LI and Shubo LI 2018).

It has been reported in the literature that the most common additive in magnesium alloy which improves the mechanical properties such as tensile strength, yield strength and texture is zinc (Yin et al. 2008, Yuan and Zheng 2014, Wang et al. 2017). Sasaki et al. investigated the improved age hardening effect of Mg-Sn alloy upon the addition of Zn (Sasaki et al. 2006). Du et al. inspected the impact of Zn on the crystallographic anisotropy of magnesium alloy during α-Mg dendritic growth (Du et al. 2019). The consequence of Zn and Ca addition on microstructure and mechanical properties of Mg-1.0Sn alloy sheet was investigated by Chai et al (Chai et

al. 2019). Badawy et al. inspected the electrochemical behavior of magnesium and its two alloys Mg-Al-Zn and Mg-Al-Zn-Mn alloy in acidic, neutral and basic media to investigate the corrosion diminishing property of the additive elements, chiefly zinc (Badawy et al. 2010). The beneficial properties of the magnesium alloy upon the addition of zinc are mainly useful as synthetic implants in biomedical applications. Several studied reports show the increased corrosion resistance property of the magnesium alloys on addition of zinc in simulated body fluid (Zhang et al. 2010, Cai et al. 2012, Zander and Zumdick 2015). Boczkal et al. studied the effect of Zn addition on mechanical property and structure characteristics of biodegradable Mg-Y and Mg-Li alloy (Boczkal et al. 2018). At the same time the deleterious effect of zinc addition to magnesium has also been documented by many researchers (Yamasaki et al. 2007, Song et al. 2012). Ha et al. discovered that zinc addition simultaneously increased both the passive film protectiveness and the rate of hydrogen evolution in Mg-Zn binary alloy. But the rate of hydrogen evolution was predominant and thus increased the overall rate of corrosion (Ha et al. 2013).

In general the microstructure of any alloy has a profound influence on its overall properties. The microstructure influence on the corrosion rate of AZ91D alloy was given by Song et al (Song et al. 1998a). This investigation explained that the size and the distribution of intermetallic β-phase were the influencing factors in deciding the corrosion rate of AZ91D alloy. The effect of β-phase morphology on the corrosion rate of an alloy was documented in several studies (Song et al. 1998b, Mathieu et al. 2003, Zhao et al. 2008a, Lyndon et al. 2013). According to the studied data, a small particle size and uniform β-phase resisted the corroding tendency, whereas an agglomerated and large particle size β-phase acted as cathode and hence induced micro-galvanic corrosion. The incorporation of certain additive elements acts as cathode to the large anode magnesium matrix and hence most of the magnesium alloys undergo micro-galvanic corrosion. The consequence of grain size and twins on corrosion of AZ31B magnesium alloys was evaluated by Aung and Zhou (Aung and Zhou 2010). There are many studies which established the influential role of

microstructure on the micro-galvanic corrosion of magnesium alloys (Ambat et al. 2000, Pardo et al. 2008b, Zhang et al. 2008;2011b, Peng et al. 2009, Song and Xu 2010, Shi et al. 2013, Liu et al. 2014, Zeng et al. 2014, Zhao et al. 2014). Verissimo et al. investigated the effect of Zn segregation and finer dendritic grains structure on the corrosion behavior of Mg-Zn alloy in NaCl solution (Verissimo et al. 2017). Sadeghi et al. examined the effect of 0.4 and 0.8 wt% addition of Sr on the microstructure of AZ31 magnesium alloy and its consequence on the corrosion behavior (Sadeghi et al. 2018). Nowadays different techniques are used to alter the microstructure, composition of the magnesium alloys and they studied its impact on the corrosion behavior (Ahmadkhaniha et al. 2018, Dai et al. 2018, Mahallawy et al. 2018, Wu et al. 2018, Zhang et al. 2018a;b, Dong et al. 2019, Jamalian and Field 2019, Wang et al. 2019).

In recent years the rare earth containing (ZE series) magnesium alloys are considered for their corrosion performance as it finds a number of outdoor applications. Zhao et al. documented the corrosion behavior of ZE41 magnesium alloy in varying pH and chloride ion concentrations to study the influential role of pH and chloride ion concentration on ZE41 corrosion (Zhao et al. 2008b). Bobby et al. examined the corrosion behavior of series of rare earth containing magnesium alloys and compared with AZ80 (Bobby et al. 2008). Neil et al. investigated the influence of microstructure on initiation and propagation of ZE41 alloy in NaCl solution (Neil et al. 2009). The corrosion tendency of four commercial alloys namely as-cast ZE41, sand-cast WE43-T6, wrought WE43-T6 and WE54-T6 were examined by Coy et al. They investigated by using scanning kelvin probe force microscopy (SKPFM) and reported that out of the four alloys, ZE41 showed the highest susceptibility to corrosion in NaCl solution (Coy et al. 2010). Neil et al. studied the effect of heat treatment on the corrosion behavior of ZE41 magnesium alloy (Neil et al. 2011). The corrosion behavior of ZE41 alloy in combined medium of chloride and sulfate, effect of pH and sulfate ion concentration on the corrosion rate were electrochemically investigation by Dinodi and Shetty (Dinodi and Shetty 2014a, 2013). Corrosion rate

of rare earth element containing three Mg alloys were investigated by Leleu et al. in Na_2SO_4 solution by impedance measurements and inductive coupled plasma-optical emission spectroscopy (Leleu et al. 2019).

Aluminum has been regarded as an advantageous element in the corrosion resistance improvement of magnesium alloy (Makar and Kruger 1990, Baliga and Tsakiropoulos 1993). Song et al. compared the corrosion behavior of AZ21, AZ501 and AZ91 in sodium chloride solution and concluded that the composition and compositional distribution of phase was crucial in overall corrosion resistance of the dual phase alloy (Song et al. 1998b). Baril et al. investigated the corrosion behavior of as-cast three magnesium aluminum alloys in 0.1 M sodium sulfate. They proposed that enrichment of aluminum in the corrosion product was responsible for the change of phenomenology appeared in the impedance diagrams (Baril et al. 2001). The addition of aluminum introduced the corrosion resistant secondary phase (β-$Mg_{17}Al_{12}$) in magnesium matrix. It was found that, increasing the aluminum content in the magnesium alloy decreases the corrosion rate of α-magnesium matrix (Song et al. 2004). Song reviewed the outstanding influence of alloying elements in the magnesium alloy containing aluminum as a primary alloying element and those magnesium alloys, free of aluminum (Song 2005). Cheng et al. compared the corrosion performance of three magnesium aluminum alloys (AZ31, AZ91 and AM60) with ZK60 magnesium alloy in 1 M sodium chloride solution (Cheng et al. 2009). Matsubara et al. reported the effect of impurity, iron, on the corrosion of aluminum containing magnesium alloy (Matsubara et al. 2013). But the addition of calcium has been reported as a beneficial element for magnesium alloy (Liu et al. 2014b; Mandal et al. 2014). Yang et al. varied the concentration of calcium in Mg-Al-Mn alloy to know the effect of concentration of calcium on the corrosion rate (Yang et al. 2016). Esmaily et al. explained the dependency of aluminum content and temperature on the corrosion behavior of magnesium aluminum alloy (Esmaily et al. 2016). The role of Sn on the microstructure and corrosion behavior of wrought Mg-5Al alloy was investigated by Metalnikov et al (Metalnikov et al. 2019). Similarly

the effect of Sm addition on the corrosion behavior of AZ91 alloy has been documented by Hu et al (Hu et al. 2019).

The corrosion behavior of magnesium alloys containing aluminum, manganese (AM series) and aluminum, zinc (AZ series) have been studied well in the literature (Mathieu et al. 2002, Cheng et al. 2009, Pardo et al. 2010, Wang et al. 2010b, Liao et al. 2012, Shi et al. 2012, Feliu Jr et al. 2014, Song et al. 2014, Zhao et al. 2014). Badawy et al. investigated the electrochemical behavior of Mg, Mg-Al-Zn and Mg-Al-Zn-Mn alloy in aqueous acidic, neutral and basic solution and concluded that the presence of alloying elements such as Al, Zn and Mn decreased the rate of corrosion of the alloy (Badawy et al. 2010).

Apart from aqueous solution, the corrosion behaviors of magnesium alloys were studied in organic medium such as ethylene glycol. The importance of corrosion behavior study of magnesium in ethylene glycol was explained by Song and StJohn (Song and StJohn 2004). Slavcheva et al. studied the influence of chloride anion on the corrosion of AZ91 magnesium alloy in aqueous ethylene glycol solution (Slavcheva et al. 2005). Song and StJohn explored the corrosion performance of AZ91D and AM-SC1 magnesium alloys in several commercial coolants. This investigation concluded that the tested commercial coolants caused general and galvanic corrosion in both the magnesium alloy, but the rate of corrosion was less on AZ91D than on AM-SC1 magnesium alloy (Song and StJohn 2005). Song et al. examined the corrosion performance of AM-SC1 magnesium alloy in commercially available engine coolant (Song et al. 2005). The detailed investigation on the effect of ethylene glycol concentration on the corrosion of AZ91D alloy was documented by Fekry and Fatayerji (Fekry and Fatayerji 2009). This study also documented the effect of concentration of chloride and fluoride ions on the corrosion rate of AZ91D alloy. Wang et al. electrochemically measured the corrosion rate of AZ91D magnesium alloy in different concentrations of ethylene glycol/water solution and reported that the increase in the concentration of ethylene glycol decreased the corrosion rate of AZ91D alloy and formed protective film after sufficient immersion time; and the

protective film was observed to be having self-healing effect on the corrosion pit (Wang et al. 2012).

1.17.2. Literature review for corrosion inhibitor of magnesium and magnesium alloys

Many compounds have been scrutinized as corrosion inhibitors for pure magnesium and magnesium alloys in aqueous and aqueous organic media. This wide class of inhibitors includes organic, inorganic and combination of organic and inorganic compounds. Considerable amount of investigations on corrosion inhibitors were performed in the aqueous medium. But the studies on corrosion inhibitors in the aqueous organic medium are very few. Some of the efficient magnesium inhibitors reported in the literature in aqueous and aqueous organic medium are listed in Table 1.5 and Table 1.6, respectively.

Table 1.5 Prominent corrosion inhibitors for magnesium and magnesium alloys in aqueous medium.

Inhibitor employed	Material	Medium	Observation
Linear sodium carboxylate (7 to 12 carbon atom)	Mg-3% Zn-15% Al alloys	ASTMD 1384 solution	Inhibition efficiency increased with the increase in the concentration, length of the aliphatic chain and immersion time in the inhibitive media (Daloz et al. 1998).
Ionic liquid (Tri(hexyl)tetradecyl phosphonium bis(trifluoromethane sulfonyl) amide)	AZ31 Mg Alloy	Humid environment and 0.1 M NaCl solution	The extreme reactivity of the metal in ionic liquid formed the surface film, giving the protection against humid environment and chloride ions (Forsyth et al. 2006).

Bis[triethoxysilylpropyl] tetrasulfide silane	AZ31 Mg alloy	0.005 M NaCl	The performance of the silane solution was improved by adding the additives like cerium ions or lanthanum ions (Montemor and Ferreira 2007).
Sodium carboxylate	Pure Mg	ASTM D1384-87 standard water	The inhibition efficiency of sodium deconate was more than sodium heptanoate (Mesbah et al. 2007).
Ionic liquid (trihexyl (tetradecyl) phosphonium diphenylphosphate)	ZE41	0.1 M NaCl	The ionic liquid treated surface showed more corrosion resistance and surface film was monitored by impedance spectra (Howlett et al. 2008).
Sodium monocarboxylate (caprate, laurate and myristate)	AZ31 Mg alloy	ASTMD 1387 saline solution	The inhibiting action of sodium carboxylate depended on the aliphatic chain length, which controlled the anion solubility and kinetics of magnesium carboxylate formation (Zucchi et al. 2009).
Sodium salt of fluoride, carbonate, phosphate, oxalate, silicate and phenyl phosphonate	Mg foil	5% NaCl solution at different pH	Phosphate addition noticeably decreased the localised corrosion and inhibition efficiency increased with the decrease in the pH of the electrolyte (Williams et al. 2010).

1,2,4-Triazole, NaF and $Ce(NO_3)_3$	Coated AZ31 Mg alloy	0.05M NaCl solution	1,2,4,-triazole showed the highest inhibition efficiency at a concentration of 0.01 M (Karavai et al. 2010).
5-(3-Aminophenyl)-tetrazole	Mg/Mn alloy	3.5% NaCl solution	The rate of corrosion decreased with the increase in the concentration of the inhibitor and exposure time in the inhibitive solution (Sherif and Almajid 2011).
Sodium silicate	AZ91D Mg alloy	ASTM D1384-87 corrosive water	Sodium silicate effectively enhanced the corrosion resistance at an optimum concentration of 10 mmol L^{-1} at a pH range of 10.5 to 12.5 (Gao et al. 2011).
Amino acid	Mg-Al-Zn alloy	Aqueous buffer with pH 7	Phenyl alanine showed highest inhibition efficiency at a concentration of 2×10^{-3} mol dm^{-3} and inhibition efficiency depended on the structure of the amino acid (Helal and Badawy 2011).
5-(3-Aminophenyl)-tetrazole	Mg/Mn alloy	Arabian Gulf water	The inhibitor molecule decreased the rate of corrosion by repairing the weak area of the alloy surface and inhibition efficiency increased with the increase in the inhibitor content and immersion time (Sherif 2011).
Sodium benzoate and sodium dodecyl benzene sulphonate	AZ31 Mg alloy	3.5% NaCl solution	SDBS exhibited higher inhibition efficiency than SB, at lower concentration (Li et al. 2011).

Sodium salt of N-lauroylsarcosine, N-lauroyl-N-methyltaurine, dodecylbenzensulph-onic acid and sodium lauryl sulfate	AZ31 Mg alloy	0.1 M NaCl and 0.05 M Na_2SO_4	The influences of surfactant type, concentration and immersion time were evaluated, which suggested that over the time the thickness of the inhibiting layer increased and became less defective (Frignani et al. 2012).
Tetraphenylporphyri-n	AZ91D Mg alloy	0.05 wt% NaCl	Tetraphenylporphyrin-Mg complex film was formed on the alloy surface by chelating with Mg via N-atom of the inhibitor which reduced the porosity of $Mg(OH)_2$ surface film and thus reduced the Mg alloy dissolution (Hu et al. 2012).
Cerium nitrate	AM60	0.1 M NaCl	The rate of corrosion decreased with the increase in the concentration of Ce(III) upto 1 mM (Heakal et al. 2012).
Schiff base compound	Mg with 0.88 wt% Al	0.01 M HCl	Schiff base compound acted as a mixed type inhibitor and adsorbed by physical adsorption process (Seifzadeh et al. 2013).

2-Hydroxy-4-methoxy-acetophenone (paeonol)	AZ91D Mg alloy	0.05 wt% NaCl	The highest inhibition efficiency was achieved with 50 ppm paeonol concentration which inhibited the anodic reaction by chelating with Mg (Hu et al. 2013).
Schiff base	AZ31 Mg alloy	0.05 mol/L HCl solution	The studied Schiff base compound acted as mixed type inhibitor. The inhibition efficiency increased with the increase in the concentration of the additive (Thirugnanaselvi et al. 2014).
Alkyl carboxylate (stearate, palmitate and myristate)	ZE41 Mg alloy	NaCl and Na_2SO_4 combined solution	The alkyl carboxylates acted as mixed type inhibitors with major anodic action. The protection was due to the formation of dense modified surface film as a result of precipitation of surface adsorbed alkyl carboxylate with magnesium (Dinodi and Shetty 2014b).
N, N′-Bis (2-pyridylmethylidene)-1,2-diiminoethane	AZ91D Mg alloy	0.01 mol/L HCl	The compound acted as a mixed type inhibitor and obeyed Langmuir adsorption (Seifzadeh et al. 2014).
Rare earth cations, fluoride, chromate, and phosphate anions	AZ31 Mg alloy	5% w/v sodium chloride solution	Chromate and phosphate gave the most efficient inhibition, and all the inhibitors acted as cathodic depolarizers (Williams et al. 2014).

Polyaspartic acid	WE43 Mg alloy	3.5 wt.% NaCl solution	The maximum inhibition efficiency of 94.2% was achieved with a concentration of 400 ppm polyaspartic acid (Yang et al. 2015).
Benzotriazole	AMlite Mg alloy	0.1 M NaCl solution	The effects of pH and benzotriazole concentration were investigated and it was found that 15 g L^{-1} benzotriazole gave good inhibition efficiency (Wang et al. 2015).
Sodium alginate	AZ31 Mg alloy	3.5 wt% sodium chloride solution	A maximum inhibition efficiency of 90% was achieved with 500 ppm of sodium alginate. The adsorbed sodium alginate mixed with original $Mg(OH)_2$ surface film to form compact and continuous film (Dang et al. 2015).
Ammonium phosphate dibasic, 8-hydroxyquinoline, calcium fluoride, sodium fluoride, sodium dodecylbenzenesulfonate and zinc nitrate	ZK30 Mg alloy	5 mM NaCl solution	8-hydroxyquinoline gave good inhibition efficiency in 5 mM NaCl solution and acted as cathodic inhibitor for ZK30 magnesium alloy (Kartsonakis et al. 2015).
2-Hydroxy-acetophenone	AZ91D Mg alloy	ASTM D1384-87 corrosive water	The inhibition efficiency first increased and then decreased with the increase in the concentration of the inhibitor, maximum inhibition

			efficiency was achieved at a concentration of 50 ppm (Hu et al. 2015).
Potassium cyanide, sodium salicylate, 5-methylsalicylic acid, sodium thiocyanate, di-potassiumoxalat monohydrate	99.95% pure Mg	0.5% sodium chloride solution	The inhibition efficiency of the iron complexing agents directly related to their stability constants (Lamaka et al. 2016).
N′-Bis (2-pyridylmethylidene)-1,2-diiminoethane	AZ31 Mg alloy	0.01 M HCl	The compound acts as a mixed type inhibitor and obeyed Langmuir adsorption isotherm (Guo et al. 2016).
Schiff base compound	AZ91D Mg alloy	0.01M H_2SO_4	The compound served as a mixed type inhibitor (Seifzadeh et al. 2016a).
N,N Bis(salicylidene)-2-hydroxy-1, 3-propanediamine Schiff base	Commercial Mg bar	0.01 M HCl	The compound acted as a mixed type inhibitor. The inhibition efficiency increased with the increase in the concentration of the inhibitor and adsorption followed Fruendlich adsorption isotherm (Seifzadeh et al. 2016b).
Triethanolamine	AZ91D Mg alloy	3.5 wt% NaCl solution	Triethanolamine acted as a mixed type inhibitor and obeyed Langmuir adsorption isotherm (Shang et al. 2016).

1-Butyl-3-methylimidazoliumdibutylphosphate ionic liquid	AZ31B Mg alloy	ultrapure water	The ionic liquid decreased the rate of corrosion by forming the film (Zheng et al. 2017).
Sodium fluoride	AZ31B Mg alloy	composite solution of $MgSO_4$-$Mg(NO_3)_2$	The corrosion inhibition efficiency of 80% was achieved with a concentration of 30 mmol L^{-1} of sodium fluoride (Xu et al. 2017).
Sodium citrate, sodium dodecylbenzenesulphonate, diammonium phosphate and sodium vanadate	AM60 Mg Alloy	0.1 M sodium chloride solution	The organic inhibitors were more effective than inorganic inhibitors and a highest inhibition efficiency of 93% was achieved with SDBS (Liu et al. 2018).
Sodium salt of 2,5-pyridinedicarboxylic acid, 3-methylsalicylic acid and fumaric acid	Pure Mg having high level Fe impurity	pH neutral NaCl electrolyte	2,5-pyridinedicarboxylate and fumarate served as mixed type inhibitors, whereas 3-methylsalicylate acted as cathodic inhibitor (Yang et al. 2018).
Sodium dodecyl sulfate	AZ91 Mg alloy	3.5 wt% NaCl solution	In the presence of sodium dodecyl sulfate microgalvanic corrosion was suppressed due to the adsorption of the inhibitor molecules on cathodic intermetallics (Lu et al. 2019).

Table 1.6 Corrosion inhibitors for magnesium and magnesium alloy in aqueous organic medium.

Inhibitor employed	Material	Medium	Observation
Derivatives of lactobionic acid and quinolone	AZ91 magnesium alloy	50 wt% aqueous solution of ethylene glycol	The derivatives of lactobionic acid showed higher corrosion inhibition as mixed type inhibitor (Slavcheva and Schmitt 2002).
Lactobiono-tallowamide	AZ91 magnesium alloy	50 wt% aqueous solution of ethylene glycol	Lactobiono-tallowamide showed 77% inhibition efficiency at a concentration of 0.2 g L^{-1} and behaved as mixed type inhibitor (Slavcheva et al. 2005).
Paracetamol	AZ91D magnesium alloy	30% ethylene glycol and 70% water	The rate of corrosion decreased with the increase in the concentration of the ethylene glycol. 0.05 mM paracetamol provided effective inhibition (Fekry and Fatayerji 2009).

Aliphatic and aromatic carboxylates and inorganic salt	GW103 magnesium alloy	50 wt% aqueous solution of ethylene glycol	The mixture showed good inhibition at ambient temperature and at a concentration of 1000 ppm. A synergistic mechanism was suggested for the inhibition of sodium phosphate with SDBS (Huang et al. 2011).
Salicyclic Schiff base compound	AZ91 magnesium alloy	30% ethylene glycol and 70% water	High inhibition efficiency was obtained at elevated temperature (Seifzadeh and Basharnavaz 2013).
Pyrazine and piperazine	GW103 magnesium alloy	50 wt% aqueous solution of ethylene glycol	The inhibition efficiency of pyrazine was more than that of piperazine (Huang et al. 2013b).
Na_3PO_4 and SDBS, Na_3PO_4 and benzoate	GW103 and AZ91D Mg alloys	50 vol% aqueous solution of ethylene glycol	The mixture of Na_3PO_4 and benzoate inhibited the corrosion of Mg alloy, where as the mixture of Na_3PO_4 and SDBS accelerated the galvanic corrosion (Huang et al. 2013a).

1.17.2.1 Synergistic inhibitors for magnesium alloys

Nowadays the combinations of two or more inhibitors are considered for the corrosion inhibition of magnesium alloy. Gao et al. examined the synergistic inhibition effect of 8-hydroxyquinoline (8HQ) with anionic surfactant sodium dodecylbenzene sulphonate on the corrosion of AZ91D magnesium alloy in ASTM D1384-87 corrosive solution by calculating the synergism parameter (Gao et al. 2010). Hu et al. observed the synergistic inhibition behavior of organic sodium aminopropyltriethoxysilicate with inorganic zinc nitrate in ASTM D1384-87 corrosive water for the corrosion of Mg-10Gd-3Y magnesium alloy (Hu et al. 2011). Huang et al. proposed synergistic mechanism to explain the inhibition behavior of combination of sodium phosphate and sodium dodecylbenzene sulphonate on the corrosion performance of GW103 magnesium alloy in ethylene glycol solution (Huang et al. 2011). Zhang et al. considered the mixture of sodium silicate and sodium alginate as synergistic corrosion inhibitor for the corrosion of AZ91D magnesium alloy in 3.5 wt% NaCl corrosive solution (Zhang et al. 2015). The combined inhibition effect of sodium alginate and sodium phosphate in 3.5 wt% NaCl solution for the corrosion of AZ31 magnesium alloy was investigated by Hou et al (Hou et al. 2016). The synergistic inhibition effect of three inhibitors namely sodium silicate, sodium alginate and sodium tungstate on the corrosion behavior of AZ91D magnesium alloy in 3.5% NaCl solution was examined by Li et al. through polarization study, electrochemical impedance spectroscopy and weight loss measurement methods (Li et al. 2017a).

1.17.2.2 Morpholine and its derivaties as corrosion inhibitors

Morpholine and large variety of its derivatives were used as volatile corrosion inhibitors (VCI) for the protection of metallic structures (Vuorinen et al. 1994). The heterocyclic compound morpholine is chemically amino ether. In the literature morpholine and its derivaties have been reported as being used for the protection of various ferrous and non ferrous alloys. Desai et al. studied morpholine

as a mixed type corrosion inhibitor for aluminum alloys in hydrochloric acid medium (Desai et al. 1969). Ahmed et al. investigated the inhibition performance of morpholine and thiosemicarbazide derivatives on the corrosion of aluminium in acid solution (Ahmed et al. 1988). Vuorinen et al. evaluated various derivaties of cyclohexylamine and morpholine as efficient volatile corrosion inhibitors for mild steel (Vuorinen et al. 1994). Subramanian et al. studied the corrosion inhibition performance of morpholine and its derivaties such as morpholine carbonate, morpholine borate, morpholine phosphate on mild steel (Subramanian et al. 2000). The corrosion of pure aluminium in near neutral chloride solution was controlled by using morpholine methylene phosphonic acid (Stefenel et al. 2001). Hafiz et al. synthesized ethanolaminemorpholine oleate and studied the corrosion inhibition property of the same in acid solution for mild steel (Hafiz et al. 2003). Zhang et al. synthesized and tested morpholinium oligomer as VPI in ASTM standard D1384 water for the temporary protection of mild steel (Zhang et al. 2005). Nasrazadani et al. investigated the effect of morpholine, 1,8-diazabicyclo[5.4.0]undec-7-ene, and dimethylamine on the corrosion inhibition of low carbon steel in autoclave exposed to steam (Nasrazadani et al. 2007). 2-Acetylpyridine-N(4)-morpholine thiosemicarbazone was synthesized and studied by Kumar et al. for the corrosion inhibition of mild steel in acid medium (Kumar et al. 2011). Jayanthi et al. examined the corrosion inhibition property of morpholine on the corrosion of mild steel in 2 N sulphuric acid and phosphoric acid (Jayanthi et al. 2012). Cheng et al. reported the corrosion inhibitors containing 4-(N,N-dibutylaminomethyl) morpholine salt, which exhibited 98.46% of inhibition efficiency for A3 carbon steel of blast furnace gas pipeline (Cheng et al. 2014). A cationic surfactant of morpholine derivative was synthesized and examined by Hegazy and Aiad as novel corrosion inhibitor for the protection of carbon steel in the production of phosphoric acid (Hegazy and Aiad 2015). Belarbi et al. reported the mitigation of top of the line corrosion of carbon steel by using diethylamine and morpholine (Belarbi et al. 2016). The electrochemical techniques like potentiodynamic polarization and impedance spectroscopy, weight loss measurements and scanning electron microscopy were used by Nasser and Sathiq

to study the inhibition property of N-[morpholin-4-yl(phenyl)methyl]acetamide in hydrochloric acid on mild steel (Nasser and Sathiq 2016). Zulfareen et al. synthesized, characterized and tested the protection efficiency of N-(4-(morpholinomethyl carbamoyl phenyl) furan-2-carboxamide in hydrochloric acid for brass (Zulfareen et al. 2016). El-Mahdy et al. synthesised 2,4-dihydrazino-6-morpholino-1,3,5-triaizne and 2,4-dihydrazino-6-piperidino-1,3,5-triaizne and tested as promising corrosion inhibitor in hydrochloric acid for the protection of steel (El-Mahdy et al. 2016). In recent days morpholine based carboxamide derivatives were considered as corrosion inhibitors for the corrosion of mild steel in hydrochloric acid (Nnaji et al. 2017).

1.18. SCOPE AND OBJECTIVES OF THE WORK

1.18.1. Scope of the present work

In the current era magnesium aluminum alloys entice metallurgist's attention because of its exquisite properties. The exceptional properties of the magnesium alloy unearth number of applications in automotive and aerospace industries where weight reduction is momentous (Song 2011). In automobile applications various magnesium alloys are admissible as engine block materials. These engine blocks are circulated with 30-70% (v/v) aqueous ethylene glycol solution as coolant. The engine parts come in contact with the coolant are susceptible for corrosion and the rate of corrosion intensifies in the presence of contaminants like NaCl, Na_2SO_4 or $NaHCO_3$ (Fekry and Fatayerji 2009). The detailed literature review explores the extensive study of magnesium alloys in various aqueous solutions (Badawy et al. 2010; Li et al. 2015; Pardo et al. 2008a). However, to date, there has been a limited work on the corrosion behavior of magnesium alloys in aqueous organic medium (Fekry and Fatayerji 2009; Huang et al. 2011, 2012, 2013b; a). So in the present study corrosion behavior of one such Mg-Al-Zn alloy in 30% (v/v) aqueous ethylene glycol medium containing chloride and sulfate ions as contaminants are considered.

Generally an automotive engine is exposed to a coolant at ambient temperature for a considerable duration in its service time. It was proved in literature,

that, for magnesium alloys, the corrosiveness of the coolants are more at low temperature than at higher temperatures (Song and StJohn 2004). So, the corrosion performance of an engine material in a coolant at room temperature has a vital contribution to the service life of the engine and the result of study at ambient temperature of the coolant can provide a base for the study of the corrosion of magnesium in hot coolants (Song and StJohn 2004). Therefore in the present study experiments were performed in the temperature range of 30 °C to 50 °C. During the use of the coolant, the oxidation product of ethylene glycol may produce glycolic acid and thereby vary the pH of the solution (Zaharieva et al. 2009). Therefore corrosion studies were performed at acidic, neutral and basic conditions to understand the role of pH on the corrosion rate of Mg-Al-Zn alloy.

Considerable amount of research for the protection of magnesium alloys are by various coatings, electroplating and sol-gel coating technologies. Unfortunately, all these techniques cohort with some major or minor handicaps in terms of cost and environmental aspects. But the use of inhibitor is an effective and economic way of environmental alteration methods and the use of inhibitor for the protection of magnesium alloy is sporadic. Hence it is essential to consider the protection of magnesium alloy by using inhibitors in aqueous ethylene glycol medium in the presence of contaminants.

1.18.2. Objectives of the current work

The main objectives of the current work are as listed in the followings:

1. To study the corrosion behavior of Mg-Al-Zn alloy in 30% (v/v) aqueous ethylene glycol in the presence of different concentration of chloride and sulfate ions at different temperatures.
2. To evaluate the effect of pH on the corrosion behavior on Mg-Al-Zn alloy in 30% (v/v) aqueous ethylene glycol medium containing chloride and sulfate ions.

3. To investigate the corrosion inhibition efficiency of inhibitors on Mg-Al-Zn alloy in 30% (v/v) aqueous ethylene glycol medium containing chloride and sulfate ions.
4. To carry out the experiments at different temperatures in order to determine the activation parameters for the corrosion and its inhibition process.
5. To deduce the thermodynamic parameters for the process of inhibitor adsorption and to propose a suitable mechanism for the corrosion inhibition in corrosive solution.

1.19. FRAMEWORK OF THE THESIS

The current thesis has been divided into four chapters. The detailed descriptions of the content of each chapter of the thesis are summarized as follows.

The **chapter 1** introduces the history, some fundamental aspects of corrosion, corrosion measuring methods, various corrosion mitigating techniques and basics of corrosion inhibitor. This chapter emphasizes the importance of magnesium alloys in the weight sensitive applications. The classifications of magnesium alloy and importance of alloying elements in magnesium alloy manufacturing are explained in details. Further, the literature of magnesium and magnesium alloy corrosion and its inhibition are included in the review of literature section. At the end of the chapter the scope and objectives of the present work are stated by considering the importance of magnesium alloy and by identifying the frailty in the present corrosion combating measures.

The **chapter 2** is focused about the descriptions of adapted experimental methods. The procedure for the preparations of test specimen and electrolyte solutions has been enlightened. This chapter demonstrates the operational stipulations related to the employed electrochemical techniques along with the calculations which results the deduction of numerical data of the present work.

The **chapter 3** accounts for the comprehensive results of the current study along with graphical and numerical interpretations. The electrochemical corrosion

behaviour of Mg-Al-Zn alloy were explored in 30% aqueous ethylene glycol medium containing different concentrations of chloride and sulfate ions, different pH and at a temperature range of 30 °C to 50 °C with an increment of 5 °C in each trail. Sodium dodecyl benzene sulphonate with trisodium phosphate and sodium benzoate were employed as synergistic corrosion inhibitors. Similarly morpholine, N-methyl morpholine and dimethyl morpholine were also studied as corrosion inhibitors in both the corrosive media. The activation parameters for the corrosion and its inhibition process were calculated. The thermodynamic parameters for the inhibitor adsorption were deduced by verifying different adsorption isotherms. Surface morphology and compositions of the corroded and inhibited surfaces were explored by SEM and EDX analyses. The mechanisms for the inhibition process in the presence of different inhibitors in the corrosive media are proposed.

The **chapter 4** summarizes the work embodied in the thesis and enumerates the major conclusions of the overall work.

CHAPTER – 2: MATERIALS AND METHODS

2.1. MATERIALS

In the present study Mg-Al-Zn alloy was considered for all the carried out investigations. The as received rod shaped magnesium alloy was analyzed by atomic absorption spectroscopy (AAS TIFAC GBC 932 plus) to ascertain the composition of the alloy. The elemental composition of the alloy in average weight percent is depicted in Table 2.1.

Table 2.1 Elemental composition of Mg-Al-Zn alloy.

Elements	Weight %
Aluminum	8.30
Zinc	0.60
Manganese	0.35
Silicon	0.20
Copper	0.12
Iron	0.20
Magnesium	Balance

To maintain a constant area of exposure in all the electrochemical studies, the rod shaped alloy was metallographically mounted in epoxy resin as shown in the Fig. 2.1. This method enabled an area of 0.834 cm^2 and it was constant in all the reported studies of this thesis.

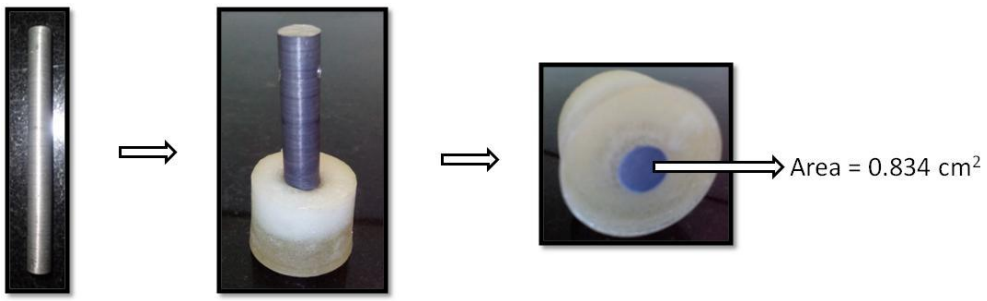

Fig. 2.1 Mounted alloy sample in epoxy resin.

The mounted Mg-Al-Zn alloy was employed with a series of metallographic practices such as belt grinding, abrading on emery papers of grade 600 to 2000, followed by mirror finish by polishing over polishing wheel smeared with levigated alumina. After polishing, the specimen was washed assiduously with double distilled water to remove SiC particles and impurities. Finally, washed with acetone, dried thoroughly in air prior to submerge in electrolyte.

2.2. MEDIA

The opted corrosive media are 30% aqueous ethylene glycol containing sodium chloride and sodium sulfate. Hereafter, for convenience 30% aqueous ethylene glycol medium containing sodium chloride and sodium sulfate are referred to as chloride medium and sulfate medium, respectively. The experiments were performed under unstirred condition at a temperature of 30 °C, 35 °C, 40 °C, 45 °C and 50 °C using calibrated thermostat with ±0.5 °C variation.

2.2.1. Preparation of chloride media

The aqueous ethylene glycol was prepared by mixing 30% by volume of analytical grade ethylene glycol with double distilled water. To this 2 mM, 4 mM, 6 mM, 8 mM and 10 mM chloride ions were added by using analytical grade sodium chloride.

2.2.2. Preparation of sulfate media

To the above explained 30% aqueous ethylene glycol solution analytical grade sodium sulfate was added to prepare 2 mM, 4 mM, 6 mM, 8 mM and 10 mM sulfate ion containing corrosive medium.

2.2.3. Preparation of chloride and sulfate media with various pH

To understand the impact of pH on the corrosion rate of Mg-Al-Zn alloy experiments are carried out in an acidic pH of 4, neutral pH of 7 and basic pH of 10 and 12. The pH study was carried out in selected media of 2 mM, 6 mM and 10 mM chloride and sulfate ion concentrations. The studied pH solutions were prepared by

adding H_2SO_4, HCl and NaOH; and the pH values of the solution were monitored using a calibrated pH meter. The numbers of chloride and sulfate ions given by the acid solutions were subtracted to prepare actual chloride and sulfate media.

2.3. INHIBITORS

All the inhibitors were studied in chloride and sulfate media at a temperature of 30 °C to 50 °C with an increment of 5 °C each time.

2.3.1. Inhibitor mixture containing sodium dodecyl benzene sulphonate (SDBS) and trisodium phosphate (TSP)

SDBS solutions of different concentrations were prepared in the corrosive media by dissolving analytical grade SDBS from Aldrich. 8 mM concentration of SDBS shows highest inhibition and this was considered for further study with different ratios of TSP. The solutions with 4 mM, 8 mM, 16 mM and 32 mM concentrations of TSP were prepared by dissolving analytical grade TSP in a corrosive media containing 8 mM SDBS and tested for its inhibition performance.

2.3.2. Inhibitor mixture containing sodium dodecyl benzene sulphonate (SDBS) and sodium benzoate (SB)

To the SDBS solution containing corrosive ions, showing maximum inhibition effect, different ratios of SB were added. The studied concentrations of SB were 8 mM, 16 mM, 32 mM and 64 mM.

2.3.3. Morpholine and its derivatives as inhibitors

Morpholine and commercially available two of its derivatives, N-methyl morpholine and 2, 6-dimethyl morpholine were tested for their inhibition properties. The structures and concentrations of the studied three inhibitors are listed in the Table 2.2.

Table 2.2 Structures and concentrations of the studied inhibitor.

Inhibitor	Structure	Studied concentrations
Morpholine		200 mM, 600 mM, 800 mM and 1000 mM.
N-methyl morpholine		400 mM, 600 mM, 800 mM and 1000 mM.
2, 6-dimethyl morpholine	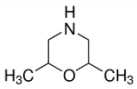	100 mM, 200 mM, 600 mM and 800 mM.

2.4. METHODS

2.4.1. Electrochemical techniques

All the performed electrochemical studies used electrochemical work station of Gill AC equipped with ACM instrument of Version 5 software. A conventional method of three electrode system Pyrex glass cell was opted for all the electrochemical investigations. This consisted of molded Mg-Al-Zn alloy as working electrode, platinum electrode as counter electrode and saturated calomel electrode (SCE) as reference electrode and all the potential reported in the present study are with respect to SCE. At the beginning of all the experiments, the working electrode was allowed to achieve a steady state potential and this was confirmed by monitoring the variation of electrode potential with time. After the steady state attainment of the equilibrium potential corresponds to the OCP of the electrode, potentiodymic polarization and impedance studies were carried out. The polarization studies were performed on the same electrode soon after the impedance studies without subjecting further surface modifying treatments. To ensure reproducibility of the obtained result all the studies were repeated minimum three times and average value of the three consecutive results were recorded. The adopted instrumentation for all the studies is as shown in the Fig. 2.2.

Fig. 2.2 The adopted laboratory instrumentation for electrochemical studies.

2.4.1.1. Potentiodynamic polarization method

In potentiodynamic polarization method the steady state working electrode was polarized +250 mV anodically and −250 mV cathodically at a scan rate of 1 mV s^{-1} from OCP. The tabulated potentiodynamic polarization parameters were deduced by applying Tafel extrapolation technique on the polarization plots.

2.4.1.2. Electrochemical impedance spectroscopy studies

In EIS, a sinusoidal AC voltage of small amplitude 10 mV over a wide range of frequency 100 KHz to 0.01 Hz was applied at OCP. The obtained Nyquist and Bode plots were analyzed to interpret impedance data. This interpretation was done by simulating the Nyquist plots to the suitable equivalent electrical circuit by using ZSimpWin software version 3.21. The simulation study gives the impedance parameters such as film resistance (R_f), film capacitance (C_f), diffusion resistance (R_{dif}), diffusion capacitance (C_{dif}) and total polarization resistance (R_p).

2.4.2. Surface studies

The surface morphology and surface composition analysis of the test coupon were carried out by recording the corresponding scanning electron microscopy (SEM) image and energy dispersion X-ray (EDX) spectra. JEOL JSM-6380LA analytical scanning electron microscope and Zeiss Sigma FESEM with Oxford EDS instrument

were used to image the morphology and to determine the surface composition of the freshly polished, corroded and inhibited surfaces, respectively.

2.5. CALCULATIONS

2.5.1. Corrosion rate

Corrosion current density was calculated by extrapolating the Tafel branches to the corrosion potential. Corrosion rate (υ_{corr}) was determined by substituting the corrosion current density in the following equation (ASTM Standard G102 1999):

$$\upsilon_{corr} = \frac{K \times i_{corr} \times EW}{\rho} \quad (2.1)$$

where υ_{corr} is the corrosion rate in mm y^{-1}, K is a constant and its value is 0.00327 mm g μA^{-1} cm^{-1} y^{-1}, which gives the corrosion rate unit in mm y^{-1}, i_{corr} is the corrosion current density in μA cm^{-2}, ρ is the density of the material under study in g cm^{-3} and is 1.81 g cm^{-3} in the present instance and EW is the equivalent weight of the material which was obtained using the following formula (ASTM Standard G102 1999):

$$EW = \frac{1}{\sum[\frac{n_i \times f_i}{W_i}]} \quad (2.2)$$

where n_i, f_i and W_i are the valence, weight fraction and atomic weight of the i^{th} element of the alloy, respectively, and are tabulated in the Table 2.3. By substituting the n_i, f_i and W_i values of the Mg-Al-Zn alloy in equation 2.2, EW was calculated.

Table 2.3 The n_i, f_i and W_i values of the Mg-Al-Zn alloying elements.

Element	Valence	Weight fraction	Atomic weight
Magnesium	2	90.23	24.305
Aluminium	3	8.3	26.981
Manganese	1	0.35	54.938
Zinc	2	0.6	65.380
Silicon	4	0.2	28.085
Copper	1	0.12	63.546
Iron	2	0.2	55.845

2.5.2. Inhibition efficiency

The ability of the inhibitor to cover the surface of the alloy decides its efficiency. The inhibition efficiency (η) and surface coverage (θ) are related as following:

$$\eta\,(\%) = \theta \times 100 \tag{2.3}$$

The value of surface coverage was obtained from electrochemical study results. The surface coverage was calculated from Tafel polarization studies by using the following equation:

$$\theta = \frac{i_{\mathrm{corr}} - i_{\mathrm{corr(inh)}}}{i_{\mathrm{corr}}} \tag{2.4}$$

where i_{corr} and $i_{\mathrm{corr(inh)}}$ are current density in the absence and presence of inhibitor, respectively.

The total polarization resistance acquired from impedance studies was used to calculate the surface coverage as per the following equation:

$$\theta = \frac{R_{\mathrm{p(inh)}} - R_{\mathrm{p}}}{R_{\mathrm{p(inh)}}} \tag{2.5}$$

where R_{p} and $R_{\mathrm{p(inh)}}$ are respectively, the total polarization resistance in the absence and in the presence of the inhibitor. The total polarization resistance is the sum of all the resistance components in the electrical equivalent circuit fitted to the impedance plots.

2.5.3. Activation parameters

The rate of corrosion was evaluated at various temperatures, facilitates the computation of important activation parameters such as apparent activation energy (E_{a}), apparent enthalpy of activation ($\Delta H^{\#}$) and apparent entropy ($\Delta S^{\#}$) of activation. Arrhenius law equation quoted below was considered for the calculation of apparent activation energy:

$$\upsilon_{\text{corr}} = A\, e^{-E_a/RT} \tag{2.6}$$

where υ_{corr} is the corrosion rate, A is proportionality constant which depends on the type of alloy, R is the universal gas constant, T is the absolute temperature. Arrhenius plots were obtained by plotting the ln (υ_{corr}) versus the reciprocal of temperature (1/T). The E_a values were deduced from the slope ($-E_a/R$) of the obtained straight line graph.

Apparent enthalpy ($\Delta H^{\#}$) and apparent entropy ($\Delta S^{\#}$) of activation were evaluated from the slope ($-\Delta H^{\#}/R$) and intercept (ln (R/Nh) + $\Delta S^{\#}/R$) values of the straight line graph obtained by plotting ln (υ_{corr}/T) verses (1/T) of the Transition state equation as mentioned below:

$$\upsilon_{\text{corr}} = \frac{RT}{Nh}\, e^{\frac{\Delta S^{\#}}{R}}\, e^{-\frac{\Delta H^{\#}}{RT}} \tag{2.7}$$

where h and N are the Planck's constant and Avogadro's number, respectively.

2.5.4. Thermodynamic parameters

Thermodynamic parameters for the adsorption of the inhibitor on the alloy surface were calculated by fitting the experimental values to different adsorption isotherms. Best fitting adsorption isotherm was considered for calculation. Adsorption isotherms are the graphical representations of the variation of extent of adsorption with pressure by keeping temperature as constant. In the case of adsorption at the solution/solid interface instead of pressure adsorbate concentration is considered. These adsorption isotherm are admissible where the inhibition is brought by the adsorption of inhibitor by covering the surface of the metal. The equlibrium between the concenration of the inhibitor in bulk electrolyte and on the surface of the metal is given by the mathematical forms of the adsorption isotherms. The mathematical forms of a few of the common adsorption isotherms, considered for corrosion inhibition are listed in Table 2.4.

Table 2.4 List of mathematical forms and verification plots of the common adsorption isotherms.

Adsorption isotherm	Equation	Verification Plot
Langmuir	$\theta/(1-\theta) = \beta C$	(C/θ) vs. C
Frumkin	$[\theta/(1-\theta)]\, e^{f\theta} = \beta C$	θ vs. log C
Bockris-Swinkels	$\theta/(1-\theta)^n.[\ \theta + n(1-\theta)]^{n-1}/n^n = C.e^{-\beta}/55.4$	$\theta/(1-\theta)$ vs. log C
Temkin	$\theta = (1/f) \ln KC$	θ vs. log C
Virial Parson	$\theta.e^{2f\theta} = \beta C$	θ vs. log(θ/C)
Flory Huggins	$\log(\theta/C) = \log \chi K + \chi \log (1-\theta)$	log (θ/C) vs. log(1-θ)
El – Awady	$\log [\theta/(1-\theta)] = \log K + Y \log C$	log [θ/ (1-θ)] vs log C

The parameters in the table are explained as follows: θ is the surface coverage, β=ΔG/2.303RT where ΔG is the free energy change during the adsorption, R is the universal gas constant, T is the absolute temperature, C is inhibitor concentration in bulk electrolyte, χ is size ratio, which indicates the number of water molecules replaced during the inhibitor adsorption, f is the inhibitor interaction parameter, K and Y are constants.

The above listed adsorption isotherms are graphically fitted to get the linear relationship between the obtained values of surface coverage and concentration of the inhibitor. The regression co-efficient (R^2) of all the adsorption isotherms were compared. The standard free energy of adsorption ($\Delta G°_{ads}$) was calculated from the reaction isotherm equation as follows:

$$\Delta G^{o}_{ads} = -RT\ln\left[55.5 \times \frac{\theta}{C(1-\theta)}\right] \quad (2.8)$$

In the above equation 55.5 is the molar concentration of the water in solution with unit mol dm^{-3}, R is the universal gas constant and T is the absolute temperature.

The standard enthalpy of adsorption ($\Delta H°_{ads}$) and standard entropy of adsorption ($\Delta S°_{ads}$) were estimated by using rearranged Gibbs-Helmholtz equation as represented below:

$$\Delta G^{o}_{ads} = \Delta H^{o}_{ads} - T\Delta S^{o}_{ads} \quad (2.9)$$

The plot of standard free energy of adsorption along y-axis and absolute temperature along x-axis gives the straight line graph with slope equal to $-\Delta S°_{ads}$ and intercept is $\Delta H°_{ads}$.

2.5.5. Synergistic parameters

The interaction between the two inhibitors can lead to either synergistic or antagonistic inhibition effect. The synergistic parameter (S) was calculated by the following equation (Aramaki and Hackerman 1969):

$$S = \frac{1-\theta_{1+2}}{1-\theta'_{1+2}} \quad (2.10)$$

where $\theta_{1+2} = (\theta_1+\theta_2) - (\theta_1\theta_2)$, θ_1 = surface coverage by inhibitor 1 and θ_2 = surface coverage by inhibitor 2, respectively when used individually, θ'_{1+2}= surface coverage by a mixture of inhibitors 1 and 2. The value of S is greater than 1 for synergistic effect, and less than 1 for antagonistic inhibition effect (Ekpe et al. 1995).

CHAPTER – 3: RESULTS AND DISCUSSIONS

3.1. CORROSION BEHAVIOUR OF Mg-Al-Zn ALLOY IN 30% AQUEOUS ETHYLENE GLYCOL CONTAINING CHLORIDE AND SULFATE IONS

3.1.1. Potentiodynamic polarization analyses

The potentiodynamic polarization studies on the corrosion behavior of Mg-Al-Zn alloy in 30% aqueous ethylene glycol were carried out under a range of conditions such as different concentrations of chloride and sulfate ions, different temperatures and varying medium pH. It was reported in the literature that for magnesium and magnesium alloys Tafel extrapolation method cannot be applied for the determination of corrosion rate in corrosive medium containing aggressive ions. This is due to the anodic hydrogen evolution and the break down of the formed surface film at more negative potential than their OCP. Therefore, Tafel plots do not obey the traditional Tafel equation or other diffusion associated equations around their OCPs (Song 2005, 2009; Song and Xu 2010). However, in ethylene glycol the polarization curve shows the breakdown potential more positive than their corrosion potential and hence Tafel extrapolation method can be used in ethylene glycol medium (Huang et al. 2011).

Fig. 3.1 (a) and Fig. 3.1 (b) show the potentiodynamic polarization curves for the corrosion of Mg-Al-Zn alloy in 30% aqueous ethylene glycol containing different concentration of chloride ions and sulfate ions at 50 °C. All the representative plots in this thesis illustrate the said conditions and henceforth it goes without mentioning that similar plots have been acquired at other respective conditions under examination. Hereafter the chloride and sulfate ions are combinedly called as aggressive ions unless it is mentioned separately as chloride and sulfate ions. In Fig. 3.1 anodic curves represent the dissolution of magnesium alloy, whereas the cathodic curves represent the hydrogen evolution reaction. From Fig. 3.1, it is clear that the polarization curves shift towards higher current density region with the increase in aggressive ion

concentration. This indicates the increased corrosion rate of the magnesium alloy at higher corrosive concentrations.

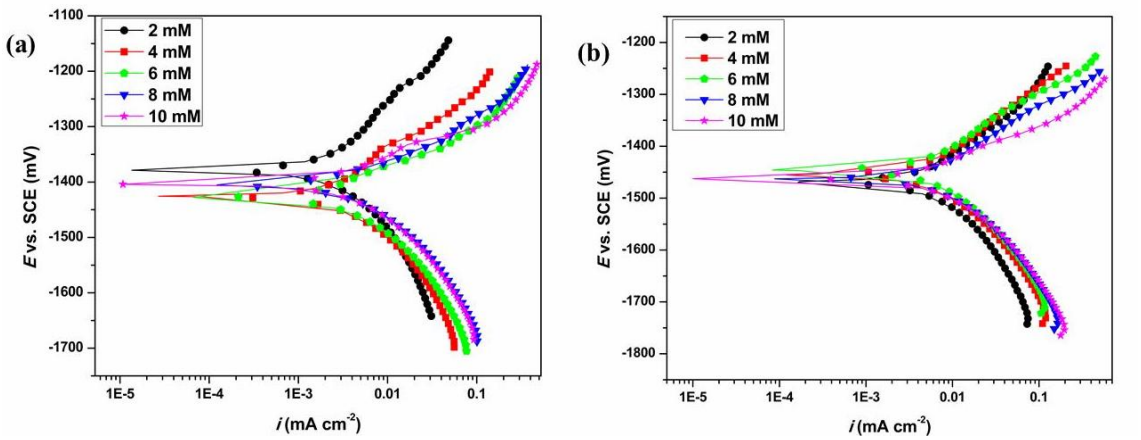

Fig. 3.1 Potentiodynamic polarization plots for the corrosion of Mg-Al-Zn alloy in 30% aqueous ethylene glycol containing different concentrations of (a) chloride ions at 50 °C and (b) sulfate ions at 50 °C.

The anodic polarization curves show inflection points characterized by two different slopes at potentials more positive than corrosion potential. This results from some kind of kinetic barrier effect, most probably by the deposition of corrosion product surface film followed by its dissolution at increased anodic overvoltage (Zhao et al. 2008b, Wang et al. 2010a). With the increase in potential, the pitting susceptibility increases, because, an increase in the applied potential may increase the electric field across the passive film and thus enhance the adsorption of aggressive ions on the passive surface (Jafarian et al. 2008). The cathodic polarization curves are characterized with distinctly linear Tafel regions, and they represent the hydrogen evolution reactions through the reduction of water. The overall shapes of the polarization curves remain same in the presence of different concentrations of aggressive ions, which indicate the unaltered corrosion mechanism with change in the concentrations of the aggressive ions. The cathodic polarization curves were used to measure the electrochemical parameters by extrapolating the linear Tafel region of the curve to the OCP, as the anodic curve possess non-linear Tafel region. The

potentiodynamic polarization parameters such as i_{corr}, E_{corr} and b_c are tabulated in Table 3.1 and Table 3.2 for different concentration of chloride and sulfate ions, respectively, at different temperatures. The tabulated values of υ_{corr} were calculated by using the equation 2.1 mentioned in section 2.5.1.

From Table 3.1 and Table 3.2, it is evident that the rate of corrosion increases with the increment in the aggressive ion concentration. This is attributed to the dissolution of the partially formed $Mg(OH)_2$ surface film in the presence of aggressive ions. In the presence of aggressive ions like chloride and sulfate, $Mg(OH)_2$ surface film forms the readily soluble magnesium salts such as magnesium chloride and magnesium sulfate (Wang et al. 2010a). As a result of this increased surface film dissolution, the rate of Mg-Al-Zn alloy corrosion increases with the increased aggressive ion concentration. In the tabulated values, no correlation with the variation of υ_{corr} value with E_{corr} value is observed. The response of the corroding system towards the change in the ionic concentration of the medium is further encountered in the noticeable variation in the value of b_c. The variation in b_c show the impact of ionic concentration on the kinetics of cathodic reaction. Among the two aggressive solutions the rate of corrosion is more in corrosive solution containing sulfate ions. Several studies have established that, for magnesium and magnesium alloys the corrosion rate is more in chloride containing corrosives due to its small radius and hence easier drilling through the film (Song et al. 1998b, Zhang et al. 2007, Pardo et al. 2010, Wang et al. 2010a). But Fekry and Fatayerji have reported that the presence of less than 0.05 M concentration of chloride ions show some inhibition effect in 30% ethylene glycol and 70% water medium (Fekry and Fatayerji 2009). In this study also less than 0.05 M chloride ion concentration is considered. Because of the inhibition effect of lower concentration chloride ions, the general trend of higher corrosiveness of chloride medium than that of sulfate medium is not observed.

3.1.2. Electrochemical impedance spectroscopy studies

Electrochemical impedance spectroscopy is a non-destructive technique which provides minimal perturbative signal and can be used to study the response of

corroding electrodes to small amplitude alternating potential signals of largely varying frequency (Perez 2004). Nyquist plots at various conditions were considered to explain the impedance behavior of the Mg-Al-Zn alloy. Fig. 3.2 (a) and Fig. 3.2 (b) show the Nyquist plots for the corrosion of Mg-Al-Zn alloy in 30% aqueous ethylene glycol containing different concentrations of chloride ions at 50 °C and sulfate ions at 50 °C, respectively.

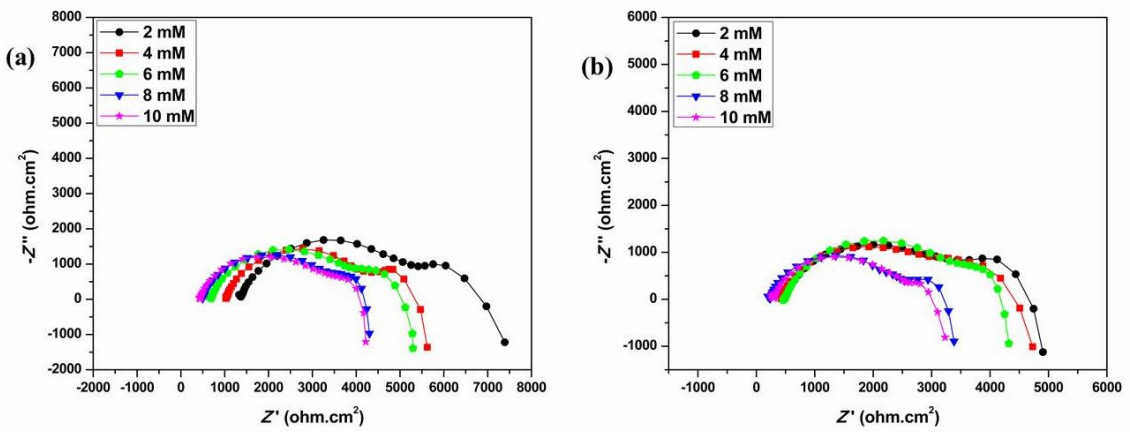

Fig. 3.2 The Nyquist plots for the corrosion of Mg-Al-Zn alloy in 30% aqueous ethylene glycol containing different concentrations of (a) chloride ions at 50 °C and (b) sulfate ions at 50 °C.

These Nyquist plots consist of two depressed semicircles at higher and medium frequency and the beginning of an inductive loop at lower frequency region. The higher frequency semicircle is comparably larger than the medium frequency semicircle. The charge transfer process of corrosion and the effect of surface film results the higher frequency semicircle. Most of the aluminum containing magnesium alloys exhibit two capacitive loops at higher and medium frequencies as the results of interfacial Faradaic charge transfer and surface film formation, respectively (Rosalbino et al. 2006, Badawy et al. 2010, Gao et al. 2010, Huang et al. 2013a). The medium frequency semicircle is because of the diffusion of the electrolyte through the corrosion product. The medium frequency capacitive loop represents the combination of pseudo resistance and capacitance of the film formation and dissolution process

(Song and Xu 2012). Inductive loop at lower frequency indicates the relaxation of adsorbed $Mg(OH)_{ads}^{+}$ and Mg^{+}_{ads} on the metal surface (Pebere et al. 1990, Baril and Pébère 2001, Mathieu et al. 2003, Zucchi et al. 2006, Frignani et al. 2012, Dinodi and Shetty 2014b). In Nyquist plots the diameter of the capacitive loop represents the corrosion resistance property of the alloy (Pebere et al. 1990, Gao et al. 2010). In Fig. 3.2 the diameter of the capacitive loops shrink with the rise in the aggressive ion concentration. This symbolizes the decreasing corrosion resistance of the material with enhanced aggressive ion concentration.

The electrochemical impedance results are best understood by simulating the electrochemical behavior of the interface between the alloy and medium by equivalent electrical circuit model. The impedance data points, neglecting the low frequency inductive loop, can be analysed using apt equivalent electrical circuit for the studied system and is as shown in the Fig. 3.3 (Song and Xu 2010, Jamesh et al. 2011). A representative simulation plot using ZSimWin software of version 3.21 is shown in Fig. 3.4. In all the simulation analyses the errors in the impedance data measurement were less than 5%. The equivalent circuit consists of a solution resistance (R_s) and a series of three parallel combinations of resistance and double layer constant phase element (CPE). They are the parallel combinations of the charge transfer resistance (R_{ct}) with double layer CPE (Q_{dl}), the surface film resistance (R_f) with film CPE (Q_f) and the diffusion resistance (R_{dif}) with diffusion CPE (Q_{dif}). The former two parallel combinations are assigned for the higher frequency response and the later is accredited for the medium frequency response. The similar combination of circuit elements have been reported in the literature (Fletcher 1994). The depressed nature of Nyquist semicircles is due to the surface heterogeneities such as porosity and roughness (Jüttner 1990). Electrode surface heterogeneity and porosity can be accounted by substituting the constant phase element (Q) to the ideal capacitive element (C) (Fan et al. 2006) and is related by the following equation:

$$C = Q(\omega_{\max})^{n-1} \tag{3.1}$$

In this equation Q represents the CPE constant; ω_{max} indicates the frequency where the imaginary part of the impedance is maximum, n represents the CPE exponent and measures the heterogeneity of the surface. The value of n varies from −1 to 1 through 0, CPE resembles an ideal capacitive behavior at n = 1, an ideal inductive behavior at n = –1 and an ideal resistive nature at n = 0.

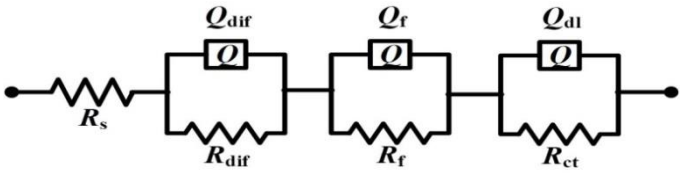

Fig. 3.3 Equivalent electrical circuit used for the simulation of experimental impedance data points.

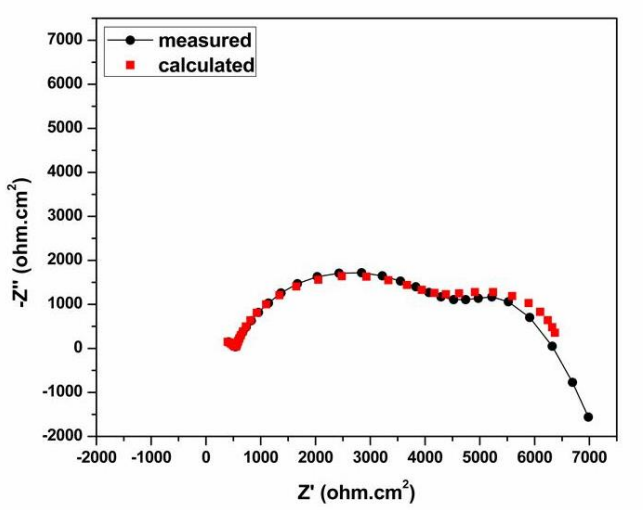

Fig. 3.4 Simulation plot for the corrosion of Mg-Al-Zn alloy in 30% aqueous ethylene glycol containing 10 mM chloride ions at 30 °C.

The relation between capacitance, dielectric constant and thickness of the double layer is given by Helmholtz model (Srinivasan 2006, Qiang et al. 2018, Tan et al. 2018):

$$C = \frac{\varepsilon^0 \varepsilon A}{d} \qquad (3.2)$$

where C denotes capacitance, d represents thickness of the double layer, ε is the local dielectric constant, ε^{o} is the permittivity of the air and A is the geometric surface area of the electrode.

The polarization resistance R_p is inversely proportional to the corrosion rate (Zucchi et al. 2006). The value of R_p was calculated using equation 3.3.

$$R_p = R_{ct} + R_f + R_{dif} \tag{3.3}$$

The values of R_p for the corrosion of Mg-Al-Zn alloy in 30% aqueous ethylene glycol containing chloride and sulfate ions are listed in Table 3.1 and Table 3.2, respectively. It is evident from the values of R_p that the corrosion rate increases with the increase in the concentration of aggressive ion as indicated by the reduction in the R_p values. These trends are in good agreement with the trends observed in potentiodynamic polarization studies.

3.1.3. Effect of temperature

Temperature is an environmental factor, which is having an impact on the corrosion rate of Mg-Al-Zn alloy. Like other chemical reactions, electrochemical reaction, corrosion, is also influenced by the increase in the temperature of the medium (Uhlig and Revie 2008). The effect of temperature on the corrosion rate of Mg-Al-Zn alloy was studied by conducting the experiments at different temperatures in the range of 30 °C to 50 °C with an increment of 5 °C at each trial. Fig. 3.5 (a) and Fig. 3.5 (b) show the potentiodynamic polarization plots for the corrosion of Mg-Al-Zn alloy in 30% aqueous ethylene glycol containing 6 mM chloride ions and 6 mM sulfate ions, respectively, at different temperatures. Fig. 3.6 (a) and Fig. 3.6 (b), respectively, show the Nyquist plots for the same in 6 mM chloride ions and 6 mM sulfate ions. The nature of the plots remains unaltered at higher temperature, which indicates the influential role of temperature on the rate of corrosion and not on the mechanism of corrosion.

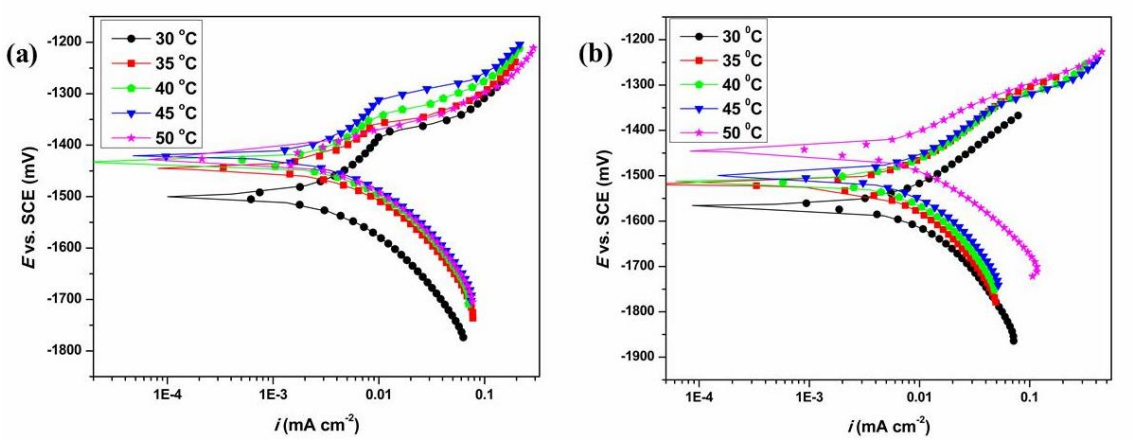

Fig. 3.5 Potentiodynamic polarization plots for the corrosion of Mg-Al-Zn alloy in 30% aqueous ethylene glycol containing (a) 6 mM chloride ions and (b) 6 mM sulfate ions at different temperatures.

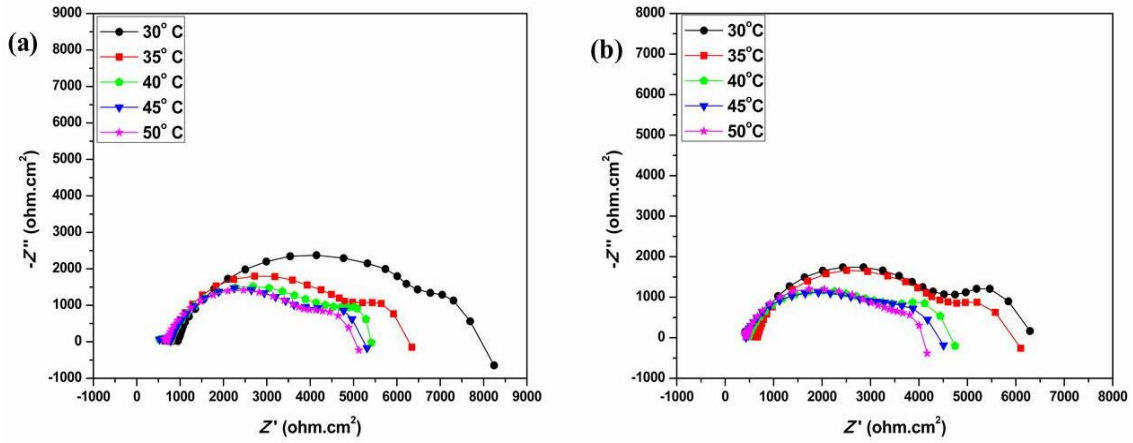

Fig. 3.6 Nyquist plots for the corrosion of Mg-Al-Zn alloy in 30% aqueous ethylene glycol containing (a) 6 mM chloride ions and (b) 6 mM sulfate ions at different temperatures.

From Fig. 3.5 and Fig. 3.6 it can be observed that the polarization curves shift towards the higher current density domain and diameter of the capacitive semicircles diminishes with the increase in the temperature of the medium. Both the factors indicate the increased corrosion rate with the increase in the temperature of the medium. Further the impact of temperature is conformed by the variation in the

electrochemical parameters enlisted in the Table 3.1 and Table 3.2. In both chloride and sulfate media, at any specific medium concentration the rate of Mg-Al-Zn alloy corrosion increases with the increase in the temperature. The increased corrosion rate at higher temperature is the result of increased surface film dissolution and decreased hydrogen overvoltage. At higher temperature the solubility of the formed magnesium hydroxide increases and thus promotes the higher corrosion rate.

The study of corrosion rate in a range of temperature not only informs the consequence of temperature but also facilitates the evaluation of activation parameters. Arrehnius law equation and transition state equation (Equations 2.6 and 2.7, respectively, in chapter-2) were employed for the calculation of apparent activation energy (E_a), apparent enthalpy of activation ($\Delta H^{\#}$) and apparent entropy of activation ($\Delta S^{\#}$). Fig. 3.7 (a) and Fig. 3.7 (b), correspondingly, represent the Arrhenius plots for the corrosion of Mg-Al-Zn alloy in 30% aqueous ethylene glycol containing chloride and sulfate ions. The ln (υ_{corr}/T) versus ($1/T$) plots for the same are shown in Fig. 3.8 (a) and Fig. 3.8 (b), respectively. The calculated activation parameters for the corrosion of Mg-Al-Zn alloy corrosion in 30% aqueous ethylene glycol containing chloride and sulfate ions, respectively, are tabulated in Table 3.3 and Table 3.4. The activation energy is a sign of energy barrier for the occurrence of corrosion (Schorr and Yahalom 1972). The gradual decrease in the activation energy with the increase in the concentration of chloride and sulfate ion indicates that the Mg-Al-Zn alloy corrosion is energetically advantageous in more concentrated media than in less concentrated media (Ashassi-Sorkhabi et al. 2005). The values of apparent enthalpy of activation vary according to the values of activation energy. The association of the reactants during the formation of the activated complex in the corrosion rate-determining step is indicated by the negative values of the apparent entropy. This suggests that the randomness of the system decreases during the association step of the Mg-Al-Zn corrosion (Bentiss et al. 2005).

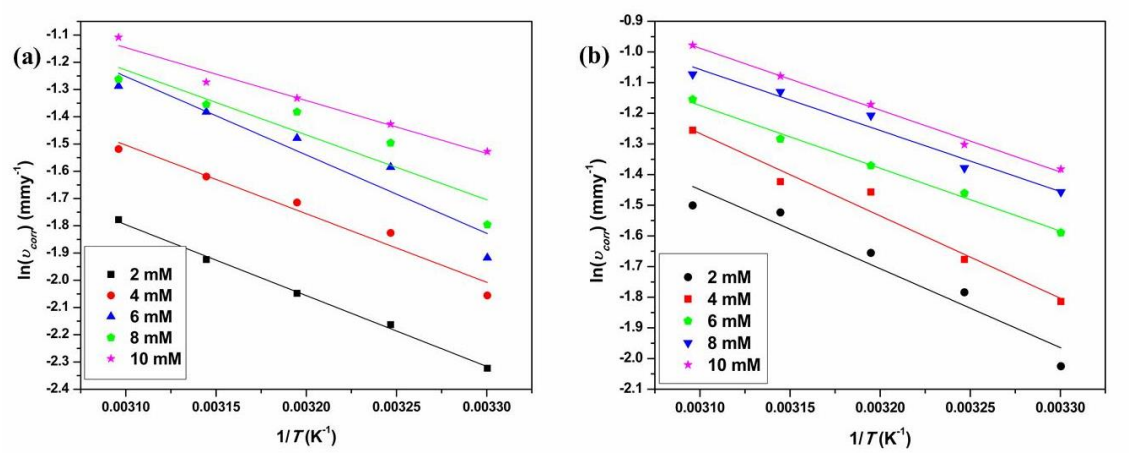

Fig. 3.7 Arrhenius plots for the corrosion of Mg-Al-Zn alloy in 30% aqueous ethylene glycol containing different concentrations of (a) chloride ions and (b) sulfate ions.

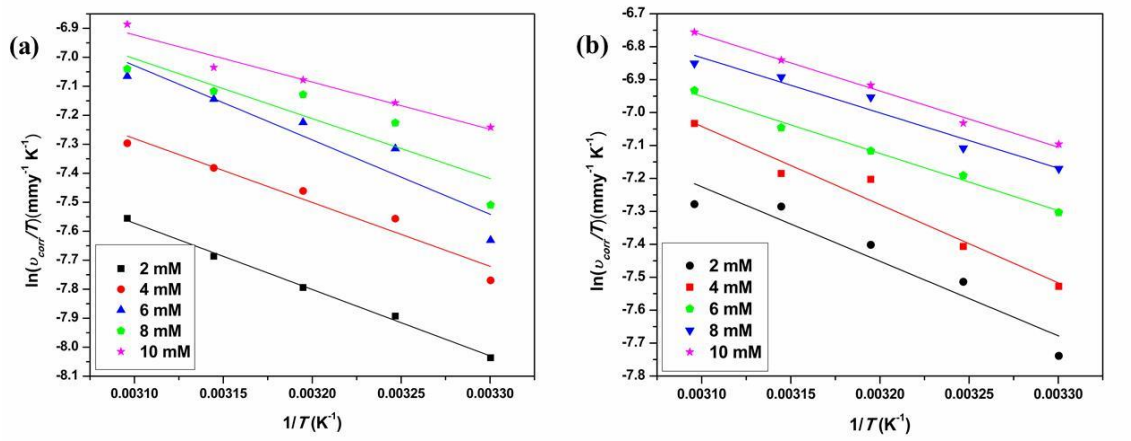

Fig. 3.8 Plots of ln (v_{corr} /T) vs 1/T for the corrosion of Mg-Al-Zn alloy in 30% aqueous ethylene glycol containing different concentration of (a) chloride ions and (b) sulfate ions.

3.1.4. Effect of pH

The corrosion rate of magnesium alloy is associated with the characteristics of its surface film. In aqueous solution, the surface film of the magnesium alloy consists of mainly $Mg(OH)_2$. The influence of pH on corrosion of magnesium alloy needs to take into the account of Mg, Al, Zn Pourbaix diagram. Fig. 3.9 shows the Pourbaix

diagram of Mg, Al, Zn (Badawy et al. 2010). In Fig. 3.9 the corrosion product $Mg(OH)_2$ is stable only in the alkaline region of pH above 10.5. Aluminum is passive in the pH range of 4 to 9 and production of magnesium aluminates and stabilization of $Mg(OH)_2$ occurs above pH 9. Zinc also shows the passive behavior in the pH range between 8.5 and 10.5.

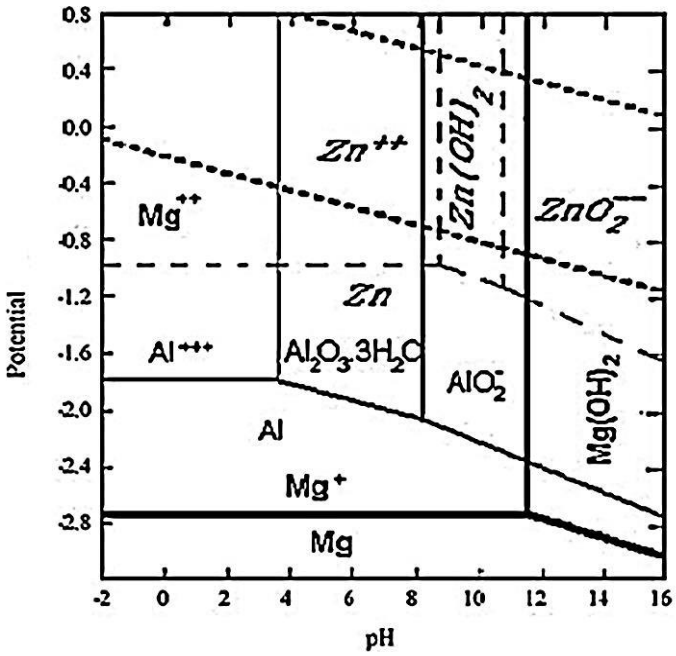

Fig. 3.9 Pourbaix diagram of Mg, Al, Zn (Badawy et al. 2010)**.**

Thermodynamics and the Pourbaix diagram predict that there should be no film on magnesium surface in acidic and neutral pH solutions. However, even though the surface film is not thermodynamically stable at low pH values, the surface film may be formed, provided, the dissolution kinetics are slower than the formation kinetics. Furthermore, even in bulk solution of acidic pH (pH=4), an alkaline pH zone near the corroding magnesium electrode develops in the electrolyte as a result of cathodic reaction of hydroxyl ion generation. This alkalization is associated with the formation of surface film. The increased corrosion rate of Mg-Al-Zn alloy on decreasing the pH of the media and increasing aggressive ion concentration are studied by potentiodynamic polarization and electrochemical impedance spectroscopy. Fig. 3.10

(a) and Fig. 3.10 (b) show the potentiodynamic polarization curves for the corrosion of Mg-Al-Zn alloy in 30% aqueous ethylene glycol containing 10 mM chloride ions and 2 mM sulfate ions, respectively, at different pH at a temperature of 30 °C. Fig. 3.11 (a) and Fig. 3.11 (b) show the Nyquist plots for the same in the presence of 10 mM chloride ions and 2 mM sulfate ions, respectively. In potentiodynamic polarization plots, the polarization curves shift to the higher current density region and in Nyquist plots the diameters of the semicircle decreases, both demonstrate the increased corrosion rate on changing the medium pH from alkaline to acidic condition. This trend is consistent with the corrosion behavior of magnesium alloy, governed by a partially protective surface film. At pH=12, the polarization curve shift to anodic region with a large shift in its E_{corr} value. Corrosion reaction occurs predominantly at the breaks or imperfections of the partially protective $Mg(OH)_2$ film. The fraction of film free surface increases with the decrease in pH of the media and with the increase in aggressive ion concentration. However, the value of corrosion rate in alkaline media is small, but significant because the $Mg(OH)_2$ surface film is with a pilling Bed-worth ratio ~ 0.81 (Pilling and Bedworth 1923) and hence incapable of imparting complete passivity to the underlying metal (Zhao et al. 2008b, Badawy et al. 2010). The obtained electrochemical parameters are tabulated in Table 3.5 which gives further support to the observed trends in the potentiodynamic polarization plots and Nyquist plots. In the Table the corrosion rate is more in acidic solution than in neutral solution and lower in basic solution. The increased corrosion rate in acidic solution is due to the increased dissolution of $Mg(OH)_2$. In neutral medium, less corrosion rate than in acidic medium is observed because of the partially soluble $Mg(OH)_2$ layer in neutral solution. Whereas in basic solution the formed $Mg(OH)_2$ is insoluble and hence shows the less corrosion rate (Badawy et al. 2010).

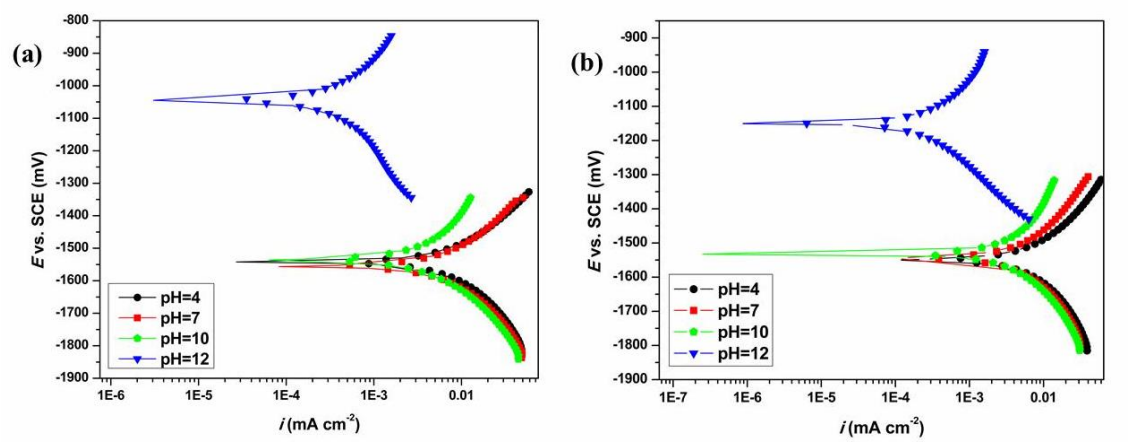

Fig. 3.10 Potentiodynamic polarization curves for the corrosion of Mg-Al-Zn alloy in 30% aqueous ethylene glycol containing (a) 10 mM chloride ions and (b) 2 mM sulfate ions at different pH and at 30 °C.

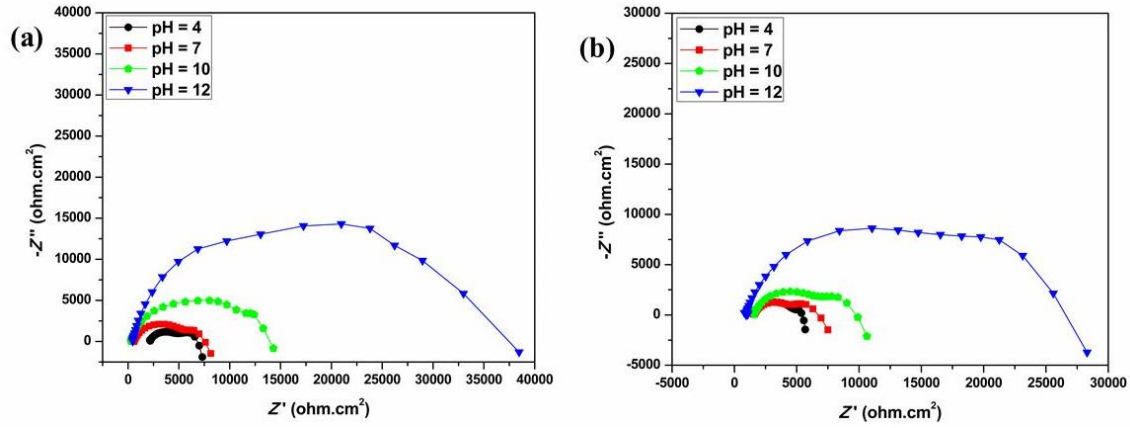

Fig. 3.11 Nyquist plots for the corrosion of Mg-Al-Zn alloy in 30% aqueous ethylene glycol containing (a) 10 mM chloride ions and (b) 2 mM sulfate ions at different pH and at 30 °C.

3.1.5. Mechanism of Mg-Al-Zn alloy corrosion

3.1.5.1. Microgalvanic corrosion of Mg-Al-Zn alloy

The microstructure of Mg-Al-Zn alloys consist of primary α-phase and a divorced eutectic β-phase, which is distributed along the grain boundaries (Froes et al. 1998). The α-Mg matrix is α-Mg-Al-Zn solid solution with the same crystal structure

as pure magnesium and the β-phase is with a composition of $Mg_{17}Al_{12}$. They are also found to have inter metallic inclusions of $MnAl_2$ (Pardo et al. 2008b). The α-Mg matrix with a very negative free corrosion potential acts as anodic with respect to the β-phase of $Mg_{17}Al_{12}$, undergoes corrosion by micro galvanic coupling between anodic α-Mg phase and cathodic β-$Mg_{17}Al_{12}$ phase (Song et al. 1998a, Ambat et al. 2000, Aung and Zhou 2002, Jönsson et al. 2007, Zhao et al. 2008a). However, the β-$Mg_{17}Al_{12}$ phase may act as a barrier against corrosion propagation if it is in the form of a continuous network. The corrosion of the alloy in the aqueous ethylene glycol media in the presence of aggressive ions indicates the discontinuities in the β-phase. According to the results published in the literature, magnesium alloys exhibit higher corrosion resistance than pure magnesium (Badawy et al. 2010). The improvement of the corrosion behavior of Mg alloys in the presence of alloying elements has been attributed to a number of factors such as refining of the β-phase and formation of more continuous network, suppression of β-phase formation by forming another intermetallic, which is less harmful to the α-Mg matrix, and incorporation of the added elements into the protective film and thus increasing its stability (Wu et al. 2005, Fan et al. 2006). Small additions of Mn have been reported to increase the corrosion resistance of magnesium alloys and reduce the effects of metallic impurities (Polmear 1992, Carlson and Jones 1993).

3.1.5.2. Anodic magnesium dissolution and negative difference effect

In aqueous solution hydrated metal ions act as hard Lewis acids. According to HSAB (hard and soft acids and bases) principle, hard Lewis acid hydrated metal ions tend to combine with hard Lewis bases such as hydroxide ions to form partial covalent or ionic compounds. The soluble or insoluble forms of these compounds influence the successive progress in metal distruction by causing corrosion acceleration (Sato 2012).

The corrosion reactions of pure magnesium hold good for magnesium alloys as well. Unlike other metals magnesium shows a very strange electrochemical phenomenon which is known as negative difference effect. Generally, with the

increase in the applied potential the rate of anodic reaction increases whereas the rate of cathodic reaction decreases. However, for pure magnesium and its alloys, it is practically found that, with the increase in applied potential both magnesium dissolution and hydrogen evolution reaction rates increases (rather than decreasing) (Song and Atrens 1999).

The corrosion of magnesium alloys in aqueous medium proceeds through an electrochemical reaction between magnesium and water to produce magnesium hydroxide and hydrogen as in the following equation (Greenblatt 1956).

$$Mg + 2H_2O \rightarrow Mg(OH)_2 + H_2 \quad (3.4)$$

The steady state working potential and the standard electrode potential of magnesium are about –1.5 V and –2.38 V (vs SCE), respectively. The difference between the steady state working potential and the standard electrode potential has been accredited to the formation of $Mg(OH)_2$ surface film on the metal surface (Udhayan and Bhatt 1996). The anodic dissolution of magnesium is composed of two oxidation reactions: oxidation of magnesium into monovalent Mg^+ ions and divalent Mg^{2+} ions as represented in equation 3.5 and equation 3.6, respectively (Baghni 2004).

$$Mg \rightarrow Mg^+ + e^- \quad (3.5)$$

$$Mg \rightarrow Mg^{2+} + 2e^- \quad (3.6)$$

The oxidation of magnesium into monovalent magnesium ion takes place at more active potentials around –2.78 V (vs SCE). Whereas oxidation of magnesium into divalent magnesium ion arises at slightly higher potentials of –1.56 V (vs SCE) in parallel with the former oxidation process (Natta 2001). The formed monovalent magnesium ion is unstable, further it undergoes oxidation to divalent magnesium ion, which involves a series of reactions comprising the formation of unstable intermediates like magnesium hydride as shown in equations 3.7 to 3.10 below:

$$Mg^{+} + 2H^{+} + 3e^{-} \rightarrow MgH_2 \quad (3.7)$$

$$MgH_2 + 2H_2O \rightarrow Mg^{2+} + 2OH^{-} + 2H_2 \quad (3.8)$$

$$Mg^{2+} + 2OH^{-} \rightarrow Mg(OH)_2 \quad (3.9)$$

$$2Mg^{+} + 2H_2O \rightarrow Mg^{2+} + Mg(OH)_2 + H_2 \quad (3.10)$$

It is reported in literature, that the surface film of magnesium is composed of multilayers with inner cellular layer of MgO-$Mg(OH)_2$, a thin film of MgO and outer thick $Mg(OH)_2$ porous layer (Nordlien et al. 1997). This surface film is porous and defective with pilling-Bedworth ratio of ~ 0.81, corrosion reactions takes place at the pores and breakes of this partially protective surface layer (Song and Atrens 1999, 2003, 2007). The ethylene glycol present in the corrosion medium may not cause significant effect on the nonprotective nature of the film, as it can only slightly modify the film without changing the porosity of the film significantly (Huang et al. 2011). In the presence of chloride and sulfate ions, Mg^{2+} ion forms the magnesium chloride and magnesium sulfate which are more soluble than $Mg(OH)_2$ and induce the higher corrosion rate (Wang et al. 2010a , Gao et al. 2011).

3.1.6. Surface analyses

The corrosive impact on the Mg-Al-Zn alloy is further justified by studing the surface morphology by means of SEM. The SEM image of the freshly polished Mg-Al-Zn alloy surface and the corresponding EDX spectra are shown in Fig. 3.12 (a) and Fig. 3.12 (b), respectively. The smooth alloy surface with intermetallic particles are observed in SEM image and intense peak of magnesium followed by other major alloying elements are observed in EDX spectrum of the Mg-Al-Zn alloy surface. In order to visualize the microstructure of Mg-Al-Zn alloy, the freshly polished alloy surface was etched in the acetic picral solution. After etching SEM and optical images were recorded by using JEOL JSM-6380LA analytical scanning electron microscope and optical microscope Zeiss AXIO Lab.A1, respectively. The microstructures of Mg-Al-Zn alloy are shown in SEM and optical image in the Fig.

3.13 (a) and Fig. 3.13 (b), respectively. In Fig. 3.13, the presence of grains and grain boundaries with $MnAl_2$ intermetallic particles on the surface of the alloy are clearly visible. Mg-Al-Zn alloy surface mainly consists of α-Mg matrix represented as α-phase and precipitates of $Mg_{17}Al_{12}$ as a second phase with dendritic and island-like structures depicted as β-phase are shown in the Fig. 3.13 (a) (Li et al. 2015).

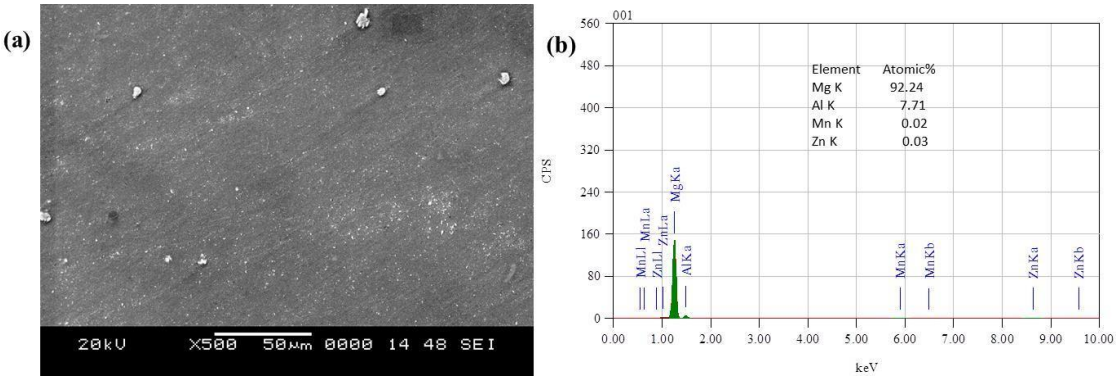

Fig. 3.12 (a) SEM image and (b) EDX spectra of freshly polished surface of Mg-Al-Zn alloy.

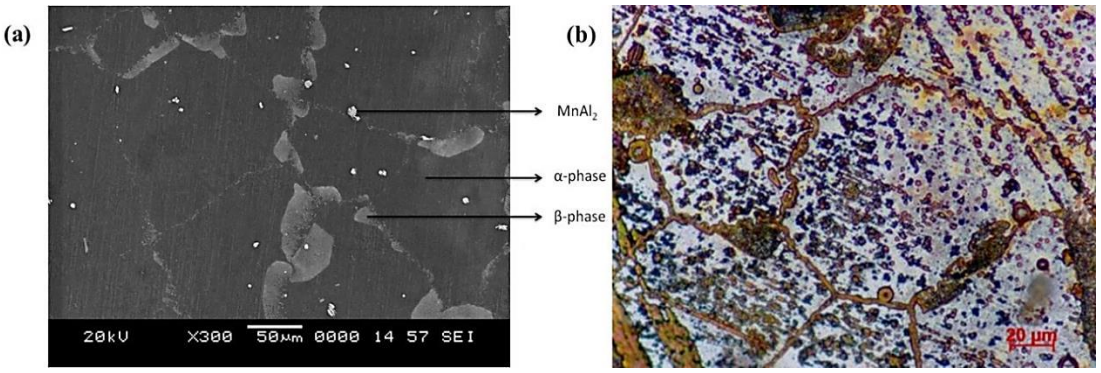

Fig. 3.13 (a) SEM image and (b) optical image of freshly polished Mg-Al-Zn alloy surface after etching in the acetic-picral solution.

The presence of $MnAl_2$ intermetallic partcicles are further confirmed by specifically recording the EDX spectra, precise to the mentioned regions. Fig. 3.14 (a) and Fig. 3.14 (b) show the EDX spectra recorded for the specified region in the SEM image of the intermetallic particle and bare Mg-Al-Zn alloy, respectively. The EDX spectra of intermetallic particle exhibit the peaks of magnesium, aluminum and

manganese with higher atomic percentage. Whereas in the EDX spectra of bare alloy, the atomic percentage of magnesium and aluminum are more. This confirms the existance of $MnAl_2$ intermetallic particle on the surface of the Mg-Al-Zn alloy and also this finding is in agreement with the reported composition of the $MnAl_2$ intermetallic particles in magnesium aluminum alloys (Pardo et al. 2008a). The distribution of major alloying elements in Mg-Al-Zn alloy was determined using EDX mapping and is as shown in the Fig. 3.15.

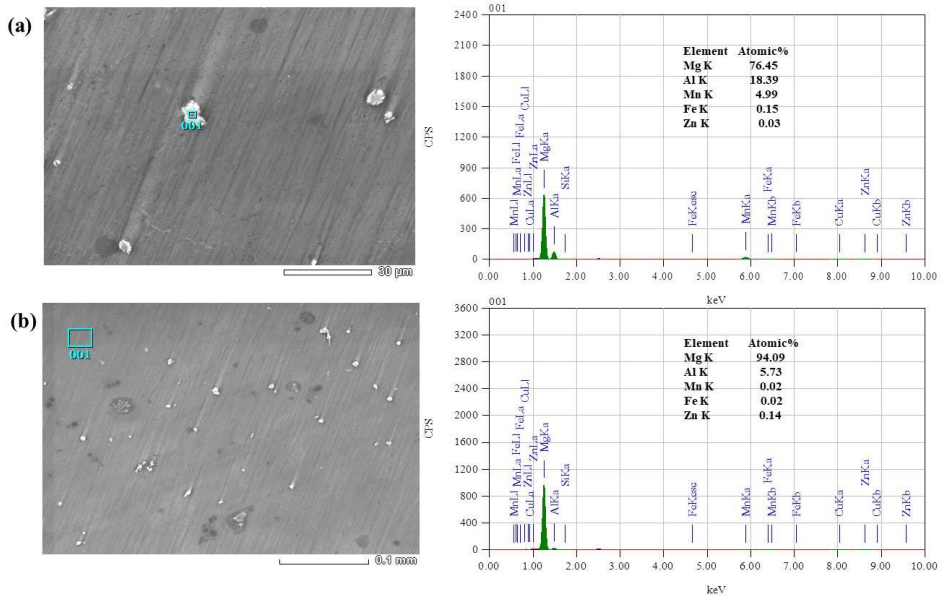

Fig. 3.14 EDX spectra of (a) intermetallic particle and (b) bare alloy along with the specified region of the SEM images.

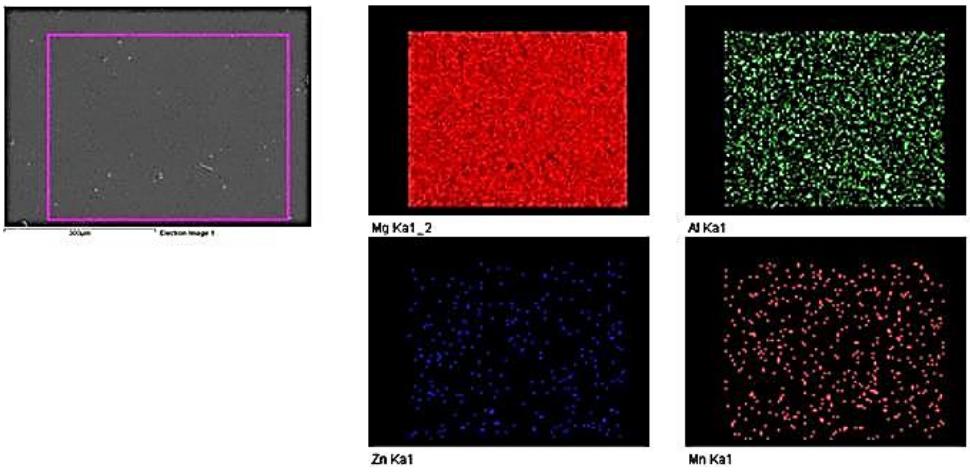

Fig. 3.15 EDX mapping of Mg-Al-Zn alloy showing the distribution of various elements in the alloy.

The SEM image and EDX spectra of the corroded alloy surface after 24 h immersion in 30% aqueous ethylene glycol containing 10 mM chloride ions and 10 mM sulfate ions are as shown in the Fig. 3.16 (a), Fig. 3.17 (a) and Fig. 3.16 (b), Fig. 3.17 (b), respectively.

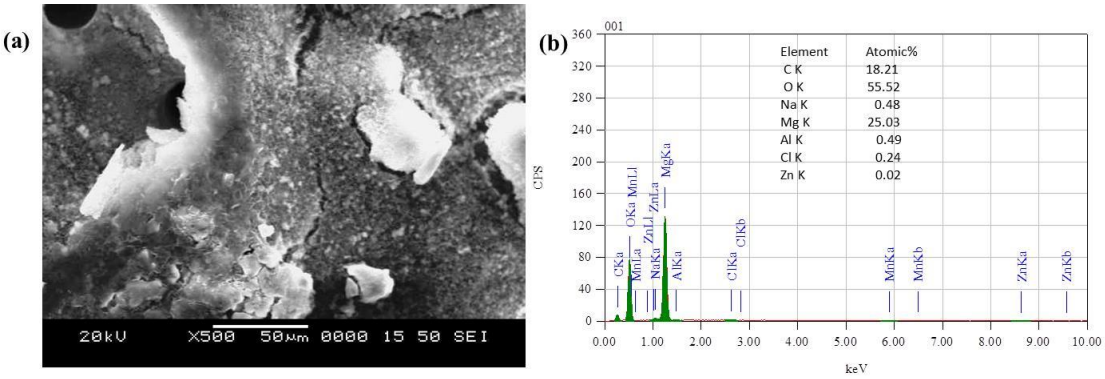

Fig. 3.16 (a) SEM image of the corroded Mg-Al-Zn alloy surface, after immersing in 30% aqueous ethylene glycol containing 10 mM chloride ions for 24 h (b) corresponding EDX spectra.

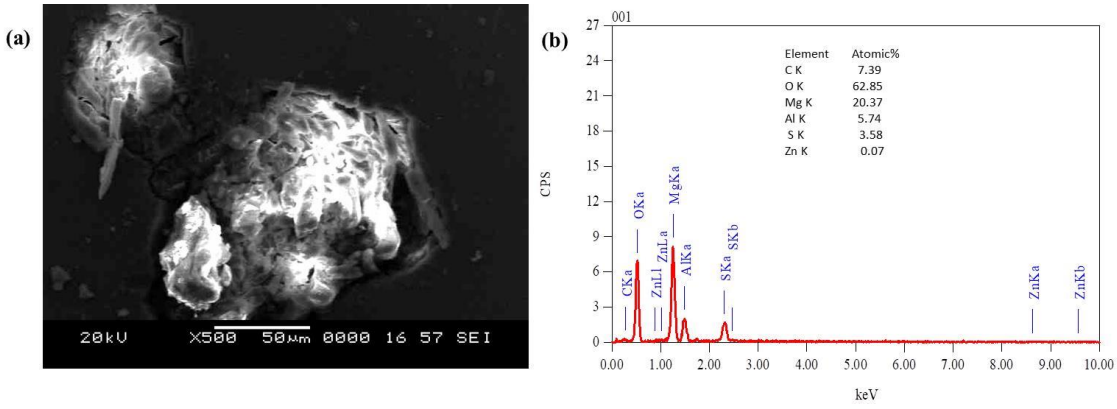

Fig. 3.17 (a) SEM image (b) EDX spectra of Mg-Al-Zn alloy surface, after immersing in 30% aqueous ethylene glycol containing 10 mM sulfate ions for 24 h.

The alloy surface is corroded and covered by corrosion product. In Fig. 3.16 (a) smaller pits are covered by denser corrosion product, whereas in Fig. 3.17 (a) larger pits with less corrosion product are observed. The presence of corrosion product on the surface of the alloy is endorsed by the existence of strong peak of oxygen in the EDX spectra. In the Fig. 3.16 (b) and Fig. 3.17 (b) EDX spectra show the strong peak of magnesium along with the peak of carbon and other alloying elements. The presence of ethylene glycol in the modified surface film contributes for the appearance of carbon peak in the EDX spectra of the corroded surface. Similarly peaks corresponding to sodium, sulphur and chlorine can be attributed to the presence of electrolyte.

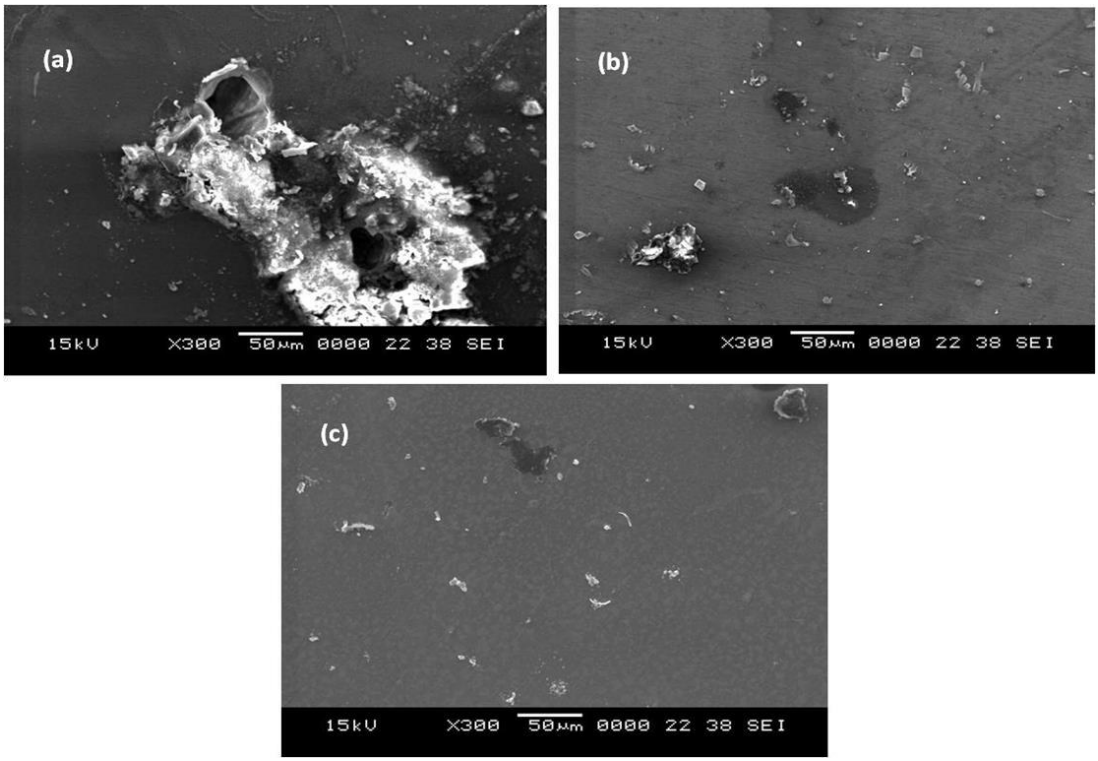

Fig. 3.18 SEM images of Mg-Al-Zn alloy surface after 24 h of immersion in 30% aqueous ethylene glycol containing 10 mM chloride ions with (a) acidic pH of 4, (b) neutral pH of 7 and (c) alkaline pH of 12.

To study the effect of pH on the rate of corrosion, the alloy specimen was immersed in 30% aqueous ethylene glycol containing 10 mM chloride ions and 10

mM sulfate ions with acidic, neutral and basic solution of pH 4, 7 and 10, respectively, and the corresponding SEM images are as shown in Fig. 3.18 (a), Fig. 3.18 (b), Fig. 3.18 (c) and Fig. 3.19 (a), Fig. 3.19 (b), Fig. 3.19 (c). From the Fig. 3.18 and Fig. 3.19 it is clear that, the specimen immersed in the acidic pH of 4 shows the more roughened surface with pits, whereas specimen immersed in the neutral surface shows less roughened surface. Similarly the specimen immersed in basic solution of pH 12 show smooth surfaces with no pits. The surface with no roughned structure confirms the reduced corrosion rate in alkaline solution.

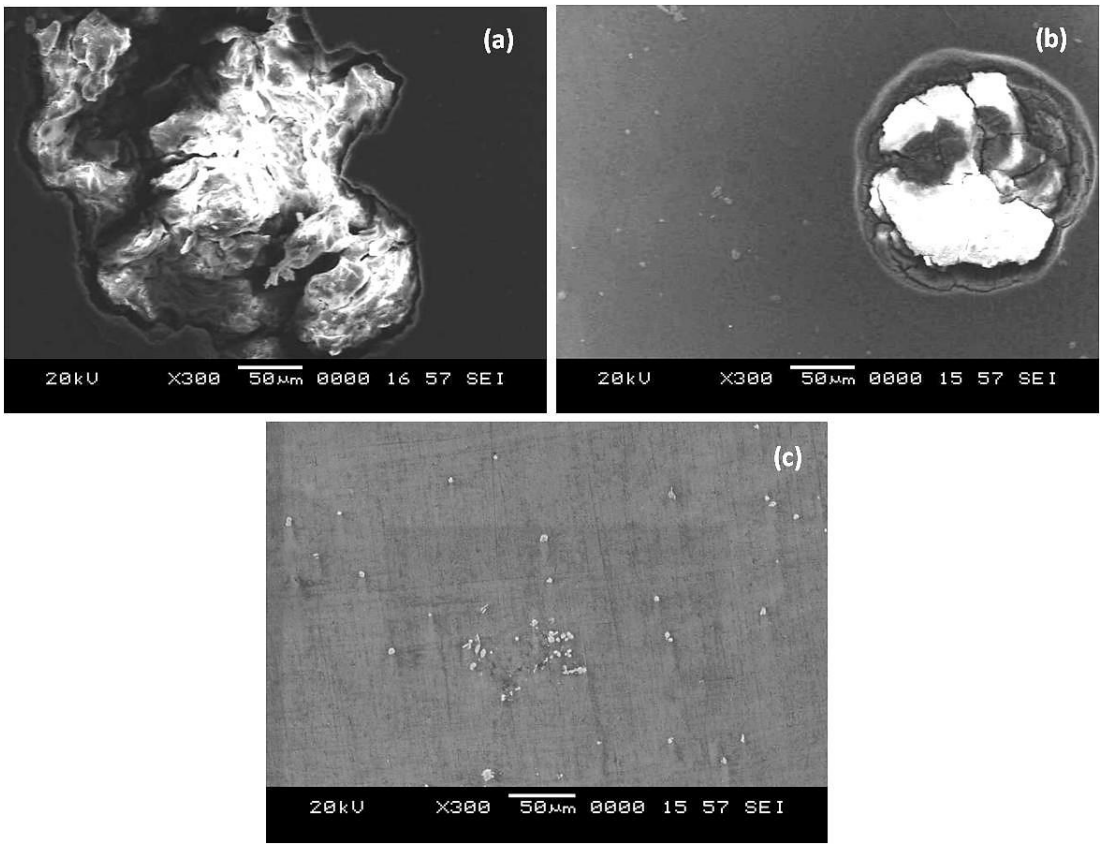

Fig. 3.19 SEM images of Mg-Al-Zn alloy surface after 24 h of immersion in 30% aqueous ethylene glycol containing 10 mM sulfate ions with (a) acidic pH of 4, (b) neutral pH of 7 and (c) alkaline pH of 12.

Table 3.1 Tafel polarization and electrochemical impedance parameters for the corrosion of Mg-Al-Zn alloy in 30% aqueous ethylene glycol containing different concentrations of chloride ions at different temperatures.

Chloride ion concentration (mM)	Temperature (°C)	E_{corr} vs. SCE (mV)	$-b_c$ (mV dec^{-1})	i_{corr} (µA cm^{-2})	υ_{corr} (mm y^{-1})	R_p (ohm cm^2)
2	30	−1476	356	4.58	0.10	9501
	35	−1466	363	5.36	0.12	8034
	40	−1486	332	6.02	0.13	6932
	45	−1470	370	6.79	0.15	6725
	50	−1379	442	7.85	0.17	5581
4	30	−1504	282	5.95	0.13	7972
	35	−1430	300	7.53	0.16	6358
	40	−1452	296	8.39	0.18	5574
	45	−1423	316	9.23	0.20	4820
	50	−1426	343	10.22	0.22	4627
6	30	−1499	270	6.85	0.15	7582
	35	−1445	279	9.53	0.21	6085
	40	−1433	297	10.59	0.23	4880
	45	−1420	317	11.68	0.25	4742
	50	−1428	338	12.82	0.28	4548
8	30	−1410	279	7.71	0.17	7389
	35	−1440	240	10.43	0.22	5636
	40	−1470	337	11.69	0.25	4523
	45	−1452	302	12.01	0.26	4242
	50	−1406	296	13.17	0.28	4031
10	30	−1458	286	10.09	0.22	6915
	35	−1446	269	11.18	0.24	5509
	40	−1416	310	12.27	0.26	4411
	45	−1461	306	13.05	0.28	4156
	50	−1405	339	15.37	0.33	3969

Table 3.2 Tafel polarization and electrochemical impedance parameters for the corrosion of Mg-Al-Zn alloy in 30% aqueous ethylene glycol containing different concentrations of sulfate ions at different temperatures.

Sulfate ion concentration (mM)	Temperature (°C)	E_{corr} vs. SCE (mV)	$-b_c$ (mV dec^{-1})	i_{corr} (µA cm^{-2})	υ_{corr} (mm y^{-1})	R_p (ohm cm^2)
2	30	–1546	284	6.14	0.13	5947
	35	–1556	349	7.80	0.17	5687
	40	–1469	311	8.90	0.19	5046
	45	–1463	309	10.15	0.22	4411
	50	–1468	285	10.36	0.22	4261
4	30	–1547	311	7.60	0.16	5905
	35	–1538	329	8.72	0.19	5680
	40	–1457	275	10.85	0.23	4704
	45	–1460	249	11.22	0.24	4394
	50	–1455	266	13.25	0.28	4183
6	30	–1566	308	9.47	0.20	5893
	35	–1520	373	10.79	0.23	5631
	40	–1513	376	11.81	0.25	4643
	45	–1500	379	12.87	0.28	4329
	50	–1446	335	14.63	0.31	3760
8	30	–1481	299	10.84	0.23	5000
	35	–1534	344	11.72	0.25	4503
	40	–1457	255	13.92	0.30	4211
	45	–1461	249	15.01	0.32	4032
	50	–1463	250	15.92	0.34	3366
10	30	–1530	386	11.68	0.25	4714
	35	–1521	402	12.65	0.27	4347
	40	–1460	344	14.43	0.31	3928
	45	–1458	327	15.82	0.34	3457
	50	–1462	318	17.49	0.38	3148

Table 3.3 Activation parameters for the corrosion of Mg-Al-Zn alloy in 30% aqueous ethylene glycol containing chloride ions.

Chloride ion concentration (mM)	E_a (kJ mol^{-1})	$\Delta H^{\#}$ (kJ mol^{-1})	$\Delta S^{\#}$ (J mol^{-1} K^{-1})
2	21.6	19.0	−201.5
4	20.9	18.3	−201.3
6	23.9	21.3	−189.9
8	19.8	17.2	−202.5
10	16.1	13.5	−213.2

Table 3.4 Activation parameters for the corrosion of Mg-Al-Zn alloy in 30% aqueous ethylene glycol containing sulfate ions.

Sulfate ion concentration (mM)	E_a (kJ mol^{-1})	$\Delta H^{\#}$ (kJ mol^{-1})	$\Delta S^{\#}$ (J mol^{-1} K^{-1})
2	21.4	18.8	−199.3
4	22.3	19.7	−194.9
6	17.0	14.4	−210.6
8	16.6	14.0	−211.1
10	16.8	14.2	−209.8

Table 3.5 Electrochemical parameters for the corrosion of Mg-Al-Zn alloy in 30% aqueous ethylene glycol of different pH, containing different concentrations of chloride ions at 30 °C.

Chloride ion concentration (mM)	pH of the medium	E_{corr} vs. SCE (mV)	$-b_c$ (mV dec^{-1})	i_{corr} (µA cm^{-2})	υ_{corr} (mm y^{-1})	R_p (ohm cm^2)
2	4	−1562	299	6.24	0.13	6729
	7	−1475	324	4.58	0.10	9503
	10	−1334	223	1.24	0.03	27770
	12	−1251	165	0.79	0.02	42540
6	4	−1583	343	8.22	0.18	4976
	7	−1569	332	6.88	0.15	7525
	10	−1380	238	2.51	0.05	20330
	12	−1167	228	1.05	0.02	40630
10	4	−1542	304	15.22	0.33	4840
	7	−1556	290	10.23	0.22	6993
	10	−1536	263	4.91	0.11	14742
	12	−1047	356	1.57	0.03	38560

Table 3.6 Electrochemical parameters for the corrosion of Mg-Al-Zn alloy in 30% aqueous ethylene glycol of different pH, containing different concentrations of sulfate ions at 30 °C.

Sulfate ion concentration (mM)	pH of the media	E_{corr} vs. SCE (mV)	$-b_c$ (mV dec^{-1})	i_{corr} (μA cm^{-2})	υ_{corr} (mm y^{-1})	R_p (ohm cm^2)
2	4	−1548	285	8.41	0.18	4299
	7	−1544	315	6.18	0.13	5915
	10	−1534	287	4.52	0.10	8272
	12	−1152	305	1.30	0.03	26920
6	4	−1520	217	14.28	0.31	3391
	7	−1529	279	9.50	0.20	5664
	10	−1532	304	7.47	0.16	7030
	12	−1337	317	1.95	0.04	22780
10	4	−1489	259	18.94	0.41	3025
	7	−1518	289	11.69	0.25	4758
	10	−1521	315	9.29	0.20	5832
	12	−1380	198	2.22	0.05	20780

3.2. CORROSION INHIBITION OF Mg-Al-Zn ALLOY IN 30% AQUEOUS ETHYLENE GLYCOL CONTAINING AGGRESSIVE IONS BY A MIXTURE OF INHIBITORS, SODIUM DODECYL BENZENE SULPHONATE (SDBS) AND TRISODIUM PHOSPHATE (TSP)

3.2.1. Effect of ethylene glycol on the corrosion rate of Mg-Al-Zn alloy

In aqueous solutions the magnesium alloy surface is covered by the porous, defective surface film of $Mg(OH)_2$ (Wang et al. 2012). Ethylene glycol is an organic molecule which easily gets adsorbed on the surface of the alloy (Slavcheva and Schmitt 2002). In the presence of ethylene glycol, the surface film is slightly modified. The larger ethylene glycol molecule easily gets adsorbed on the surface and replaces the previously adsorbed water molecules. This decreases the direct contact of the alloy sample with water molecules, alters the $Mg(OH)_2$ film on the surface and decreases the conductivity of the medium (Wang et al. 2012). This can be evidenced by the potentiodynamic polarization plots and electrochemical impedance spectra as shown in Fig. 3.20 (a) and Fig. 3.20 (b), respectively. Therefore the rate of corrosion decreases in the presence of ethylene glycol and hence acts as a self inhibitor in the coolants; but it requires inhibitor for warranted service of the coolants (Song and StJohn 2004).

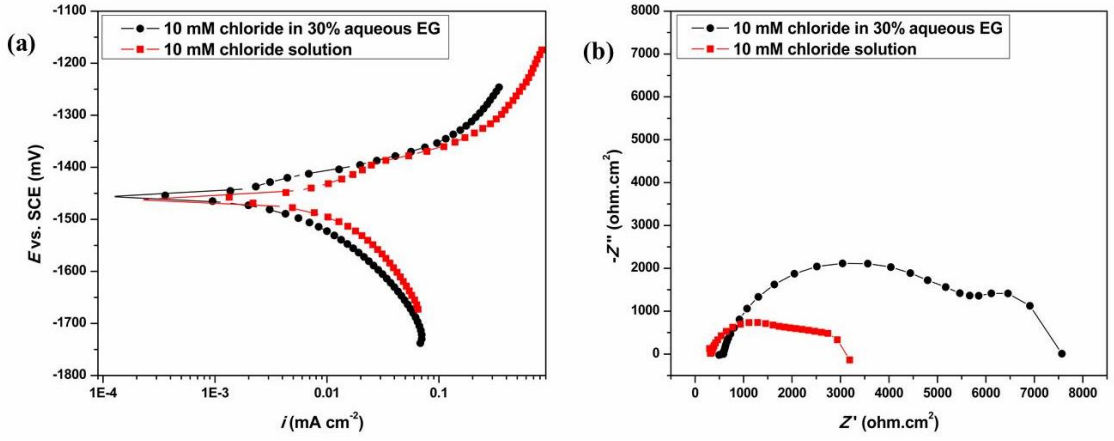

Fig. 3.20 (a) Potentiodynamic polarization plots (b) Nyquist plots for the corrosion of Mg-Al-Zn alloy in 10 mM chloride solution, in the presence and in the absence of 30% ethylene glycol at 30 °C.

3.2.2. Potentiodynamic polarization analyses

The corrosion inhibition property of the surfactant SDBS on Mg-Al-Zn alloy was studied in 30% aqueous ethylene glycol containing different concentrations of aggressive ions in a temperature range of 30 °C to 50 °C. Fig. 3.21 (a) and Fig. 3.21 (b) show the potentiodynamic polarization curves for the corrosion of Mg-Al-Zn alloy in 10 mM chloride and 10 mM sulfate medium, respectively, at 30 °C and 40 °C in the presence of different concentrations of SDBS.

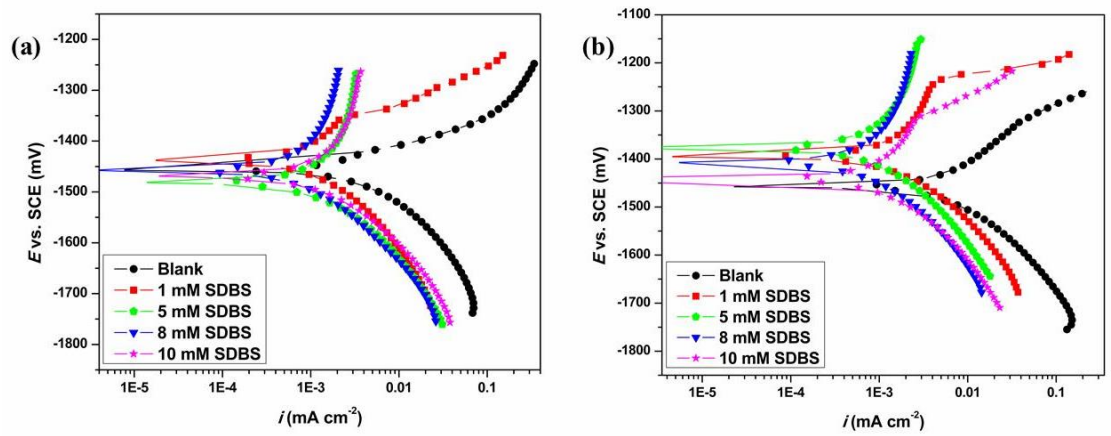

Fig. 3.21 Potentiodynamic polarization plots for the corrosion of Mg-Al-Zn alloy in different concentrations of SDBS in a corrosive medium of (a) 10 mM chloride ions at 30 °C (b) 10 mM sulfate ions at 40 °C.

The maximum inhibition effect was observed in the presence of 8 mM SDBS in chloride and sulfate media and hence the same concentration was considered for further inhibition studies in combination with TSP. Fig. 3.22 (a) and Fig. 3.22 (b) show the potentiodynamic polarization curves for the corrosion of Mg-Al-Zn alloy in the presence of different concentrations of TSP and 8 mM SDBS in 10 mM chloride and 2 mM sulfate media at 30 °C and 50 °C, respectively. In Fig. 3.21 and Fig. 3.22 anodic curves represent the dissolution of magnesium alloy whereas the cathodic curves represent the hydrogen evolution reaction.

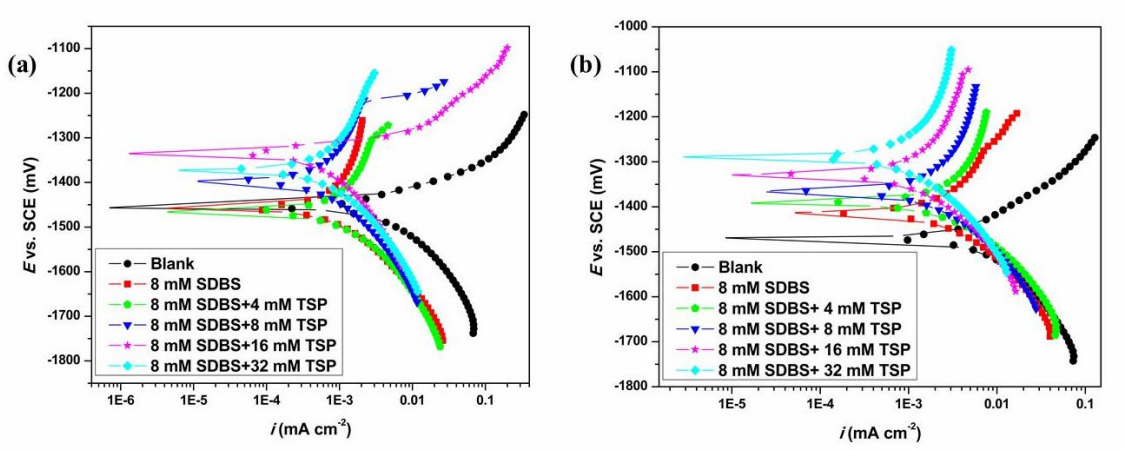

Fig. 3.22 Potentiodynamic polarization plots for the corrosion of Mg-Al-Zn alloy in different concentrations of TSP and 8 mM SDBS in a corrosive medium of (a) 10 mM chloride ions at 30 °C and (b) 2 mM sulfate ions at 50 °C.

The polarization parameters such as i_{corr}, E_{corr} and b_c were obtained by extrapolating the cathodic branch of the polarization curve to the open circuit potential. Corrosion rate and percentage inhibition efficiency, η (%) were calculated using equation 2.1 and 2.3, as stated in chapter 2. The obtained potentiodynamic polarization parameters for the corrosion of Mg-Al-Zn alloy in chloride and sulfate media containing 8 mM SDBS and different concentrations of TSP at different temperatures are tabulated in Table 3.7 (a), Table 3.7 (b), Table 3.7 (c) and Table 3.8 (a), Table 3.8 (b), Table 3.8 (c), respectively.

The change in the value of E_{corr} in the presence of 8 mM SDBS is insignificant in comparision with the E_{corr} values of the alloy in the absence of inhibitor. The shift in E_{corr} value upon the addition of TSP along with SDBS, is more than 85 mV vs SCE towards anodic direction. In general any compound can be classified into anodic or cathodic type of corrosion inhibitor, if a minimum corrosion potential shift should be of 85 mV from the corrosion potential value of the blank (Fekry and Ameer 2010, Torres et al. 2011). Therefore mixture of SDBS and TSP can be considered as an anodic type inhibitor. It is also observed that the corrosion current density decreases as the concentrations of TSP increases. It is evident from Fig. 3.22 (a) and Fig. 3.22

(b) that the anodic region gets passivated in the presence of TSP. The observations indicate that the mixture of inhibitors suppress the anodic reaction more than the cathodic reaction. The anodic polarization curves also show points of inflection at higher potentials like in the absence of inhibitor. The values of i_{corr} are minimum and the inhibition efficiencies are maximum when the ratio of SDBS to TSP is 1:2. Beyond this ratio, the inhibition efficiency does not change significantly.

3.2.3. Electrochemical impedance spectroscopy

The results of EIS studies give the information regarding the interfacial process of adsorption of inhibitor on the alloy surface (Mansfeld 1990). Fig. 3.23 (a) and Fig. 3.23 (b) show the Nyquist plots for the corrosion of Mg-Al-Zn alloy in the presence of different concentrations of SDBS in a corrosive media of 10 mM chloride ions at 30 °C and 10 mM sulfate ions at 40 °C, respectively. In line with the results of potentiodynamic results, highest inhibition efficiency was achieved with 8 mM concentration of SDBS, and the same concentration was considered for further inhibition study, in combination with TSP. Fig. 3.24 (a) and Fig. 3.24 (b) show the Nyquist plots for the corrosion of Mg-Al-Zn alloy in the presence of different concentrations of TSP and 8 mM SDBS in 10 mM chloride and 2 mM sulfate media at 30 °C and 50 °C, respectively.

These Nyquist plots consist of two depressed semicircles at higher and medium frequency regions and the beginning of an inductive loop at lower frequency region. The addition of SDBS increases the diameter of the semicircles, which indicates the reduced corrosion rate. But in the presence of TSP, the diameter of the medium frequency semicircle shows the larger size increase, which indicates the formation of adsorbed film of inhibitor mixture on the passivation film (Frignani et al. 2012), converting the surface film compact and complete; and making the ingress of the electrolyte on to the alloy surface more difficult.

In order to understand the electrochemical behavior of the interface between the alloy and medium electrochemical results are simulated by using equivalent

electrical circuit. The equivalent electrical circuit explained in the section 3.1.2 was used to simulate the electrochemical impedance data points. The value of η (%) was calculated from the equation 2.3 and 2.5 as stated in the chapter-2. The impedance parameters for the corrosion of Mg-Al-Zn alloy in the presence of different concentrations of TSP and 8 mM SDBS in the corrosive medium containing different concentration of chloride and sulfate ions at different temperature are shown in Table 3.9 (a), Table 3.9 (b), Table 3.9 (c) and Table 3.10 (a), Table 3.10 (b), Table 3.10 (c), respectively.

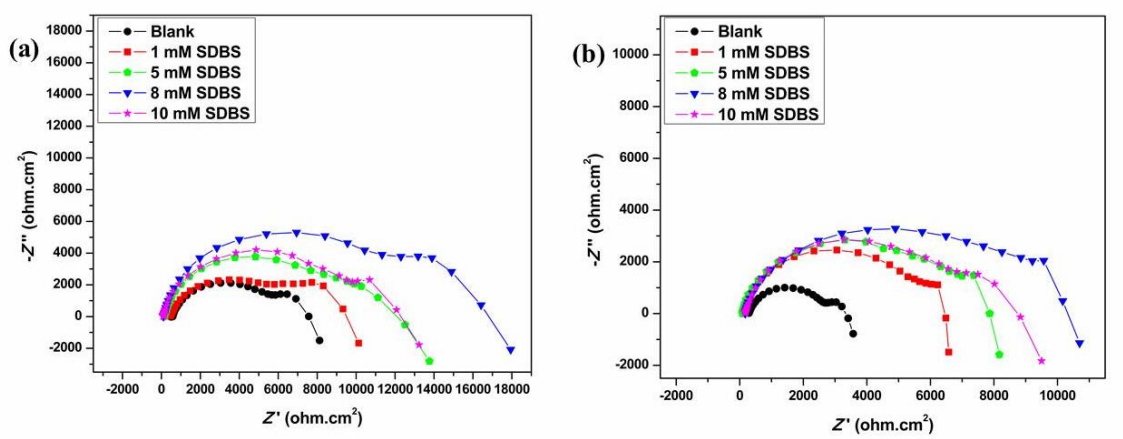

Fig. 3.23 Nyquist plots for the corrosion of Mg-Al-Zn alloy in different concentrations of SDBS in a corrosive medium of (a) 10 mM chloride ions at 30 °C and (b) 10 mM sulfate ions at 40 °C.

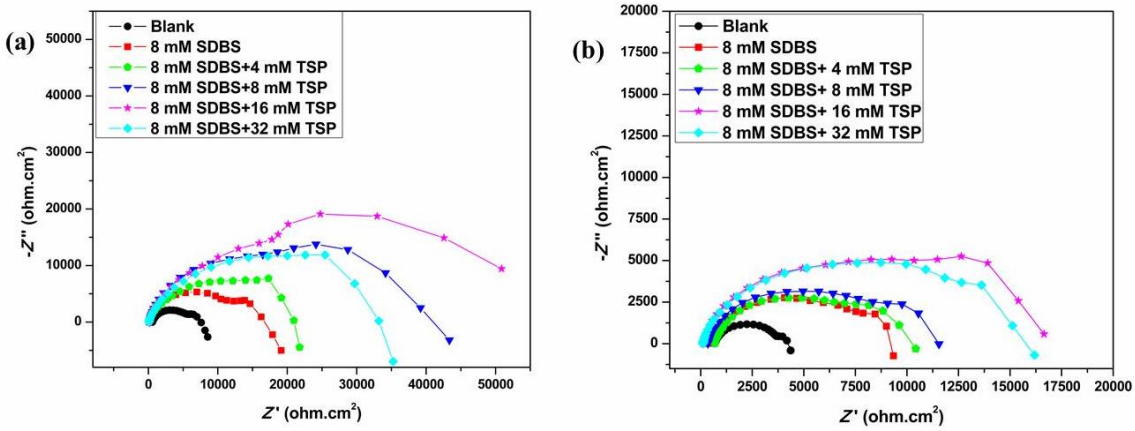

Fig. 3.24 Nyquist plots for the corrosion of Mg-Al-Zn alloy in different concentrations of TSP and 8 mM SDBS in a corrosive medium of (a) 10 mM chloride ions at 30 °C and (b) 2 mM sulfate ions at 50 °C.

The addition of inhibitor replaces the previously adsorbed ethylene glycol and water molecules. Therefore, with the increase in the concentration of the inhibitor mixture, the impedance parameters are bound to change. The increase in the value of R_f on the addition of inhibitor mixtures signifies the increased protection of the surface film; and the increase in R_{dif} indicates the increased hindrance for the diffusion of ions through the surface film. The decreased values of C_f and C_{dif} demonstrate the increased electrical double layer thickness and reduction in the dielectric constant. The changes in the values of R_f and C_f in the presence of inhibitors, indicate the incorporation of inhibitor molecules in the surface film, rendering it compact with less defects. The variation in the values of inhibition efficiency with the increase in the concentration of TSP is in good agreement with those obtained from potentiodynamic polarization studies. Huang et al., have found that with the increasing concentration of TSP and the decreasing concentration of SDBS, i.e., with the increased ratio of TSP to SDBS, the inhibitor film formed on the surface of the alloy becomes more and more thin. Therefore inhibitor efficiency decreases with the increasing concentration of TSP after certain ratio of TSP (Huang et al. 2011).

Frequency specific impedance behavior of the system is described by Bode plots, whereas Nyquist plots do not show the specific frequency where the data points are recorded. Fig. 3.25 (a) and Fig. 3.25 (b) show the Bode magnitude plots for the corrosion of Mg-Al-Zn alloy in the presence of different concentrations of TSP and 8 mM SDBS in 10 mM chloride and 2 mM sulfate media at 30 °C and 50 °C, respectively, and Fig. 3.26 (a) and Fig. 3.26 (b) show the corresponding Bode phase angle plots. Bode plots demonstrate that, the addition of TSP increases the low frequency impedance modulus (Z_{mod}) and the medium frequency phase maximum (θ_{max}). The increase in the values of Z_{mod} and θ_{max} indicate the good inhibition effect of the inhibitor. The medium frequency phase maximum accounts for the corrosive species diffusion through the surface film. As the value of θ_{max} increases, the diffusion of the corrosive species through the surface film decreases, thereby

increasing the protection value of the surface film on the alloy surface (Gao et al. 2010).

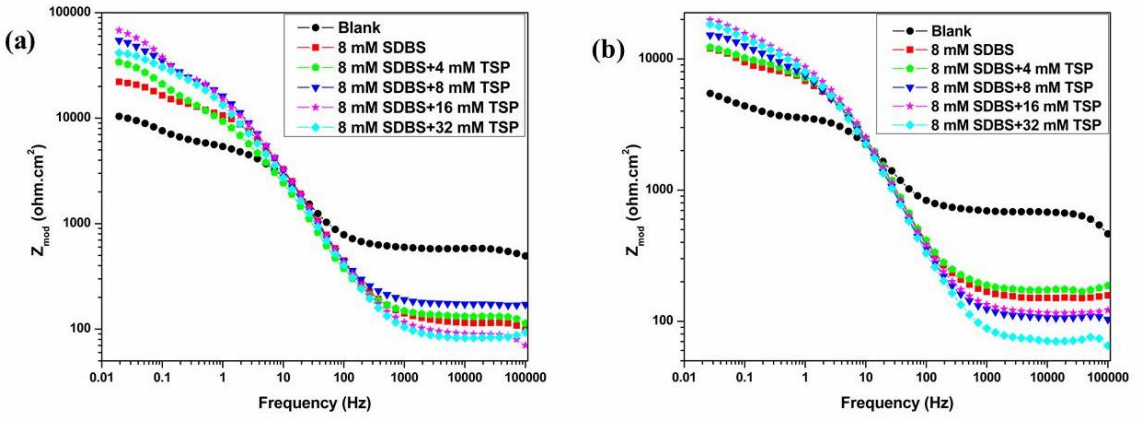

Fig. 3.25 Bode magnitude plots for the corrosion of Mg-Al-Zn alloy in different concentrations of TSP and 8 mM SDBS in a corrosive medium of (a) 10 mM chloride ions at 30 °C and (b) 2 mM sulfate ions at 50 °C.

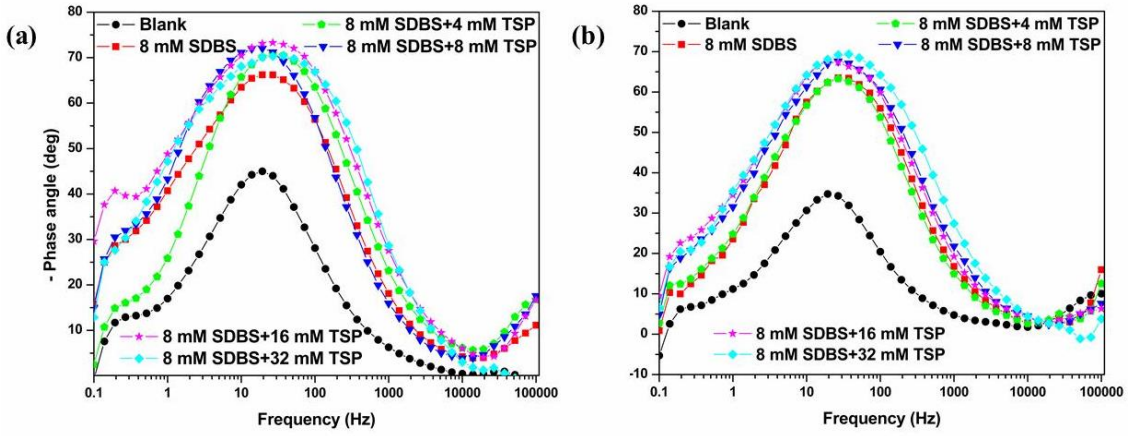

Fig. 3.26 Bode phase angle plots for the corrosion of Mg-Al-Zn alloy in different concentrations of TSP and 8 mM SDBS in a corrosive medium of (a) 10 mM chloride ions at 30 °C and (b) 2 mM sulfate ions at 50 °C.

3.2.4. Effect of temperature

The increase in the temperature of the medium influences the rate of corrosion and also the inhibition efficiency of the inhibitor (Uhlig and Revie 2008). The

electrochemical parameters summarized in Table 3.7, Table 3.8, Table 3.9 and Table 3.10 indicate that the inhibition efficiency decreases with the increase in the temperature of the media. The decrease in the values of R_f and R_{dif}, as observed in the impedance parameters, indicate the reduction in the effectiveness of the inhibitor surface film to protect the alloy surface. This could be attributed to the increased desorption of the inhibitor molecules from the surface of the alloy as the temperature increases, which is the characteristic features of physisorption (Antropov 1967).

The effect of variation in the temperature on the interaction between the metal and inhibitor can be used to assess the important activation parameters. Arrhenius law equation mentioned in the equation 2.6 of the chapter-2 was used to calculate E_a for the corrosion of the alloy in the absence and in the presence of inhibitors. Arrhenius plots for the corrosion of Mg-Al-Zn alloy in a corrosive solution containing 10 mM chloride ions and 2 mM sulfate ions are shown in Fig. 3.27 (a) and Fig. 3.27 (b), respectively.

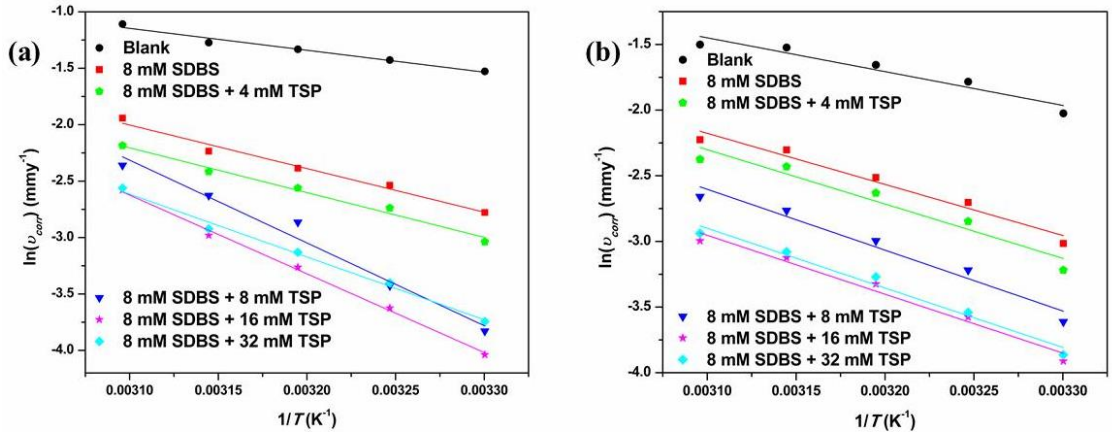

Fig. 3.27 Arrhenius plots for the corrosion of Mg-Al-Zn alloy in the presence of 8 mM SDBS and different concentrations of TSP in a corrosive solution of (a) 10 mM chloride ions and (b) 2 mM sulfate ions.

Apparent enthalpy of activation and apparent entropy of activation were calculated from the transition state theory equation 2.7 presented in chapter-2. Fig. 3.28 (a) and Fig. 3.28 (b) show the plots of ln (υ_{corr}/T) versus ($1/T$) for the corrosion of

Mg-Al-Zn alloy in a corrosive solution containing 10 mM chloride ions and 2 mM sulfate ions, respectively. Table 3.11 and Table 3.12 list the calculated activation parameters. The value of E_a is higher in the presence of the inhibitors than that in the absence of inhibitors; and E_a value increases with the increase in the concentration of inhibitor. Activation energy indicates the energy barrier for the occurrence of corrosion (Schorr and Yahalom 1972). Increase in the concentration of inhibitor energetically hinders the Mg-Al-Zn alloy corrosion by forming the denser surface film on the alloy surface through adsorption.

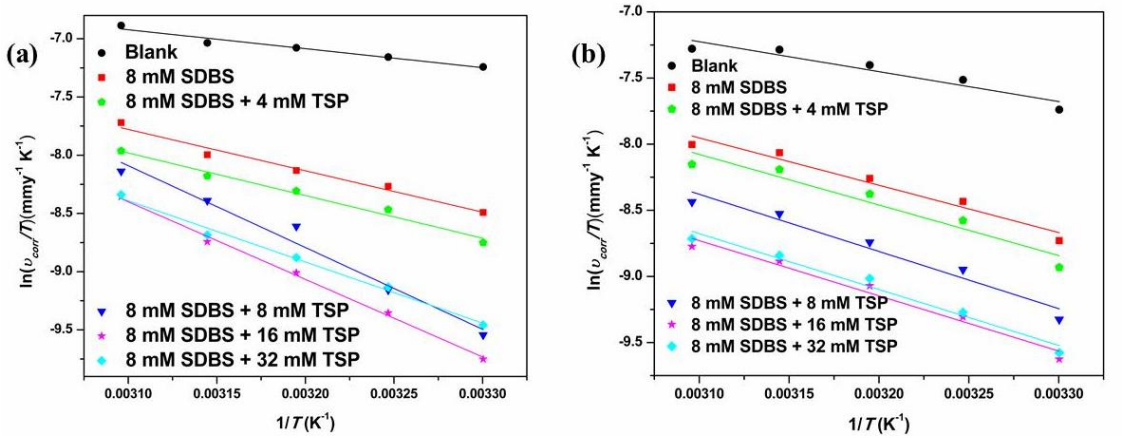

Fig. 3.28 Plots of ln (υ_{corr}/T) versus ($1/T$) for the corrosion of Mg-Al-Zn alloy in the presence of 8 mM SDBS and different concentrations of TSP in a corrosive solution of (a) 10 mM chloride ions and (b) 2 mM sulfate ions.

3.2.5. Adsorption isotherm

Adsorption isotherm explains the nature of interaction between the inhibitor molecule and the surface of the alloy. It is defined as a graphical representation of the variation in the extent of inhibitor adsorption on the surface of the alloy at constant temperature and varies with pressure or concentration of the inhibitor. In aqueous solution the surface of the alloy is always covered by adsorbed water molecules. During the inhibition process inhibitor molecules substitute the previously adsorbed water molecules and get adsorbed on the surface as represented in the following equation:

$$(\text{Inhibitor})_{\text{solution}} + (\chi\, H_2O)_{\text{adsorbed}} \rightleftharpoons (\text{Inhibitor})_{\text{adsorbed}} + (\chi\, H_2O)_{\text{solution}} \qquad (3.11)$$

In the above equation χ denotes the number of the water molecules displaced upon the adsorption of single inhibitor molecule. The value of χ depends on the individual inhibitor and surface charge on the alloy.

The surface coverage (θ), decides the efficiency of the adsorbed inhibitor on the surface of the alloy. The equation 2.3 was used to calculate the value of θ at different concentrations of TSP (C_{inh}). Attempts were made to fit the values of θ and C_{inh} graphically, into different adsorption isotherms such as Langmuir, Temkin, Frumkin and Flory–Huggins isotherms, etc. However, the best graphical fitment with linear regression coefficient (R^2) close to one was obtained with Langmuir isotherm, which is given by the following equation.

$$\frac{C_{\text{inh}}}{\theta} = C_{\text{inh}} + \left(\frac{1}{K}\right) \qquad (3.12)$$

In the above equation K is the equilibrium constant for the adsorption-desorption process on the surface of the alloy.

Fig. 3.29 (a) and Fig. 3.29 (b) represents the Langmuir adsorption isotherms for the adsorption of TSP on the surface of the Mg-Al-Zn alloy in corrosive medium containing 10 mM chloride ions and 2 mM sulfate ions, respectively at different temperatures. The value of K was evaluated from the reciprocal of the intercept of the plots.

The thermodynamic parameters such as standard free energy of adsorption ($\Delta G°_{\text{ads}}$), standard enthalpy of adsorption ($\Delta H°_{\text{ads}}$) and standard entropy of adsorption ($\Delta S°_{\text{ads}}$) were evaluated using the reaction isotherm equation and Gibbs-Helmholtz equation mentioned in the equation 2.8 and 2.9. The calculated thermodynamic parameters at different temperatures for the adsorption of TSP on Mg-Al-Zn alloy surface in corrosive medium containing different concentration of chloride and sulfate ions are enlisted in Table 3.13 and Table 3.14, respectively. The average linear regression coefficient (R^2) was close but not equal to unity, indicating a slight deviation from the ideal Langmuir isotherm. This deviation may be due to the consequence of mutual interaction of the adsorbed inhibitor molecules on the surface

of the alloy (Masel 1996). The values of standard free energy of adsorption are negative and in between −27.22 to −31.36 kJ mol^{-1}. In general the values of standard free energy of adsorption −20 kJ mol^{-1} and −40 kJ mol^{-1} indicate the threshold energy for physisorption and chemisorption processes. In the current study the obtained values indicate the adsorption of the inhibitor molecules through physisorption as well as chemisorption type. But the values of standard enthalpy of adsorption indicate the predominant physisorption process, whereas chemisorption involves the formation of strong covalent bonds and the values are almost 100 kJ mol^{-1} (Martinez and Stern 2002, Bentiss et al. 2005).

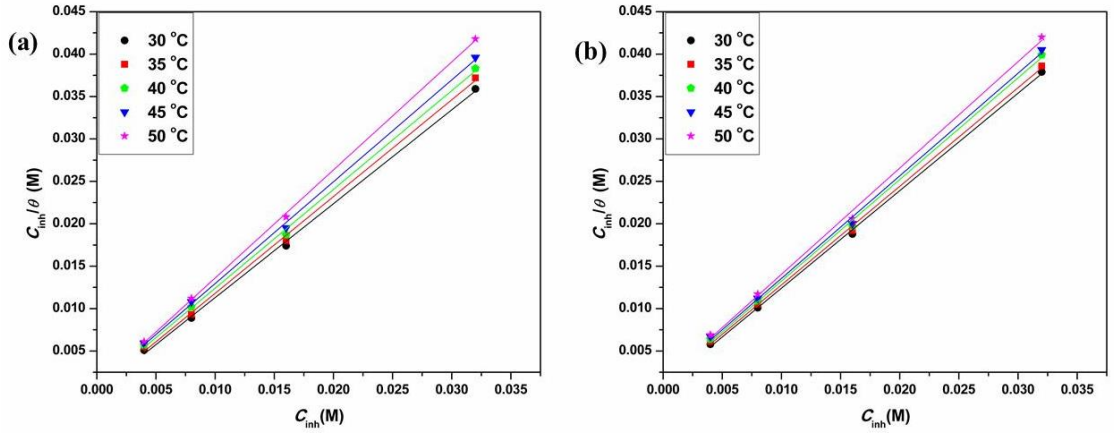

Fig. 3.29 Langmuir adsorption isotherms for the adsorption of TSP on Mg-Al-Zn alloy surface at different temperatures in a corrosive medium of (a) 10 mM chloride ions and (b) 2 mM sulfate ions.

3.2.6. Surface analyses

Surface analyses were carried out to examine the surface morphology of the Mg-Al-Zn alloy in corrosive media containing inhibitors. The surface of the Mg-Al-Zn alloy was studied by utilizing SEM and EDX techniques. Fig. 3.30 (a) and Fig. 3.30 (b) show the SEM image and EDX spectra of the Mg-Al-Zn alloy after 24 h of immersion in the corrosive medium of 10 mM chloride ions containing 8 mM SDBS. Fig. 3.31 (a) and Fig. 3.31 (b) show the same in 10 mM sulfate medium. It is seen

from Fig. 3.30 (a) and Fig. 3.31 (a) that in the presence of SDBS, the alloy surface is relatively less deteriorated as compared in the absence of it.

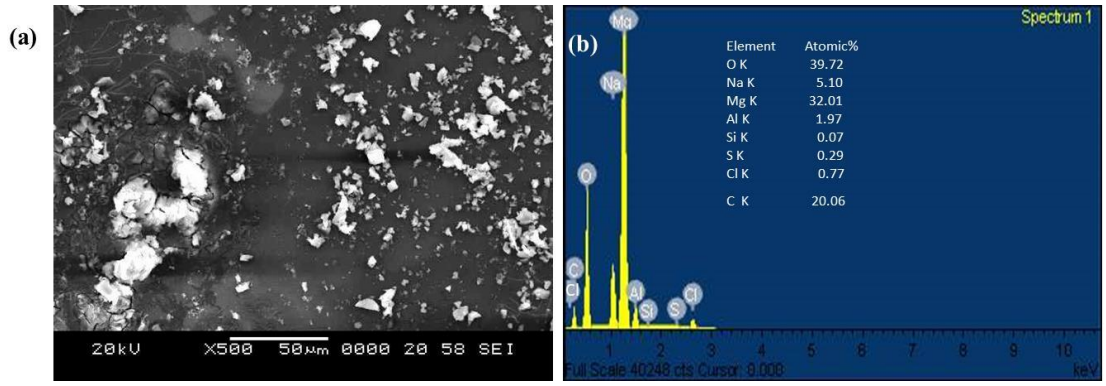

Fig. 3.30 (a) SEM image of Mg-Al-Zn alloy surface after 24 h of immersion in the corrosive medium of 10 mM chloride solution containing 8 mM SDBS and (b) the corresponding EDX spectra.

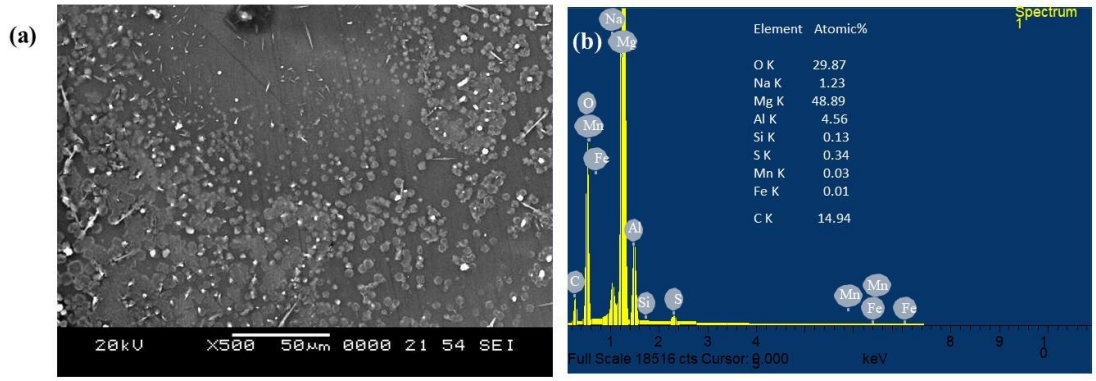

Fig. 3.31 (a) SEM image of Mg-Al-Zn alloy surface after 24 h of immersion in the corrosive medium of 10 mM sulfate solution containing 8 mM SDBS and (b) the corresponding EDX spectra.

In Fig. 3.30 (b) intense peaks of carbon, chlorine, sodium and sulfur along with magnesium and oxygen were observed and in Fig. 3.31 (b) except chlorine peak all other peaks as in Fig. 3.30 (b) were noticed. The observed peaks might be due to the adsorption of SDBS and presence of electrolyte on the surface of the alloy.

Fig. 3.32 (a) and Fig. 3.32 (b) show the SEM image and EDX spectrum of the Mg-Al-Zn alloy after 24 h of immersion in the corrosive medium of 10 mM chloride ions containing 8 mM SDBS and 16 mM TSP. Fig. 3.33 (a) and Fig. 3.33 (b) show the same in 10 mM sulfate medium. In the presence of TSP, the surface is still less deteriorated with a mud crack appearance, which could be due to the dehydration of the film in the vacuum of the SEM chamber. Peak of phosphorous in Fig. 3.32 (b) and Fig. 3.33 (b) indicates the presence of phosphate on the surface of the alloy, might be due to the formation of $Mg_3(PO_4)_2$ in the presence of TSP.

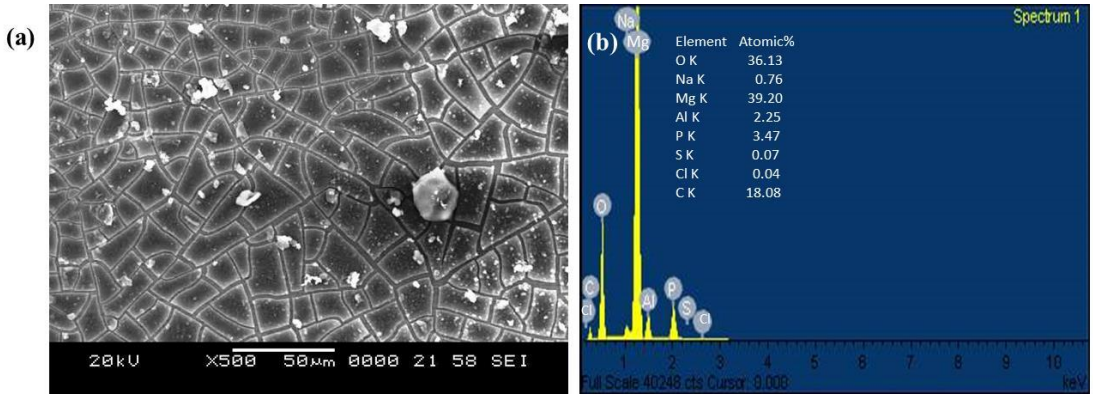

Fig. 3.32 (a) SEM image of Mg-Al-Zn alloy surface after 24 h of immersion in the corrosive medium of 10 mM chloride solution containing 8 mM SDBS and 16 mM TSP and (b) the corresponding EDX spectra.

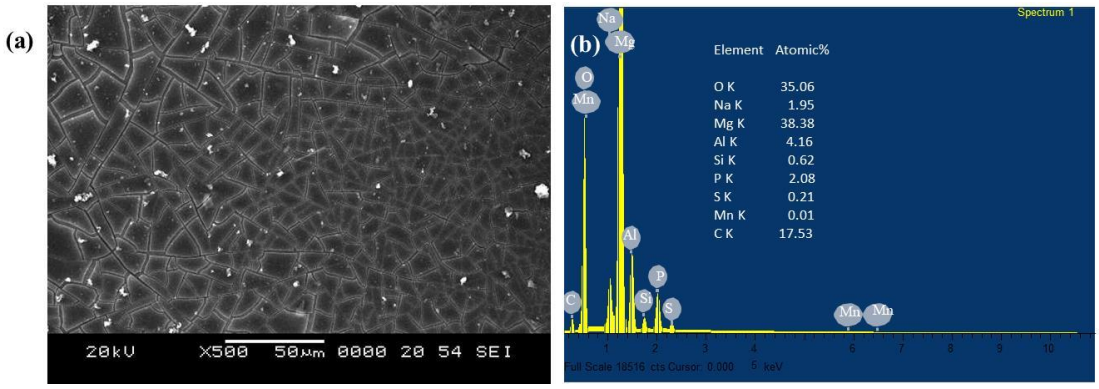

Fig. 3.33 (a) SEM image of Mg-Al-Zn alloy surface after 24 h of immersion in the corrosive medium of 10 mM sulfate solution containing 8 mM SDBS and 16 mM TSP and (b) the corresponding EDX spectra.

Table 3.7 (a) Potentiodynamic polarization parameters for the corrosion of Mg-Al-Zn alloy in 30% aqueous ethylene glycol containing 2 mM chloride ions, 8 mM SDBS and different concentrations of TSP at different temperatures.

Temperature (°C)	Inhibitor concentration (mM)	E_{corr} vs. SCE (mV)	i_{corr} (μA cm^{-2})	$-b_c$ (mV dec^{-1})	η (%)
30	Blank	−1476	4.58	356	-
	8 (SDBS)	−1423	2.06	310	55.0
	4 (TSP)	−1376	1.47	290	67.9
	8	−1258	0.87	279	81.0
	16	−1268	0.73	274	84.1
	32	−1274	0.69	255	84.9
35	Blank	−1466	5.36	363	-
	8 (SDBS)	−1510	2.52	305	53.0
	4 (TSP)	−1430	1.99	284	62.9
	8	−1340	1.16	263	78.4
	16	−1231	0.97	243	81.9
	32	−1286	1.03	220	80.8
40	Blank	−1486	6.02	332	-
	8 (SDBS)	−1469	3.09	291	48.7
	4 (TSP)	−1363	2.53	269	58.0
	8	−1326	1.73	250	71.3
	16	−1263	1.25	238	79.2
	32	−1228	1.27	213	78.9
45	Blank	−1470	6.79	370	-
	8 (SDBS)	−1471	3.85	306	43.3
	4 (TSP)	−1352	3.00	281	55.8
	8	−1332	2.20	276	67.6
	16	−1226	1.60	253	76.4
	32	−1254	1.62	235	76.1
50	Blank	−1379	7.85	442	-
	8 (SDBS)	−1460	4.74	308	39.6
	4 (TSP)	−1338	3.72	286	52.6
	8	−1302	2.73	272	65.2
	16	−1262	2.10	266	73.2
	32	−1268	2.12	263	73.0

Table 3.7 (b) Potentiodynamic polarization parameters for the corrosion of Mg-Al-Zn alloy in 30% aqueous ethylene glycol containing 6 mM chloride ions, 8 mM SDBS and different concentrations of TSP at different temperatures.

Temperature (°C)	Inhibitor concentration (mM)	E_{corr} vs. SCE (mV)	i_{corr} (μA cm^{-2})	$-b_c$ (mV dec^{-1})	η (%)
30	Blank	−1499	6.85	270	-
	8 (SDBS)	−1535	2.76	241	59.7
	4 (TSP)	−1399	1.88	234	72.6
	8	−1409	1.04	228	84.8
	16	−1315	0.83	217	87.9
	32	−1247	0.90	201	86.9
35	Blank	−1445	9.53	279	-
	8 (SDBS)	−1494	4.20	255	55.9
	4 (TSP)	−1391	2.95	252	69.0
	8	−1372	1.77	237	81.4
	16	−1287	1.43	222	85.0
	32	−1320	1.60	218	83.2
40	Blank	−1433	10.59	297	-
	8 (SDBS)	−1435	5.15	287	51.4
	4 (TSP)	−1373	3.59	273	66.1
	8	−1328	2.66	255	74.9
	16	−1316	1.83	247	82.7
	32	−1258	2.01	228	81.0
45	Blank	−1420	11.68	317	-
	8 (SDBS)	−1449	5.88	290	49.7
	4 (TSP)	−1399	4.25	274	63.6
	8	−1261	3.30	262	71.7
	16	−1314	2.38	240	79.6
	32	−1276	2.49	219	78.7
50	Blank	−1428	12.82	338	-
	8 (SDBS)	−1448	6.86	307	46.5
	4 (TSP)	−1336	5.12	271	60.1
	8	−1329	4.00	234	68.8
	16	−1281	3.13	227	75.6
	32	−1272	3.22	206	74.9

Table 3.7 (c) Potentiodynamic polarization parameters for the corrosion of Mg-Al-Zn alloy in 30% aqueous ethylene glycol containing 10 mM chloride ions, 8 mM SDBS and different concentrations of TSP at different temperatures.

Temperature (°C)	Inhibitor concentration (mM)	E_{corr} vs. SCE (mV)	i_{corr} (μA cm^{-2})	$-b_c$ (mV dec^{-1})	η (%)
30	Blank	−1458	10.09	286	-
	8 (SDBS)	−1459	2.89	295	71.4
	4 (TSP)	−1466	2.23	274	77.9
	8	−1397	1.01	238	90.0
	16	−1340	0.82	248	91.9
	32	−1374	1.10	251	89.1
35	Blank	−1446	11.18	269	-
	8 (SDBS)	−1497	3.68	261	67.1
	4 (TSP)	−1400	3.01	254	73.1
	8	−1279	1.51	237	86.5
	16	−1317	1.24	246	88.9
	32	−1345	1.55	231	86.1
40	Blank	−1416	12.27	310	-
	8 (SDBS)	−1369	4.28	270	65.1
	4 (TSP)	−1390	3.59	241	70.7
	8	−1351	2.65	239	78.4
	16	−1355	1.78	228	85.5
	32	−1319	2.03	213	83.5
45	Blank	−1461	13.05	306	-
	8 (SDBS)	−1414	4.98	260	61.8
	4 (TSP)	−1351	4.15	246	68.2
	8	−1315	3.36	241	74.3
	16	−1299	2.36	232	81.9
	32	−1331	2.50	226	80.8
50	Blank	−1405	15.37	339	-
	8 (SDBS)	−1360	6.67	266	56.6
	4 (TSP)	−1347	5.23	245	66.0
	8	−1283	4.39	237	71.4
	16	−1278	3.53	220	77.0
	32	−1287	3.59	217	76.6

Table 3.8 (a) Potentiodynamic polarization parameters for the corrosion of Mg-Al-Zn alloy in 30% aqueous ethylene glycol containing 2 mM sulfate ions, 8 mM of SDBS and different concentrations of TSP at different temperatures.

Temperature (°C)	Inhibitor concentration (mM)	E_{corr} vs. SCE (mV)	i_{corr} (μA cm^{-2})	$-b_c$ (mV dec^{-1})	η (%)
30	Blank	−1546	6.14	284	-
	8 (SDBS)	−1447	2.27	254	63.0
	4 (TSP)	−1377	1.87	278	69.6
	8	−1342	1.28	251	79.2
	16	−1478	0.92	241	85.1
	32	−1300	0.95	245	84.5
35	Blank	−1556	7.80	349	-
	8 (SDBS)	−1505	3.11	251	60.2
	4 (TSP)	−1446	2.68	229	65.6
	8	−1465	1.85	203	76.2
	16	−1445	1.30	171	83.3
	32	−1406	1.34	197	82.8
40	Blank	−1469	8.90	311	-
	8 (SDBS)	−1428	3.77	254	57.6
	4 (TSP)	−1421	3.33	233	62.5
	8	−1431	2.34	221	73.7
	16	−1367	1.69	208	81.0
	32	−1334	1.77	228	80.2
45	Blank	−1463	10.15	309	-
	8 (SDBS)	−1415	4.63	286	54.4
	4(TSP)	−1439	4.11	259	59.5
	8	−1413	2.92	230	71.3
	16	−1349	2.04	194	79.9
	32	−1293	2.13	220	79.1
50	Blank	−1468	10.36	285	-
	8 (SDBS)	−1435	5.03	271	51.4
	4 (TSP)	−1392	4.35	247	58.0
	8	−1368	3.27	225	68.5
	16	−1329	2.32	216	77.6
	32	−1290	2.46	228	76.3

Table 3.8 (b) Potentiodynamic polarization parameters for the corrosion of Mg-Al-Zn alloy in 30% aqueous ethylene glycol containing 6 mM sulfate ions, 8 mM of SDBS and different concentrations of TSP at different temperatures.

Temperature (°C)	Inhibitor concentration (mM)	E_{corr} vs. SCE (mV)	i_{corr} (μA cm^{-2})	$-b_c$ (mV dec^{-1})	η (%)
30	Blank	−1566	9.47	308	-
	8 (SDBS)	−1446	3.08	250	67.5
	4 (TSP)	−1471	2.64	232	72.1
	8	−1461	1.42	189	85.0
	16	−1324	0.70	162	92.7
	32	−1309	0.71	153	92.5
35	Blank	−1520	10.79	373	-
	8 (SDBS)	−1414	3.76	260	65.2
	4 (TSP)	−1415	3.14	269	70.9
	8	−1483	1.96	220	81.8
	16	−1388	0.96	214	91.1
	32	−1402	1.26	228	88.3
40	Blank	−1513	11.81	376	-
	8 (SDBS)	−1392	4.36	283	63.0
	4 (TSP)	−1422	3.68	280	68.9
	8	−1439	2.58	228	78.1
	16	−1385	1.21	208	89.7
	32	−1365	1.51	231	87.2
45	Blank	−1500	12.87	379	-
	8 (SDBS)	−1388	5.10	282	60.4
	4 (TSP)	−1408	4.22	235	67.2
	8	−1442	3.01	225	76.6
	16	−1374	1.60	180	87.6
	32	−1324	1.72	191	86.6
50	Blank	−1446	14.63	335	-
	8 (SDBS)	−1405	6.32	290	56.8
	4 (TSP)	−1385	4.99	247	65.9
	8	−1403	3.78	238	74.2
	16	−1351	2.22	228	84.8
	32	−1305	2.38	230	83.8

Table 3.8 (c) Potentiodynamic polarization parameters for the corrosion of Mg-Al-Zn alloy in 30% aqueous ethylene glycol containing 10 mM sulfate ions, 8 mM of SDBS and different concentrations of TSP at different temperatures.

Temperature (°C)	Inhibitor concentration (mM)	E_{corr} vs. SCE (mV)	i_{corr} (μA cm^{-2})	$-b_c$ (mV dec^{-1})	η (%)
30	Blank	−1530	11.68	386	-
	8 (SDBS)	−1495	3.12	217	73.3
	4 (TSP)	−1453	2.38	184	79.6
	8	−1479	1.21	169	89.6
	16	−1413	0.61	152	94.8
	32	−1357	0.62	154	94.7
35	Blank	−1521	12.65	402	-
	8 (SDBS)	−1430	3.99	280	68.5
	4 (TSP)	−1442	3.01	169	76.2
	8	−1478	1.70	143	86.6
	16	−1434	0.96	139	92.4
	32	−1409	1.13	151	91.1
40	Blank	−1460	14.43	344	-
	8 (SDBS)	−1412	4.92	257	65.9
	4 (TSP)	−1417	3.65	194	74.7
	8	−1460	2.17	183	85.0
	16	−1403	1.43	176	90.1
	32	−1394	1.54	168	89.3
45	Blank	−1458	15.82	327	-
	8 (SDBS)	−1406	5.80	269	63.3
	4 (TSP)	−1405	4.62	218	70.8
	8	−1427	3.16	200	80.0
	16	−1415	1.87	187	88.2
	32	−1372	1.91	174	87.9
50	Blank	−1462	17.49	318	-
	8 (SDBS)	−1400	6.94	242	60.3
	4 (TSP)	−1393	5.59	248	68.0
	8	−1423	4.15	224	76.3
	16	−1387	2.32	203	86.7
	32	−1322	2.39	206	86.3

Table 3.9 (a) Electrochemical impedance parameters for the corrosion of Mg-Al-Zn alloy in 30% aqueous ethylene glycol containing 2 mM chloride ion, 8 mM SDBS and different concentrations of TSP at different temperatures.

Temperature (°C)	Inhibitor concentration (mM)	R_f (Ω cm²)	R_{dif} (Ω cm²)	R_p (Ω cm²)	C_f (μF cm^{-2})	C_{dif} (μF cm^{-2})	η (%)
30	Blank	4053	1888	9501	23.4	186.1	-
	8 (SDBS)	9354	3070	19680	20.5	121.7	51.7
	4 (TSP)	14420	8190	30570	19.3	109.2	68.9
	8	17910	12450	49140	18.7	83.4	80.7
	16	28570	18160	60540	16.3	56.5	84.3
	32	28420	9845	51965	16.4	68.1	81.7
35	Blank	3885	1738	8034	24.4	195.1	-
	8 (SDBS)	8666	2944	15794	21.4	148.5	49.1
	4 (TSP)	12245	6718	22748	20.0	123.0	64.7
	8	16330	10320	35190	19.4	110.3	77.2
	16	26410	12010	45830	17.4	77.4	82.5
	32	22000	12510	41790	18.0	69.7	80.8
40	Blank	3269	1659	6932	25.6	208.3	-
	8 (SDBS)	7020	2868	13188	23.0	156.5	47.4
	4 (TSP)	10417	5102	17352	21.9	144.2	60.1
	8	15490	7820	25270	20.4	125.5	72.6
	16	24040	9120	35380	19.1	112.8	80.4
	32	24340	8140	34020	19.3	118.2	79.6
45	Blank	3052	1587	6725	27.6	228.1	-
	8 (SDBS)	5927	2796	11592	24.9	177.3	42.0
	4 (TSP)	8900	3873	14833	23.9	158.2	54.7
	8	12790	4940	20870	21.3	139.8	67.8
	16	17010	8510	29910	20.2	121.4	77.5
	32	16660	4601	25181	20.6	130.4	73.3
50	Blank	2488	1503	5581	30.7	250.7	-
	8 (SDBS)	4613	2279	9086	26.8	191.0	38.6
	4 (TSP)	6492	2816	11291	25.3	171.4	50.6
	8	8313	3880	14740	23.0	142.0	62.1
	16	10020	6907	21427	20.9	129.3	74.0
	32	9590	4480	18840	21.3	138.6	70.4

Table 3.9 (b) Electrochemical impedance parameters for the corrosion of Mg-Al-Zn alloy in 30% aqueous ethylene glycol containing 6 mM chloride ion, 8 mM SDBS and different concentrations of TSP at different temperatures.

Temperature (°C)	Inhibitor concentration (mM)	R_f (Ω cm^2)	R_{dif} (Ω cm^2)	R_p (Ω cm^2)	C_f (μF cm^{-2})	C_{dif} (μF cm^{-2})	η (%)
30	Blank	3597	1820	7582	23.9	236.5	-
	8 (SDBS)	10428	2455	16365	15.5	190.4	53.7
	4 (TSP)	15200	8407	27487	13.4	157.1	72.4
	8	18090	11320	40120	12.4	123.0	81.1
	16	27750	14230	52500	10.8	108.5	85.6
	32	26020	12490	48890	11.1	116.7	84.5
35	Blank	2879	1713	6085	25.0	242.4	-
	8 (SDBS)	7045	2258	12170	16.2	209.1	50.0
	4 (TSP)	9845	7920	20420	14.1	174.8	70.2
	8	15450	10110	29830	13.3	151.2	79.6
	16	19260	13930	39540	12.3	132.3	84.6
	32	18570	11670	37010	12.5	135.3	83.6
40	Blank	2577	1608	4880	26.9	252.8	-
	8 (SDBS)	5674	1926	9595	17.1	226.1	49.1
	4 (TSP)	7668	6172	15236	15.4	200.4	68.0
	8	11810	8797	21057	14.2	173.4	76.8
	16	14800	11240	28210	13.1	158.8	82.7
	32	14620	10180	26660	13.5	165.1	81.7
45	Blank	2214	1569	4742	28.3	257.0	-
	8 (SDBS)	4890	1900	8399	19.0	245.3	43.5
	4 (TSP)	6272	4974	13523	17.6	231.0	64.9
	8	10450	6403	17733	16.7	218.6	73.3
	16	12600	10710	24980	15.1	198.0	81.0
	32	12280	9050	23100	15.7	203.2	79.5
50	Blank	1886	1487	4548	31.5	269.8	-
	8 (SDBS)	3493	1865	7571	23.9	250.0	39.9
	4 (TSP)	5572	4726	12172	21.5	242.3	62.6
	8	7642	5695	15168	20.4	224.8	70.0
	16	9720	6690	17830	18.8	203.4	74.5
	32	9520	5900	16930	19.4	209.2	73.1

Table 3.9 (c) Electrochemical impedance parameters for the corrosion of Mg-Al-Zn alloy in 30% aqueous ethylene glycol containing 10 mM chloride ion, 8 mM SDBS and different concentrations of TSP at different temperatures.

Temperature (°C)	Inhibitor concentration (mM)	R_f (Ω cm²)	R_{dif} (Ω cm²)	R_p (Ω cm²)	C_f (μF cm^{-2})	C_{dif} (μF cm^{-2})	η (%)
30	Blank	2102	1516	6915	25.4	302.1	-
	8 (SDBS)	11180	3770	19370	12.7	283.7	64.3
	4 (TSP)	16640	5003	23793	11.3	255.7	70.9
	8	20890	13850	44610	9.6	186.4	84.5
	16	36070	26970	68660	7.2	103.3	89.9
	32	25450	8340	36580	8.4	264.6	81.1
35	Blank	2002	1485	5509	25.8	320.1	-
	8 (SDBS)	9184	3591	14731	13.6	291.3	62.6
	4 (TSP)	11305	4970	17750	12.6	258.3	69.0
	8	19070	8515	34425	11.8	232.4	84.0
	16	22510	21580	48220	10.3	181.1	88.6
	32	19580	8660	28610	11.4	201.1	80.7
40	Blank	1823	1363	4411	29.4	332.1	-
	8 (SDBS)	6552	3312	11396	14.2	311.9	61.3
	4 (TSP)	7077	3810	13280	13.7	285.6	66.8
	8	11790	9100	23780	12.5	255.4	81.5
	16	14970	9695	28375	11.3	242.4	84.5
	32	12180	8090	22060	11.8	248.0	80.0
45	Blank	1733	1303	4156	32.7	337.3	-
	8 (SDBS)	5020	2803	9922	15.8	322.2	58.1
	4 (TSP)	6404	3686	12057	14.5	309.7	65.5
	8	8079	8850	18100	13.2	283.0	77.0
	16	11220	8944	22664	11.7	270.7	81.7
	32	8279	7950	18920	12.9	276.0	78.0
50	Blank	1434	1283	3969	36.1	345.4	-
	8 (SDBS)	4143	2636	8656	17.9	334.8	54.1
	4 (TSP)	5643	3040	10852	15.3	318.6	63.4
	8	6120	8760	16993	14.0	285.3	76.6
	16	9770	8773	19603	12.2	279.9	79.8
	32	9320	7750	17330	13.3	291.0	77.1

Table 3.10 (a) Electrochemical impedance parameters for the corrosion of Mg-Al-Zn alloy in 30% aqueous ethylene glycol containing of 2 mM sulfate ions, 8 mM SDBS and different concentrations of TSP at different temperatures.

Temperature (°C)	Inhibitor concentration (mM)	R_f (Ω cm^2)	R_{dif} (Ω cm^2)	R_p (Ω cm^2)	C_f (μF cm^{-2})	C_{dif} (μF cm^{-2})	η (%)
30	Blank	3247	2156	5947	34.6	228.4	-
	8 (SDBS)	8577	3974	16294	16.3	163.4	63.5
	4 (TSP)	9490	4491	20031	13.1	148.2	70.3
	8	11740	6690	25490	11.6	130.0	76.7
	16	14360	8360	36360	7.3	116.5	83.6
	32	14230	8170	35210	8.2	119.1	83.1
35	Blank	3164	1960	5687	40.3	230.1	-
	8 (SDBS)	8397	2428	14201	18.9	177.2	59.9
	4 (TSP)	8455	3894	16094	16.6	153.7	64.7
	8	9429	6020	22140	13.6	144.9	74.3
	16	11370	7290	30610	10.2	129.3	81.4
	32	11050	7080	30290	10.0	133.2	81.2
40	Blank	2937	1809	5046	45.3	241.2	-
	8 (SDBS)	6472	2160	11494	26.7	185.9	56.1
	4 (TSP)	7975	3690	13580	21.3	175.0	62.8
	8	8447	5260	18340	17.7	155.6	72.5
	16	12010	6330	24890	13.6	144.2	79.7
	32	11100	5760	23220	14.6	147.4	78.3
45	Blank	2785	1508	4411	49.7	260.0	-
	8 (SDBS)	6370	1965	9475	28.7	198.0	53.4
	4 (TSP)	7437	2491	11148	24.6	187.5	60.4
	8	7929	3882	14572	20.9	178.3	69.7
	16	10830	4982	19492	16.9	150.5	77.4
	32	10470	4527	18247	17.4	153.6	75.8
50	Blank	2693	1116	4261	54.3	272.1	-
	8 (SDBS)	6009	1559	8769	32.7	205.9	51.4
	4 (TSP)	6654	1770	9920	26.0	198.6	57.0
	8	7540	3140	12110	22.8	184.0	64.8
	16	8690	4286	15956	19.9	166.4	73.3
	32	8100	4660	15600	20.7	169.6	72.7

Table 3.10 (b) Electrochemical impedance parameters for the corrosion of Mg-Al-Zn alloy in 30% aqueous ethylene glycol containing of 6 mM sulfate ions, 8 mM SDBS and different concentrations of TSP at different temperatures.

Temperature (°C)	Inhibitor concentration (mM)	R_f (Ω cm^2)	R_{dif} (Ω cm^2)	R_p (Ω cm^2)	C_f (μF cm^{-2})	C_{dif} (μF cm^{-2})	η (%)
30	Blank	2981	1839	5893	38.9	286.2	-
	8 (SDBS)	7149	4082	17611	19.4	184.1	66.5
	4 (TSP)	9970	4929	21139	15.8	171.9	72.1
	8	12300	7615	30415	12.1	157.1	80.6
	16	25860	10290	49080	10.7	140.1	88.0
	32	22680	9498	46898	10.6	147.8	87.4
35	Blank	2806	1642	5631	47.6	292.1	-
	8 (SDBS)	5982	3915	15890	24.4	189.2	64.6
	4 (TSP)	9830	4254	19194	19.3	180.5	70.7
	8	11290	6160	26090	17.9	169.4	78.4
	16	18880	9840	40920	15.9	158.7	86.2
	32	15980	9008	37078	16.1	164.8	84.8
40	Blank	2689	1526	4643	52.2	296.3	-
	8 (SDBS)	5869	2619	12326	29.0	206.9	62.3
	4 (TSP)	7170	3631	14691	22.7	193.3	68.4
	8	9330	4726	19016	20.0	178.6	75.6
	16	12220	8657	27187	16.5	169.4	82.9
	32	12060	6756	26446	17.7	171.7	82.4
45	Blank	2531	1433	4329	58.8	304.0	-
	8 (SDBS)	5334	2311	10711	31.1	235.8	59.6
	4 (TSP)	6901	3277	12772	25.2	215.8	66.1
	8	8730	3381	15581	22.9	198.5	72.2
	16	11400	5610	21380	18.7	179.4	79.7
	32	11010	4664	19384	19.5	182.7	77.7
50	Blank	2511	1075	3760	61.5	322.5	-
	8 (SDBS)	5178	1696	8643	36.1	247.9	56.5
	4 (TSP)	6659	2501	10571	28.3	239.8	64.4
	8	7810	2770	12900	25.6	214.2	70.8
	16	10440	3898	16388	20.9	202.1	77.0
	32	10430	3150	15060	21.1	208.2	75.0

Table 3.10 (c) Electrochemical impedance parameters for the corrosion of Mg-Al-Zn alloy in 30% aqueous ethylene glycol containing of 10 mM sulfate ions, 8 mM SDBS and different concentrations of TSP at different temperatures.

Temperature (°C)	Inhibitor concentration (mM)	R_f (Ω cm²)	R_{dif} (Ω cm²)	R_p (Ω cm²)	C_f (μF cm^{-2})	C_{dif} (μF cm^{-2})	η (%)
30	Blank	2780	1681	4714	41.3	337.0	-
	8 (SDBS)	6866	5495	16245	22.6	208.9	71.0
	4 (TSP)	8661	7433	20483	18.5	191.4	77.0
	8	9670	9251	31601	15.1	186.4	85.1
	16	24480	12498	50838	11.7	169.2	90.7
	32	21730	10989	48909	11.9	172.4	90.4
35	Blank	2679	1395	4347	49.8	346.7	-
	8 (SDBS)	6594	4461	12659	25.9	227.9	65.7
	4 (TSP)	6811	6328	16935	21.7	216.4	74.3
	8	9084	6972	27302	19.5	193.3	84.1
	16	18800	11920	40100	14.7	179.5	89.1
	32	16380	10693	36863	15.1	184.4	88.2
40	Blank	2434	1330	3928	55.2	351.5	-
	8 (SDBS)	6293	3919	10836	28.0	241.1	63.7
	4 (TSP)	6589	4041	14148	24.2	238.3	72.2
	8	7181	5815	21505	22.1	202.3	81.7
	16	11620	8490	31020	17.9	194.0	87.3
	32	11570	7247	29137	18.6	198.7	86.5
45	Blank	2145	1201	3457	62.3	364.3	-
	8 (SDBS)	4610	3534	8730	33.7	244.5	60.4
	4 (TSP)	6374	3768	12008	28.6	241.1	71.2
	8	6926	4370	16920	24.4	216.7	79.6
	16	10810	5165	24005	19.5	206.1	85.6
	32	10200	4881	22091	20.8	211.0	84.3
50	Blank	1980	994	3148	66.8	388.8	-
	8 (SDBS)	3443	2753	7024	35.5	254.7	55.2
	4 (TSP)	5817	2469	9729	31.7	250.5	67.6
	8	8145	3442	13192	29.2	225.5	76.1
	16	10040	3877	18447	23.8	214.1	82.9
	32	9880	3190	16230	23.8	219.1	80.6

Table 3.11 Activation parameters for the corrosion of Mg-Al-Zn alloy in 30% aqueous ethylene glycol containing chloride ions, 8 mM SDBS and different concentrations of TSP.

Concentration of chloride ions (mM)	Inhibitor concentration (mM)	E_a (kJ mol^{-1})	$\Delta H^{\#}$ (kJ mol^{-1})	$\Delta S^{\#}$ (J mol^{-1} K^{-1})
2	Blank	21.6	19.0	−201.5
	8 (SDBS)	34.4	31.8	−166.3
	4 (TSP)	36.3	33.7	−162.0
	8	47.2	44.6	−130.7
	16	41.5	38.9	−151.1
	32	44.1	41.5	−142.8
6	Blank	23.9	21.3	−189.9
	8 (SDBS)	35.3	32.7	−159.6
	4 (TSP)	39.1	36.5	−150.7
	8	54.8	52.2	−103.6
	16	51.0	48.4	−117.9
	32	49.7	47.1	−121.6
10	Blank	16.1	13.5	−213.2
	8 (SDBS)	32.1	29.5	−170.7
	4 (TSP)	33.0	30.4	−169.6
	8	61.0	58.4	−83.8
	16	58.0	55.4	−95.6
	32	46.3	43.7	−131.9

Table 3.12 Activation parameters for the corrosion of Mg-Al-Zn alloy in 30% aqueous ethylene glycol containing different concentrations of sulfate ions, 8 mM SDBS and different concentrations of TSP.

Concentration of sulfate ions (mM)	Inhibitor concentration (mM)	E_a (kJ mol^{-1})	$\Delta H^{\#}$ (kJ mol^{-1})	$\Delta S^{\#}$ (J mol^{-1} K^{-1})
2	Blank	21.4	18.8	−199.3
	8 (SDBS)	32.4	29.8	−171.4
	4 (TSP)	34.4	31.8	−166.1
	8	38.5	35.9	−155.8
	16	39.8	37.2	−154.3
	32	37.8	35.2	−160.7
6	Blank	17.0	14.4	−210.6
	8 (SDBS)	28.5	25.9	−182.1
	4 (TSP)	25.5	22.9	−193.4
	8	38.4	35.8	−155.3
	16	45.7	43.1	−137.8
	32	45.1	42.5	−138.5
10	Blank	16.8	14.2	−209.8
	8 (SDBS)	32.1	29.5	−169.8
	4 (TSP)	34.7	32.1	−163.8
	8	50.0	47.4	−119.1
	16	54.5	51.9	−109.2
	32	53.4	50.8	−112.2

Table 3.13 Thermodynamic parameters for the adsorption of TSP on the surface of Mg-Al-Zn alloy in 30% aqueous ethylene glycol containing chloride ions and 8 mM SDBS.

Concentration of chloride ions (mM)	**Temperature (°C)**	**$\Delta G°_{ads}$ (kJ mol^{-1})**	**$\Delta H°_{ads}$ (kJ mol^{-1})**	**$\Delta S°_{ads}$ (JK^{-1}mol^{-1})**	**R^2**
2	30	−27.6	−31.9	−13.9	0.999
	35	−28.1			0.998
	40	−27.2			0.998
	45	−27.3			0.998
	50	−27.6			0.998
6	30	−28.8	−34.8	−19.4	0.999
	35	−29.3			0.998
	40	−28.4			0.998
	45	−28.5			0.999
	50	−28.8			0.999
10	30	−31.4	−59.2	−93.5	0.998
	35	−30.4			0.998
	40	−29.2			0.998
	45	−29.0			0.999
	50	−29.7			0.999

Table 3.14 Thermodynamic parameters for the adsorption of TSP on Mg-Al-Zn alloy in 30% aqueous ethylene glycol containing different concentrations of sulfate ions and 8 mM SDBS.

Concentration of sulfate ions (mM)	**Temperature (°C)**	**$\Delta G°_{ads}$ (kJ mol^{-1})**	**$\Delta H°_{ads}$ (kJ mol^{-1})**	**$\Delta S°_{ads}$ (JK^{-1}mol^{-1})**	**R^2**
2	30	−27.8	−19.6	26.4	0.999
	35	−27.6			0.999
	40	−27.9			0.998
	45	−27.9			0.998
	50	−28.3			0.997
6	30	−27.4	−14.7	42.8	0.999
	35	−28.2			0.998
	40	−28.2			0.997
	45	−28.1			0.998
	50	−28.5			0.998
10	30	−28.5	−30.3	−4.9	1.000
	35	−29.1			0.999
	40	−29.2			0.999
	45	−28.6			0.999
	50	−28.6			0.998

3.3. CORROSION INHIBITION OF Mg-Al-Zn ALLOY IN 30% AQUEOUS ETHYLENE GLYCOL CONTAINING CHLORIDE IONS AND SULFATE IONS BY A MIXTURE OF INHIBITORS, SODIUM DODECYL BENZENE SULPHONATE (SDBS) AND SODIUM BENZOATE (SB)

3.3.1. Potentiodynamic polarization analyses

The potentiodynamic polarization plots for the corrosion of Mg-Al-Zn alloy in the presence of SDBS and different concentration of SB in 10 mM chloride medium at 35 °C and 2 mM sulfate medium at 40 °C are shown in the Fig. 3.34 (a) and Fig. 3.34 (b), respectively.

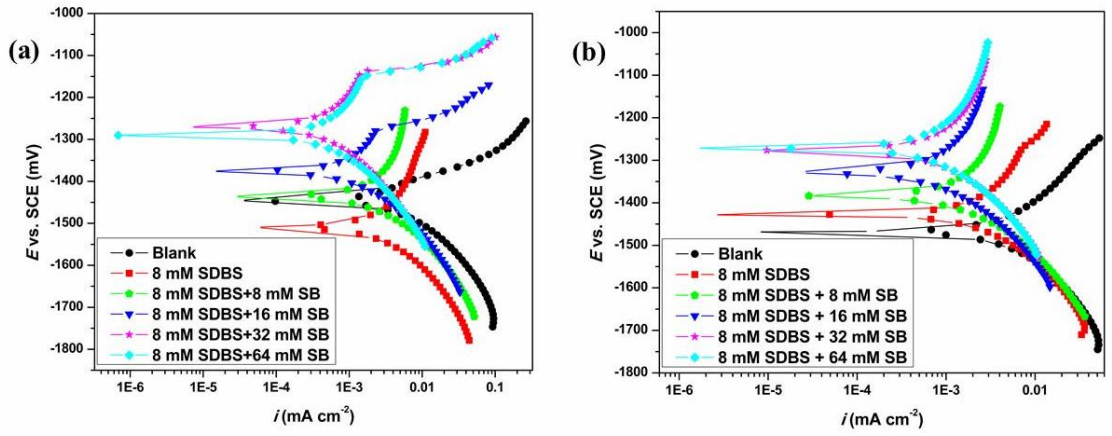

Fig. 3.34 Potentiodynamic polarization plots for the corrosion of Mg-Al-Zn alloy in the presence of SDBS and different concentrations of SB in (a) 10 mM chloride ions at 35 °C and (b) 2 mM sulfate ions at 40 °C.

From the potentiodynamic polarization curves it is clear that, on introducing SB to the corrosive solution containing SDBS, the polarization curves are drifted towards the lower current density region. Further, the unaltered shape of the Tafel curves epitomized that mixture of inhibitors prevents the alloy dissolution without influencing the mechanism of corrosion. In Tafel curves anodic branches show the inflection point at higher applied potential and a pseudo passive state is obsevered over the potential from corrosion potential to the inflection point. At the inflection point localized corrosion and pit propagation take place with rapid increase in the

anodic current (Pardo et al. 2008a). Therefore cathodic curves are considered in applying Tafel extrapolation method to calculate the corrosion rate.

The electrochemical parameters derived from the potentiodynamic polarization studies are listed in Table 3.15 (a), Table 3.15 (b), Table 3.15 (c) and Table 3.16 (a), Table 3.16 (b), Table 3.16 (c) for the chloride and sulfate media, respectively. It is observed from the Tables that, the addition of SB along with SDBS to the corrosion medium decreases the corrosion current, shifts the E_{corr} value to the more positive side. The displacement in the E_{corr} value on the addition of SB to the corrosive media is more than 85 mV vs. SCE. Therefore mixture of SDBS and SB exerts anodic inhibition effect on the corrosion of the alloy. The inhibition efficiency is maximum when the ratio of SDBS to SB is 1:4; beyond this ratio, the change in the inhibition efficiency is insignificant.

3.3.2. Electrochemical impedance spectroscopy

Fig. 3.35 (a) and Fig. 3.35 (b), respectively, represent the Nyquist plots for the corrosion of Mg-Al-Zn alloy in 10 mM chloride medium at 35 °C and 2 mM sulfate medium at 40 °C containing 8 mM SDBS and different concentrations of SB. Addition of SB increases the diameter of the capacitive loops. In capacitive loop the diameter of the medium frequency semicircle increases to a larger extent as compared with that of high frequency capacitive loop. Electrical equivalent circuit discussed in section 3.1.2 (Fig. 3.3), was used to analyze the impedance parameters.

The impedance parameters such as R_f, C_f, R_{dif}, C_{dif} and η (%) obtained from analysing the impedance spectra at different temperatures are tabulated in Tables 3.12 to 3.14. The values of R_f, R_{dif} increases, the values of C_f and C_{dif} decreases and the inhibition efficiency increases with the increase in the concentration of SB up to a limit. The results are similar to those observed in the presence of TSP. Within the experimental errors the variation in the values of η with the increase in the concentration of SB are in good agreement with those obtained from potentiodynamic polarization studies.

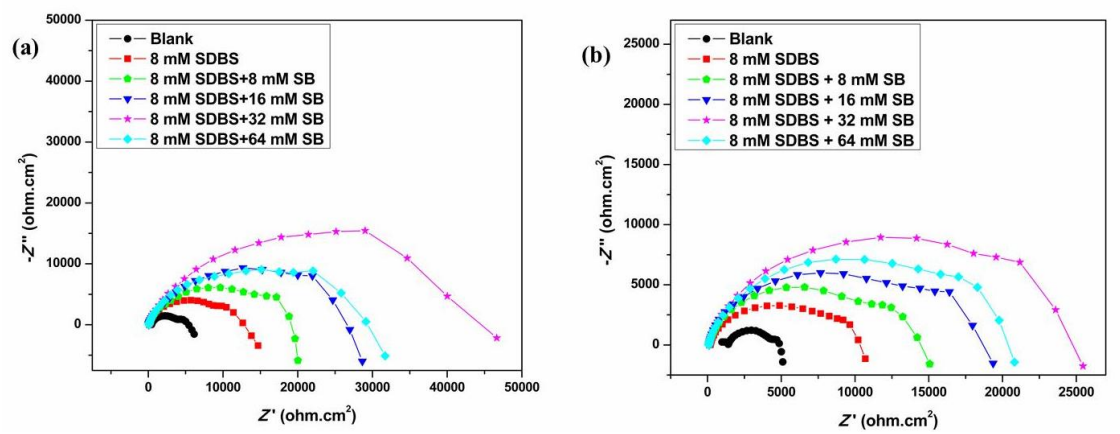

Fig. 3.35 Nyquist plots for the corrosion of Mg-Al-Zn alloy in the presence of SDBS and different concentrations of SB in (a) 10 mM chloride medium at 35 °C and (b) 2 mM sulfate medium at 40 °C.

Fig. 3.36 (a), Fig. 3.36 (b) and Fig. 3.37 (a), Fig. 3.37 (b), respectively, represents the Bode magnitude plots and Bode phase angle plots, for the corrosion of Mg-Al-Zn alloy in 10 mM chloride medium at 35 °C and 2 mM sulfate medium at 40 °C containing 8 mM SDBS and different concentrations of SB.

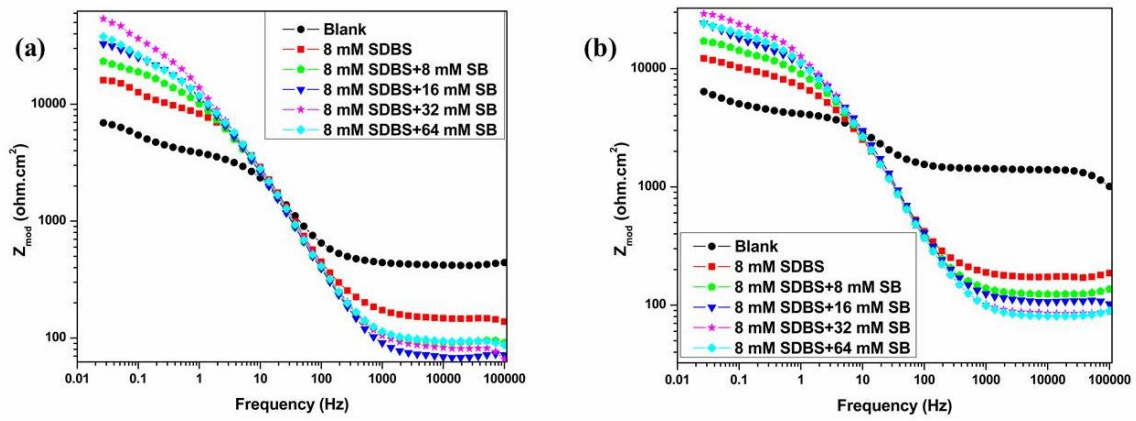

Fig. 3.36 Bode magnitude plots for the corrosion of Mg-Al-Zn alloy in the presence of SDBS and different concentrations of SB in (a) 10 mM chloride medium at 35 °C and (b) 2 mM sulfate medium at 40 °C.

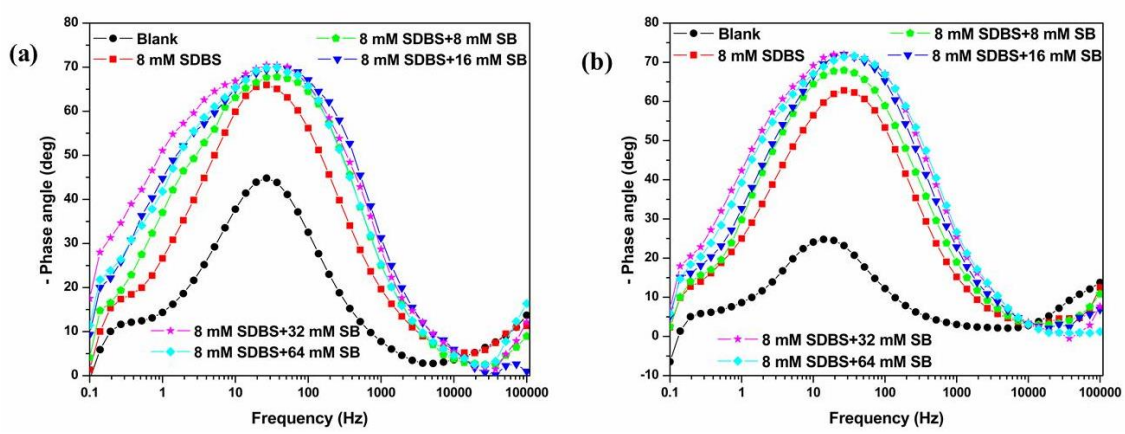

Fig. 3.37 Bode phase angle plots for the corrosion of Mg-Al-Zn alloy in the presence of SDBS and different concentrations of SB in (a) 10 mM chloride medium at 35 °C and (b) 2 mM sulfate medium at 40 °C.

These plots indicate the increase in inhibition efficiency with the increase in the concentration of SB, as shown by the increased values of low frequency impedance modulus (Z_{mod}) and medium frequency phase angle maximum (θ_{max}).

3.3.3. Effect of temperature

The inhibition efficiency of the mixture of SDBS and SB decreases with the increase in the temperature of the medium as evidenced from the results presented in Table 3.15 (a) to Table 3.18 (c). The trend indicates physisorption of the inhibitor molecules on the alloy surface.

Fig. 3.38 (a) and Fig. 3.38 (b) represent Arrhenius plots for the corrosion of Mg-Al-Zn alloy in 10 mM chloride medium at 35 °C and 2 mM sulfate medium at 40 °C containing 8 mM SDBS and different concentrations of SB. Fig. 3.39 (a) and Fig. 3.39 (b) show the corresponding plots of ln (υ_{corr}/T) versus ($1/T$). Table 3.19 and Table 3.20, present the calculated activation parameters. In both the media, the activation energy increases with the increase in the SB concentration, which indicates the increased barrier effect for the occurrence of corrosion, in turn implying an increased protection by the inhibitor film formed on the alloy surface. The sequence of change

in $\Delta H^{\#}$ values is similar to that of activation energy. The decreased apparent entropy of the reaction suggests that the activated complex in the rate determining step undergoes association of the reactants.

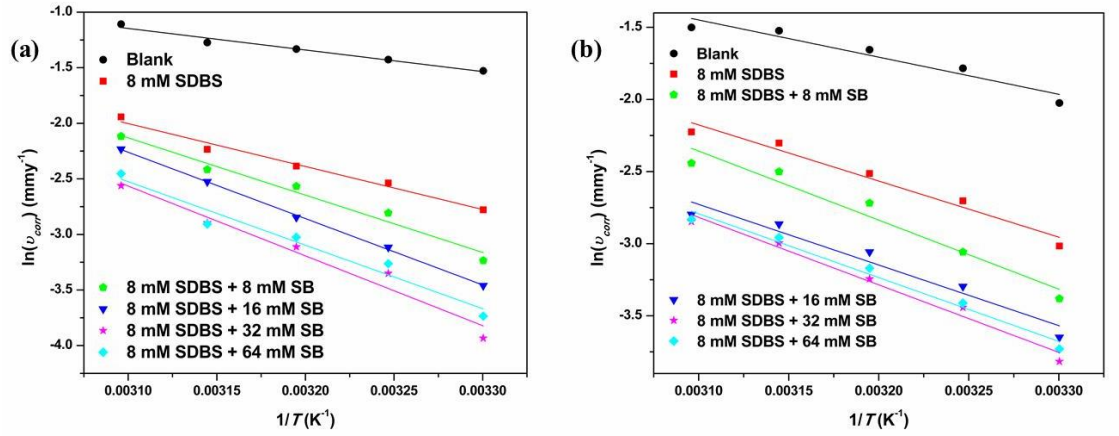

Fig. 3.38 Arrhenius plots for the corrosion of Mg-Al-Zn alloy in the presence of 8 mM SDBS and different concentrations of SB in a corrosive solution of (a) 10 mM chloride medium and (b) 2 mM sulfate medium.

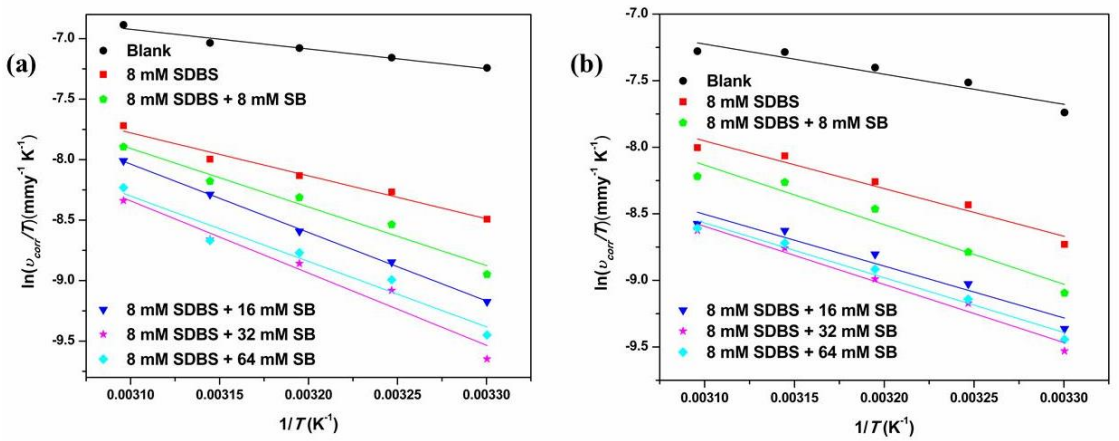

Fig. 3.39 Plots of ln (υ_{corr}/T) versus ($1/T$) for the corrosion of Mg-Al-Zn alloy in the presence of 8 mM SDBS and different concentrations of SB in a corrosive solution of (a) 10 mM chloride medium and (b) 2 mM sulfate medium.

3.3.4. Adsorption isotherm

The relation between θ and concentration of the mixture of inhibitors were graphically fitted into Langmuir adsorption isotherm after attempting to fit with Langmuir, Temkin, Frumkin and Flory-Huggins isotherms. Fig. 3.40 (a) and Fig. 3.40 (b) represent the Langmuir adsorption isotherms for the adsorption of SB on Mg-Al-Zn alloy surface at different temperatures in 10 mM chloride medium and 2 mM sulfate medium, respectively. The plots show an average R^2 close to unity. Standard free energy of adsorption, standard enthalpy of adsorption and standard entropy of adsorption in chloride and sulfate media are calculated and tabulated in Table 3.21 and Table 3.22, respectively. The values of standard free energy of adsorption are negative and lie in between −26.21 to −30.48 kJ mol^{-1}, which indicate that SB gets adsorbed on the surface of the alloy through physisorption as well as chemisorption. But the values of standard enthalpy of adsorption indicate the predominant physisorption process.

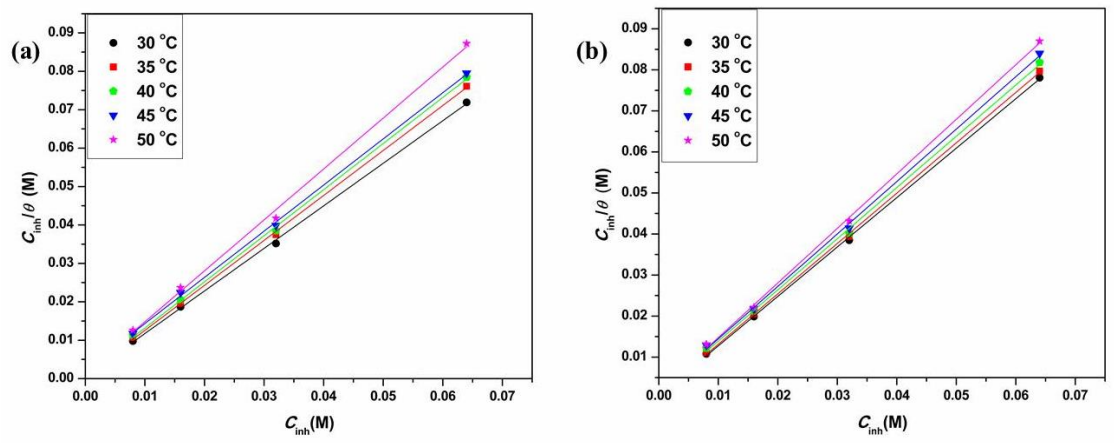

Fig. 3.40 Langmuir adsorption isotherms for the adsorption of SB on Mg-Al-Zn alloy surface at different temperatures in (a) 10 mM chloride medium and (b) 2 mM sulfate medium.

3.3.5. Surface analyses

Fig. 3.41 (a) and Fig. 3.41 (b), respectively represent the SEM image and EDX spectra of the Mg-Al-Zn alloy surface after immersion in the corrosion medium

containing 10 mM chloride ion, 8 mM SDBS and 32 mM SB. Fig. 3.42 (a) and Fig. 3.42 (b) represent the corresponding SEM image and EDX spectra in the corrosion medium containing 10 mM sulfate ion.

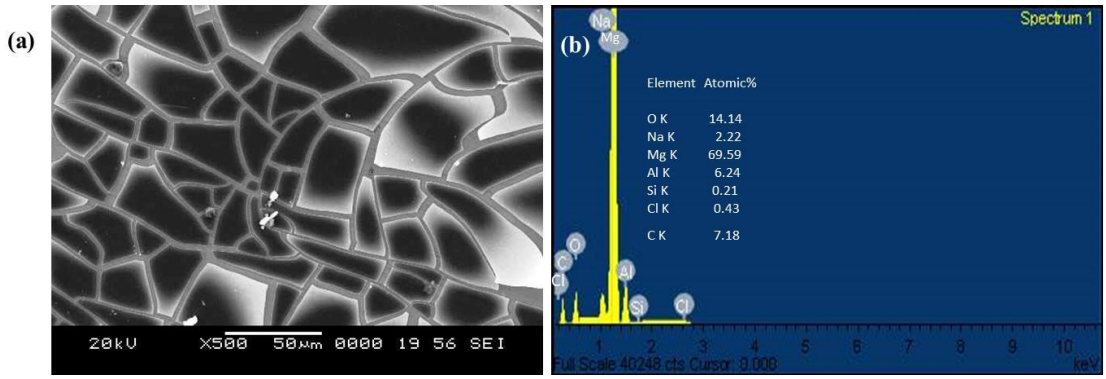

Fig. 3.41 (a) SEM image of Mg-Al-Zn alloy surface after 24 h of immersion in the corrosion medium containing 10 mM chloride ions, 8 mM SDBS and 32 mM SB and (b) corresponding EDX spectra.

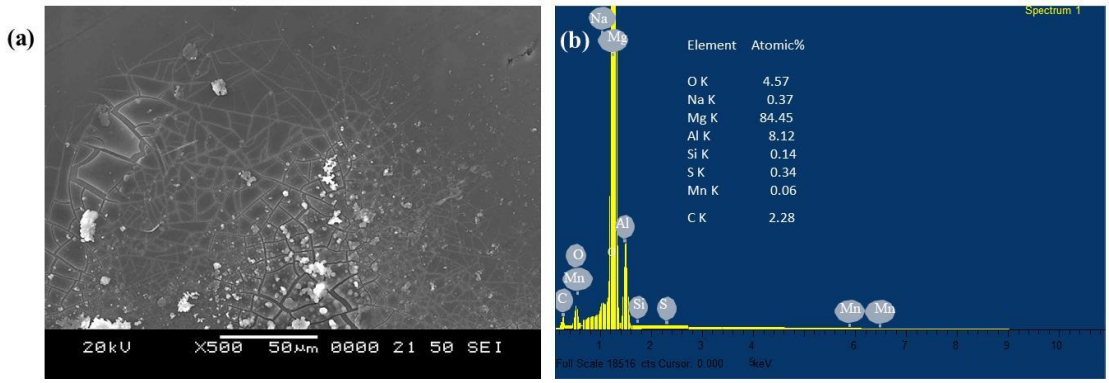

Fig. 3.42 (a) SEM image of Mg-Al-Zn alloy surface after 24 h of immersion in the corrosion medium containing 10 mM sulfate ions, 8 mM SDBS and 32 mM SB and (b) corresponding EDX spectra.

The presence of SDBS and SB together in the corrosion medium results in the less deteriorated surface with a mud crack appearance. The less intensed oxgen peaks in the EDX spectra (Fig. 3.41 (b) and Fig. 3.42 (b)) of the alloy surface indicate the decreased corrosion of the alloy. The presence of C and S on the alloy surface indicate the presence inhibitors on the surface of the alloy.

Table 3.15 (a) Potentiodynamic polarization parameters for the corrosion of Mg-Al-Zn alloy in 30% aqueous ethylene glycol containing 2 mM chloride ions, 8 mM SDBS and different concentrations of SB at different temperatures.

Temperature (°C)	Inhibitor concentration (mM)	E_{corr} vs. SCE (mV)	i_{corr} (μA cm^{-2})	$-b_c$ (mV dec^{-1})	η (%)
30	Blank	−1476	4.58	356	-
	8 (SDBS)	−1423	2.06	310	55.0
	8 (SB)	−1339	1.16	283	74.7
	16	−1344	0.97	268	78.8
	32	−1312	0.74	254	83.8
	64	−1271	0.78	247	83.0
35	Blank	−1466	5.36	363	-
	8 (SDBS)	−1510	2.52	305	53.0
	8 (SB)	−1331	1.65	269	69.2
	16	−1356	1.47	241	72.6
	32	−1242	1.15	230	78.5
	64	−1268	1.09	236	79.7
40	Blank	−1486	6.02	332	-
	8 (SDBS)	−1469	3.09	291	48.7
	8 (SB)	−1398	2.13	268	64.6
	16	−1348	1.92	240	68.1
	32	−1302	1.41	226	76.6
	64	−1272	1.48	223	75.4
45	Blank	−1470	6.79	370	-
	8 (SDBS)	−1471	3.85	306	43.3
	8 (SB)	−1306	2.65	243	61.0
	16	−1329	2.35	222	65.4
	32	−1288	1.76	209	74.1
	64	−1275	1.79	207	73.6
50	Blank	−1379	7.85	442	-
	8 (SDBS)	−1460	4.74	308	39.6
	8 (SB)	−1336	3.36	256	57.2
	16	−1293	2.91	247	62.9
	32	−1312	2.50	222	68.2
	64	−1297	2.51	217	68.0

Table 3.15 (b) Potentiodynamic polarization parameters for the corrosion of Mg-Al-Zn alloy in 30% aqueous ethylene glycol containing 6 mM chloride ions, 8 mM SDBS and different concentrations of SB at different temperatures.

Temperature (°C)	Inhibitor concentration (mM)	E_{corr} vs. SCE (mV)	i_{corr} (μA cm^{-2})	$-b_c$ (mV dec^{-1})	η (%)
30	Blank	−1499	6.85	270	-
	8 (SDBS)	−1535	2.76	221	59.7
	8 (SB)	−1322	1.45	216	78.8
	16	−1336	1.17	214	82.9
	32	−1347	0.84	208	87.7
	64	−1300	0.83	200	87.9
35	Blank	−1445	9.53	279	-
	8 (SDBS)	−1494	4.20	255	55.9
	8 (SB)	−1368	2.63	233	72.4
	16	−1361	2.03	219	78.7
	32	−1336	1.68	205	82.4
	64	−1325	1.71	190	82.1
40	Blank	−1433	10.59	297	-
	8 (SDBS)	−1435	5.15	287	51.4
	8 (SB)	−1302	3.42	234	67.7
	16	−1316	2.56	221	75.8
	32	−1295	2.19	210	79.3
	64	−1266	2.14	204	79.8
45	Blank	−1420	11.68	317	-
	8 (SDBS)	−1449	5.88	290	49.7
	8 (SB)	−1302	4.20	261	64.0
	16	−1306	3.80	253	67.5
	32	−1282	2.80	235	76.0
	64	−1283	2.75	232	76.5
50	Blank	−1428	12.82	338	-
	8 (SDBS)	−1448	6.86	307	46.5
	8 (SB)	−1315	5.13	277	60.0
	16	−1296	4.71	252	63.3
	32	−1294	3.50	240	72.7
	64	−1289	3.48	225	72.9

Table 3.15 (c) Potentiodynamic polarization parameters for the corrosion of Mg-Al-Zn alloy in 30% aqueous ethylene glycol containing 10 mM chloride ions, 8 mM SDBS and different concentrations of SB at different temperatures.

Temperature (°C)	Inhibitor concentration (mM)	E_{corr} vs. SCE (mV)	i_{corr} (μA cm^{-2})	$-b_c$ (mV dec^{-1})	η (%)
30	Blank	−1458	10.09	286	-
	8 (SDBS)	−1459	2.89	295	71.4
	8 (SB)	−1364	1.83	272	81.9
	16	−1341	1.46	282	85.5
	32	−1375	0.91	268	91.0
	64	−1368	1.11	210	89.0
35	Blank	−1446	11.18	269	-
	8 (SDBS)	−1520	3.68	261	67.1
	8 (SB)	−1436	2.81	237	74.9
	16	−1377	2.06	221	81.6
	32	−1272	1.63	216	85.4
	64	−1292	1.78	204	84.1
40	Blank	−1416	12.27	310	-
	8 (SDBS)	−1369	4.28	270	65.1
	8 (SB)	−1309	3.57	252	70.9
	16	−1297	2.70	245	78.0
	32	−1266	2.07	233	83.1
	64	−1273	2.26	229	81.6
45	Blank	−1461	13.05	306	-
	8 (SDBS)	−1414	4.98	260	61.8
	8 (SB)	−1290	4.15	258	68.2
	16	−1288	3.72	253	71.5
	32	−1298	2.57	229	80.3
	64	−1289	2.54	220	80.5
50	Blank	−1405	15.37	339	-
	8 (SDBS)	−1360	6.67	266	56.6
	8 (SB)	−1278	5.60	256	63.6
	16	−1291	4.99	236	67.5
	32	−1283	3.59	225	76.6
	64	−1248	4.00	217	73.4

Table 3.16 (a) Tafel polarization parameters for the corrosion of Mg-Al-Zn alloy in 30% aqueous ethylene glycol containing 2 mM sulfate ions, 8 mM SDBS and different concentrations of SB at different temperatures.

Temperature (°C)	Inhibitor concentration (mM)	E_{corr} vs. SCE (mV)	i_{corr} (μA cm^{-2})	$-b_c$ (mV dec^{-1})	η (%)
30	Blank	−1546	6.14	284	-
	8 (SDBS)	−1447	2.27	254	63.0
	8 (SB)	−1436	1.58	243	74.2
	16	−1374	1.20	239	80.4
	32	−1275	1.04	224	83.0
	64	−1332	1.11	232	82.0
35	Blank	−1556	7.80	349	-
	8 (SDBS)	−1505	3.11	251	60.2
	8 (SB)	−1405	2.20	243	71.8
	16	−1406	1.72	233	77.9
	32	−1320	1.47	217	81.2
	64	−1285	1.54	225	80.3
40	Blank	−1469	8.90	311	-
	8 (SDBS)	−1428	3.77	254	57.6
	8 (SB)	−1385	3.06	251	65.6
	16	−1328	2.18	231	75.5
	32	−1277	1.81	226	79.7
	64	−1271	1.94	213	78.2
45	Blank	−1463	10.15	309	-
	8 (SDBS)	−1415	4.63	286	54.4
	8 (SB)	−1361	3.84	257	62.2
	16	−1338	2.66	249	73.8
	32	−1303	2.31	240	77.3
	64	−1293	2.42	242	76.2
50	Blank	−1468	10.36	285	-
	8 (SDBS)	−1435	5.03	271	51.4
	8 (SB)	−1325	4.04	251	61.0
	16	−1293	2.86	238	72.4
	32	−1278	2.68	224	74.1
	64	−1278	2.73	236	73.6

Table 3.16 (b) Tafel polarization parameters for the corrosion of Mg-Al-Zn alloy in 30% aqueous ethylene glycol containing 6 mM sulfate ions, 8 mM SDBS and different concentrations of SB at different temperatures.

Temperature (°C)	Inhibitor concentration (mM)	E_{corr} vs. SCE (mV)	i_{corr} (μA cm^{-2})	$-b_c$ (mV dec^{-1})	η (%)
30	Blank	−1566	9.47	308	-
	8 (SDBS)	−1446	3.08	250	67.5
	8 (SB)	−1390	1.99	265	79.0
	16	−1362	1.46	260	84.6
	32	−1400	1.20	242	87.3
	64	−1417	1.26	206	86.6
35	Blank	−1520	10.79	373	-
	8 (SDBS)	−1414	3.76	260	65.2
	8 (SB)	−1353	2.43	280	77.5
	16	−1406	2.01	263	81.4
	32	−1372	1.55	250	85.6
	64	−1357	1.76	247	83.7
40	Blank	−1513	11.81	376	-
	8 (SDBS)	−1392	4.36	283	63.0
	8 (SB)	−1363	2.95	279	75.0
	16	−1351	2.68	276	77.3
	32	−1327	1.89	268	84.0
	64	−1314	2.21	259	81.3
45	Blank	−1500	12.87	379	-
	8 (SDBS)	−1388	5.10	282	60.4
	8 (SB)	−1329	3.41	288	73.5
	16	−1341	3.10	280	75.9
	32	−1325	2.39	255	81.4
	64	−1348	2.54	263	80.3
50	Blank	−1446	14.63	335	-
	8 (SDBS)	−1405	6.32	290	56.8
	8 (SB)	−1314	4.35	276	70.3
	16	−1315	3.97	268	72.9
	32	−1289	3.25	249	77.8
	64	−1307	3.31	255	77.4

Table 3.16 (c) Tafel polarization parameters for the corrosion of Mg-Al-Zn alloy in 30% aqueous ethylene glycol containing 10 mM sulfate ions, 8 mM SDBS and different concentrations of SB at different temperatures.

Temperature (°C)	Inhibitor concentration (mM)	E_{corr} vs. SCE (mV)	i_{corr} (μA cm^{-2})	$-b_c$ (mV dec^{-1})	η (%)
30	Blank	−1530	11.68	386	-
	8 (SDBS)	−1495	3.12	217	73.3
	8 (SB)	−1308	2.02	284	82.7
	16	−1314	1.22	259	89.6
	32	−1321	0.96	224	91.8
	64	−1316	1.15	229	90.2
35	Blank	−1521	12.65	402	-
	8 (SDBS)	−1430	3.99	280	68.5
	8 (SB)	−1352	2.41	273	80.9
	16	−1333	1.59	249	87.4
	32	−1305	1.15	223	90.9
	64	−1347	1.44	244	88.6
40	Blank	−1460	14.43	344	-
	8 (SDBS)	−1412	4.92	257	65.9
	8 (SB)	−1341	3.11	273	78.4
	16	−1314	2.15	266	85.1
	32	−1363	1.69	250	88.3
	64	−1268	1.83	252	87.3
45	Blank	−1458	15.82	327	-
	8 (SDBS)	−1406	5.80	269	63.3
	8 (SB)	−1334	3.73	268	76.4
	16	−1301	2.81	254	82.2
	32	−1289	2.28	250	85.6
	64	−1325	2.36	250	85.1
50	Blank	−1462	17.49	318	-
	8 (SDBS)	−1400	6.94	242	60.3
	8 (SB)	−1311	4.60	277	73.7
	16	−1302	3.45	249	80.3
	32	−1285	3.00	231	82.8
	64	−1277	3.23	235	81.5

Table 3.17 (a) Electrochemical impedance parameters for the corrosion of Mg-Al-Zn alloy in 30% aqueous ethylene glycol, containing 2 mM chloride ions, 8 mM SDBS and different concentrations of SB at different temperatures.

Temperature (°C)	Inhibitor concentration (mM)	R_f (Ω cm²)	R_{dif} (Ω cm²)	R_p (Ω cm²)	C_f (μF cm^{-2})	C_{dif} (μF cm^{-2})	η (%)
30	Blank	4053	1888	9501	23.4	186.1	-
	8 (SDBS)	9354	3070	19680	20.5	121.7	51.7
	8 (SB)	22200	9520	37780	15.1	102.5	74.9
	16	28140	10140	42960	13.6	97.6	77.9
	32	30670	15830	54630	12.8	81.0	82.6
	64	30520	14367	53197	12.3	83.3	82.1
35	Blank	3885	1738	8034	24.4	195.1	-
	8 (SDBS)	8666	2944	15794	21.4	148.5	49.1
	8 (SB)	15190	6780	27240	17.3	122.8	70.5
	16	16360	7350	29970	14.6	105.2	73.2
	32	24500	10850	41780	13.9	92.7	80.8
	64	25130	9680	41410	13.6	93.7	80.6
40	Blank	3269	1659	6932	25.6	208.3	-
	8 (SDBS)	7020	2868	13188	23.0	156.5	47.4
	8 (SB)	12590	4900	19600	18.8	129.9	64.6
	16	13700	5403	21693	15.1	115.2	68.0
	32	15000	7830	29510	14.3	102.5	76.5
	64	14930	7880	29200	14.6	103.0	76.3
45	Blank	3052	1587	6725	27.6	228.1	-
	8 (SDBS)	5927	2796	11592	24.9	177.3	42.0
	8 (SB)	11710	4840	17930	20.7	152.9	62.5
	16	12080	5690	20380	17.7	140.2	67.0
	32	14850	7484	26974	16.8	123.2	75.1
	64	14540	6860	26020	17.1	123.6	74.2
50	Blank	2488	1503	5581	30.7	250.7	-
	8 (SDBS)	4613	2279	9086	26.8	191.0	38.6
	8 (SB)	8640	3270	12625	22.2	165.1	55.8
	16	9470	4200	14790	18.6	143.0	62.3
	32	10740	6090	18320	17.4	136.9	69.5
	64	9968	6019	17879	18.4	139.9	68.8

Table 3.17 (b) Electrochemical impedance parameters for the corrosion of Mg-Al-Zn alloy in 30% aqueous ethylene glycol, containing 6 mM chloride ions, 8 mM SDBS and different concentrations of SB at different temperatures.

Temperature (°C)	Inhibitor concentration (mM)	R_f (Ω cm²)	R_{dif} (Ω cm²)	R_p (Ω cm²)	C_f (μF cm^{-2})	C_{dif} (μF cm^{-2})	η (%)
30	Blank	3597	1820	7582	23.9	236.5	-
	8 (SDBS)	10428	2455	16365	15.5	190.4	53.7
	8 (SB)	18160	8340	32610	13.8	149.0	76.7
	16	20400	9681	38111	11.5	135.9	80.1
	32	33680	13950	50740	9.9	114.6	85.1
	64	31710	13580	49360	10.0	117.9	84.6
35	Blank	2879	1713	6085	25.0	242.4	-
	8 (SDBS)	7045	2258	12170	16.2	209.1	50.0
	8 (SB)	12500	7760	22770	15.0	189.0	73.3
	16	14640	8632	27672	14.2	180.2	78.0
	32	18830	10830	36160	10.7	173.1	83.2
	64	17660	10440	34560	11.0	175.5	82.4
40	Blank	2577	1608	4880	26.9	252.8	-
	8 (SDBS)	5674	1926	9595	17.1	226.1	49.1
	8 (SB)	8840	6280	16123	16.9	197.8	69.7
	16	10180	7724	20344	15.6	184.1	76.0
	32	12410	9320	25600	13.1	180.3	80.9
	64	12060	8970	25210	13.6	182.9	80.6
45	Blank	2214	1569	4742	28.3	257.0	-
	8 (SDBS)	4890	1900	8399	19.0	245.3	43.5
	8 (SB)	7170	4430	13260	17.7	228.4	64.2
	16	8910	5790	15700	16.5	219.0	69.8
	32	10300	7190	20750	15.7	204.2	77.1
	64	10230	6440	20140	16.0	211.7	76.5
50	Blank	1886	1487	4548	31.5	269.8	-
	8 (SDBS)	3493	1865	7571	23.9	250.0	39.9
	8 (SB)	5390	3850	11381	19.7	248.1	60.0
	16	6987	4230	12555	18.7	231.3	63.8
	32	9209	6170	16400	16.4	225.7	72.3
	64	9140	5540	15760	16.6	229.9	71.1

Table 3.17 (c) Electrochemical impedance parameters for the corrosion of Mg-Al-Zn alloy in 30% aqueous ethylene glycol, containing 10 mM chloride ions, 8 mM SDBS and different concentrations of SB at different temperatures.

Temperature (°C)	Inhibitor concentration (mM)	R_f (Ω cm^2)	R_{dif} (Ω cm^2)	R_p (Ω cm^2)	C_f (μF cm^{-2})	C_{dif} (μF cm^{-2})	η (%)
30	Blank	2102	1516	6915	25.4	302.1	-
	8 (SDBS)	11180	3770	19370	12.7	283.7	64.3
	8 (SB)	19110	5220	31490	9.8	246.7	78.0
	16	22160	9909	38989	8.1	205.9	82.3
	32	32160	15720	55210	7.4	166.0	87.5
	64	26170	7017	39717	8.5	220.4	82.6
35	Blank	2002	1485	5509	25.8	320.1	-
	8 (SDBS)	9184	3591	14731	13.6	291.3	62.6
	8 (SB)	12410	4790	20700	11.0	250.3	73.4
	16	15860	8860	27230	9.6	240.5	79.8
	32	31160	9329	41919	8.0	227.0	86.9
	64	20650	7001	29371	9.5	232.5	81.2
40	Blank	1823	1363	4411	29.4	332.1	-
	8 (SDBS)	6552	3312	11396	14.2	311.9	61.3
	8 (SB)	8396	4510	14630	12.3	298.7	69.8
	16	9190	7920	20130	10.9	282.1	78.1
	32	12060	8960	25740	9.1	272.3	82.9
	64	10202	6060	21700	10.1	278.2	79.7
45	Blank	1733	1303	4156	32.7	337.3	-
	8 (SDBS)	5020	2803	9922	15.8	322.2	58.1
	8 (SB)	6446	4240	12711	14.8	307.8	67.3
	16	8841	7180	16759	14.0	287.4	75.2
	32	10230	7798	22218	10.9	276.6	81.3
	64	9044	6018	19058	11.6	279.4	78.2
50	Blank	1434	1283	3969	36.1	345.4	-
	8 (SDBS)	4143	2636	8656	17.9	334.8	54.1
	8 (SB)	5557	3460	10560	15.8	316.3	62.4
	16	7788	6450	14745	14.7	291.1	73.1
	32	9680	7680	19320	11.5	278.0	79.5
	64	8460	4560	15370	11.9	282.5	74.2

Table 3.18 (a) Electrochemical impedance parameters for the corrosion of Mg-Al-Zn alloy in 30% aqueous ethylene glycol containing 2 mM sulfate ions, 8 mM SDBS and different concentrations of SB at different temperatures.

Temperature (°C)	Inhibitor concentration (mM)	R_f (Ω cm²)	R_{dif} (Ω cm²)	R_p (Ω cm²)	C_f (μF cm^{-2})	C_{dif} (μF cm^{-2})	η (%)
30	Blank	3247	2156	5947	34.6	228.4	-
	8 (SDBS)	8577	3974	16294	16.3	163.4	63.5
	8 (SB)	10360	5697	22097	13.0	144.4	73.1
	16	13607	6629	32849	10.1	123.6	81.9
	32	22890	9080	38040	7.2	109.0	84.4
	64	20860	8669	35419	8.7	112.0	83.2
35	Blank	3164	1960	5687	40.3	230.1	-
	8 (SDBS)	8397	2428	14201	18.9	177.2	60.0
	8 (SB)	9310	4746	19336	15.9	157.0	70.6
	16	11702	6218	26388	12.6	133.4	78.4
	32	19170	8120	33290	9.4	112.2	82.9
	64	17560	7610	29590	10.9	118.6	80.8
40	Blank	2937	1809	5046	45.3	241.2	-
	8 (SDBS)	6472	2160	11494	26.7	185.9	56.1
	8 (SB)	8447	4488	16118	22.4	169.3	68.7
	16	9540	5957	20417	16.8	142.2	75.3
	32	12670	6254	25044	13.9	131.0	79.9
	64	10370	6120	21140	14.5	137.0	76.1
45	Blank	2785	1508	4411	49.7	260.0	-
	8 (SDBS)	6370	1965	9475	27.7	198.0	53.4
	8 (SB)	6733	3384	12804	25.0	184.0	65.5
	16	8080	5145	16615	21.0	160.0	73.5
	32	9310	5674	19134	17.3	149.5	76.9
	64	8610	5278	17538	18.8	151.5	74.8
50	Blank	2693	1116	4261	54.3	272.1	-
	8 (SDBS)	6009	1559	8769	29.7	205.9	51.4
	8 (SB)	6295	2847	11007	27.2	191.4	61.3
	16	7310	4527	13807	24.2	182.9	69.1
	32	8970	5045	16815	21.7	168.6	74.7
	64	7510	4317	15177	23.3	172.0	71.9

Table 3.18 (b) Electrochemical impedance parameters for the corrosion of Mg-Al-Zn alloy in 30% aqueous ethylene glycol containing 6 mM sulfate ions, 8 mM SDBS and different concentrations of SB at different temperatures.

Temperature (°C)	Inhibitor concentration (mM)	R_f (Ω cm^2)	R_{dif} (Ω cm^2)	R_p (Ω cm^2)	C_f (μF cm^{-2})	C_{dif} (μF cm^{-2})	η (%)
30	Blank	2981	1839	5893	38.9	286.2	-
	8 (SDBS)	7149	4082	17611	19.4	184.1	66.5
	8 (SB)	9680	5529	25699	13.7	167.6	77.1
	16	18980	8740	36660	10.8	148.6	83.9
	32	25390	9144	44364	8.9	127.8	86.7
	64	22270	8734	40744	9.9	131.0	85.5
35	Blank	2806	1642	5631	47.6	292.1	-
	8 (SDBS)	5982	3915	15890	24.4	189.2	64.6
	8 (SB)	8640	4586	22286	20.1	178.9	74.7
	16	11880	7530	29910	16.9	151.7	81.2
	32	22070	8879	37319	11.7	136.6	84.9
	64	20734	8483	33983	13.8	140.7	83.4
40	Blank	2689	1526	4643	52.2	296.3	-
	8 (SDBS)	5869	2619	12326	29.0	206.9	62.3
	8 (SB)	7350	3249	16909	22.2	195.3	72.5
	16	10180	7255	22055	19.6	179.4	78.9
	32	13350	8512	26112	16.3	140.5	82.2
	64	10290	8000	23480	17.6	143.8	80.2
45	Blank	2531	1433	4329	58.8	304.0	-
	8 (SDBS)	5334	2311	10711	31.1	235.8	59.6
	8 (SB)	6551	3036	14106	26.1	213.4	69.3
	16	9610	6534	18544	21.4	201.0	76.7
	32	10550	7080	22140	18.5	184.0	80.4
	64	9950	6927	19937	20.6	191.8	78.3
50	Blank	2511	1075	3760	61.5	322.5	-
	8 (SDBS)	5178	1696	8643	36.1	247.9	56.5
	8 (SB)	6162	2134	11464	31.1	235.5	67.2
	16	8347	4686	15126	25.4	215.2	75.1
	32	9150	5816	17766	22.0	202.1	78.8
	64	8538	5277	15927	23.3	207.4	76.4

Table 3.18 (c) Electrochemical impedance parameters for the corrosion of Mg-Al-Zn alloy in 30% aqueous ethylene glycol containing 10 mM sulfate ions, 10 mM SDBS and different concentrations of SB at different temperatures.

Temperature (°C)	Inhibitor concentration (mM)	R_f (Ω cm²)	R_{dif} (Ω cm²)	R_p (Ω cm²)	C_f (μF cm^{-2})	C_{dif} (μF cm^{-2})	η (%)
30	Blank	2780	1681	4714	41.3	337.0	-
	8 (SDBS)	6866	5495	16245	22.6	208.9	71.0
	8 (SB)	11650	10200	27160	15.6	198.7	82.6
	16	18290	13220	37850	13.5	189.0	87.5
	32	28260	15330	54080	10.1	142.4	91.3
	64	27050	14300	48720	11.4	151.7	90.3
35	Blank	2679	1395	4347	49.8	346.7	-
	8 (SDBS)	6594	4461	12659	25.9	227.9	65.7
	8 (SB)	7567	8522	21004	21.0	208.0	79.3
	16	16720	9447	31287	17.4	194.9	86.1
	32	21830	12236	40816	14.5	154.4	89.3
	64	20250	11160	38360	15.6	158.3	88.7
40	Blank	2434	1330	3928	55.2	351.5	-
	8 (SDBS)	6293	3919	10836	28.0	241.1	63.8
	8 (SB)	7290	7851	17291	23.1	224.7	77.3
	16	11230	8645	24835	19.3	212.4	84.2
	32	13510	10720	30340	17.1	197.0	87.1
	64	12270	10470	29400	18.1	200.2	86.6
45	Blank	2145	1201	3457	62.3	364.3	-
	8 (SDBS)	4610	3534	8730	33.7	244.5	60.4
	8 (SB)	6362	4813	13063	27.7	237.0	73.5
	16	9610	7130	19190	22.9	220.2	82.0
	32	10420	7997	24257	19.7	208.9	85.7
	64	9587	6444	23914	19.9	210.0	85.5
50	Blank	1980	994	3148	66.8	388.8	-
	8 (SDBS)	3443	2753	7024	35.5	254.7	55.2
	8 (SB)	5340	3322	11222	30.4	244.3	71.9
	16	8160	5951	14951	26.0	233.1	78.9
	32	9991	6784	18784	22.6	221.4	83.2
	64	9112	6221	17411	23.1	229.4	81.9

Table 3.19 Activation parameters for the corrosion of Mg-Al-Zn alloy in 30% aqueous ethylene glycol containing chloride ions, 8 mM SDBS and different concentrations of SB.

Concentration of chloride ions (mM)	Inhibitor concentration (mM)	E_a (kJ mol^{-1})	$\Delta H^{\#}$ (kJ mol^{-1})	$\Delta S^{\#}$ (J mol^{-1} K^{-1})
2	Blank	21.6	19.0	−201.5
	8 (SDBS)	34.4	31.8	−166.3
	8 (SB)	42.4	39.8	−144.0
	16	43.5	40.9	−141.7
	32	46.4	43.8	−134.3
	64	45.8	43.2	−136.3
6	Blank	23.9	21.3	−189.9
	8 (SDBS)	35.3	32.7	−159.6
	8 (SB)	48.9	46.3	−119.9
	16	55.7	53.1	−99.7
	32	56.7	54.4	−89.9
	64	54.3	51.7	−106.4
10	Blank	16.1	13.5	−213.2
	8 (SDBS)	32.1	29.5	−170.7
	8 (SB)	42.8	40.2	−138.6
	16	49.6	47.0	−118.6
	32	52.2	49.6	−113.1
	64	47.5	44.9	−127.2

Table 3.20 Activation parameters for the corrosion of Mg-Al-Zn alloy in 30% aqueous ethylene glycol containing different concentrations of sulfate ions, 8 mM SDBS and different concentrations of SB.

Concentration of sulfate ions (mM)	Inhibitor concentration (mM)	E_a (kJ mol^{-1})	$\Delta H^{\#}$ (kJ mol^{-1})	$\Delta S^{\#}$ (J mol^{-1} K^{-1})
2	Blank	21.4	18.8	−199.3
	8 (SDBS)	32.4	29.8	−171.4
	8 (SB)	34.8	33.0	−158.2
	16	34.9	33.2	−157.2
	32	40.6	36.3	−156.4
	64	36.8	34.2	−162.8
6	Blank	17.0	14.4	−210.6
	8 (SDBS)	28.5	25.9	−182.1
	8 (SB)	30.6	28.0	−178.8
	16	40.1	37.5	−149.7
	32	42.6	38.3	−147.9
	64	37.5	34.9	−159.4
10	Blank	16.8	14.2	−209.8
	8 (SDBS)	32.1	29.5	−169.8
	8 (SB)	34.2	31.6	−167.1
	16	43.3	40.7	−141.0
	32	47.7	45.1	−128.9
	64	41.1	38.5	−149.0

Table 3.21 Thermodynamic parameters for the adsorption of SB on Mg-Al-Zn alloy surface in 30% aqueous ethylene glycol containing chloride ions and 8 mM SDBS.

Concentration of chloride ions (mM)	**Temperature (°C)**	**$\Delta G°_{ads}$ (kJ mol^{-1})**	**$\Delta H°_{ads}$ (kJ mol^{-1})**	**$\Delta S°_{ads}$ (JK^{-1}mol^{-1})**	**R^2**
2	30	−27.4	−28.6	−6.0	1.000
	35	−26.2			1.000
	40	−26.6			0.999
	45	−26.3			0.999
	50	−27.2			0.999
6	30	−27.2	−45.3	−58.6	1.000
	35	−27.7			1.000
	40	−27.2			1.000
	45	−26.3			0.999
	50	−26.4			0.999
10	30	−28.6	−43.5	−49.5	0.999
	35	−28.4			0.999
	40	−28.0			0.999
	45	−26.7			0.999
	50	−28.2			0.997

Table 3.22 Thermodynamic parameters for the adsorption of SB on Mg-Al-Zn alloy in 30% aqueous ethylene glycol containing different concentrations of sulfate ions, 8 mM SDBS and different concentrations of SB.

Concentration of sulfate ions (mM)	Temperature (°C)	$\Delta G°_{ads}$ (kJ mol^{-1})	$\Delta H°_{ads}$ (kJ mol^{-1})	$\Delta S°_{ads}$ ($JK^{-1}mol^{-1}$)	R^2
2	30	−28.5	−34.7	−21.3	1.000
	35	−28.3			1.000
	40	−27.5			0.999
	45	−27.5			0.999
	50	−28.3			0.999
6	30	−28.6	−31.1	−6.7	1.000
	35	−29.6			0.999
	40	−29.2			0.999
	45	−28.9			0.999
	50	−28.8			1.000
10	30	−29.6	−24.4	16.8	0.999
	35	−30.0			0.999
	40	−29.1			1.000
	45	−29.0			1.000
	50	−30.5			0.999

3.4. MECHANISM OF CORROSION INHIBITION BY SYNERGISTIC MIXTURES

3.4.1. Inhibition mechanism of SDBS

The corrosion of magnesium alloy forms the porous, semi-protective $Mg(OH)_2$ film on its surface. SDBS possesses potential electron rich adsorption sites in sulfur and oxygen of the sulfonate group; and in the benzene ring which facilitate the adsorption of SDBS on the surface of the alloy, that is not covered by the $Mg(OH)_2$ semi protective film. Initially inhibition efficiency increases with the raise in the concentration of the SDBS, when the concentration is sufficiently high, a hem-micelle barrier composed of SDBS, is formed on the surface of the alloy (El Rehim et al. 2008). While the electron rich centers of SDBS help in adsorption, the long alkyl chain repels the electrolyte. The SDBS preferably gets adsorbed on the cathodic regions on the alloy surface, as the anodic sites are covered with the corrosion product layer. Though anchored at the cathodic region, the inhibitor molecule spreads over the anodic regions also through its alkyl chains, thereby providing the barrier effect over the surface of the alloy. Therefore the shift in the E_{corr} values in the presence of SDBS is very small, as observed from the potentiodynamic polarization studies. At higher temperature, the rate of adsorption is less than the rate of desorption and hence induce lower inhibition effect.

3.4.2. Inhibition mechanism of TSP

The anodic dissolution of magnesium forms divalent Mg^{2+} ions as shown in equation (3.6). When TSP is added into the corrosive medium, the divalent Mg^{2+} ion reacts with the phosphate ions by the following reaction:

$$3\ Mg^{2+} + 2\ PO_4^{3-} \rightarrow Mg_3(PO_4)_2 \qquad (3.13)$$

This $Mg_3(PO_4)_2$ deposits on the surface through the pores of the surface film. The solubility product of $Mg_3(PO_4)_2$ (1.04×10^{-24}) is less than that of $Mg(OH)_2$ (1.2×10^{-11}). The $Mg_3(PO_4)_2$ film is relatively more compact and dense than the

original semi protective surface film of $Mg(OH)_2$. Thus, the barrier effect is significantly increased at the anodic regions of the alloy surface, as the deposition of $Mg_3(PO_4)_2$ film is governed by the formation of Mg^{2+} ions at the anodic regions. Therefore, TSP is supposed to act as an anodic inhibitor and therefore, shifts the E_{corr} value in the more positive direction on the addition of TSP. As the temperature of the medium increases, the diffusion rate of Mg^{2+} and PO_4^{3-} increases and diffuse far away before deposition. The previously deposited $Mg_3(PO_4)_2$ film migrate to the entire surface of the alloy and thus gives less inhibition efficiency (Williams et al. 2010, Huang et al. 2011, 2012).

3.4.3. Inhibition mechanism of SB

When dissolved in the solution, SB undergoes partial dissociation as per the following reaction (Zhao and Chen 2012):

$$phCOONa \longleftrightarrow phCOO^- + Na^+ \quad (3.14)$$

$$phCOO^- + H^+ \longleftrightarrow phCOOH \quad (3.15)$$

The benzoate ions combine with Mg^{2+} ions formed at the anodic region, depositing as magnesium benzoate ($Mg(phCOO)_2$), and thereby modifying the original surface film of the corrosion product. The anodic dissolution rate is notably decreased as the deposition of magnesium benzoate increases at the anodic region with large shift in the E_{corr} values to the more positive direction. At higher temperature the increased diffusion rate of benzoate ion decreases the combination to form magnesium benzoate and causes higher corrosion rate.

3.4.4. Inhibition mechanism of SDBS and TSP combination

The mechanism for the inhibition effect by the combination of TSP and SDBS is explained as follows. The $Mg_3(PO_4)_2$ deposited by the reaction of Mg^{2+} ion and phosphate ion, will reduce the porosity of the original $Mg(OH)_2$ surface film, by modifying it through preferential deposition on the anodic sites of the alloy such as magnesium matrix. The presence of SDBS further stabilizes the film by its adsorption

on the modified film, in the pores of the modified film and also on inter metallic particles (Huang et al. 2011). Hence the combination of TSP and SDBS exerts the inhibitive effect by reducing both the dissolution of magnesium at the anodic sites and liberation of hydrogen at the cathodic sites. However, the anodic shift in the E_{corr} value suggests the predominant anodic control that implies that the effect of TSP is significantly higher than that of SDBS, when both are present together. The adsorbed SDBS significantly decrease the anodic dissolution by adsorbing on the pores of the surface film and averting the access of aggressive species through the pores. The decreased efficiency at higher temperature is due to the decreased rate of formation of $Mg_3(PO_4)_2$ and increased rate of desorption of SDBS on the surface of the alloy (Huang et al. 2011). When the ratio of TSP is small, only SDBS adsorption takes place but no enough TSP to form the modified deposited film. As the concentration of TSP is increased, the densification of the surface film increases and correspondingly the inhibition efficiency also increases. The increased R_f, R_{dif} and decreased C_f, C_{dif} with the increase in the ratio of SDBS to TSP collectively point out the increament in the barrier effect of the surface film. Beyond a limit, the surface film gets saturated, and no further densification takes place; and further increase in TSP content does not increase the inhibition efficiency significantly.

3.4.5. Inhibition mechanism of SDBS and SB combination

A similar mechanism, as discussed above, can be proposed for the inhibition effect of SDBS and SB combination. The deposition of magnesium benzoate on the anodic region of the alloy decreases the anodic dissolution of magnesium. The adsorption of SDBS through the pores of the modified film further stabilizes the film. The adsorption of both SDBS and SB provides a more compact barrier film for the passage of metal atoms from lattice into the electrolyte (Li et al. 2011). The increased value of R_f and R_{dif} and decreased value of C_f and C_{dif} with the addition of SB accounts for the improved corrosion protection ability of the surface barrier film. So the modified surface film formed in the presence of both SDBS and SB effectively retards the ingress of corrosive ion and dissolution of the magnesium substrate.

3.4.6. Synergistic effect

The interaction between the two inhibitors can lead to either synergistic or antagonistic inhibition effect. If the combined effect of two inhibitors is greater than the sum of the individual effect of the two inhibitors, it is termed as synergistic inhibition effect. The synergistic parameter can be calculated by the following equation (Aramaki and Hackerman 1969):

$$S = \frac{1-\theta_{1+2}}{1-\theta'_{1+2}} \tag{3.16}$$

where $\theta_{1+2} = (\theta_1+\theta_2) - (\theta_1\theta_2)$, θ_1 = surface coverage by inhibitor 1 (SDBS) and θ_2 = surface coverage by inhibitor 2 (TSP or SB), respectively, θ'_{1+2}= surface coverage by a mixer of inhibitors 1 and 2. The value of *S* is greater than 1 for synergistic effect, and is less than 1 for antagonistic inhibition effect (Ekpe et al. 1995). The θ values for the individual inhibitors and their combinations were calculated from polarization studies and used in the calculation of *S* value for the interaction of SDBS with TSP and SB. The *S* value for the interaction of 8 mM SDBS with 8 mM TSP and 8 mM SB are calculated in 30% aqueous ethylene glycol containing 10 mM chloride ions and 10 mM sulfate ions and listed in Table 3.23 (a) and Table 3.23 (b), respectively. The values of *S* obtained for the combination of SDBS with TSP and SB are greater than 1, which suggests the significant synergistic effect by the mixture of inhibitors.

Table 3.23 (a) Synergistic parameters for the interaction of SDBS with TSP and SB on the alloy surface in 30% aqueous ethylene glycol containing 10 mM chloride ions.

θ_{SDBS}	θ_{TSP}	θ_{SB}	$\theta_{SDBS+TSP}$	$\theta_{SDBS+SB}$	***S* for SDBS and TSP**	***S* for SDBS and SB**
0.714	0.558	0.220	0.900	0.819	1.26	1.23

Table 3.23 (b) Synergistic parameters for the interaction of SDBS with TSP and SB on the alloy surface in 30% aqueous ethylene glycol containing 10 mM sulfate ions.

θ_{SDBS}	θ_{TSP}	θ_{SB}	$\theta_{SDBS+TSP}$	$\theta_{SDBS+SB}$	***S* for SDBS and TSP**	***S* for SDBS and SB**
0.733	0.490	0.190	0.896	0.827	1.31	1.25

3.4.7. Effect of medium concentration

The increased inhibition efficiency of the inhibitor in the higher aggressive ion concentration may be due to the increased dissolution of $Mg(OH)_2$ surface film at higher ionic concentration. Increased dissolution of $Mg(OH)_2$ facilitate the formation of Mg^{2+} ions, which act as a site for possible physisorption and thus increase the inhibitor efficiency (Zucchi et al. 2006). The rate of corrosion is more in sulfate containing corrosive media, which facilitate the generation of more and more Mg^{2+} ions facilitating higher physisorption, resulting in higher inhibition efficiency than in chloride containing corrosive media.

3.5. CORROSION INHIBITION OF Mg-Al-Zn ALLOY IN 30% AQUEOUS ETHYLENE GLYCOL CONTAINING CHLORIDE IONS AND SULFATE IONS BY MORPHOLINE

3.5.1. Potentiodynamic polarization analyses

The potentiodynamic polarization plots for the corrosion of Mg-Al-Zn alloy in 6 mM chloride medium at 35 °C and 2 mM sulfate medium at 35 °C containing different concentration of morpholine are shown in Fig. 3.43 (a) and Fig. 3.43 (b), respectively.

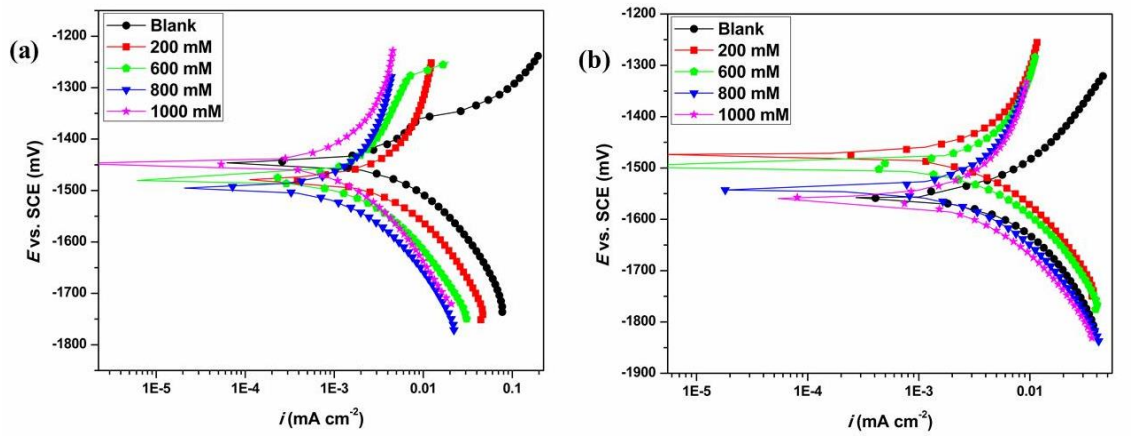

Fig. 3.43 Potentiodynamic polarization plots for the corrosion of Mg-Al-Zn alloy in the presence of different concentrations of morpholine in (a) 6 mM chloride medium at 35 °C and (b) 2 mM sulfate medium at 35 °C.

The polarization curves in Fig. 3.43, for the corrosive media containing morpholine are shifted towards the lower current density region. The unaffected shape of the polarization curves in the Fig. 3.43 demonstrates the non-involvement of the morpholine in the mechanism of the Mg-Al-Zn alloy corrosion. The cathodic branches of the polarization curves were considered in Tafel extrapolation method to calculate the polarization parameters and the calculated values are tabulated in the Table 3.24 (a), Table 3.24 (b), Table 3.24 (c) and Table 3.25 (a), Table 3.25 (b), Table 3.25 (c) for chloride and sulfate media, respectively. From the tabulated values it is

concluded that the corrosion rate of the Mg-Al-Zn alloy decreases with the increase in the concentration of the morpholine and with the rise in the ionic concentration of the medium.

The highest efficiency was achieved with 800 mM morpholine in both chloride and sulfate media. The maximum efficiency shown by morpholine at 30 °C in 10 mM chloride medium is 90.4% and in 10 mM sulfate medium is 94.6% at a concentration of 800 mM. Further, increase in the concentration of the morpholine in both the corrosive media does not increase the efficiency significantly. It follows from the corrosion potential values in the Table 3.24 and Table 3.25 that the shift in E_{corr} value upon the addition of morpholine is not more than 85 mV vs SCE and hence morpholine is considered as a mixed type inhibitor (Fekry and Ameer 2010, Torres et al. 2011).

3.5.2. Electrochemical impedance spectroscopy

The Nyquist plots for the corrosion of Mg-Al-Zn alloy in the presence of different concentrations of morpholine in a corrosive solution of 6 mM chloride medium at 35 °C and 2 mM sulfate medium at 35 °C are shown in Fig. 3.44 (a) and Fig. 3.44 (b), respectively.

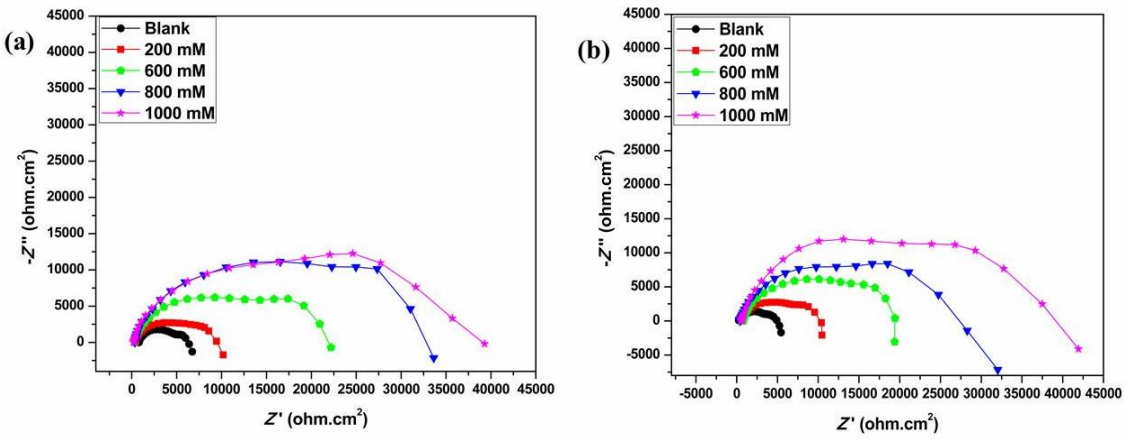

Fig. 3.44 Nyquist plots for the corrosion of Mg-Al-Zn alloy in the presence of different concentrations of morpholine in (a) 6 mM chloride medium at 35 °C and (b) 2 mM sulfate medium at 35 °C.

The Nyquist plots consist of two capacitive loops followed by an inductive loop at higher, medium and lower frequencies, respectively. With the increase in the morpholine concentration in both the media, a successive augment of capacitive loops results, without any change in their shapes. This indicates that the addition of morpholine reduce the Mg-Al-Zn alloy corrosion without altering its mechanism.

The simulation studies were carried out for all the impedance results for different concentrations of morpholine at different temperatures in both the media. The equivalent circuit shown in Fig. 3.3 fits into the experimental data. The impedance parameters like R_f, C_f, R_{dif}, C_{dif} and η (%) obtained from the simulation studies are tabulated in Table 3.26 (a), Table 3.26 (b), Table 3.26 (c) and Table 3.27 (a), Table 3.27 (b), Table 3.27 (c) for chloride and sulfate media, respectively. The results are similar to the one obtained from potentiodynamic polarization studies with the inhibition efficiency increasing with the increase in the concentration of morpholine. Further, higher values of efficiency are observed in sulfate media than in the chloride media. Also increased efficiencies were observed with the increase in the ionic concentration of the corrosive media. In the Tables increased values in film resistance, diffusion resistance and decreased values in the film capacitance, diffusion capacitance on successive addition of morpholine reflects the improvement in the inhibitive ability and thickness of the surface film formed on the surface of the Mg-Al-Zn alloy.

The morpholine inhibition towards the corrosion of Mg-Al-Zn alloy is further substantiated from the Bode plots. The Bode magnitude plots for the corrosion of Mg-Al-Zn alloy in the presence of different concentrations of morpholine in a corrosive solution of 6 mM chloride at 35 °C and 2 mM sulfate medium at 35 °C are shown in Fig. 3.45 (a) and Fig. 3.45 (b), respectively. The Bode phase angle plots for the same are depicted in Fig. 3.46 (a) and Fig. 3.46 (b), respectively.

As seen from Fig. 3.45 and Fig. 3.46 gradual increase in impedance modulus at low frequency and phase maximum at medium frequency is consistent with the

increase in the concentration of morpoline, which together indicates a better corrosion inhibition performance.

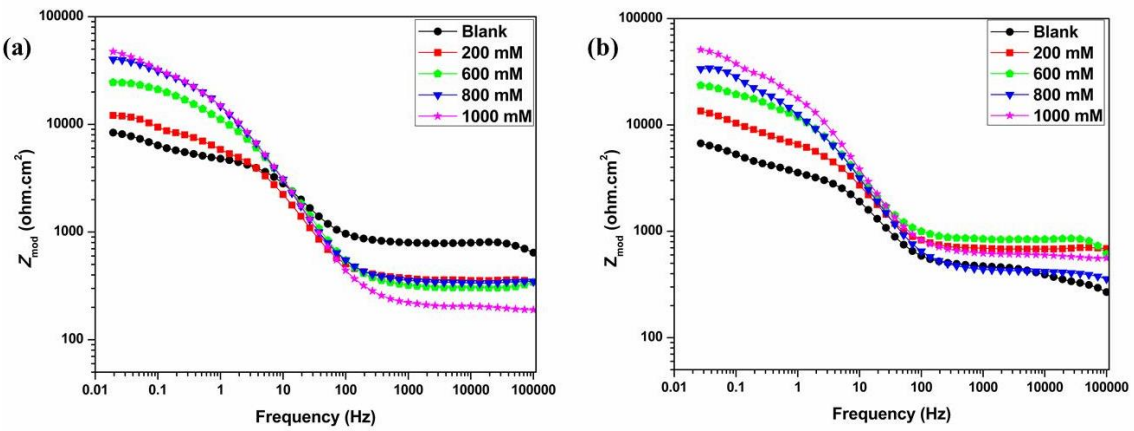

Fig. 3.45 Bode magnitude plots for the corrosion of Mg-Al-Zn alloy in the presence of different concentrations of morpholine in (a) 6 mM chloride medium at 35 °C and (b) 2 mM sulfate medium at 35 °C.

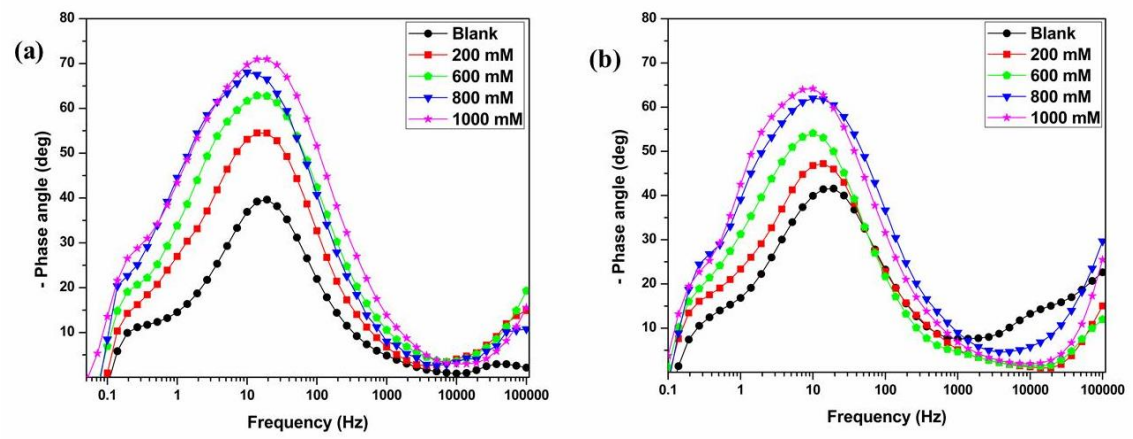

Fig. 3.46 Bode phase angle plots for the corrosion of Mg-Al-Zn alloy in the presence of different concentrations of morpholine in (a) 6 mM chloride medium at 35 °C and (b) 2 mM sulfate medium at 35 °C.

3.5.3. Effect of temperature

The increase in the temperature of the medium decreases the corrosion inhibition efficiency of the morpholine in the corrosive media as seen from the Table

3.24, Table 3.25, Table 3.26 and Table 3.27. The increased film capacitance and decreased film resisitance with the successive increase in the medium temperature further supports the observed trend of efficiency.

Fig. 3.47 (a) and Fig. 3.47 (b), respectively, represents the Arrhenius plots for the corrosion of Mg-Al-Zn alloy in the presence of different concentrations of morpholine in a corrosive solution of 6 mM chloride medium and 2 mM sulfate medium. The plots of ln (υ_{corr}/T) versus ($1/T$) for the same are shown in Fig. 3.48 (a) and Fig. 3.48 (b), respectively. The obtained activation parameters for the corrosion of Mg-Al-Zn alloy in chloride and sulfate media in the presence of different concentrations of morpholine are enlisted in Table 3.28 and Table 3.29, respectively. The increased activation energy with the increase in the concentration of morpholine indicates the increased obstruction for the occurance of Mg-Al-Zn alloy corrosion. The pattern of variation in $\Delta H^{\#}$ values is similar to that of activation energy values. The decreased entropy of the reaction during activation indicates the association of the reactants in the rate determining step of the Mg-Al-Zn alloy corrosion.

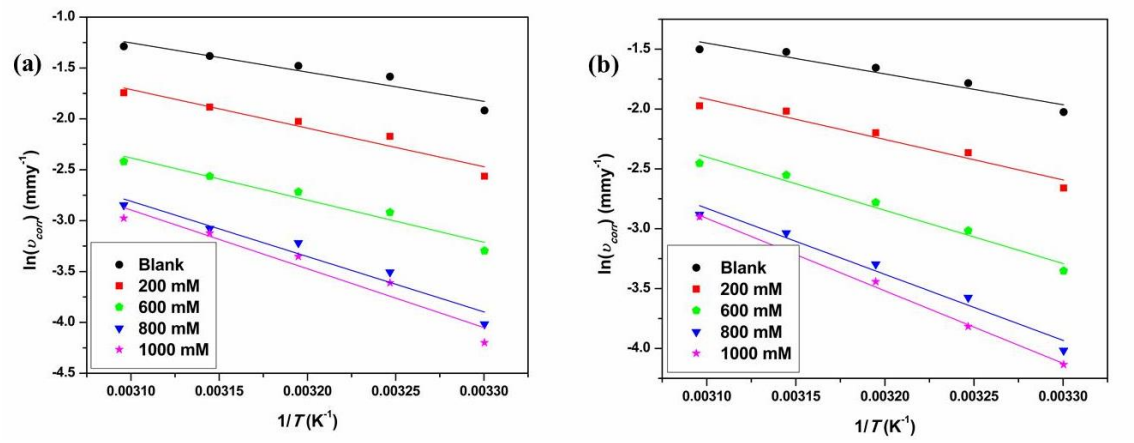

Fig. 3.47 Arrhenius plots for the corrosion of Mg-Al-Zn alloy in the presence of different concentrations of morpholine in a corrosive solution of (a) 6 mM chloride medium and (b) 2 mM sulfate medium.

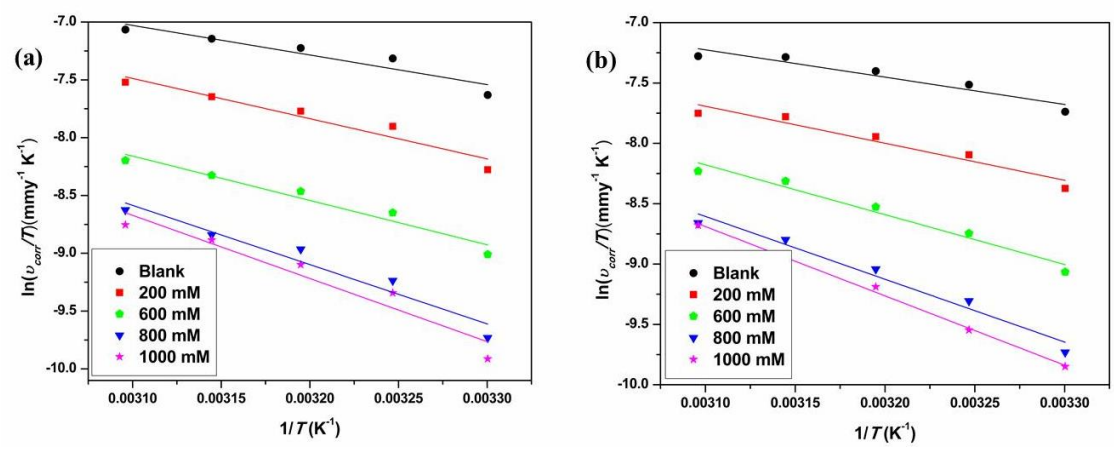

Fig. 3.48 Plots of ln (υ_{corr}/T) versus ($1/T$) for the corrosion of Mg-Al-Zn alloy in the presence of different concentrations of morpholine in a corrosive solution of (a) 6 mM chloride medium and (b) 2 mM sulfate medium.

3.5.4. Adsorption isotherm

Langmuir, Temkin, Frumkin and Flory-Huggins isotherms were tried to fit the graphical variation of the surface coverage and concentration of the inhibitor. It was found that the interfacial adsorption of morpholine can be best fitted using Langmuir adsorption isotherm. The Langmuir adsorption isotherm for the adsorption of mixture of inhibitor on Mg-Al-Zn alloy surface at different temperature in 6 mM chloride and 2 mM sulfate media are represented in Fig. 3.49 (a) and Fig. 3.49 (b), respectively.

The assessed thermodynamic parameters at different temperatures for the adsorption of morpholine on Mg-Al-Zn alloy surface in chloride and sulfate media are tabulated in Table 3.30 and Table 3.31, respectively. The slight deviation in the linear regression coefficient value of the Langmuir adsorption isotherm indicates the mutual interaction of the adsorbed morpholine molecules on the surface of the Mg-Al-Zn alloy. The decrease in standard free energy of the system is denoted by negative values of the ΔG^{o}_{ads}. The negative value of ΔG^{o}_{ads} implies the spontaneity in the adsorption of morpholine on the surface of the alloy (El Bribri et al. 2013). The values of ΔG^{o}_{ads} are in the range of –12.7 to 14.2 kJ mol^{-1}, which hint the physisorption process involving weak electrostatic interactions (Bentiss et al. 2005). Further the

lower value of $\Delta H°_{ads}$ with negative sign accounts the possible physisorption with low strength of the formed bond (Martinez and Stern 2002).

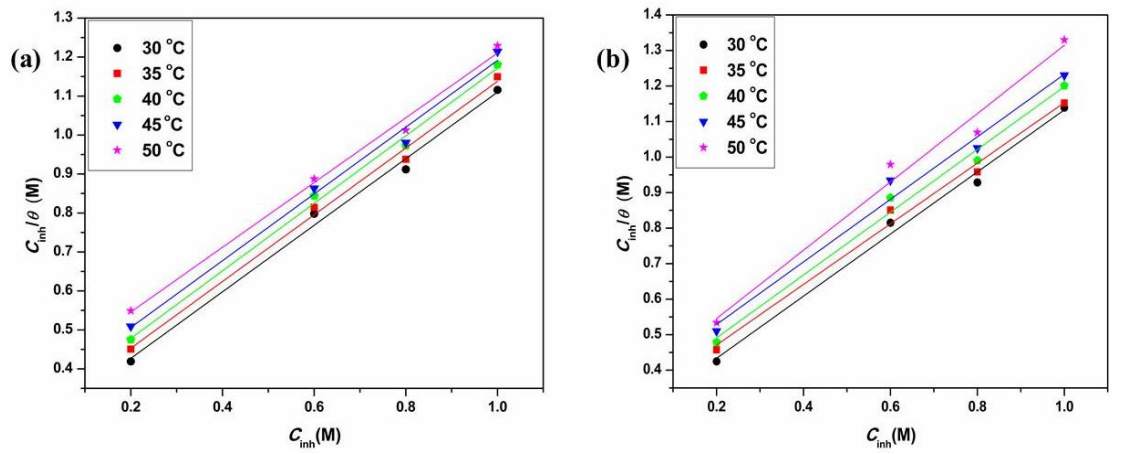

Fig. 3.49 Langmuir adsorption isotherms for the adsorption of morpholine on Mg-Al-Zn alloy surface at different temperatures in (a) 6 mM chloride medium and (b) 2 mM sulfate medium.

3.5.5. Surface analyses

The SEM image and EDX spectra of Mg-Al-Zn alloy surface after 24 h of immersion in 10 mM chloride medium containing 800 mM morpholine are studied and presented in Fig. 3.50 (a) and Fig. 3.50 (b), respectively.

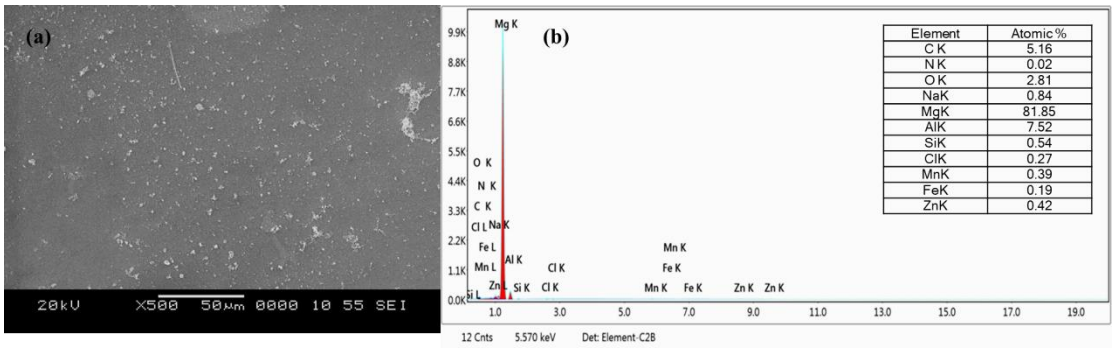

Fig. 3.50 (a) SEM image of Mg-Al-Zn alloy surface after 24 h of immersion in the corrosive medium containing 10 mM chloride ions, 800 mM morpholine and (b) corresponding EDX spectra.

The SEM image and EDX spectra of the alloy surface after 24 h of immersion in 10 mM sulfate medium are shown in the Fig. 3.51 (a) and Fig. 3.51 (b), respectively. The SEM image of the inhibited surface is smoother with fewer pits in comparision with the SEM image of the corroded surface. In inhibited surface the size of the pits are small and are covered by inhibitor film. The EDX spectra given in the Fig. 3.50 (b) and Fig. 3.51 (b) further corroborate the modified surface film. In EDX spectra along with metallic peak, less intense peak of oxygen and peak of carbon are observed, which signify the modified Mg-Al-Zn alloy surface by organic inhibitor.

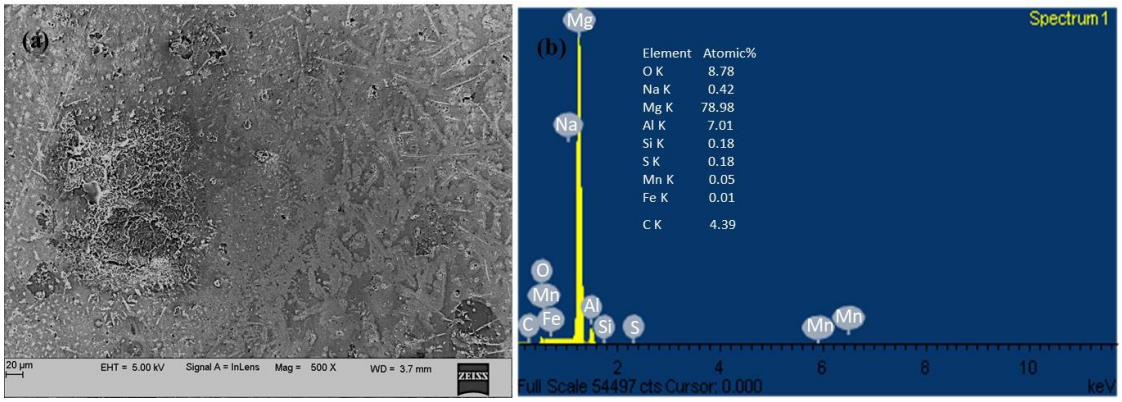

Fig. 3.51 (a) SEM image of Mg-Al-Zn alloy surface after 24 h of immersion in the corrosive medium containing 10 mM sulfate ions, 800 mM morpholine and (b) corresponding EDX spectra.

Table 3.24 (a) Tafel polarization parameters for the corrosion of Mg-Al-Zn alloy in a corrosive solution containing 2 mM chloride ions and different concentrations of morpholine at different temperatures.

Temperature (°C)	Inhibitor concentration (mM)	E_{corr} vs. SCE (mV)	i_{corr} (μA cm^{-2})	$-b_c$ (mV dec^{-1})	η (%)
30	Blank	−1476	4.58	356	-
	200	−1529	2.66	218	41.9
	600	−1538	1.32	205	71.2
	800	−1502	0.76	204	83.4
	1000	−1533	0.62	199	86.5
35	Blank	−1466	5.36	363	-
	200	−1538	3.24	209	39.6
	600	−1521	1.65	191	69.2
	800	−1498	1.06	186	80.2
	1000	−1476	0.96	185	82.1
40	Blank	−1486	6.02	332	-
	200	−1535	3.78	227	37.2
	600	−1546	1.94	190	67.8
	800	−1517	1.39	178	76.9
	1000	−1528	1.25	170	79.2
45	Blank	−1470	6.79	370	-
	200	−1529	4.41	224	35.1
	600	−1539	2.25	222	66.9
	800	−1517	1.79	196	73.6
	1000	−1521	1.59	187	76.6
50	Blank	−1379	7.85	442	-
	200	−1422	5.28	245	32.7
	600	−1407	2.87	236	63.4
	800	−1448	2.32	213	70.4
	1000	−1406	2.00	200	74.5

Table 3.24 (b) Tafel polarization parameters for the corrosion of Mg-Al-Zn alloy in a corrosive solution containing 6 mM chloride ions and different concentrations of morpholine at different temperatures.

Temperature (°C)	Inhibitor concentration (mM)	E_{corr} vs. SCE (mV)	i_{corr} (μA cm^{-2})	$-b_c$ (mV dec^{-1})	η (%)
30	Blank	−1499	6.85	270	-
	200	−1489	3.58	265	47.7
	600	−1421	1.70	242	75.2
	800	−1497	0.84	185	87.7
	1000	−1458	0.71	177	89.6
35	Blank	−1445	9.53	279	-
	200	−1478	5.30	248	44.4
	600	−1481	2.51	227	73.7
	800	−1496	1.40	181	85.3
	1000	−1448	1.24	203	87.0
40	Blank	−1433	10.59	297	-
	200	−1476	6.13	255	42.1
	600	−1426	3.06	243	71.1
	800	−1496	1.88	196	82.2
	1000	−1437	1.62	191	84.7
45	Blank	−1420	11.68	317	-
	200	−1459	7.09	282	39.3
	600	−1394	3.56	256	69.5
	800	−1468	2.15	224	81.6
	1000	−1421	2.06	197	82.4
50	Blank	−1428	12.82	338	-
	200	−1430	8.15	290	36.4
	600	−1381	4.15	249	67.6
	800	−1458	2.69	249	79.0
	1000	−1419	2.39	229	81.4

Table 3.24 (c) Tafel polarization parameters for the corrosion of Mg-Al-Zn alloy in a corrosive solution containing 10 mM chloride ions and different concentrations of morpholine at different temperatures.

Temperature (°C)	Inhibitor concentration (mM)	E_{corr} vs. SCE (mV)	i_{corr} (μA cm^{-2})	$-b_c$ (mV dec^{-1})	η (%)
30	Blank	−1458	10.09	286	-
	200	−1419	5.03	236	50.1
	600	−1442	2.23	223	77.9
	800	−1415	0.97	230	90.4
	1000	−1455	0.70	222	93.1
35	Blank	−1446	11.18	269	-
	200	−1436	5.89	251	47.3
	600	−1443	2.78	239	75.1
	800	−1414	1.53	205	86.3
	1000	−1456	1.12	220	90.0
40	Blank	−1416	12.27	310	-
	200	−1446	6.66	299	45.7
	600	−1390	3.49	287	71.6
	800	−1358	1.98	270	83.9
	1000	−1339	1.65	241	86.6
45	Blank	−1461	13.05	306	-
	200	−1414	7.54	274	42.2
	600	−1424	4.01	250	69.3
	800	−1463	2.54	242	80.5
	1000	−1433	2.19	227	83.2
50	Blank	−1405	15.37	339	-
	200	−1434	9.26	301	39.8
	600	−1441	5.07	291	67.0
	800	−1398	3.44	287	77.6
	1000	−1364	2.77	247	82.0

Table 3.25 (a) Tafel polarization parameters for the corrosion of Mg-Al-Zn alloy in a corrosive solution containing 2 mM sulfate ions and different concentrations of morpholine at different temperatures.

Temperature (°C)	Inhibitor concentration (mM)	E_{corr} vs. SCE (mV)	i_{corr} (μA cm^{-2})	$-b_c$ (mV dec^{-1})	η (%)
30	Blank	−1546	6.14	284	-
	200	−1544	3.25	254	47.1
	600	−1539	1.62	241	73.6
	800	−1528	0.85	228	86.2
	1000	−1529	0.75	210	87.8
35	Blank	−1556	7.80	349	-
	200	−1479	4.39	274	43.7
	600	−1492	2.30	254	70.5
	800	−1540	1.29	241	83.5
	1000	−1560	1.03	236	86.8
40	Blank	−1469	8.90	311	-
	200	−1498	5.18	266	41.8
	600	−1468	2.87	245	67.8
	800	−1418	1.71	221	80.8
	1000	−1408	1.49	218	83.3
45	Blank	−1463	10.15	309	-
	200	−1474	6.17	283	39.2
	600	−1414	3.63	263	64.2
	800	−1467	2.23	244	78.0
	1000	−1487	1.90	227	81.3
50	Blank	−1468	10.36	285	-
	200	−1476	6.48	250	37.5
	600	−1430	4.01	236	61.3
	800	−1467	2.61	231	74.8
	1000	−1441	2.57	213	75.2

Table 3.25 (b) Tafel polarization parameters for the corrosion of Mg-Al-Zn alloy in a corrosive solution containing 6 mM sulfate ions and different concentrations of morpholine at different temperatures.

Temperature (°C)	Inhibitor concentration (mM)	E_{corr} vs. SCE (mV)	i_{corr} (μA cm^{-2})	$-b_c$ (mV dec^{-1})	η (%)
30	Blank	−1566	9.47	308	-
	200	−1504	4.65	246	50.9
	600	−1555	2.12	240	77.6
	800	−1531	0.88	232	90.7
	1000	−1525	0.77	214	91.9
35	Blank	−1520	10.79	373	-
	200	−1485	5.64	271	47.7
	600	−1476	2.61	259	75.8
	800	−1476	1.44	223	86.7
	1000	−1505	1.27	212	88.2
40	Blank	−1513	11.81	376	-
	200	−1529	6.67	256	43.5
	600	−1536	3.25	234	72.5
	800	−1530	1.89	232	84.0
	1000	−1505	1.75	217	85.2
45	Blank	−1500	12.87	379	-
	200	−1508	7.65	283	40.6
	600	−1471	3.87	267	69.9
	800	−1528	2.53	261	80.3
	1000	−1478	2.26	250	82.4
50	Blank	−1446	14.63	335	-
	200	−1488	9.11	270	37.7
	600	−1493	4.80	245	67.2
	800	−1490	3.34	238	77.2
	1000	−1422	2.86	223	80.5

Table 3.25 (c) Tafel polarization parameters for the corrosion of Mg-Al-Zn alloy in a corrosive solution containing 10 mM sulfate ions and different concentrations of morpholine at different temperatures.

Temperature (°C)	Inhibitor concentration (mM)	E_{corr} vs. SCE (mV)	i_{corr} (μA cm^{-2})	$-b_c$ (mV dec^{-1})	η (%)
30	Blank	−1530	11.68	386	-
	200	−1529	5.29	206	54.7
	600	−1558	2.36	194	79.8
	800	−1523	0.63	181	94.6
	1000	−1537	0.57	181	95.1
35	Blank	−1521	12.65	402	-
	200	−1469	6.05	256	52.2
	600	−1508	2.86	252	77.4
	800	−1477	0.97	247	92.3
	1000	−1458	0.90	231	92.9
40	Blank	−1460	14.43	344	-
	200	−1504	7.24	257	49.8
	600	−1460	3.50	237	75.7
	800	−1504	1.38	248	90.4
	1000	−1522	1.34	228	90.7
45	Blank	−1458	15.82	327	-
	200	−1438	8.53	258	46.1
	600	−1471	4.15	224	73.8
	800	−1506	1.84	213	88.4
	1000	−1473	1.73	209	89.1
50	Blank	−1462	17.49	318	-
	200	−1404	9.70	254	44.5
	600	−1455	5.15	238	70.6
	800	−1417	2.38	235	86.4
	1000	−1494	2.21	224	87.4

Table 3.26 (a) Electrochemical impedance parameters for the corrosion of Mg-Al-Zn alloy in a corrosive solution containing 2 mM chloride ions and different concentrations of morpholine at different temperatures.

Temperature (°C)	Inhibitor concentration (mM)	R_f (Ω cm^2)	R_{dif} (Ω cm^2)	R_p (Ω cm^2)	C_f (μF cm^{-2})	C_{dif} (μF cm^{-2})	η (%)
30	Blank	4053	1888	9501	23.4	186.1	-
	200	6389	4295	15837	21.9	177.7	40.0
	600	13560	5575	32205	19.4	165.1	70.5
	800	20220	16500	52210	17.1	149.1	81.8
	1000	35250	17470	62050	14.6	136.3	84.7
35	Blank	3885	1738	8034	24.4	195.1	-
	200	5586	3515	13115	22.0	183.8	38.7
	600	15640	4125	25705	20.4	170.0	68.7
	800	18450	8722	36752	19.5	167.1	78.1
	1000	19130	9810	42950	18.7	163.4	81.3
40	Blank	3269	1659	6932	25.6	208.3	-
	200	4259	3056	10748	21.1	189.6	35.5
	600	10095	3917	20030	19.2	176.8	65.4
	800	14530	7690	28290	16.2	169.9	75.5
	1000	18450	8676	33696	15.5	166.7	79.4
45	Blank	3052	1587	6725	27.6	228.1	-
	200	4008	2117	10115	24.5	218.3	33.5
	600	9008	3572	18529	22.2	205.8	63.7
	800	12520	7560	24560	19.3	196.0	72.6
	1000	13950	8540	27230	17.3	187.3	75.3
50	Blank	2488	1503	5581	30.7	250.7	-
	200	3690	1857	8193	27.4	231.0	31.9
	600	5498	2560	14429	24.8	224.8	61.3
	800	9660	4886	18456	22.0	213.0	69.8
	1000	10220	5570	20590	19.4	204.5	72.9

Table 3.26 (b) Electrochemical impedance parameters for the corrosion of Mg-Al-Zn alloy in a corrosive solution containing 6 mM chloride ions and different concentrations of morpholine at different temperatures.

Temperature (°C)	Inhibitor concentration (mM)	R_f (Ω cm²)	R_{dif} (Ω cm²)	R_p (Ω cm²)	C_f (μF cm^{-2})	C_{dif} (μF cm^{-2})	η (%)
30	Blank	3597	1820	7582	23.9	236.5	-
	200	9160	2373	14453	19.3	204.7	47.5
	600	13330	9490	29590	16.1	190.9	74.4
	800	23240	12139	51379	13.6	180.3	85.2
	1000	27350	12920	54980	11.8	151.3	86.2
35	Blank	2879	1713	6085	25.0	242.4	-
	200	6366	2048	11025	24.0	227.7	44.8
	600	9967	7626	22036	18.6	209.2	72.4
	800	10916	11380	34690	15.8	199.8	82.5
	1000	11940	11958	38888	13.4	169.4	84.4
40	Blank	2577	1608	4880	26.9	252.8	-
	200	5340	1921	8475	25.4	239.0	42.4
	600	8025	6645	16675	20.9	210.2	70.7
	800	9585	6692	24932	16.5	205.0	80.4
	1000	9926	7045	27695	12.6	186.5	82.4
45	Blank	2214	1569	4742	28.3	257.0	-
	200	4315	1635	7570	27.2	247.6	37.4
	600	6959	5312	15150	23.6	222.7	68.7
	800	9052	5844	21454	19.8	219.7	77.9
	1000	9905	6801	23521	15.9	204.3	79.8
50	Blank	1886	1487	4548	31.5	269.8	-
	200	3023	1579	6951	29.2	256.0	34.6
	600	6168	3879	12615	26.8	255.4	63.9
	800	7241	5407	18637	22.9	225.4	75.6
	1000	8233	6185	21195	20.8	217.0	78.5

Table 3.26 (c) Electrochemical impedance parameters for the corrosion of Mg-Al-Zn alloy in a corrosive solution containing 10 mM chloride ions and different concentrations of morpholine at different temperatures.

Temperature (°C)	Inhibitor concentration (mM)	R_f (Ω cm²)	R_{dif} (Ω cm²)	R_p (Ω cm²)	C_f (μF cm^{-2})	C_{dif} (μF cm^{-2})	η (%)
30	Blank	2102	1516	6915	25.4	302.1	-
	200	4925	6155	13205	18.3	205.4	47.6
	600	11960	9190	28420	15.0	188.3	75.7
	800	22390	16653	46973	12.6	174.8	85.3
	1000	26320	17420	51140	10.4	150.2	86.5
35	Blank	2002	1485	5509	25.8	320.1	-
	200	3535	3029	9894	21.7	230.5	44.3
	600	10874	9015	20575	18.6	211.8	73.2
	800	18660	8633	33253	15.5	203.4	83.4
	1000	20960	8491	37331	12.3	197.5	85.2
40	Blank	1823	1363	4411	29.4	332.1	-
	200	3314	2317	7701	24.9	288.3	42.7
	600	7530	5171	14811	22.7	258.9	70.2
	800	9033	6814	21234	19.8	233.9	79.2
	1000	11690	7870	24700	16.3	217.4	82.1
45	Blank	1733	1303	4156	32.7	337.3	-
	200	2765	2021	7040	29.5	316.4	41.0
	600	5844	3432	12659	26.7	293.7	67.2
	800	8060	5887	18047	23.8	266.1	77.0
	1000	10920	7520	21620	19.1	253.2	80.8
50	Blank	1434	1283	3969	36.1	345.4	-
	200	2536	1908	6488	31.9	339.0	38.8
	600	4274	2987	11047	28.7	320.8	64.1
	800	7489	4890	15930	25.8	304.4	75.1
	1000	9880	5980	18550	23.9	294.1	78.6

Table 3.27 (a) Electrochemical impedance parameters for the corrosion of Mg-Al-Zn alloy in a corrosive solution containing 2 mM sulfate ions and different concentrations of morpholine at different temperatures.

Temperature (°C)	Inhibitor concentration (mM)	R_f (Ω cm²)	R_{dif} (Ω cm²)	R_p (Ω cm²)	C_f (μF cm^{-2})	C_{dif} (μF cm^{-2})	η (%)
30	Blank	3247	2156	5947	34.6	228.4	-
	200	6110	3519	11379	28.5	219.5	47.7
	600	11210	4952	22102	23.3	205.7	73.1
	800	16620	7829	43029	19.8	195.8	86.2
	1000	18090	8500	47600	16.6	188.5	87.5
35	Blank	3164	1960	5687	40.3	230.1	-
	200	4672	3186	10037	38.0	229.2	43.3
	600	11040	4045	19135	32.4	216.0	70.3
	800	12070	6290	32060	28.7	203.2	82.3
	1000	15040	7760	43150	21.0	195.5	86.8
40	Blank	2937	1809	5046	45.3	241.2	-
	200	3805	2164	8544	39.8	233.3	40.9
	600	8160	3553	16073	34.1	224.5	68.6
	800	10220	5120	25380	29.9	217.7	80.1
	1000	12690	6910	30720	23.7	210.9	83.6
45	Blank	2785	1508	4411	49.7	260.0	-
	200	3381	1953	7004	46.9	251.0	37.0
	600	7955	2751	13191	37.3	238.1	66.6
	800	9590	3440	19150	32.4	223.7	77.0
	1000	10510	5400	23780	30.9	215.4	81.5
50	Blank	2693	1116	4261	54.3	272.1	-
	200	3083	1692	6628	49.1	265.7	35.7
	600	7670	2048	11308	41.4	244.7	62.3
	800	8460	2964	16274	37.9	232.7	73.8
	1000	9320	3423	18233	34.9	224.2	76.6

Table 3.27 (b) Electrochemical impedance parameters for the corrosion of Mg-Al-Zn alloy in a corrosive solution containing 6 mM sulfate ions and different concentrations of morpholine at different temperatures.

Temperature (°C)	Inhibitor concentration (mM)	R_f (Ω cm^2)	R_{dif} (Ω cm^2)	R_p (Ω cm^2)	C_f (μF cm^{-2})	C_{dif} (μF cm^{-2})	η (%)
30	Blank	2981	1839	5893	38.9	286.2	-
	200	6927	4676	11816	36.0	279.6	50.1
	600	15690	7090	26760	26.7	255.5	78.0
	800	29460	10090	49910	20.7	246.4	88.2
	1000	30760	12500	57370	19.6	228.5	89.7
35	Blank	2806	1642	5631	47.6	292.1	-
	200	5290	3840	10796	43.7	281.3	47.8
	600	11160	5910	21970	34.1	256.1	74.4
	800	23100	6771	38521	29.2	248.2	85.4
	1000	27830	7243	43063	26.1	244.4	86.9
40	Blank	2689	1526	4643	52.2	296.3	-
	200	4122	2908	8232	47.2	290.0	43.6
	600	8085	5350	16770	39.7	278.4	72.3
	800	16280	5830	28380	36.7	262.2	83.6
	1000	17410	6190	32700	29.5	253.9	85.8
45	Blank	2531	1433	4329	58.8	304.0	-
	200	3049	2251	7215	54.9	293.6	40.0
	600	6482	4762	13932	43.6	287.3	68.9
	800	11730	5463	22553	37.8	271.8	80.8
	1000	13070	5650	25030	35.3	262.3	82.7
50	Blank	2511	1075	3760	61.5	322.5	-
	200	2466	1923	5902	58.7	304.8	36.3
	600	4210	3815	11405	49.2	294.9	67.0
	800	9010	5030	16250	43.4	276.6	76.9
	1000	10270	5360	19630	38.3	268.6	80.8

Table 3.27 (c) Electrochemical impedance parameters for the corrosion of Mg-Al-Zn alloy in a corrosive solution containing 10 mM sulfate ions and different concentrations of morpholine at different temperatures.

Temperature (°C)	Inhibitor concentration (mM)	R_f (Ω cm²)	R_{dif} (Ω cm²)	R_p (Ω cm²)	C_f (μF cm^{-2})	C_{dif} (μF cm^{-2})	η (%)
30	Blank	2780	1681	4714	41.3	337.0	-
	200	3202	4428	10410	34.7	311.4	54.7
	600	9930	8810	21230	29.6	294.9	77.8
	800	27770	17120	60290	27.5	283.0	92.2
	1000	29240	19960	67610	24.1	263.6	93.0
35	Blank	2679	1395	4347	49.8	346.7	-
	200	3030	3878	8933	46.3	331.8	51.3
	600	8890	7470	17910	41.4	324.7	75.7
	800	24560	14310	45830	37.0	295.4	90.5
	1000	28410	15110	49240	35.5	266.6	91.2
40	Blank	2434	1330	3928	55.2	351.5	-
	200	2912	2619	7606	53.4	346.0	48.4
	600	7540	5961	15071	49.1	330.0	73.9
	800	13640	9260	34560	44.7	319.6	88.6
	1000	17060	9647	39587	42.5	311.7	90.1
45	Blank	2145	1201	3457	62.3	364.3	-
	200	2350	2412	6405	57.5	354.8	46.0
	600	6770	3840	11930	52.8	344.4	71.0
	800	10430	6210	26240	46.5	327.0	86.8
	1000	12570	6895	29515	42.5	304.6	88.3
50	Blank	1980	994	3148	66.8	388.8	-
	200	2233	1665	5511	64.9	375.6	42.9
	600	5220	3000	10020	57.3	361.6	68.6
	800	9370	3554	18824	52.3	344.7	83.3
	1000	10120	4153	22473	49.5	340.4	86.0

Table 3.28 Activation parameters for the corrosion of Mg-Al-Zn alloy in 30% aqueous ethylene glycol containing chloride ions and different concentrations of morpholine.

Concentration of chloride ion (mM)	**Inhibitor concentration (mM)**	E_a **(kJ mol^{-1})**	$\Delta H^{\#}$ **(kJ mol^{-1})**	$\Delta S^{\#}$ **(J mol^{-1} K^{-1})**
2	Blank	21.6	19.0	–201.5
	200	27.5	24.9	–186.5
	600	31.0	28.4	–181.0
	800	45.3	42.7	–138.2
	1000	46.9	44.3	–134.2
6	Blank	23.9	21.3	–189.9
	200	31.5	28.9	–170.1
	600	34.5	31.9	–166.6
	800	45.2	42.6	–136.8
	1000	48.0	45.4	–128.9
10	Blank	16.1	13.5	–213.2
	200	23.8	21.2	–193.5
	600	32.6	30.0	–171.3
	800	49.4	46.8	–122.2
	1000	56.2	53.6	–102.5

Table 3.29 Activation parameters for the corrosion of Mg-Al-Zn alloy in 30% aqueous ethylene glycol containing sulfate ions and different concentrations of morpholine.

Concentration of sulfate ion (mM)	**Inhibitor concentration (mM)**	E_a **(kJ mol^{-1})**	$\Delta H^{\#}$ **(kJ mol^{-1})**	$\Delta S^{\#}$ **(J mol^{-1} K^{-1})**
2	Blank	21.4	18.8	–199.3
	200	28.1	25.5	–182.5
	600	36.9	34.3	–159.1
	800	45.9	43.3	–135.0
	1000	50.4	47.8	–121.7
6	Blank	17.0	14.4	–210.6
	200	26.9	24.3	–184.0
	600	32.6	30.0	–171.5
	800	52.5	49.9	–112.7
	1000	51.4	48.8	–117.1
10	Blank	16.8	14.2	–209.8
	200	25.3	22.7	–188.3
	600	31.4	28.8	–174.7
	800	52.7	50.1	–115.0
	1000	56.1	53.5	–104.6

Table 3.30 Thermodynamic parameters for the adsorption of morpholine on Mg-Al-Zn alloy in 30% aqueous ethylene glycol containing different concentrations of chloride ions and different concentrations of morpholine.

Concentration of chloride ion (mM)	Temperature (°C)	$\Delta G°_{ads}$ (kJ mol^{-1})	$\Delta H°_{ads}$ (kJ mol^{-1})	$\Delta S°_{ads}$ ($JK^{-1}mol^{-1}$)	R^2
2	30	–12.7	5.0	58.0	0.994
	35	–12.8			0.993
	40	–12.7			0.996
	45	–13.7			0.992
	50	–13.8			0.992
6	30	–13.6	–15.6	–6.8	0.990
	35	–13.5			0.992
	40	–13.5			0.994
	45	–13.5			0.987
	50	–13.4			0.991
10	30	–13.7	–13.0	2.4	0.991
	35	–13.7			0.994
	40	–13.8			0.989
	45	–13.8			0.992
	50	–13.7			0.994

Table 3.31 Thermodynamic parameters for the adsorption of morpholine on Mg-Al-Zn alloy in 30% aqueous ethylene glycol containing different concentrations of sulfate ions and different concentrations of morpholine.

Concentration of sulfate ion (mM)	Temperature (°C)	$\Delta G°_{ads}$ (kJ mol^{-1})	$\Delta H°_{ads}$ (kJ mol^{-1})	$\Delta S°_{ads}$ ($JK^{-1}mol^{-1}$)	R^2
2	30	–13.5	–12.7	2.4	0.989
	35	–13.4			0.987
	40	–13.5			0.985
	45	–13.4			0.977
	50	–13.6			0.975
6	30	–13.8	–18.0	–13.8	0.988
	35	–13.9			0.994
	40	–13.7			0.991
	45	–13.7			0.994
	50	–13.6			0.996
10	30	–14.1	–14.3	–0.8	0.982
	35	–14.1			0.981
	40	–14.2			0.981
	45	–14.0			0.982
	50	–14.1			0.973

3.6. CORROSION INHIBITION OF Mg-Al-Zn ALLOY IN 30% AQUEOUS ETHYLENE GLYCOL CONTAINING CHLORIDE IONS AND SULFATE IONS BY N-METHYL MORPHOLINE

3.6.1. Potentiodynamic polarization analyses

The potentiodynamic polarization plots for the corrosion of Mg-Al-Zn alloy in 10 mM chloride medium and 10 mM sulfate medium at 50 °C containing different concentrations of N-methyl morpholine are shown in Fig. 3.52 (a) and Fig. 3.52 (b), respectively.

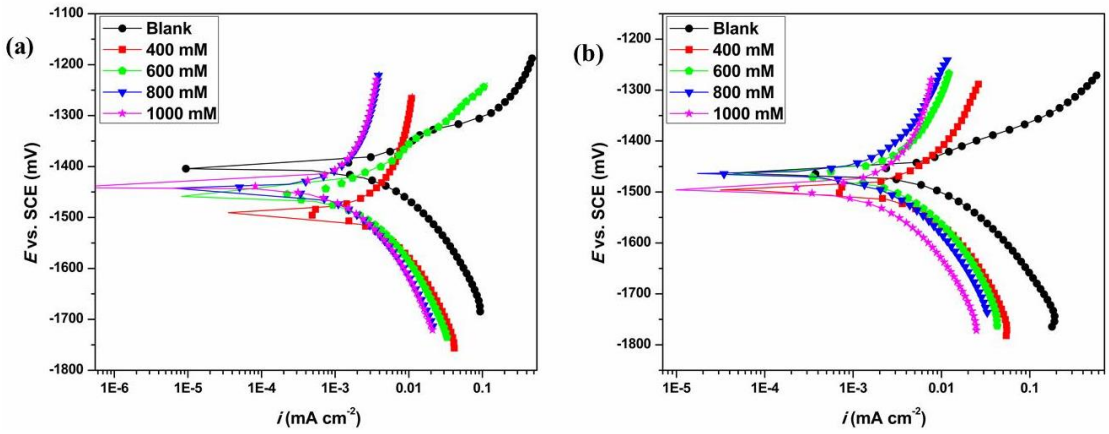

Fig. 3.52 Potentiodynamic polarization plots for the corrosion of Mg-Al-Zn alloy in the presence of different concentrations of N-methyl morpholine in a) 10 mM chloride medium at 50 °C and (b) 10 mM sulfate medium at 50 °C.

From the Fig. 3.52, the following observation were recorded: On increasing the concentration of N-methyl morpholine the polarization curves shift towards lower current density region, with no potent change in the overall shape of the polarization curves, which suggest that N-methyl morpholine decreases the rate of Mg-Al-Zn alloy corrosion without affecting the mechanism of the electrode reaction. Like morpholine, for N-methyl morpholine also the linear Tafel behavior is observed for cathodic branches of the Tafel plots and thus i_{corr} is obtained from the cathodic extrapolation of Tafel plots at its corrosion potential. The deduced potentiodynamic polarization parameters from the Tafel extrapolation method were tabulated in the Table 3.32 (a),

Table 3.32 (b), Table 3.32 (c) and Table 3.33 (a), Table 3.33 (b), Table 3.33 (c) for different concentration of N-methyl morpholine at different temperature in chloride and sulfate media, respectively.

From the tabulated values of the Table 3.32 and Table 3.33, it follows that N-methyl morpholine act as a mixed type inhibitor in both chloride and sulfate media with slight variation in cathodic slope. The inhibition efficiency increases with the rise in the concentration of N-methyl morpholine and decreases with the enhancement in the temperature of the medium. The maximum efficiency shown by N-methyl morpholine at 30 °C in 10 mM chloride medium is 87.5% and in 10 mM sulfate medium is 89.1% at a concentration of 800 mM. Further increase in the concentration of the N-methyl morpholine does not increase the inhibition efficiency notably. The observed increase in effciency is in accordance with the increase in the ionic concentration of the media.

3.6.2. Electrochemical impedance spectroscopy

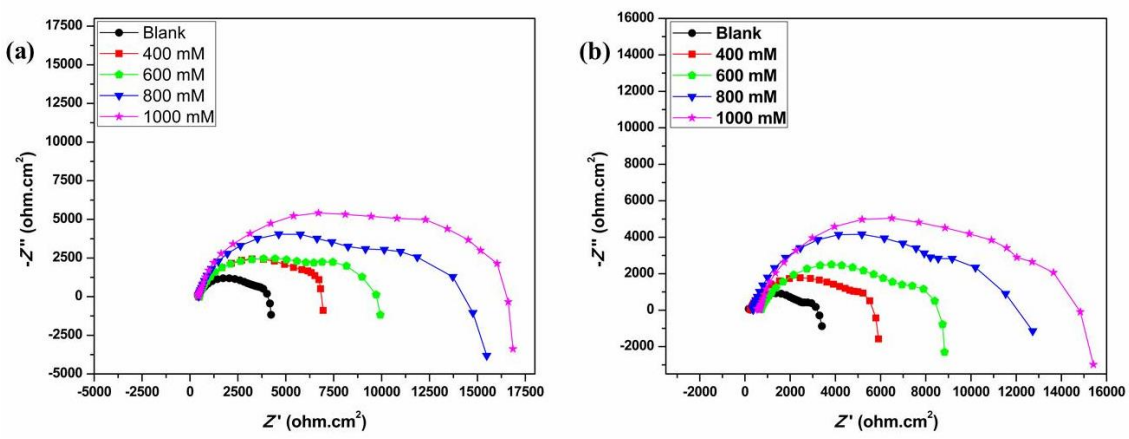

Fig. 3.53 Nyquist plots for the corrosion of Mg-Al-Zn alloy in the presence of different concentrations of N-methyl morpholine in (a) 10 mM chloride medium at 50 °C and (b) 10 mM sulfate medium at 50 °C.

The Nyquist plots for the corrosion of Mg-Al-Zn alloy in 10 mM chloride medium at 50 °C and 10 mM sulfate medium at 50 °C containing different concentrations of N-methyl morpholine are shown in Fig. 3.53 (a) and Fig. 3.53 (b),

respectively. Like in the presence of morpholine, presence of N-methyl morpholine also shows characteristic shape of Nyquist plots with two capacitive loops and the beginning of an inductive loop at higher, medium and lower frequencies, respectively. The diameter of the capacitive loop enlarges with the successive rise in N-methyl morpholine concentration in both the aggressive media. The unaltered shape of the Nyquist plot implies that the added N-methyl morpholine does not change the mechanism of the Mg-Al-Zn alloy corrosion.

The obtained Nyquist plots were simulated with the proposed equivalent circuit in Fig. 3.3 to deduce the impedance parameters such as R_f, C_f, R_{dif}, C_{dif} and η (%) and are enlisted in Table 3.34 (a), Table 3.34 (b), Table 3.34 (c) and Table 3.35 (a), Table 3.35 (b), Table 3.35 (c) for chloride and sulfate media, respectively. The obtained impedance results such as increased efficiency with the increase in the concentration of N-methyl morpholine as well as with increased ionic concentration of the media and decreased efficiency with the rise in medium temperature are in good agreement with the results of potentiodynamic polarization studies. The characteristic features of surface film such as lower film capacitance and higher film resistance are observed at the successive increase in the concentration of N-methyl morpholine.

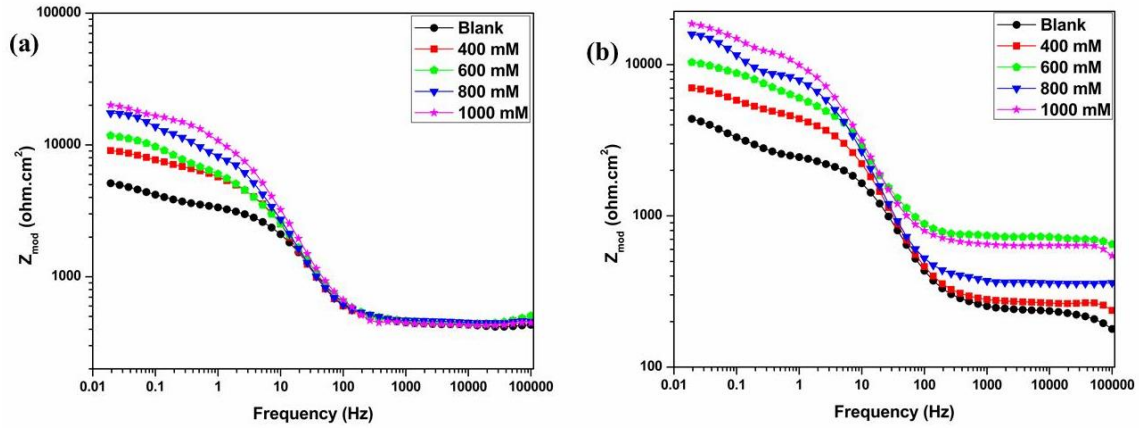

Fig. 3.54 Bode magnitude plots for the corrosion of Mg-Al-Zn alloy in the presence of different concentrations of N-methyl morpholine in (a) 10 mM chloride medium at 50 °C and (b) 10 mM sulfate medium at 50 °C.

Bode plots were constructed to understand the frequency specific impedance nature of N-methyl morpholine in aggressive media. Fig. 3.54 (a) and Fig. 3.54 (b) show the Bode magnitude plots for the corrosion of Mg-Al-Zn alloy in the presence of different concentrations of N-methyl morpholine in 10 mM chloride medium at 50 °C and 10 mM sulfate medium at 50 °C, respectively. Fig. 3.55 (a) and Fig. 3.55 (b) represent the Bode phase angle plots for the same.

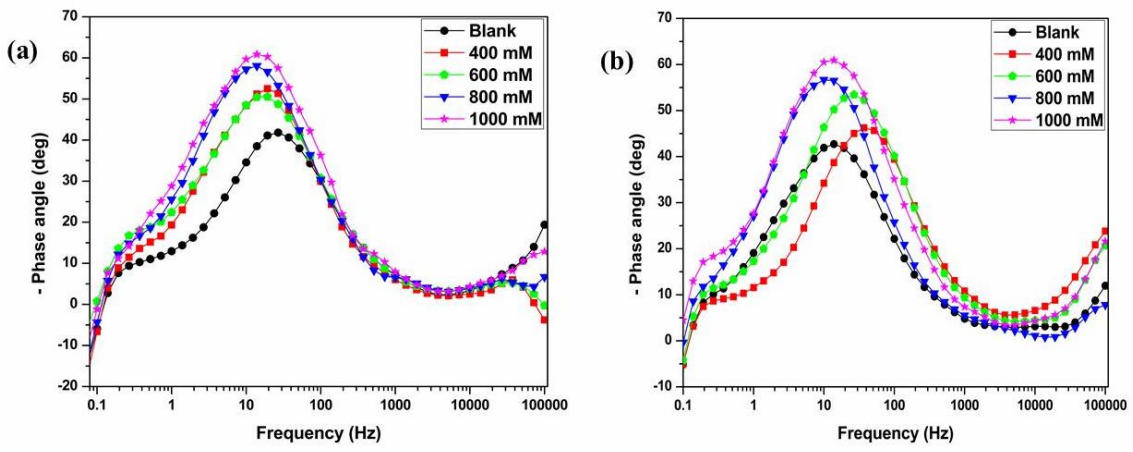

Fig. 3.55 Bode phase angle plots for the corrosion of Mg-Al-Zn alloy in the presence of different concentrations of N-methyl morpholine in (a) 10 mM chloride medium at 50 °C and (b) 10 mM sulfate medium at 50 °C.

A better efficiency of N-methyl morpholine in inhibiting the Mg-Al-Zn alloy corrosion at higher concentrations can be comprehended as the consequence of augmentation of resistance to corrosion and electrolyte inflow. Fig. 3.54 and Fig. 3.55, respectively, show the increase in low frequency impedance modulus and medium frequencies phase maximum for successive increase in the concentration of N-methyl morpholine.

3.6.3. Effect of temperature

The tabulated values in Tables 3.32, Tables 3.33, Table 3.34 and Table 3.35 evidence the effect of temperature on the inhibition efficiency of the N-methyl morpholine on Mg-Al-Zn alloy corrosion in chloride and sulfate media. In both the media, at higher temperature lower efficiency is observed which is further

authenticated by higher film capacitance and lower film resistance values as seen in the Tables 3.34 and Tables 3.35.

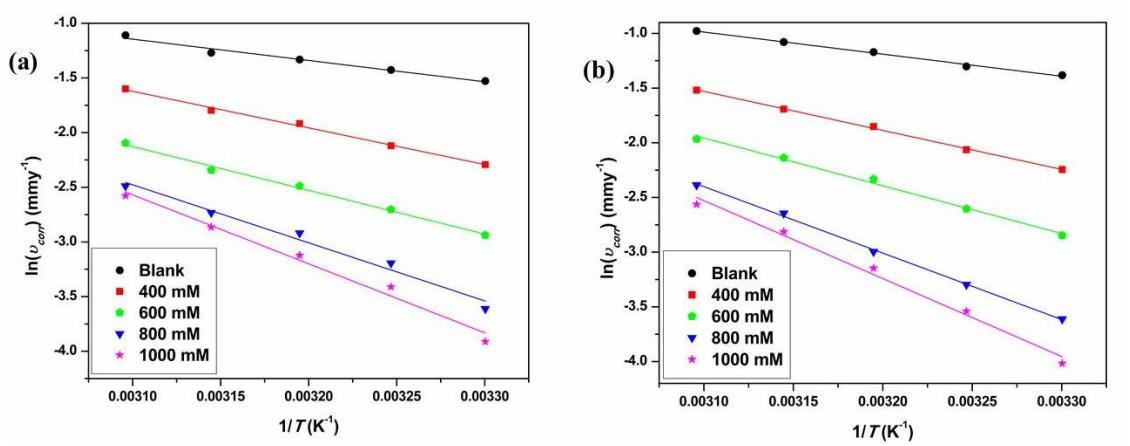

Fig. 3.56 Arrhenius plots for the corrosion of Mg-Al-Zn alloy in the presence of different concentrations of N-methyl morpholine in a corrosive solution of (a) 10 mM chloride medium and (b) 10 mM sulfate medium.

The Arrhenius plots for the corrosion of Mg-Al-Zn alloy in chloride and sulfate media containing different concentrations of N-methyl morpholine are as shown in Fig. 3.56 (a) and Fig. 3.56 (b), respectively. The plots of ln (υ_{corr}/T) versus ($1/T$) for the same are shown in Fig. 3.57 (a) and Fig. 3.57 (b), respectively.

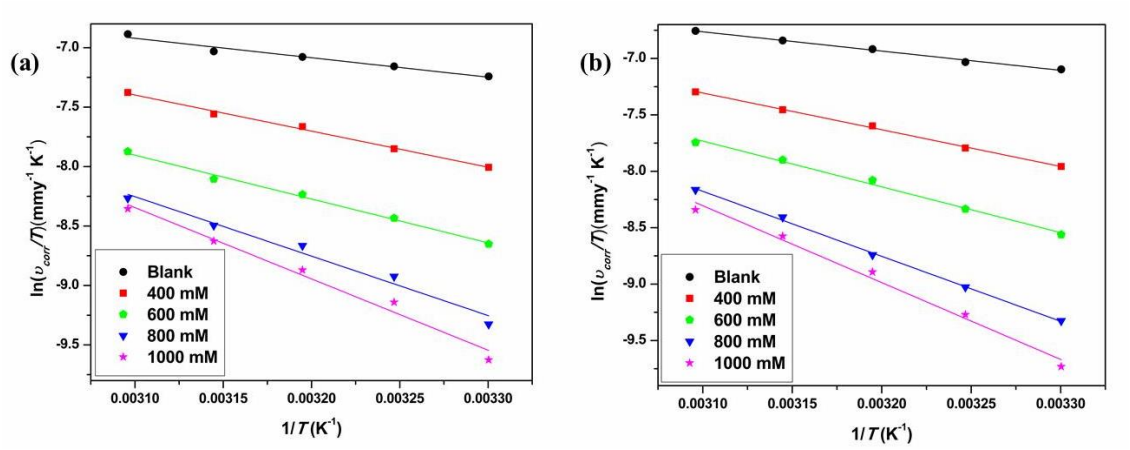

Fig. 3.57 Plots of ln (υ_{corr}/T) versus ($1/T$) for the corrosion of Mg-Al-Zn alloy in the presence of different concentrations of N-methyl morpholine in a corrosive solution of (a) 10 mM chloride medium and (b) 10 mM sulfate medium.

The calculated activation parameters for the corrosion of Mg-Al-Zn alloy in different concentrations of N-methyl morpholine containing chloride and sulfate media are summarized in Table 3.36 and Table 3.37, respectively. The energetically unfavored conditions for the occurrence of corrosion in both the media are indicated by the enlisted values of the activation energy. The variation in the values of $\Delta H^{\#}$ is similar to that of E_a. The negative values of $\Delta S^{\#}$ signify the decrease in the entropy of the system, indicating the association of the reactants during the formation of activated complex.

3.6.4. Adsorption isotherm

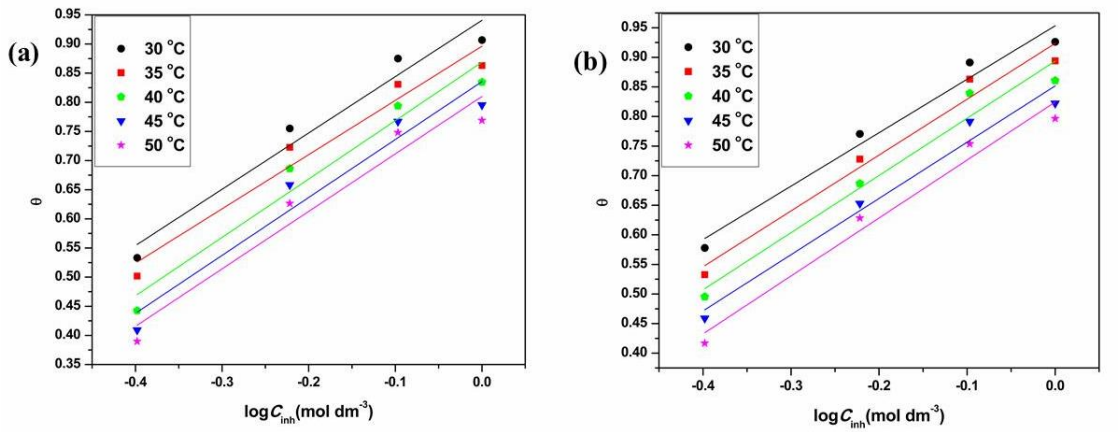

Fig. 3.58 Temkin adsorption isotherms for the adsorption of N-methyl morpholine on Mg-Al-Zn alloy surface at different temperatures in (a) 10 mM chloride medium and (b) 10 mM sulfate medium.

The adsorption of N-methyl morpholine on the surface of the Mg-Al-Zn alloy in both chloride and sulfate media obeys Temkin adsorption isotherm. The Temkin adsorption isotherms for the adsorption of N-methyl morpholine on Mg-Al-Zn alloy surface at different temperatures in chloride and sulfate media are as shown in Fig. 3.58 (a) and Fig. 3.58 (b), respectively.

The thermodynamic parameters derived from the Fig. 3.58 for the corrosion of Mg-Al-Zn alloy in chloride and sulfate media are tabulated in the Table 3.38 and Table 3.39, respectively. The slight deviation in the regression coefficient values

listed in the Table 3.38 and Table 3.39 suggest the intermolecular interaction of the adsorbed N-methyl morpholine on the surface of the Mg-Al-Zn alloy. The positive values of $\Delta S°_{ads}$ demonstrate the increase in disorderliness in the process of the adsorption of N-methyl morpholine, by replacing the adsorbed water molecules on the surface of the Mg-Al-Zn alloy. From the values of $\Delta G°_{ads}$ and $\Delta H°_{ads}$ it is concluded that N-methyl morpholine spontaneously adsorbed on the surface of the alloy by physisorption.

3.6.5. Surface analyses

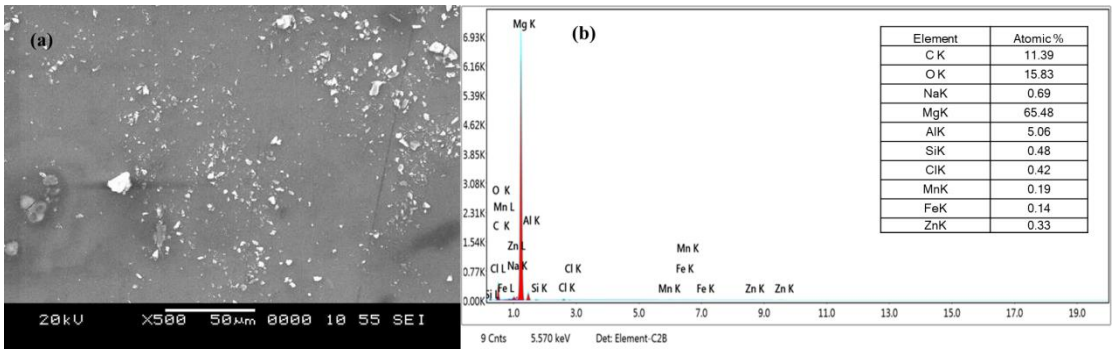

Fig. 3.59 (a) SEM image of Mg-Al-Zn alloy surface after 24 h of immersion in the corrosive medium containing 10 mM chloride ions, 800 mM N-methyl morpholine and (b) corresponding EDX spectra.

Fig. 3.59 (a) and Fig. 3.59 (b), respectively, represent the SEM and EDX spectrum of Mg-Al-Zn alloy surface after 24 h of immersion in the corrosive solution of 10 mM chloride ions having 800 mM N-methyl morpholine. The same in 10 mM sulfate medium are shown in Fig. 3.60 (a) and Fig. 3.60 (b), respectively. In Fig. 3.59 (a) and Fig. 3.60 (a), the surfaces of the alloy contain less pits and smoother than the corroded surface. The existence of carbon peak in the EDX spectra of the corroded surface in chloride and sulfate media represents the presence of inhibitor on the surface of the Mg-Al-Zn alloy.

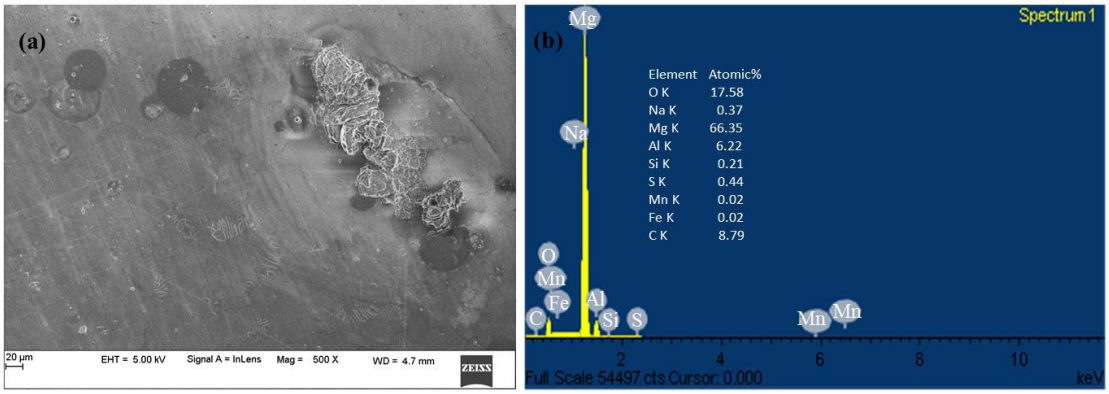

Fig. 3.60 (a) SEM image of Mg-Al-Zn alloy surface after 24 h of immersion in the corrosive medium containing 10 mM sulfate ions, 800 mM N-methyl morpholine and (b) corresponding EDX spectra.

Table 3.32 (a) Tafel polarization parameters for the corrosion of Mg-Al-Zn alloy in a corrosive solution containing 2 mM chloride ions and different concentrations of N-methyl morpholine at different temperatures.

Temperature (°C)	Inhibitor concentration (mM)	E_{corr} vs. SCE (mV)	i_{corr} (μA cm^{-2})	$-b_c$ (mV dec^{-1})	η (%)
30	Blank	–1476	4.58	356	-
	400	–1496	2.39	296	47.8
	600	–1491	1.59	281	65.3
	800	–1450	0.92	271	79.9
	1000	–1444	0.86	259	81.2
35	Blank	–1466	5.36	363	-
	400	–1519	2.97	320	44.6
	600	–1521	2.05	304	61.8
	800	–1519	1.39	295	74.1
	1000	–1527	1.19	268	77.8
40	Blank	–1486	6.02	332	-
	400	–1504	3.58	316	40.5
	600	–1514	2.51	293	58.3
	800	–1530	1.76	281	70.8
	1000	–1514	1.61	262	73.3
45	Blank	–1470	6.79	370	-
	400	–1482	4.15	321	38.9
	600	–1461	3.01	309	55.7
	800	–1504	2.19	291	67.7
	1000	–1498	2.05	273	69.8
50	Blank	–1379	7.85	442	-
	400	–1395	5.13	342	34.6
	600	–1430	3.79	309	51.7
	800	–1432	2.92	294	62.8
	1000	–1384	2.70	279	65.6

Table 3.32 (b) Tafel polarization parameters for the corrosion of Mg-Al-Zn alloy in a corrosive solution containing 6 mM chloride ions and different concentrations of N-methyl morpholine at different temperatures.

Temperature (°C)	Inhibitor concentration (mM)	E_{corr} vs. SCE (mV)	i_{corr} (μA cm^{-2})	$-b_c$ (mV dec^{-1})	η (%)
30	Blank	–1499	6.85	270	-
	400	–1518	3.38	256	50.7
	600	–1526	2.05	247	70.1
	800	–1528	1.19	216	82.6
	1000	–1543	0.93	213	86.4
35	Blank	–1445	9.53	279	-
	400	–1430	4.99	263	47.6
	600	–1490	3.12	251	67.3
	800	–1491	1.92	243	79.9
	1000	–1497	1.43	236	85.0
40	Blank	–1433	10.59	297	-
	400	–1477	5.91	280	44.2
	600	–1476	3.73	261	64.8
	800	–1467	2.55	249	75.9
	1000	–1450	2.06	231	80.5
45	Blank	–1420	11.68	317	-
	400	–1475	7.00	305	40.1
	600	–1463	4.51	278	61.4
	800	–1461	3.21	253	72.5
	1000	–1437	2.80	237	76.0
50	Blank	–1428	12.82	338	-
	400	–1476	8.11	310	36.7
	600	–1452	5.20	284	59.4
	800	–1430	4.13	267	67.8
	1000	–1430	3.43	239	73.2

Table 3.32 (c) Tafel polarization parameters for the corrosion of Mg-Al-Zn alloy in a corrosive solution containing 10 mM chloride ions and different concentrations of N-methyl morpholine at different temperatures.

Temperature (°C)	Inhibitor concentration (mM)	E_{corr} vs. SCE (mV)	i_{corr} (μA cm^{-2})	$-b_c$ (mV dec^{-1})	η (%)
30	Blank	–1458	10.09	286	-
	400	–1457	4.71	229	53.3
	600	–1429	2.47	230	75.5
	800	–1477	1.26	210	87.5
	1000	–1450	0.94	197	90.7
35	Blank	–1446	11.18	269	-
	400	–1513	5.57	257	50.2
	600	–1516	3.10	240	72.3
	800	–1502	1.89	221	83.1
	1000	–1509	1.53	213	86.3
40	Blank	–1416	12.27	310	-
	400	–1410	6.84	278	44.3
	600	–1474	3.85	273	68.6
	800	–1489	2.53	258	79.4
	1000	–1466	2.03	223	83.5
45	Blank	–1461	13.05	306	-
	400	–1489	7.71	282	40.9
	600	–1467	4.46	267	65.8
	800	–1475	3.04	257	76.7
	1000	–1506	2.67	248	79.5
50	Blank	–1405	15.37	339	-
	400	–1491	9.38	325	39.0
	600	–1459	5.74	313	62.7
	800	–1442	3.87	301	74.8
	1000	–1441	3.55	290	76.9

Table 3.33 (a) Tafel polarization parameters for the corrosion of Mg-Al-Zn alloy in a corrosive solution containing 2 mM sulfate ions and different concentrations of N-methyl morpholine at different temperatures.

Temperature (°C)	Inhibitor concentration (mM)	E_{corr} vs. SCE (mV)	i_{corr} (μA cm^{-2})	$-b_c$ (mV dec^{-1})	η (%)
30	Blank	–1546	6.14	284	-
	400	–1469	3.13	274	49.0
	600	–1495	1.77	267	71.2
	800	–1488	1.04	257	83.1
	1000	–1469	0.93	242	84.9
35	Blank	–1556	7.80	349	-
	400	–1522	4.35	292	44.2
	600	–1531	2.53	284	67.6
	800	–1522	1.62	267	79.2
	1000	–1510	1.33	250	82.9
40	Blank	–1469	8.90	311	-
	400	–1510	5.32	294	40.2
	600	–1516	3.16	271	64.5
	800	–1500	2.29	249	74.3
	1000	–1504	2.01	233	77.4
45	Blank	–1463	10.15	309	-
	400	–1520	6.36	293	37.3
	600	–1519	3.92	270	61.4
	800	–1505	2.90	263	71.4
	1000	–1494	2.52	230	75.2
50	Blank	–1468	10.36	285	-
	400	–1521	6.75	270	34.8
	600	–1516	4.37	255	57.8
	800	–1488	3.23	264	68.8
	1000	–1496	2.80	247	73.0

Table 3.33 (b) Tafel polarization parameters for the corrosion of Mg-Al-Zn alloy in a corrosive solution containing 6 mM sulfate ions and different concentrations of N-methyl morpholine at different temperatures.

Temperature (°C)	Inhibitor concentration (mM)	E_{corr} vs. SCE (mV)	i_{corr} (μA cm^{-2})	$-b_c$ (mV dec^{-1})	η (%)
30	Blank	–1566	9.47	308	-
	400	–1502	4.46	294	52.9
	600	–1539	2.38	271	74.9
	800	–1534	1.21	260	87.2
	1000	–1525	1.02	241	89.2
35	Blank	–1520	10.79	373	-
	400	–1509	5.42	293	49.8
	600	–1508	3.09	279	71.4
	800	–1498	1.81	254	83.2
	1000	–1518	1.66	247	84.6
40	Blank	–1513	11.81	376	-
	400	–1513	6.36	307	46.1
	600	–1516	3.68	290	68.8
	800	–1487	2.46	267	79.2
	1000	–1475	2.23	241	81.1
45	Blank	–1500	12.87	379	-
	400	–1495	7.29	316	43.4
	600	–1492	4.43	304	65.6
	800	–1493	3.34	283	74.0
	1000	–1500	2.95	265	77.1
50	Blank	–1446	14.63	335	-
	400	–1515	8.63	307	41.0
	600	–1500	5.33	288	63.6
	800	–1482	4.13	260	71.8
	1000	–1467	3.67	241	74.9

Table 3.33 (c) Tafel polarization parameters for the corrosion of Mg-Al-Zn alloy in a corrosive solution containing 10 mM sulfate ions and different concentrations of N-methyl morpholine at different temperatures.

Temperature (°C)	Inhibitor concentration (mM)	E_{corr} vs. SCE (mV)	i_{corr} (μA cm^{-2})	$-b_c$ (mV dec^{-1})	η (%)
30	Blank	–1530	11.68	386	-
	400	–1461	4.93	324	57.8
	600	–1494	2.68	314	77.1
	800	–1505	1.27	298	89.1
	1000	–1476	0.86	258	92.6
35	Blank	–1521	12.65	402	-
	400	–1498	5.91	330	53.3
	600	–1514	3.44	296	72.8
	800	–1496	1.73	258	86.3
	1000	–1490	1.34	236	89.4
40	Blank	–1460	14.43	344	-
	400	–1515	7.28	323	49.5
	600	–1506	4.52	284	68.7
	800	–1495	2.32	279	83.9
	1000	–1489	2.01	262	86.1
45	Blank	–1458	15.82	327	-
	400	–1505	8.56	297	45.9
	600	–1474	5.49	280	65.3
	800	–1491	3.30	259	79.1
	1000	–1491	2.81	248	82.2
50	Blank	–1462	17.49	318	-
	400	–1496	10.20	305	41.7
	600	–1466	6.50	291	62.8
	800	–1464	4.30	286	75.4
	1000	–1497	3.56	257	79.6

Table 3.34 (a) Electrochemical impedance parameters for the corrosion of Mg-Al-Zn alloy in a corrosive solution containing 2 mM chloride ions and different concentrations of N-methyl morpholine at different temperatures.

Temperature (°C)	Inhibitor concentration (mM)	R_f (Ω cm²)	R_{dif} (Ω cm²)	R_p (Ω cm²)	C_f (μF cm^{-2})	C_{dif} (μF cm^{-2})	η (%)
30	Blank	4053	1888	9501	23.4	186.1	-
	400	8810	5530	17910	21.7	175.8	47.0
	600	10660	6700	27580	18.6	166.6	65.6
	800	17310	8570	42510	17.7	141.3	77.6
	1000	22270	9520	46510	16.1	133.6	79.6
35	Blank	3885	1738	8034	24.4	195.1	-
	400	5675	5170	14109	21.2	178.4	43.1
	600	9051	5875	20917	20.2	172.6	61.6
	800	12430	7819	32289	18.1	159.2	75.1
	1000	14870	8600	34820	17.0	149.2	76.9
40	Blank	3269	1659	6932	25.6	208.3	-
	400	5267	4104	11460	24.3	196.6	39.5
	600	7258	5020	16374	22.7	174.5	57.7
	800	9131	6744	24544	19.2	167.2	71.8
	1000	12360	7390	25420	18.2	155.4	72.7
45	Blank	3052	1587	6725	27.6	228.1	-
	400	4677	3756	10558	25.1	217.7	36.3
	600	7060	4201	14711	24.7	206.7	54.3
	800	8625	6480	21220	21.6	185.9	68.3
	1000	10840	6870	22800	20.4	180.6	70.5
50	Blank	2488	1503	5581	30.7	250.7	-
	400	3983	3274	8526	28.3	241.6	34.5
	600	5297	3553	11543	26.0	229.2	51.7
	800	6748	4230	15330	23.1	215.3	63.6
	1000	7280	4600	16890	21.8	202.7	67.0

Table 3.34 (b) Electrochemical impedance parameters for the corrosion of Mg-Al-Zn alloy in a corrosive solution containing 6 mM chloride ions and different concentrations of N-methyl morpholine at different temperatures.

Temperature (°C)	Inhibitor concentration (mM)	R_f (Ω cm²)	R_{dif} (Ω cm²)	R_p (Ω cm²)	C_f (μF cm^{-2})	C_{dif} (μF cm^{-2})	η (%)
30	Blank	3579	1820	7582	23.9	236.5	-
	400	6151	4250	14639	21.4	228.2	48.2
	600	11789	5646	25666	19.0	217.3	70.5
	800	13760	9920	39860	15.7	203.1	81.0
	1000	17790	10270	47180	13.3	188.4	83.9
35	Blank	2879	1713	6085	25.0	242.4	-
	400	5023	3213	11409	23.2	237.1	46.7
	600	9135	4266	18683	21.4	220.0	67.4
	800	8131	8564	28520	19.0	204.1	78.7
	1000	12120	9510	32980	18.0	196.6	81.5
40	Blank	2577	1608	4880	26.9	252.8	-
	400	4579	2714	8650	25.0	248.9	43.6
	600	7875	3513	13171	21.2	224.8	62.9
	800	8090	6649	19629	19.5	209.0	75.1
	1000	10100	7316	23296	19.0	203.1	79.1
45	Blank	2214	1569	4742	28.3	257.0	-
	400	3885	2320	7793	27.2	251.5	39.2
	600	6671	3074	11444	24.8	237.4	58.6
	800	7490	5610	16550	20.7	213.7	71.3
	1000	8512	6250	20020	18.4	208.6	76.3
50	Blank	1886	1487	4548	31.5	269.8	-
	400	3278	1971	7032	28.8	267.8	35.3
	600	6076	2523	10513	27.9	238.1	56.7
	800	6479	4403	13563	24.4	223.3	66.5
	1000	8110	4877	16727	23.6	198.2	72.8

Table 3.34 (c) Electrochemical impedance parameters for the corrosion of Mg-Al-Zn alloy in a corrosive solution containing 10 mM chloride ions and different concentrations of N-methyl morpholine at different temperatures.

Temperature (°C)	Inhibitor concentration (mM)	R_f (Ω cm^2)	R_{dif} (Ω cm^2)	R_p (Ω cm^2)	C_f (μF cm^{-2})	C_{dif} (μF cm^{-2})	η (%)
30	Blank	2102	1516	6915	25.4	302.1	-
	400	6286	4408	14450	23.4	292.2	52.1
	600	10630	7830	28030	18.9	285.3	75.3
	800	27100	10640	48150	16.3	274.6	85.6
	1000	30640	12390	57450	15.2	259.9	88.0
35	Blank	2002	1485	5509	25.8	320.1	-
	400	5105	3510	11101	24.4	294.4	50.4
	600	9765	7134	18912	21.3	289.8	70.9
	800	19778	9210	32080	19.0	281.3	82.8
	1000	20881	10830	36020	17.5	261.4	84.7
40	Blank	1823	1363	4411	29.4	332.1	-
	400	4404	2549	8271	26.7	319.2	46.7
	600	7287	4629	14116	24.8	302.3	68.8
	800	11620	7927	22784	22.3	292.7	80.6
	1000	13080	8516	25926	19.5	280.2	83.0
45	Blank	1733	1303	4156	32.7	337.3	-
	400	2738	2019	7043	30.0	327.0	41.0
	600	6759	3185	12156	26.0	310.8	65.8
	800	9894	6342	17532	23.6	299.5	76.3
	1000	10542	7560	20970	21.8	290.6	80.2
50	Blank	1434	1283	3969	36.1	345.4	-
	400	2657	1901	6387	33.9	333.7	37.9
	600	5285	2114	9984	29.1	319.6	60.2
	800	9118	4645	15625	26.5	305.8	74.6
	1000	9950	5169	17139	23.8	292.5	76.8

Table 3.35 (a) Electrochemical impedance parameters for the corrosion of Mg-Al-Zn alloy in a corrosive solution containing 2 mM sulfate ions and different concentrations of N-methyl morpholine at different temperatures.

Temperature (°C)	Inhibitor concentration (mM)	R_f (Ω cm²)	R_{dif} (Ω cm²)	R_p (Ω cm²)	C_f (μF cm^{-2})	C_{dif} (μF cm^{-2})	η (%)
30	Blank	3247	2156	5947	34.6	228.4	-
	400	4623	3067	11657	32.9	210.2	49.0
	600	5870	6960	19860	27.5	199.0	70.1
	800	9852	7150	34300	23.1	185.1	82.7
	1000	11020	8940	38130	21.3	179.5	84.4
35	Blank	3164	1960	5687	40.3	230.1	-
	400	3945	2807	10186	37.7	218.1	44.2
	600	4842	5506	17096	31.8	204.8	66.7
	800	7630	6071	26553	28.5	186.3	78.6
	1000	9591	6886	30226	25.0	175.2	81.2
40	Blank	2937	1809	5046	45.3	241.2	-
	400	3229	2681	8517	42.9	237.6	40.8
	600	4274	3114	13691	36.4	219.0	63.1
	800	6660	4600	19640	31.7	205.5	74.3
	1000	8319	6158	22185	29.4	199.6	77.3
45	Blank	2785	1508	4411	49.7	260.0	-
	400	2907	2258	7033	43.1	247.4	37.3
	600	3941	2976	11142	38.7	229.0	60.4
	800	7299	3664	15510	34.4	209.9	71.6
	1000	8964	5526	17566	31.1	202.5	74.9
50	Blank	2693	1116	4261	54.3	272.1	-
	400	2830	2175	6534	50.9	266.1	34.8
	600	3634	2447	10007	43.7	245.7	57.4
	800	5215	3082	13122	37.0	229.8	67.5
	1000	6069	3137	14237	34.8	220.7	70.1

Table 3.35 (b) Electrochemical impedance parameters for the corrosion of Mg-Al-Zn alloy in a corrosive solution containing 6 mM sulfate ions and different concentrations of N-methyl morpholine at different temperatures.

Temperature (°C)	Inhibitor concentration (mM)	R_f (Ω cm^2)	R_{dif} (Ω cm^2)	R_p (Ω cm^2)	C_f (μF cm^{-2})	C_{dif} (μF cm^{-2})	η (%)
30	Blank	2981	1839	5893	38.9	286.2	-
	400	4249	4196	12252	36.0	274.7	51.9
	600	10820	6579	21719	29.6	251.0	72.9
	800	15260	9596	44206	26.4	245.6	86.7
	1000	16680	11061	48931	23.5	233.6	88.0
35	Blank	2806	1642	5631	47.6	292.1	-
	400	3390	3221	11126	44.2	281.4	49.4
	600	8085	4536	19067	40.9	269.6	70.5
	800	12753	7241	35146	36.4	255.6	84.0
	1000	14899	7824	37664	33.5	250.9	85.0
40	Blank	2689	1526	4643	52.2	296.3	-
	400	3082	2528	8580	48.3	288.9	45.9
	600	6548	3639	14319	41.6	270.6	67.6
	800	7717	5885	22744	37.6	257.6	79.6
	1000	9965	6884	25254	35.6	243.2	81.6
45	Blank	2531	1433	4329	58.8	304.0	-
	400	2748	2254	7504	55.1	290.8	42.3
	600	5995	3144	12694	47.2	277.2	65.9
	800	6742	4391	17232	41.0	267.1	74.9
	1000	8625	4739	19599	38.6	257.8	77.9
50	Blank	2511	1075	3760	61.5	322.5	-
	400	2641	1465	6367	58.6	298.7	40.9
	600	4331	2572	9898	50.8	280.8	62.0
	800	5866	3828	12602	46.5	273.1	70.2
	1000	5978	4241	14057	42.9	268.1	73.3

Table 3.35 (c) Electrochemical impedance parameters for the corrosion of Mg-Al-Zn alloy in a corrosive solution containing 10 mM sulfate ions and different concentrations of N-methyl morpholine at different temperatures.

Temperature (°C)	Inhibitor concentration (mM)	R_f (Ω cm²)	R_{dif} (Ω cm²)	R_p (Ω cm²)	C_f (μF cm^{-2})	C_{dif} (μF cm^{-2})	η (%)
30	Blank	2780	1681	4714	41.3	337.0	-
	400	4280	3255	10686	38.8	268.9	55.9
	600	9331	6450	21270	35.7	257.9	77.8
	800	16670	8074	37944	32.6	237.5	87.6
	1000	19670	9470	44660	29.4	222.2	89.4
35	Blank	2679	1395	4347	49.8	346.7	-
	400	3498	2816	9125	47.4	327.7	52.4
	600	8156	5133	15918	43.6	314.0	72.7
	800	13213	7538	29843	38.2	296.4	85.4
	1000	16523	8190	35894	29.2	284.6	87.9
40	Blank	2434	1330	3928	55.2	351.5	-
	400	3088	2178	7650	50.4	343.4	48.7
	600	4653	3822	12002	47.7	338.2	67.3
	800	9611	4538	23538	41.6	308.4	83.3
	1000	11013	5821	27676	39.6	294.6	85.8
45	Blank	2145	1201	3457	62.3	364.3	-
	400	2947	1931	6463	58.0	356.9	46.5
	600	3797	2406	9788	52.3	338.1	64.7
	800	6826	3414	16926	47.4	317.8	79.6
	1000	7159	4430	19939	44.9	313.0	82.7
50	Blank	1980	994	3148	66.8	388.8	-
	400	2162	1451	5401	62.2	378.3	41.7
	600	2873	1921	8243	55.2	366.5	61.8
	800	5221	2641	13041	49.9	348.9	75.9
	1000	7801	3964	15264	45.6	321.3	79.4

Table 3.36 Activation parameters for the corrosion of Mg-Al-Zn alloy in a corrosive solution containing different concentrations of chloride ions and N-methyl morpholine.

Concentration of chloride ion (mM)	**Inhibitor concentration (mM)**	E_a **(kJ mol^{-1})**	$\Delta H^{\#}$ **(kJ mol^{-1})**	$\Delta S^{\#}$ **(J mol^{-1} K^{-1})**
2	Blank	21.6	19.0	–201.5
	400	30.4	27.8	–177.9
	600	34.6	32.0	–167.3
	800	44.7	42.1	–138.2
	1000	46.7	44.1	–132.6
6	Blank	23.9	21.3	–189.9
	400	33.9	31.3	–162.9
	600	36.6	34.0	–158.1
	800	48.6	46.0	–122.8
	1000	53.4	50.8	–109.3
10	Blank	16.1	13.5	–213.2
	400	27.8	25.2	–180.8
	600	33.3	30.7	–168.2
	800	44.2	41.6	–137.3
	1000	52.5	49.9	–112.4

Table 3.37 Activation parameters for the corrosion of Mg-Al-Zn alloy in a corrosive solution containing different concentrations of sulfate ions and N-methyl morpholine.

Concentration of sulfate ion (mM)	**Inhibitor concentration (mM)**	E_a **(kJ mol^{-1})**	$\Delta H^{\#}$ **(kJ mol^{-1})**	$\Delta S^{\#}$ **(J mol^{-1} K^{-1})**
2	Blank	21.4	18.8	–199.3
	400	31.4	28.8	–171.8
	600	36.8	34.2	–158.8
	800	46.7	44.1	–130.3
	1000	46.0	43.4	–133.6
6	Blank	17.0	14.4	–210.6
	400	26.3	23.7	–186.1
	600	32.4	29.8	–171.2
	800	50.1	47.5	–118.2
	1000	50.8	48.2	–116.8
10	Blank	16.8	14.2	–209.8
	400	29.7	27.1	–174.4
	600	36.3	33.7	–157.3
	800	50.5	47.9	–117.0
	1000	59.3	56.7	–90.9

Table 3.38 Thermodynamic parameters for the adsorption of N-methyl morpholine on Mg-Al-Zn alloy in a corrosive solution containing different concentrations of chloride ions at different temperature.

Concentration of chloride ion (mM)	**Temperature (°C)**	**$\Delta G°_{ads}$ (kJ mol^{-1})**	**$\Delta H°_{ads}$ (kJ mol^{-1})**	**$\Delta S°_{ads}$ (JK^{-1}mol^{-1})**	**R^2**
2	30	–12.0	–8.2	12.4	0.941
	35	–12.1			0.972
	40	–12.1			0.954
	45	–12.2			0.950
	50	–12.3			0.958
6	30	–12.2	–6.0	20.7	0.965
	35	–12.4			0.978
	40	–12.5			0.964
	45	–12.6			0.947
	50	–12.7			0.943
10	30	–12.4	–3.6	28.8	0.943
	35	–12.4			0.937
	40	–12.7			0.935
	45	–12.8			0.916
	50	–12.9			0.920

Table 3.39 Thermodynamic parameters for the adsorption of N-methyl morpholine on Mg-Al-Zn alloy in a corrosive solution containing different concentrations of sulfate ions at different temperature.

Concentration of sulfate ion (mM)	**Temperature (°C)**	**$\Delta G°_{ads}$ (kJ mol^{-1})**	**$\Delta H°_{ads}$ (kJ mol^{-1})**	**$\Delta S°_{ads}$ (JK^{-1}mol^{-1})**	**R^2**
2	30	–12.2	–4.5	25.7	0.921
	35	–12.5			0.942
	40	–12.5			0.914
	45	–12.6			0.927
	50	–12.8			0.946
6	30	–12.3	–8.6	12.3	0.928
	35	–12.4			0.917
	40	–12.5			0.908
	45	–12.4			0.912
	50	–12.6			0.908
10	30	–12.3	–2.8	31.5	0.961
	35	–12.5			0.958
	40	–12.7			0.950
	45	–12.8			0.959
	50	–13.0			0.963

3.7. CORROSION INHIBITION OF Mg-Al-Zn ALLOY IN 30% AQUEOUS ETHYLENE GLYCOL CONTAINING CHLORIDE IONS AND SULFATE IONS BY DIMETHYL MORPHOLINE

3.7.1. Potentiodynamic polarization analyses

The potentiodynamic polarization plots for the corrosion of Mg-Al-Zn alloy in 2 mM chloride medium at 40 °C and 2 mM sulfate medium at 40 °C containing different concentrations of dimethyl morpholine are shown in Fig. 3.61 (a) and Fig. 3.61 (b), respectively.

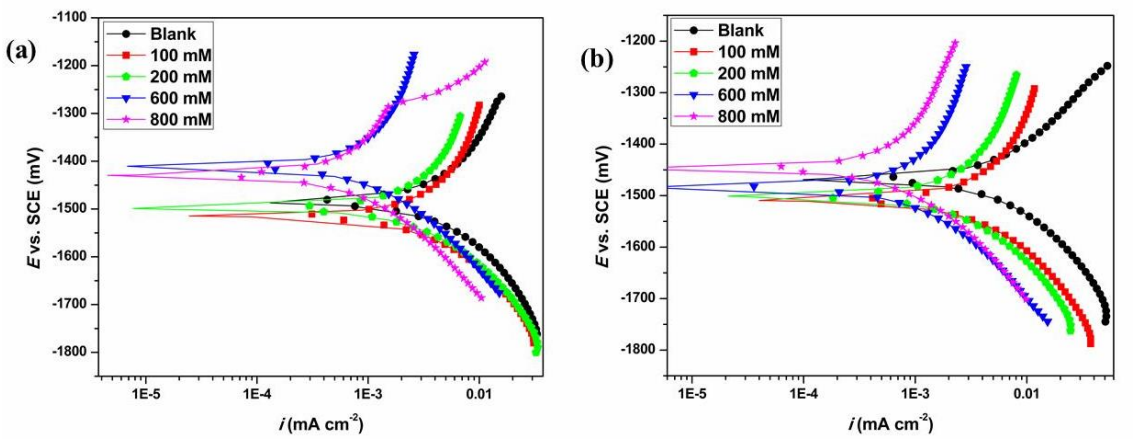

Fig. 3.61 Potentiodynamic polarization plots for the corrosion of Mg-Al-Zn alloy in the presence of different concentrations of dimethyl morpholine in (a) 2 mM chloride medium at 40 °C and (b) 2 mM sulfate medium at 40 °C.

In the presence of dimethyl morpholine the potentiodynamic polarization plots are shifted towards the lower current density region with no significant change in the shape of the polarization curve. The unaltered shape of the polarization curve suggest the non-involvement of the dimethyl morpholine in the mechanism of the Mg-Al-Zn alloy corrosion. Like N-methyl morpholine, presence of dimethyl morpholine also causes the inflection point in the anodic branch of polarization curve and hence cathodic polarization curve was considered in the calculation of corrosion current density from Tafel extrapolation method. Table 3.40 (a), Table 3.40 (b) and Table

3.41 (a), Table 3.41 (b), respectively, display the experimentally calculated polarization parameters for the corrosion of Mg-Al-Zn alloy in the presence of different concentrations of dimethyl morpholine in chloride and sulfate media.

The variations in the potentiodynamic polarization parameters are similar to potentiodynamic polarization parameters of the earlier reported inhibitors. The maximum inhibition efficiency was achieved with 600 mM dimethyl morpholine in chloride and sulfate media. The inhibition efficiency in both chloride and sulfate media increases with the increase in the concentration of dimethyl morpholine and also with the rise in ionic concentration of the media. Dimethyl morpholine reduces both anodic and cathodic reaction rate and shift in the E_{corr} value with respect to the OCP is less than 85 mV and hence it can be classified as a mixed type inhibitor.

3.7.2. Electrochemical impedance spectroscopy

The Nyquist plots for the corrosion of Mg-Al-Zn alloy in the presence of different concentrations of dimethyl morpholine in a corrosive solution of 2 mM chloride medium at 40 °C and 2 mM sulfate medium at 40 °C are shown in Fig. 3.62 (a) and Fig. 3.62 (b), respectively.

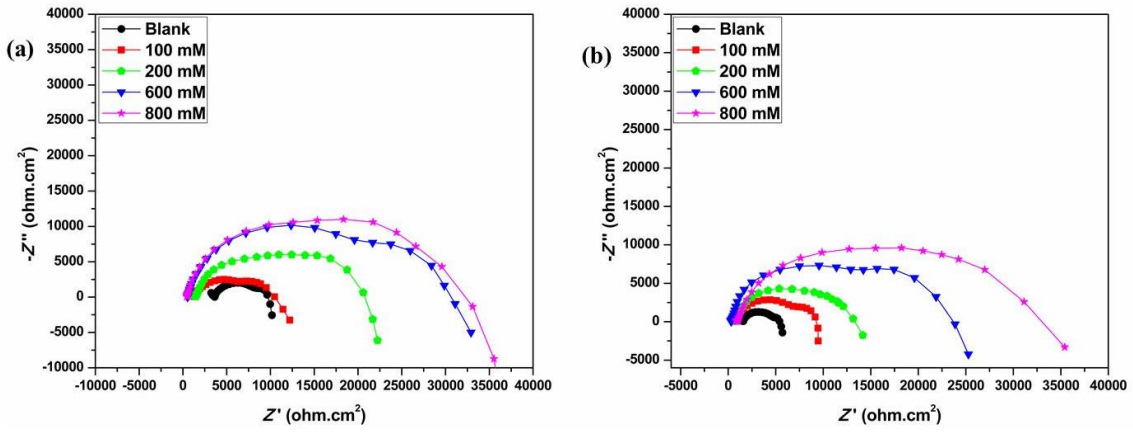

Fig. 3.62 Nyquist plots for the corrosion of Mg-Al-Zn alloy in the presence of different concentrations of dimethyl morpholine in (a) 2 mM chloride medium at 40 °C and (b) 2 mM sulfate medium at 40 °C.

Corrosion inhibition property of the dimethyl morpholine is evidenced with the successive increase in the diameter of the capacitive loops on its consecutive addition to the corrosive media. Inorder to evaluate impedance parameters each Nyquist plot was simulated with the proposed equivalent electrical circuit. The obtained impedance parameters such as R_f, C_f, R_{dif}, C_{dif} and η (%) from simulation method for chloride and sulfate media in different concentration of dimethyl morpholine at different temperatures were enumerated in Table 3.42 (a), Table 3.42 (b) and Table 3.43 (a), Table 3.43 (b), respectively. The impedance results also show that the highest inhibition efficiency is shown in the presence of 600 mM concentration of dimethyl morpholine and the results are in agreement with those of the potentiodynamic polarization results. The increased R_f, R_{dif} and decreased C_f, C_{dif} further support the obtained trend of inhibition.

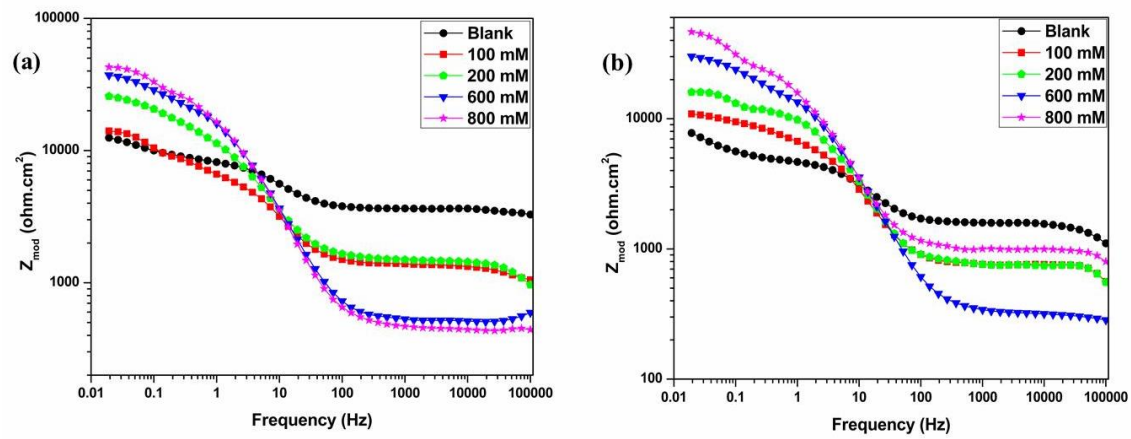

Fig. 3.63 Bode magnitude plots for the corrosion of Mg-Al-Zn alloy in the presence of different concentrations of dimethyl morpholine in (a) 2 mM chloride medium at 40 °C and (b) 2 mM sulfate medium at 40 °C.

Bode plots were constructed to understand the variation in low frequency impedance modulus and intermediate frequency phase maximum for the inhibition of dimethyl morpholine in chloride and sulfate media. Fig. 3.63 (a) and Fig. 3.63 (b) show the Bode magnitude plots for the corrosion of Mg-Al-Zn alloy in the presence of different concentrations of dimethyl morpholine in 2 mM chloride medium at 40 °C

and 2 mM sulfate medium at 40 °C, respectively. Fig. 3.64 (a) and Fig. 3.64 (b) represent the Bode phase angle plots for the same.

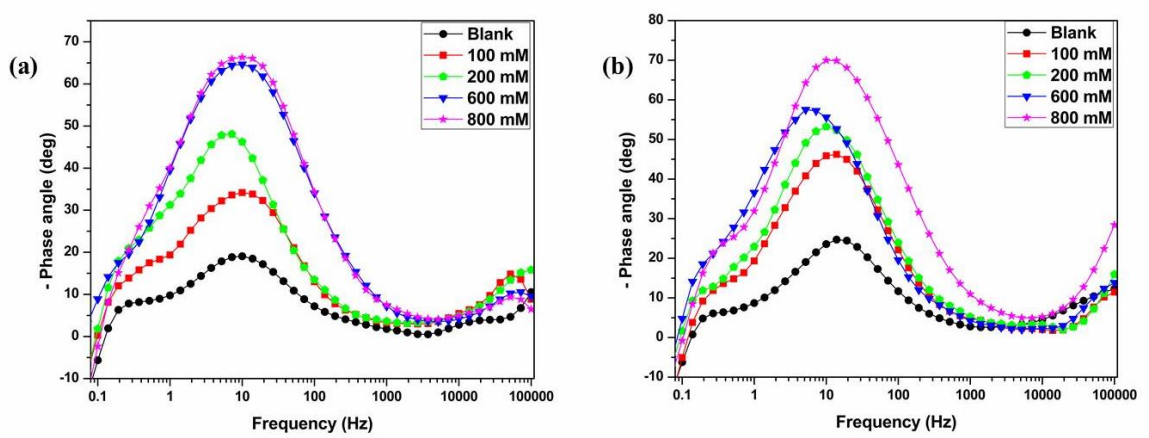

Fig. 3.64 Bode phase angle plots for the corrosion of Mg-Al-Zn alloy in the presence of different concentrations of dimethyl morpholine in (a) 2 mM chloride medium at 40 °C and (b) 2 mM sulfate medium at 40 °C.

The increment in the low frequency impedance modulus and intermediate frequency phase maximum combinedly indicate the addition of dimethyl morpholine facilitate the formation of protective surface film which functions as a barrier against corrosive access.

3.7.3. Effect of temperature

The efficiency of the dimethyl morpholine decreases with the increase in the temperature of the medium as evidenced by the electrochemical parameters enlisted in the Table 3.40, Table 3.41, Table 3.42 and Table 3.43. At higher temperature the formed films dissolves, and is indicative by the obtained higher value of film capacitance and lower value of film resistance. Fig. 3.65 (a) and Fig. 3.65 (b), respectively, show the Arrhenius plots for the corrosion of Mg-Al-Zn alloy in chloride and sulfate media containing different concentrations of dimethyl morpholine. The plots of ln (υ_{corr}/T) versus ($1/T$) for the same are shown in Fig. 3.66 (a) and Fig. 3.66 (b), respectively. The calculated activation parameters for the corrosion of Mg-Al-Zn

alloy in chloride and sulfate media having different concentration of dimethyl morpholine are listed in Table 3.44 and Table 3.45, respectively.

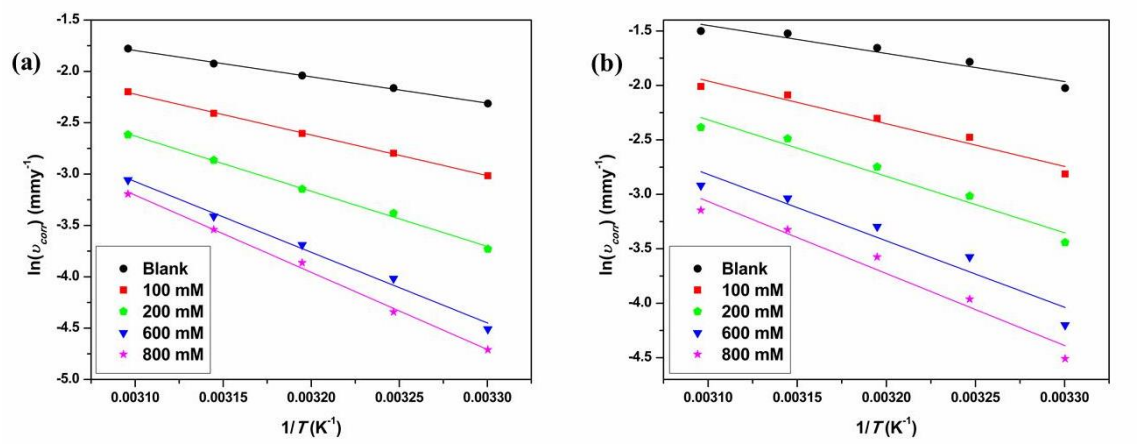

Fig. 3.65 Arrhenius plots for the corrosion of Mg-Al-Zn alloy in the presence of different concentrations of dimethyl morpholine in a corrosive solution of (a) 2 mM chloride medium and (b) 2 mM sulfate medium.

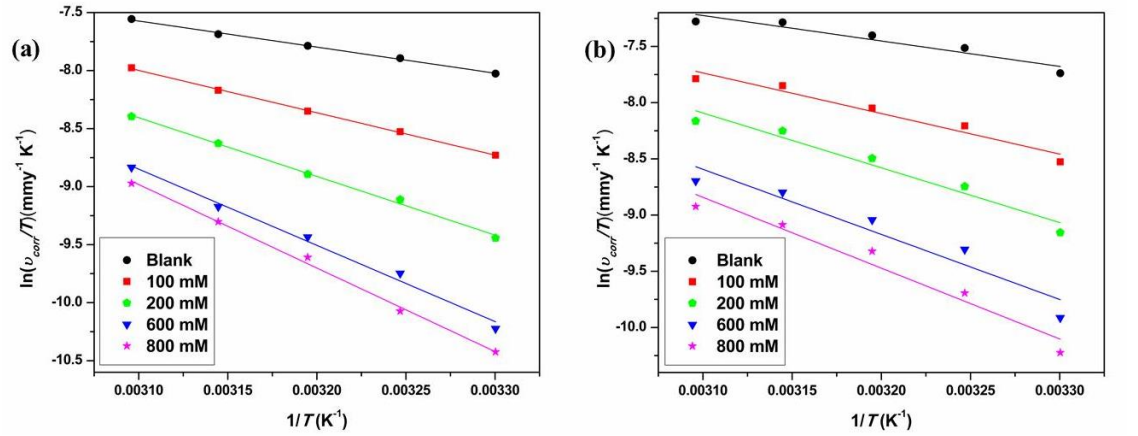

Fig. 3.66 Plots of ln (υ_{corr}/T) versus ($1/T$) for the corrosion of Mg-Al-Zn alloy in the presence of different concentrations of dimethyl morpholine in a corrosive solution of (a) 2 mM chloride medium and (b) 2 mM sulfate medium.

The increase in the energy barrier with the increase in the concentration of the dimethyl morpholine indicates the decrease in Mg-Al-Zn alloy corrosion. During Mg-Al-Zn alloy corrosion, the reactants combine together to form activated complex and

such association decrease the entropy of the system during activation, as observed in the negative values of $\Delta S^{\#}$.

3.7.4. Adsorption isotherm

Among the adsorption isotherms listed in the Table 2.4, Langmuir adsorption isotherm was most suitable to describe the adsorption of dimethyl morpholine on the surface of the Mg-Al-Zn alloy. The Langmuir adsorption isotherms for the adsorption of dimethyl morpholine on Mg-Al-Zn alloy surface at different temperatures in 2 mM chloride media and 2 mM sulfate media are depicted in Fig. 3.67 (a) and Fig. 3.67 (b), respectively.

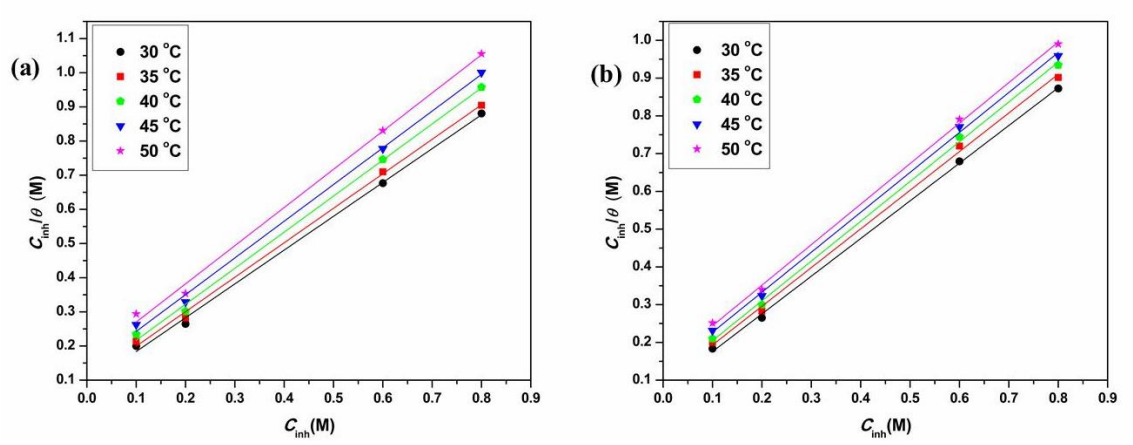

Fig. 3.67 Langmuir adsorption isotherms for the adsorption of dimethyl morpholine on Mg-Al-Zn alloy surface at different temperatures in (a) 2 mM chloride medium and (b) 2 mM sulfate medium.

The calculated thermodynamic parameters such as $\Delta G°_{ads}$, $\Delta H°_{ads}$, $\Delta S°_{ads}$ and linear regression coefficient for the adsorption of dimethyl morpholine at different temperatures in chloride and sulfate media are listed in the Table 3.46 and Table 3.47, respectively. The suitability of Langmuir isotherm to explain the adsorption of dimethyl morpholine is evidensed from the closeness of linear regression coefficient to unity. The consequence of intermolecular interaction among the adsorbed dimethyl morpholine leads to the deviation from the ideal Langmuir behavior. The obtained

thermodynamic parameters collectively suggest the spontaneity of the physisorption with the decrease in the entropy of the system.

3.7.5. Surface analyses

The SEM images and EDX spectra of Mg-Al-Zn alloy surface after 24 h of immersion in the corrosive medium containing 10 mM chloride ion, 800 mM dimethyl morpholine are as shown in the Fig. 3.68 (a) and Fig. 3.68 (b), respectively.

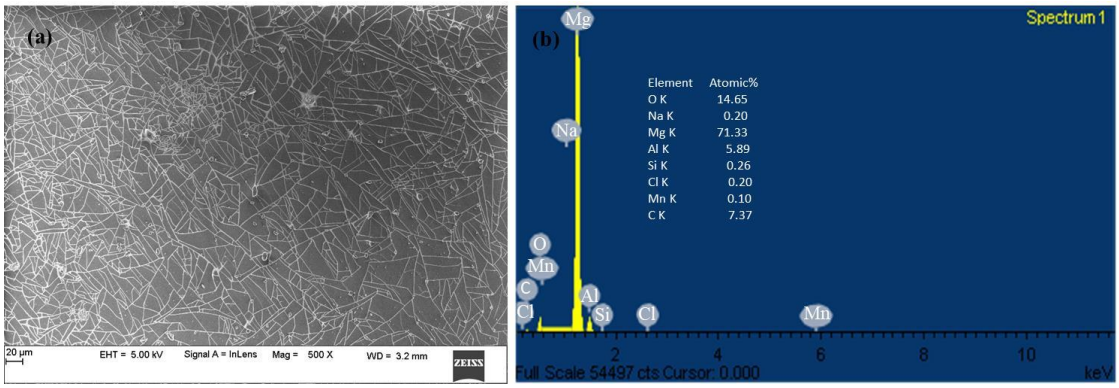

Fig. 3.68 (a) SEM image of Mg-Al-Zn alloy surface after 24 h of immersion in the corrosive medium containing 10 mM chloride ions, 800 mM dimethyl morpholine and (b) corresponding EDX spectra.

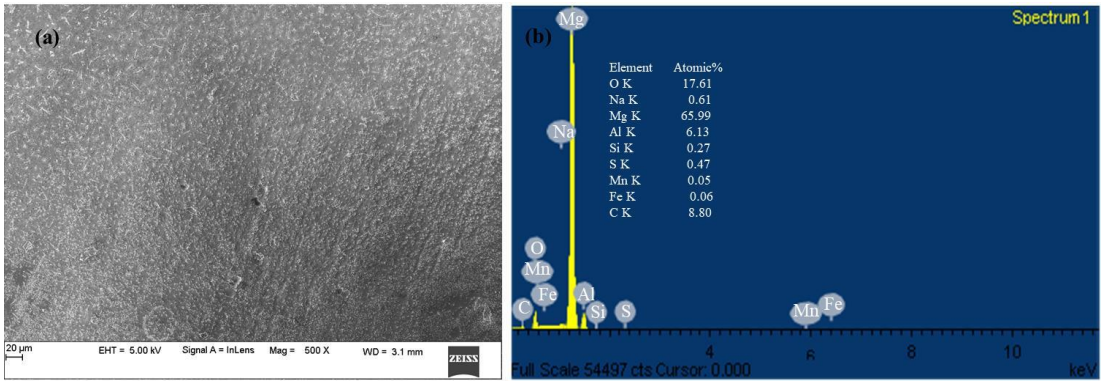

Fig. 3.69 (a) SEM image of Mg-Al-Zn alloy surface after 24 h of immersion in the corrosive medium containing 10 mM sulfate ions, 800 mM dimethyl morpholine and (b) corresponding EDX spectra.

Fig. 3.69 (a) and Fig. 3.69 (b) represent the same in a corrosive medium containing 10 mM sulfate ions. The surface of the alloy in the presence of dimethyl morpholine shows mud crack appearance in the chloride media and contains fewer pits in the sulfate media. Both these factor shows the corrosion inhibition by dimethyl morpholine in chloride and sulfate media. The EDX spectra of the alloy show the carbon peaks along with metallic peaks for both chloride and sulfate media. This indicates the presence of inhibitor on the surface of the alloy.

Table 3.40 (a) Tafel polarization parameters for the corrosion of Mg-Al-Zn alloy in a corrosive solution containing 2 mM chloride ions and different concentrations of dimethyl morpholine at different temperatures.

Temperature (°C)	Inhibitor concentration (mM)	E_{corr} vs. SCE (mV)	i_{corr} (μA cm^{-2})	$-b_c$ (mV dec^{-1})	η (%)
30	Blank	–1476	4.58	356	-
	100	–1459	2.29	250	50.0
	200	–1481	1.12	233	75.5
	600	–1460	0.52	194	88.6
	800	–1485	0.42	193	90.8
35	Blank	–1466	5.36	363	-
	100	–1499	2.85	259	46.8
	200	–1499	1.56	239	70.9
	600	–1426	0.83	203	84.5
	800	–1415	0.62	209	88.4
40	Blank	–1486	6.02	332	-
	100	–1514	3.45	264	42.7
	200	–1497	2.02	258	66.4
	600	–1410	1.18	229	80.4
	800	–1429	0.99	216	83.6
45	Blank	–1470	6.79	370	-
	100	–1531	4.20	269	38.1
	200	–1467	2.66	255	60.8
	600	–1473	1.55	238	77.2
	800	–1427	1.36	236	80.0
50	Blank	–1379	7.85	442	-
	100	–1404	5.18	291	34.0
	200	–1432	3.41	277	56.6
	600	–1411	2.18	263	72.2
	800	–1380	1.90	254	75.8

Table 3.40 (b) Tafel polarization parameters for the corrosion of Mg-Al-Zn alloy in a corrosive solution containing 10 mM chloride ions and different concentrations of dimethyl morpholine at different temperatures.

Temperature (°C)	Inhibitor concentration (mM)	E_{corr} vs. SCE (mV)	i_{corr} (μA cm^{-2})	$-b_c$ (mV dec^{-1})	η (%)
30	Blank	–1458	10.09	286	-
	100	–1468	4.38	280	56.6
	200	–1472	1.81	278	82.1
	600	–1452	0.67	254	93.4
	800	–1411	0.41	207	95.9
35	Blank	–1446	11.18	269	-
	100	–1451	5.23	254	53.2
	200	–1475	2.34	239	79.1
	600	–1398	1.18	234	89.4
	800	–1410	0.86	213	92.3
40	Blank	–1416	12.27	310	-
	100	–1470	6.08	299	50.4
	200	–1484	3.14	251	74.4
	600	–1469	1.86	250	84.8
	800	–1446	1.33	244	89.2
45	Blank	–1461	13.05	306	-
	100	–1474	7.11	289	45.5
	200	–1495	3.73	277	71.4
	600	–1460	2.35	263	82.0
	800	–1445	1.70	257	87.0
50	Blank	–1405	15.37	339	-
	100	–1470	8.88	302	42.2
	200	–1450	4.88	293	68.2
	600	–1415	3.37	263	78.1
	800	–1394	2.36	242	84.6

Table 3.41 (a) Tafel polarization parameters for the corrosion of Mg-Al-Zn alloy in a corrosive solution containing 2 mM sulfate ions and different concentrations of dimethyl morpholine at different temperatures.

Temperature (°C)	Inhibitor concentration (mM)	E_{corr} vs. SCE (mV)	i_{corr} (μA cm^{-2})	$-b_c$ (mV dec^{-1})	η (%)
30	Blank	–1546	6.14	284	-
	100	–1472	2.79	262	54.6
	200	–1477	1.51	256	75.4
	600	–1483	0.72	233	88.3
	800	–1475	0.51	208	91.7
35	Blank	–1556	7.80	349	-
	100	–1487	3.90	265	50.0
	200	–1497	2.29	257	70.6
	600	–1522	1.30	252	83.3
	800	–1486	0.88	251	88.7
40	Blank	–1469	8.90	311	-
	100	–1508	4.66	283	47.6
	200	–1501	2.96	257	66.7
	600	–1483	1.73	247	80.6
	800	–1448	1.28	239	85.6
45	Blank	–1463	10.15	309	-
	100	–1503	5.76	296	43.3
	200	–1489	3.87	269	61.9
	600	–1438	2.25	251	77.8
	800	–1431	1.68	238	83.4
50	Blank	–1468	10.36	285	-
	100	–1479	6.24	278	39.8
	200	–1420	4.26	273	58.9
	600	–1395	2.50	267	75.9
	800	–1416	1.99	252	80.8

Table 3.41 (b) Tafel polarization parameters for the corrosion of Mg-Al-Zn alloy in a corrosive solution containing 10 mM sulfate ions and different concentrations of dimethyl morpholine at different temperatures.

Temperature (°C)	Inhibitor concentration (mM)	E_{corr} vs. SCE (mV)	i_{corr} (μA cm^{-2})	$-b_c$ (mV dec^{-1})	η (%)
30	Blank	–1530	11.68	386	-
	100	–1507	4.62	267	60.4
	200	–1498	1.83	219	84.3
	600	–1491	0.65	202	94.4
	800	–1469	0.41	179	96.5
35	Blank	–1521	12.65	402	-
	100	–1507	5.47	294	56.8
	200	–1524	2.56	245	79.8
	600	–1490	1.12	218	91.1
	800	–1450	0.85	180	93.3
40	Blank	–1460	14.43	344	-
	100	–1503	6.95	275	51.8
	200	–1535	3.71	253	74.3
	600	–1448	1.44	235	90.0
	800	–1426	1.37	230	90.5
45	Blank	–1458	15.82	327	-
	100	–1499	8.10	278	48.8
	200	–1492	4.74	251	70.0
	600	–1450	1.80	238	88.6
	800	–1446	1.67	229	89.4
50	Blank	–1462	17.49	318	-
	100	–1483	9.99	301	42.9
	200	–1477	5.76	262	67.1
	600	–1431	2.22	259	87.3
	800	–1403	2.01	234	88.5

Table 3.42 (a) Electrochemical impedance parameters for the corrosion of Mg-Al-Zn alloy in a corrosive solution containing 2 mM chloride ions and different concentrations of dimethyl morpholine at different temperatures.

Temperature (°C)	Inhibitor concentration (mM)	R_f (Ω cm²)	R_{dif} (Ω cm²)	R_p (Ω cm²)	C_f (μF cm^{-2})	C_{dif} (μF cm^{-2})	η (%)
30	Blank	4053	1888	9501	23.4	186.1	-
	100	9067	3860	18990	21.3	174.9	50.0
	200	12600	8020	36600	17.1	151.6	74.0
	600	28430	12800	63440	15.5	142.2	85.0
	800	29630	18440	70180	14.4	131.3	86.5
35	Blank	3885	1738	8034	24.4	195.1	-
	100	5868	3050	14926	23.6	190.0	46.2
	200	9839	5995	26705	19.9	160.4	69.9
	600	16930	8395	46685	16.3	148.3	82.8
	800	17210	9277	51767	16.0	132.4	84.5
40	Blank	3269	1659	6932	25.6	208.3	-
	100	5056	2843	12045	24.2	191.5	42.4
	200	8520	5649	21289	21.9	163.1	67.4
	600	12720	7231	33911	17.4	151.2	79.6
	800	14380	7807	36727	16.9	147.8	81.1
45	Blank	3052	1587	6725	27.6	228.1	-
	100	4714	2621	10907	26.3	216.6	38.3
	200	6072	4620	16820	23.8	205.6	60.0
	600	9839	5525	30245	19.6	182.7	77.8
	800	11350	6874	32674	18.1	172.0	79.4
50	Blank	2488	1503	5581	30.7	250.7	-
	100	4134	2238	8459	28.3	246.1	34.0
	200	5420	3511	12801	25.5	228.1	56.4
	600	9542	4860	20260	21.3	210.9	72.5
	800	9943	5780	22450	19.5	201.9	75.1

Table 3.42 (b) Electrochemical impedance parameters for the corrosion of Mg-Al-Zn alloy in a corrosive solution containing 10 mM chloride ions and different concentrations of dimethyl morpholine at different temperatures.

Temperature (°C)	Inhibitor concentration (mM)	R_f (Ω cm²)	R_{dif} (Ω cm²)	R_p (Ω cm²)	C_f (μF cm^{-2})	C_{dif} (μF cm^{-2})	η (%)
30	Blank	2102	1516	6915	25.4	302.1	-
	100	6291	3873	15803	22.7	294.8	56.2
	200	13400	9050	35410	20.5	284.2	80.5
	600	22600	17910	67670	19.0	269.5	89.8
	800	28060	21098	73128	18.0	264.4	90.5
35	Blank	2002	1485	5509	25.8	320.1	-
	100	5040	3166	11757	24.0	309.0	53.1
	200	9447	6840	25550	21.5	274.8	78.4
	600	18300	12860	42550	19.4	266.1	87.1
	800	19830	14381	52461	18.9	259.4	89.5
40	Blank	1823	1363	4411	29.4	332.1	-
	100	3107	2904	8985	27.3	324.2	50.9
	200	7381	4313	16879	23.6	304.8	73.9
	600	12200	8826	29126	21.1	281.6	84.9
	800	15880	9910	35330	19.9	276.5	87.5
45	Blank	1733	1303	4156	32.7	337.3	-
	100	2300	2358	7438	29.0	332.3	44.1
	200	6703	3594	13984	25.1	312.8	70.3
	600	10040	6389	21699	23.4	304.6	80.8
	800	11544	9049	31839	22.2	298.2	86.9
50	Blank	1434	1283	3969	36.1	345.4	-
	100	2039	1977	6926	33.2	337.6	42.7
	200	5299	3152	12545	28.5	314.2	68.4
	600	9400	5060	18810	24.7	307.0	78.9
	800	10910	7220	25590	23.2	300.9	84.5

Table 3.43 (a) Electrochemical impedance parameters for the corrosion of Mg-Al-Zn alloy in a corrosive solution containing 2 mM sulfate ions and different concentrations of dimethyl morpholine at different temperatures.

Temperature (°C)	Inhibitor concentration (mM)	R_f (Ω cm^2)	R_{dif} (Ω cm^2)	R_p (Ω cm^2)	C_f (μF cm^{-2})	C_{dif} (μF cm^{-2})	η (%)
30	Blank	3247	2156	5947	34.6	228.4	-
	100	6085	5095	13152	29.8	218.1	54.8
	200	8295	7162	22752	25.5	204.3	73.9
	600	15700	16510	48950	20.9	181.4	87.9
	800	20411	20760	59860	17.2	175.2	90.1
35	Blank	3164	1960	5687	40.3	230.1	-
	100	5627	4401	11422	37.1	226.1	50.2
	200	6756	6578	18922	34.0	212.8	69.9
	600	12820	14810	35390	28.2	184.3	83.9
	800	14320	18690	43830	25.5	174.9	87.0
40	Blank	2937	1809	5046	45.3	241.2	-
	100	3169	3639	9529	40.1	236.2	47.0
	200	4792	5535	14816	36.4	218.8	65.9
	600	11280	10300	25900	30.9	201.0	80.5
	800	12500	15728	34708	27.1	194.1	85.5
45	Blank	2785	1508	4411	49.7	260.0	-
	100	2905	3400	7743	43.0	249.3	43.0
	200	3824	4087	11497	38.7	230.0	61.6
	600	8770	5675	18625	32.7	216.2	76.3
	800	10580	7090	25390	30.3	205.8	82.6
50	Blank	2693	1116	4261	54.3	272.1	-
	100	2744	3176	7053	48.1	260.4	39.6
	200	3533	3735	10292	44.4	240.1	58.6
	600	7000	4630	16130	38.8	229.0	73.6
	800	9920	6420	20750	35.9	217.2	79.5

Table 3.43 (b) Electrochemical impedance parameters for the corrosion of Mg-Al-Zn alloy in a corrosive solution containing 10 mM sulfate ions and different concentrations of dimethyl morpholine at different temperatures.

Temperature (°C)	Inhibitor concentration (mM)	R_f (Ω cm²)	R_{dif} (Ω cm²)	R_p (Ω cm²)	C_f (μF cm^{-2})	C_{dif} (μF cm^{-2})	η (%)
30	Blank	2780	1681	4714	41.3	337.0	-
	100	3048	3566	11853	38.6	315.6	60.2
	200	9301	8934	28512	30.2	302.4	83.5
	600	23180	15448	65338	23.5	185.5	92.8
	800	31060	24090	76280	19.8	178.8	93.8
35	Blank	2679	1395	4347	49.8	346.7	-
	100	2963	3014	9927	43.5	330.7	56.2
	200	7462	7311	20774	39.2	310.8	79.1
	600	15462	10540	45785	27.4	286.7	90.5
	800	18490	11768	48428	25.4	238.4	91.0
40	Blank	2434	1330	3928	55.2	351.5	-
	100	2756	2757	8056	49.7	336.3	51.2
	200	6186	5170	14568	41.0	316.9	73.0
	600	12050	7428	35478	30.5	294.0	88.9
	800	14910	8353	40363	27.5	288.0	90.3
45	Blank	2145	1201	3457	62.3	364.3	-
	100	2561	2214	6615	57.2	352.4	47.7
	200	5912	3727	11205	49.0	339.2	69.1
	600	9810	5641	26111	39.7	312.6	86.8
	800	12470	7180	30970	37.1	299.4	88.8
50	Blank	1980	994	3148	66.8	388.8	-
	100	2285	1669	5519	62.5	360.7	43.0
	200	4452	3605	9679	51.2	349.5	67.5
	600	8600	4430	20780	45.3	322.6	84.9
	800	10840	5764	23434	44.0	305.5	86.6

Table 3.44 Activation parameters for the corrosion of Mg-Al-Zn alloy in 30% aqueous ethylene glycol containing chloride ions and different concentrations of dimethyl morpholine.

Concentration of chloride ion (mM)	Inhibitor concentration (mM)	E_a (kJ mol^{-1})	$\Delta H^{\#}$ (kJ mol^{-1})	$\Delta S^{\#}$ (J mol^{-1} K^{-1})
2	Blank	21.6	19.0	–201.5
	100	32.9	30.3	–170.0
	200	44.6	42.0	–137.1
	600	57.2	54.6	–101.8
	800	62.4	59.8	–86.7
10	Blank	16.1	13.5	–213.2
	100	28.1	25.5	–180.5
	200	39.9	37.3	–148.9
	600	65.1	62.5	–73.5
	800	68.4	65.8	–65.7

Table 3.45 Activation parameters for the corrosion of Mg-Al-Zn alloy in 30% aqueous ethylene glycol containing sulfate ions and different concentrations of dimethyl morpholine.

Concentration of sulfate ion (mM)	Inhibitor concentration (mM)	E_a (kJ mol^{-1})	$\Delta H^{\#}$ (kJ mol^{-1})	$\Delta S^{\#}$ (J mol^{-1} K^{-1})
2	Blank	21.4	18.8	–199.3
	100	32.6	30.0	–168.8
	200	43.1	40.5	–139.2
	600	50.7	48.1	–119.8
	800	55.0	52.4	–108.6
10	Blank	16.8	14.2	–209.8
	100	31.6	29.0	–168.8
	200	47.8	45.2	–122.5
	600	48.2	45.6	–129.1
	800	62.5	59.9	–85.0

Table 3.46 Thermodynamic parameters for the adsorption of dimethyl morpholine on Mg-Al-Zn alloy in a corrosive solution containing different concentrations of chloride ions at different temperature.

Concentration of chloride ion (mM)	Temperature (°C)	$\Delta G°_{ads}$ (kJ mol^{-1})	$\Delta H°_{ads}$ (kJ mol^{-1})	$\Delta S°_{ads}$ ($JK^{-1}mol^{-1}$)	R^2
2	30	–16.3	–25.5	–30.2	0.997
	35	–16.2			0.997
	40	–16.2			0.997
	45	–15.9			0.997
	50	–15.7			0.995
10	30	–16.9	–20.9	–13.0	0.998
	35	–17.0			0.997
	40	–16.9			0.997
	45	–16.8			0.995
	50	–16.7			0.992

Table 3.47 Thermodynamic parameters for the adsorption of dimethyl morpholine on Mg-Al-Zn alloy in a corrosive solution containing different concentrations of sulfate ions at different temperature.

Concentration of sulfate ion (mM)	Temperature (°C)	$\Delta G°_{ads}$ (kJ mol^{-1})	$\Delta H°_{ads}$ (kJ mol^{-1})	$\Delta S°_{ads}$ ($JK^{-1}mol^{-1}$)	R^2
2	30	–16.6	–23.9	–23.9	0.999
	35	–16.4			0.998
	40	–16.5			0.998
	45	–16.2			0.998
	50	–16.1			0.999
10	30	–17.3	–29.8	–41.0	0.998
	35	–17.2			0.999
	40	–17.0			0.998
	45	–16.8			0.998
	50	–16.5			0.996

3.8. MECHANISM OF CORROSION INHIBITION BY MORPHOLINE AND ITS DERIVATIES

The corrosion inhibition by morpholine, N-methyl morpholine and dimethyl morpholine on the surface of Mg-Al-Zn alloy is the result of molecular adsorption. The oxide layer on the surface of the Mg-Al-Zn alloy is porous, semi-protective and its dissolution rate increases with the increase in the corrosive concentration as indicated by the reported i_{corr} values. In the absence of the inhibitors, the $MgCl_2$ and $Mg(SO_4)_2$ formed during the corrosion reaction have higher solubility than $Mg(OH)_2$; they dissolve, leaving behind the active magnesium surface for further attack.

The core moiety morpholine, in all the three inhibitors, is chemically an amino ether. The ether functional group is typically inert compared to amine group. The adsorption of the inhibitors on the Mg-Al-Zn alloy surface is through the oxides that have defects and capable of accepting electrons. Initially the adsorbed inhibitor molecules displace the previously adsorbed water molecule from the surface of the alloy. Fig. 3.70 and Fig. 3.71, respectively, show the probable mechanisms between the protonated and non-protonated amine functional group of morpholine on the positively charged alloy surface.

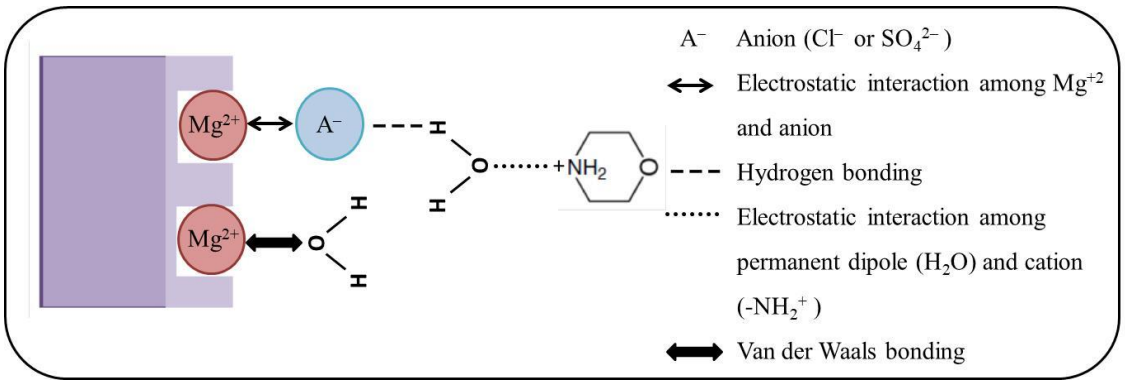

Fig. 3.70 Possible interactions between magnesium surface and protonated amine functional group.

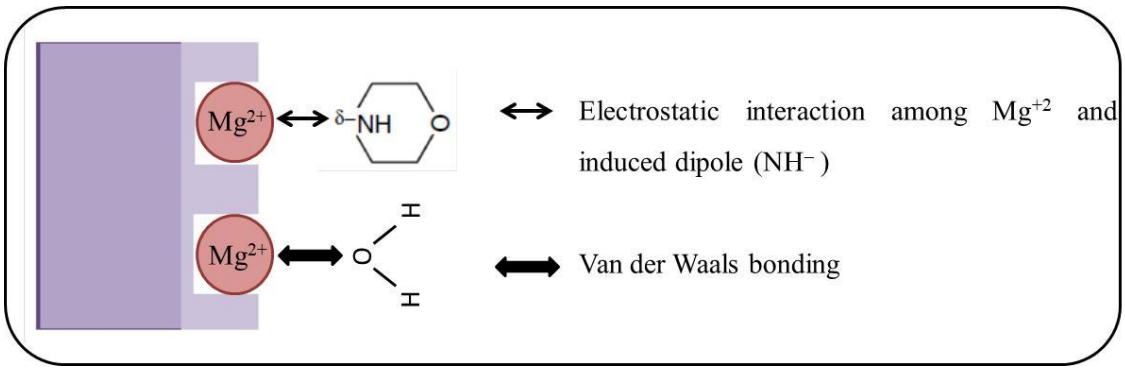

Fig. 3.71 Possible interactions between magnesium surface and non-protonated amine functional group.

The amine functional group in the morpholine and its derivatives get protonated in the aqueous solution due to its basic nature. The previously adsorbed water and anions (such as Cl^- and SO_4^{2-} ions) interact with the protonated morpholine and its derivatives forming electrostatic bonds (McCafferty 2010) (Fig. 3.70). The positively charged protonated amine molecule can adsorb on the positively charged alloy surface with the help of intermediate anions as shown in the Fig. 3.70. Where as in the case of unprotonated amines, the free electron pair of the nitrogen atom can form van der Waals bonding with the Mg-surface as shown in the Fig. 3.71 (Nasser and Sathiq 2016). The oxygen atom of the morpholine and its derivatives cannot form van der Waals bonding with Mg-surface because of its lower electron donating capability than nitrogen atom of the same molecule (Belarbi et al. 2016).

Further, the increased pH after the addition of morpholine and its derivatives decreases the corrosion rate. But the decreased corrosion rate in the presence of inhibitor is more than the lowered corrosion rate in the corresponding pH of the medium. The pH of the solution after the addition of 800 mM morpholine, 800 mM N-methyl morpholine and 600 mM dimethyl morpholine to the corrosive solution of 10 mM chloride ions are 10.5, 8.6 and 10.2, respectively. The corrosion current densities at the corresponding pH of the solutions are 2.92, 6.54 and 3.20 μA cm^{-2}, respectively. These corrosion current density values are higher than in the presence of inhibitors. This concludes that along with molecular interaction the increased pH of

the solution may play a little but not significant role in the inhibition efficiency of the inhibitor.

The evaluated thermodynamic parameters in this study suggest the possible physisorption during the interaction of the inhibitor on the surface of the alloy. The calculated standard enthalpy of adsorption and decreased inhibition efficiency with the increase in medium temperature, further support the phenomenon of physisorption. This is due to the desorption of the physisorbed organic inhibitor as the consequence of increased ionic mobility at higher temperature (Huang et al. 2011). The slight deviation from the ideal Langmuir and Temkin behavior observed in all the three inhibitors indicates the presence of intermolecular interactions among the adsorbed inhibitors. Such mutual interactions might impede the anodic dissolution of magnesium through the enhanced barrier effect against electrolyte ingress. This is evidenced by the increased inhibition efficiency of the inhibitor with the increased concentration to a certain value. The increased values of R_f and R_{dif}; and the decreased values of C_f and C_{dif} on the addition of inhibitor evidences the augmentation of the barrier effect. Further addition of inhibitor does not cause any noticeable increment in the inhibition efficiency.

The evaluated electrochemical parameters indicate the increased efficiency of the inhibitor in the higher concentrations of the aggessive ions. This may be due to the increased dissolution of $Mg(OH)_2$ surface film in higher aggressive ion concentration, which facilitates the generation of magnesium ions (Zucchi et al. 2006). The generated magnesium ions at the surface of the alloy function as the site for physisorption process. Therefore increased aggressive ion concentration results in increased physisorption which in turn increases the inhibitor efficiency. The observed higher inhibition efficiency in the sulfate ion containing corrosive medium is due to the availability of more Mg^{2+} ion for physisorption by increased dissolution of $Mg(OH)_2$ surface film in the sulfate containing corrosive media.

The highest inhibition efficiency of the three inhibitors in 10 mM SO_4^{2-} medium at 30 °C are as follows: Morpholine shows the highest inhibition efficiency

of 94.6% at an optimum concentration of 800 mM, N-methyl morpholine exhibits the highest inhibition efficiency of 89.1% at an optimum concentration of 800 mM and dimethyl morpholine exhibits the highest inhibition efficiency of 94.4% at an optimum concentration of 600 mM. The variation in the inhibition efficiency of the three inhibitors is due to the difference in their structure.

In morpholine the amine functional group is more active than ether functional group and it has the pKa of 8.72 (Bernasconi and Stronach 1991). The oxygen atom of the morpholine withdraws electron cloud from nitrogen atom and hence it has a less electron donating property than piperidine (Clayden et al. 2012). In case of N-methyl morpholine the hydrogen atom of the secondary amine group is replaced by methyl group. The sterically hindered loone pair electrons are not freely available and hence it has less donating property than morpholine with pKa of 7.61 (Hall 1957). But in the case of dimethyl morpholine the lone pair of electrons are available for donation as the electron donating property increases because of the inductive electron donation by two methyl groups, with a pKa value of 11.12 (Somasundaran 2006, Clayden et al. 2012). In line with the electron donating properties of the morpholine and its derivatives, the order of inhibition efficiency follows the order: dimethyl morpholine > morpholine > N-methyl morpholine.

CHAPTER – 4: SUMMARY AND CONCLUSIONS

4.1. SUMMARY

In this thesis, the corrosion behavior of Mg-Al-Zn alloy in aqueous ethylene glycol containing different concentrations of chloride and sulfate ions were established. The electrochemical investigations include potentiodynamic polarization and electrochemical impedance techniques to study the corrosion behavior of Mg-Al-Zn alloy. In order to apprehend the influence of environmental factors on the electrochemical corrosion reactions of Mg-Al-Zn alloy experiments were performed with varied concentration of chloride and sulfate ions, different temperature of the medium and different pH of the solution. The study of Mg-Al-Zn corrosion at various temperatures of the medium was used for the evaluation of activation parameters of the corrosion reactions. The impact of chloride and sulfate ions and pH of the medium were further demonstrated by surface analysis studies.

The synergistic mixture of SDBS with TSP and SB were examined to study the inhibition efficiency of the organic-inorganic and organic-organic mixture of inhibitors. Further three heterocyclic compounds morpholine, N-methyl morpholine and dimethyl morpholine were studied as corrosion inhibitors in aqueous ethylene glycol containing chloride and sulfate ions. All the five corrosion inhibitors were tested in various medium concentration and five different temperatures of the medium. Further, at every medium concentrations and temperature a range of inhibitor concentrations were studied to establish the optimum concentration of the inhibitor. The study of organic-inorganic and organic-organic synergistic mixture of inhibitor at various concentrations eventuated the effect of concentration ratio on the inhibition efficiency of the mixture of inhibitor. The examination of morpholine and its two derivaties results in understanding the impact of molecular structure of the inhibitor on its inhibition efficiency. The potentiodynamic polarization results of variation in inhibition efficiency with the concentration of the inhibitor are in compliance with the impedance spectroscopy results. The study of activation and

thermodynamic parameters resulted in understanding the Mg-Al-Zn dissolution and interfacial adsorption of inhibitor on the surface of the alloy, respectively. The outcome of potentiodynamic polarization parameters and impedance parameters along with SEM and EDX analyses were taken into account for proposing the plausible mechanism for inhibition of Mg-Al-Zn alloy corrosion by inhibitor. The mixture of SDBS, TSP and SDBS, SB were principally block the anodic dissolution of magnesium and hence act as anodic inhibitors. The anodic inhibition of the mixture of inhibitor is due to the formation of $Mg(PO_3)_4$ and $Mg(phCOO)_2$, respectively with TSP and SB and subsequent deposition of SDBS on the surface of the alloy. Whereas morpholine and its two derivatives equally inhibit the anodic and cathodic rection and act as mixed inhibitors. The slight deviation from ideal adsorption isotherms is due to the intermolecular interaction of the adsorbed inhibitors. The difference in the inhibition efficiency of the morpholine and its derivaties are due to the structural difference which causes the difference in adsorption ability of the inhibitor.

4.2. CONCLUSIONS

From the studied data, the following conclusions have been drawn:

1. The corrosion studies at various ionic concentration, temperature and pH of the media conclude that higher ionic concentration, higher temperature of 30% ethylene glycol medium and acidic pH induce unprotective surface film with greater dissolution tendency and hence Mg-Al-Zn alloy corrosion.

2. The corrosion rate of Mg-Al-Zn alloy is more in the sulfate ions containing corrosive media than in chloride ions containing media.

3. The potentiodynamic polarization data indicate the anodic type inhibitor behavior for the mixture of SDBS and TSP, SDBS and SB, whereas morpholine, N-methyl morpholine and dimethyl morpholine act as mixed type inhibitors.

4. The polarization and impedance studies for all the inhibitors indicate the increase in inhibition efficiency with the increase in the concentration of the inhibitor, upto an optimum concentration and above which the change is negligible.

5. The increase in the temperature of the medium is unfavorable for the formation of modified surface film and hence decreases the inhibition efficiency of the inhibitor.

6. All the studied inhibitors show the higher efficiency at higher ionic concentrations of the corrosive media than in lower corrosive concentrations and the higher inhibition efficiency is observed in sulfate containing corrosive media than in chloride containing corrosive media.

7. The adsorptions of all the inhibitors on Mg-Al-Zn alloy surface are predominantly physisorption and obey Langmuir adsorption isotherm except for N-methyl morpholine which obeys Temkin adsorption isotherm.

8. The combination of organic inoraganic mixture (SDBS and TSP) shows higher efficiency than the combination of organic organic mixture (SDBS and SB).

9. In all the three morpholine compounds, dimethyl morpholine exhibits a highest inhibition efficiency followed by morpholine and N-methyl morpholine.

4.3. SCOPE FOR FUTURE WORK

1. Electrochemical corrosion investigation of Mg-Al-Zn alloy in aqueous ethylene glycol containing combined chloride and sulfate ions can be explored.

2. The electrochemical study of corrosion inhibitor can be carried out at various immersion times to study the effectiveness of surface film at longer exposure duration.

REFERENCES

AbdelGawad, M., Mansoor, B. and Chaudhry, A.U. (2018). "Corrosion characteristics of two rare earth containing magnesium alloys." *Magnes. Technol. 2018*, The Minerals, Metals & Materials Series, D. Orlov, V. Joshi, K. N. Solanki, and N. R. Neelameggham, eds., TMS, Springer, 43–53.

Agnew, S.R. (2004). "Wrought magnesium: a 21st century outlook." *JOM*, 56(5), 20–21.

Ahmad, Z. (2006). *Principles of corrosion engineering and corrosion control*. First edition, Butterworth-Heinemann IChemE Series, USA.

Ahmadkhaniha, D., Huang, Y., Jaskari, M., Järvenpää, A., Sohi, M.H., Zanella, C., Karjalainen, L.P. and Langdon, T.G. (2018). "Effect of high-pressure torsion on microstructure, mechanical properties and corrosion resistance of cast pure Mg." *J. Mater. Sci.*, 53(24), 16585–16597.

Ahmed, A.I., Basahel, S.N. and Khalil Chemistry, R.M. (1988). "Inhibition of the acid corrosion of aluminium with some morpholine and thiosemicarbazide derivatives." *Anti-Corros. Methods Mater.*, 35(8), 4–8.

Ambat, R., Aung, N.N. and Zhou, W. (2000). "Evaluation of microstructural effects on corrosion behaviour of AZ91D magnesium alloy." *Corros. Sci.*, 42(8), 1433–1455.

Antropov, L.I. (1967). "A correlation between kinetics of corrosion and the mechanism of inhibition by organic compounds." *Corros. Sci.*, 7(9), 607–620.

Aouniti, A., Khaled, K.F. and Hammouti, B. (2013). "Correlation between inhibition efficiency and chemical structure of some amino acids on the corrosion of armco iron in molar HCl." *Int. J. Electrochem. Sci.*, 8, 5925–5943.

Aramaki, K. (2002). "Synergistic inhibition of zinc corrosion in 0.5 M NaCl by combination of cerium (III) chloride and sodium silicate." *Corros. Sci.*, 44(4), 871–886.

Aramaki, K. and Hackerman, N. (1969). "Inhibition mechanism of medium-sized polymethyleneimine." *J. Electrochem. Soc.*, 116(5), 568–574.

Armelin, E., Pla, R., Liesa, F., Ramis, X., Iribarren, J.I. and Alemán, C. (2008). "Corrosion protection with polyaniline and polypyrrole as anticorrosive additives for epoxy paint." *Corros. Sci.*, 50(3), 721–728.

Arrabal, R., Pardo, A., Merino, M.C., Mohedano, M., Casajús, P., Paucar, K. and Garcés, G. (2012). "Effect of Nd on the corrosion behaviour of AM50 and AZ91D magnesium alloys in 3.5 wt.% NaCl solution." *Corros. Sci.*, 55, 301–312.

Ashassi-Sorkhabi, H., Ghasemi, Z. and Seifzadeh, D. (2005). "The inhibition effect of some amino acids towards the corrosion of aluminum in 1 M HCl + 1 M H_2SO_4 solution." *Appl. Surf. Sci.*, 249(1–4), 408–418.

ASTM Standard G102, 1989(1999). "Standard practice for calculation of corrosion rates and related information from electrochemical measurements." *ASTM International*, West Conshohocken, PA.

Atrens, A. and Dietzel, W. (2007). "The negative difference effect and unipositive Mg^+." *Adv. Eng. Mater.*, 9(4), 292–297.

Aung, N.N. and Zhou, W. (2002). "Effect of heat treatment on corrosion and electrochemical behaviour of AZ91D magnesium alloy." *J. Appl. Electrochem.*, 32(12), 1397–1401.

Aung, N.N. and Zhou, W. (2010). "Effect of grain size and twins on corrosion behaviour of AZ31B magnesium alloy." *Corros. Sci.*, 52(2), 589–594.

Badawy, W.A., Hilal, N.H., El-Rabiee, M. and Nady, H. (2010). "Electrochemical behavior of Mg and some Mg alloys in aqueous solutions of different pH." *Electrochim. Acta*, 55(6), 1880–1887.

Baghni, M., Wu, Y., Li, J. and Zhang, W. (2004). "Corrosion behavior of magnesium and magnesium alloys." *T. Nonferr. Metal. Soc.*, 14, 1-10.

Baliga, C.B. and Tsakiropoulos, P. (1993). "Development of corrosion resistant magnesium alloys Part 2 Structure of corrosion products on rapidly solidified Mg–16Al alloys." *Mater. Sci. Technol.*, 9(6), 513–519.

Baril, G., Blanc, C. and Pébère, N. (2001). "AC impedance spectroscopy in characterizing time-dependent corrosion of AZ91 and AM50 magnesium alloys characterization with respect to their microstructures." *J. Electrochem. Soc.*, 148(12), B489–B496.

Baril, G. and Pébère, N. (2001). "The corrosion of pure magnesium in aerated and deaerated sodium sulfate solutions." *Corros. Sci.*, 43(3), 471–484.

Belarbi, Z., Farelas, F., Singer, M. and Nešić, S. (2016). "Role of amines in the mitigation of CO_2 top of the line corrosion." *Corrosion*, 72(10), 1300–1310.

Bentiss, F., Lebrini, M. and Lagrenée, M. (2005). "Thermodynamic characterization of metal dissolution and inhibitor adsorption processes in mild steel/2, 5-bis (n-thienyl)-1, 3, 4-thiadiazoles/hydrochloric acid system." *Corros. Sci.*, 47(12), 2915–2931.

Bernasconi, C.F. and Stronach, M.W. (1991). "Kinetics of amine addition to benzylidene-1, 3-indandione and other vinylic. beta.-diketones. Effect of cyclic structure and steric strain on intrinsic rate constants." *J. Am. Chem. Soc.*, 113(6), 2222–2227.

Birbilis, N., Easton, M.A., Sudholz, A.D., Zhu, S.M. and Gibson, M.A. (2009). "On the corrosion of binary magnesium-rare earth alloys." *Corros. Sci.*, 51(3), 683–689.

Blawert, C., Hort, N. and Kainer, K.U. (2004). "Automotive applications of magnesium and its alloys." *Trans. Indian Inst. Met.*, 57(4), 397–408.

Bobby K.M., Dietzel, W., Blawert, C., Atrens, A. and Lyon, P. (2008). "Stress corrosion cracking of rare-earth containing magnesium alloys ZE41, QE22 and Elektron 21 (EV31A) compared with AZ80." *Mater. Sci. Eng. A*, 480(1), 529–539.

Boczkal, S., Karaś, M., Osyczka, A.M. and Lech-Grega, M. (2018). "Biodegradable Mg–Y and Mg–Li alloys with the addition of Ca and Zn for medical applications." *TMS Annu. Meet. Exhib.*, Springer, 399–404.

Cai, S., Lei, T., Li, N. and Feng, F. (2012). "Effects of Zn on microstructure, mechanical properties and corrosion behavior of Mg–Zn alloys." *Mater. Sci. Eng. C*, 32(8), 2570–2577.

Cain, T.W., Gonzalez-Afanador, I., Birbilis, N. and Scully, J.R. (2017). "The role of surface films and dissolution products on the negative difference effect for magnesium: comparison of Cl^- versus Cl^- free solutions." *J. Electrochem. Soc.*, 164(6), C300–C311.

Cao, F., Shi, Z., Hofstetter, J., Uggowitzer, P.J., Song, G., Liu, M. and Atrens, A. (2013). "Corrosion of ultra-high-purity Mg in 3.5% NaCl solution saturated with $Mg(OH)_2$." *Corros. Sci.*, 75, 78–99.

Carlson, B.E. and Jones, J.W. (1993). "The metallurgical aspects of the corrosion behaviour of cast Mg–Al alloys." *Light Met. Process. Appl.*, 833–847.

Chai, Y., Jiang, B., Song, J., Liu, B., Huang, G., Zhang, D. and Pan, F. (2019). "Effects of Zn and Ca addition on microstructure and mechanical properties of as-extruded Mg-1.0Sn alloy sheet." *Mater. Sci. Eng. A*, 746, 82–93.

Chen, Y., Liu, K., Hu, K., Wang, Z. and Du, J. (2019). "Influence of mixed rare earth elements (Y and Ce) on the microstructure and corrosion behaviour of Mg-4Al-3Ca alloy." *Mater. Res. Express*, 6(1), 16555.

Cheng, X., Huang, Y., Deng, X., Mei, S., Zhang, H. and Zhou, F. (2014). "Research on synthesis and complex of corrosion inhibitor for blast furnace gas pipeline." *Adv. Mater. Res.* Trans. Tech. Publ., 626–629.

Cheng, Y., Qin, T.W., Wang, H.M. and Zhang, Z. (2009). "Comparison of corrosion behaviors of AZ31, AZ91, AM60 and ZK60 magnesium alloys." *Trans. Nonferrous Met. Soc. China*, 19(3), 517–524.

Clayden, J., Greeves, N. and Warren, S. (2012). *Organic Chemistry*, second edition, Oxford University Press, Oxford.

Cole, G. (2007). "Summary of magnesium vision 2020: A North American automotive strategic vision for magnesium." *Magnesium technology 2007*, R.S. Beals., A.A. Luo., N.R. Neelameggham and M.O. Pekguleryuz, eds., TMS, *Florida*, 35.

Coy, A.E., Viejo, F., Skeldon, P. and Thompson, G.E. (2010). "Susceptibility of rare-earth-magnesium alloys to micro-galvanic corrosion." *Corros. Sci.*, 52(12), 3896–3906.

Dai, J.W., Zhang, X.B., Fei, Y., Wang, Z.Z. and Sui, H.M. (2018). "Effect of solution treatment on microstructure and corrosion properties of Mg–4Gd–1Y–1Zn–0.5Ca–1Zr alloy." *Acta Metall. Sin. Engl. Lett.*, 31(8), 865–872.

Daloz, D., Rapin, C., Steinmetz, P. and Michot, G. (1998). "Corrosion inhibition of rapidly solidified Mg-3% Zn-15% Al magnesium alloy with sodium carboxylates." *Corrosion*, 54(6), 444–450.

Dang, N., Wei, Y.H., Hou, L.F., Li, Y.G. and Guo, C.L. (2015). "Investigation of the inhibition effect of the environmentally friendly inhibitor sodium alginate on magnesium alloy in sodium chloride solution." *Mater. Corros.*, 66(11), 1354–1362.

Debab, H., Douadi, T., Daoud, D., Issaadi, S. and Chafaa, S. (2018). "Electrochemical and quantum chemical studies of adsorption and corrosion inhibition of two new schiff bases on carbon steel in hydrochloric acid media." http://dspace.univ-setif.dz:8888/jspui/handle/123456789/2968 (Nov. 29, 2018).

Desai, M.N., Shah, C.B., Desai, Y.B., Desai, S.M. and Gandhi, M.H. (1969). "Morpholine as a corrosion inhibitor for aluminium alloys in hydrochloric acid." *Br. Corros. J.*, 4(6), 315–317.

Dinodi, N. and Shetty, A. (2014a). "Investigation of influence of medium pH and sulfate ion concentrations on corrosion behavior of magnesium alloy ZE41." *Surf. Eng. Appl. Electrochem.*, 50(2), 149–156.

Dinodi, N. and Shetty, A.N. (2013). "Electrochemical investigations on the corrosion behaviour of magnesium alloy ZE41 in a combined medium of chloride and sulfate." *J. Magnes. Alloys*, 1(3), 201–209.

Dinodi, N. and Shetty, A.N. (2014b). "Alkyl carboxylates as efficient and green inhibitors of magnesium alloy ZE41 corrosion in aqueous salt solution." *Corros. Sci.*, 85, 411–427.

Dong, J.H., Tan, L.L., Ren, Y.B. and Yang, K. (2019). "Effect of microstructure on corrosion behavior of Mg–Sr alloy in Hank's solution." *Acta Metall. Sin. Engl. Lett.*, 32(3), 305-320.

Du, J., Zhang, A., Guo, Z., Yang, M., Li, M., Liu, F. and Xiong, S. (2019). "Effect of additional solute elements (X= Al, Ca, Y, Ba, Sn, Gd and Zn) on crystallographic anisotropy during the dendritic growth of magnesium alloys." *J. Alloys Compd.*, 775, 322–329.

Dunn, D.S., Yang, L., Wu, C. and Cragnolino, G.A. (2004). "Effect of inhibiting oxyanions on the localized corrosion susceptibility of waste package container materials." *Scientific basis for nuclear waste management XXVIII*, Materials Research Society, Boston, CC1.7.1–CC1.7.6.

Ebenso, E.E., Obot, I.B. and Murulana, L.C. (2010). "Quinoline and its derivatives as effective corrosion inhibitors for mild steel in acidic medium." *Int. J. Electrochem. Sci.*, 5, 1574–1586.

Ekpe, U.J., Ibok, U.J., Ita, B.I., Offiong, O.E. and Ebenso, E.E. (1995). "Inhibitory action of methyl and phenyl thiosemicarbazone derivatives on the corrosion of mild steel in hydrochloric acid." *Mater. Chem. Phys.*, 40(2), 87–93.

El Bribri, A., Tabyaoui, M., Tabyaoui, B., El Attari, H. and Bentiss, F. (2013). "The use of Euphorbia falcata extract as eco-friendly corrosion inhibitor of carbon steel in hydrochloric acid solution." *Mater. Chem. Phys.*, 141(1), 240–247.

El Rehim, S.S.A., Amin, M.A., Moussa, S.O. and Ellithy, A.S. (2008). "The corrosion inhibition of aluminum and its copper alloys in 1.0 M H_2SO_4 solution using linear-sodium dodecyl benzene sulfonate as inhibitor." *Mater. Chem. Phys.*, 112(3), 898–906.

El-Fattah, M.A., El-Wahab, H.A., Bashandy, M.S., El-Eisawy, R.A., El-hai, F.A. and Saeed, M. (2017). "Potential application of some coumarin derivatives incorporated thiazole ring as ecofriendly antimicrobial, flame retardant and corrosion inhibitor additives for polyurethane coating." *Prog. Org. Coat.*, 111, 57–66.

El-Mahdy, G.A., Al-Rasheed, H.H., Al Alshaikh, M., Al-Lohedan, H.A. and El-Faham, A. (2016). "2, 4-Dihydrazino-6-Morpholino-1, 3, 5-Triaizne (DHMT) and 2, 4-Dihydrazino-6-Piperidino-1, 3, 5-Triaizne (DHPT) as promising corrosion inhibitors of steel in acidic media." *Int. J. Electrochem. Sci.*, 11(7), 5459–5472.

Esmaily, M., Blücher, D.B., Svensson, J.E., Halvarsson, M. and Johansson, L.G. (2016). "New insights into the corrosion of magnesium alloys-The role of aluminum." *Scr. Mater.*, 115, 91–95.

Fan, Y., Wu, G. and Zhai, C. (2006). "Influence of cerium on the microstructure, mechanical properties and corrosion resistance of magnesium alloy." *Mater. Sci. Eng. A*, 433(1), 208–215.

Fang, J. and Li, J. (2002). "Quantum chemistry study on the relationship between molecular structure and corrosion inhibition efficiency of amides." *J. Mol. Struct. Theochem*, 593(1–3), 179–185.

Fekry, A.M. and Ameer, M.A. (2010). "Corrosion inhibition of mild steel in acidic media using newly synthesized heterocyclic organic molecules." *Int. J. Hydrog. Energy*, 35(14), 7641–7651.

Fekry, A.M. and Fatayerji, M.Z. (2009). "Electrochemical corrosion behavior of AZ91D alloy in ethylene glycol." *Electrochim. Acta*, 54(26), 6522–6528.

Feliu Jr, S., Samaniego, A., Barranco, V., El-Hadad, A.A., Llorente, I. and Adeva, P. (2014). "The effect of low temperature heat treatment on surface chemistry and corrosion resistance of commercial magnesium alloys AZ31 and AZ61 in 0.6 M NaCl solution." *Corros. Sci.*, 80, 461–472.

Fletcher, S. (1994). "Tables of degenerate electrical networks for use in the equivalent-circuit analysis of electrochemical systems." *J. Electrochem. Soc.*, 141(7), 1823–1826.

Flick, E.W. (1993). *Corrosion inhibitors: an industrial guide*. Noyes Publications Park Ridge, NJ.

Fontana, M.G. (2005). *Corrosion engineering*. third edition, McGraw-Hill, New York.

Forsyth, M., Forsyth, C.M., Wilson, K., Behrsing, T. and Deacon, G.B. (2002). "ATR characterisation of synergistic corrosion inhibition of mild steel surfaces by cerium salicylate." *Corros. Sci.*, 44(11), 2651–2656.

Forsyth, M., Howlett, P.C., Tan, S.K., MacFarlane, D.R. and Birbilis, N. (2006). "An ionic liquid surface treatment for corrosion protection of magnesium alloy AZ31." *Electrochem. Solid-State Lett.*, 9(11), B52–B55.

Frankel, G.S., Samaniego, A. and Birbilis, N. (2013). "Evolution of hydrogen at dissolving magnesium surfaces." *Corros. Sci.*, 70, 104–111.

Frignani, A., Grassi, V., Zanotto, F. and Zucchi, F. (2012). "Inhibition of AZ31 Mg alloy corrosion by anionic surfactants." *Corros. Sci.*, 63, 29–39.

Frignani, A., Trabanelli, G., Wrubl, C. and Mollica, A. (1996). "N-Lauroyl sarcosine sodium salt as a corrosion inhibitor for type 1518 carbon steel in neutral saline environments." *Corrosion*, 52(3), 177–182.

Froes, F.H., Eliezer, D. and Aghion, E. (1998). "The science, technology, and applications of magnesium." *JOM*, 50(9), 30–34.

Gadag, R.V. and Shetty, A.N. (2010). "Corrosion and its control." *Engineering chemistry*, second edition, IK International, New Delhi, 54-77.

Gandel, D.S., Easton, M.A., Gibson, M.A., Abbott, T. and Birbilis, N. (2014). "The influence of zirconium additions on the corrosion of magnesium." *Corros. Sci.*, 81, 27–35.

Gao, H., Li, Q., Chen, F.N., Dai, Y., Luo, F. and Li, L.Q. (2011). "Study of the corrosion inhibition effect of sodium silicate on AZ91D magnesium alloy." *Corros. Sci.*, 53(4), 1401–1407.

Gao, H., Li, Q., Dai, Y., Luo, F. and Zhang, H.X. (2010). "High efficiency corrosion inhibitor 8-hydroxyquinoline and its synergistic effect with sodium dodecylbenzenesulphonate on AZ91D magnesium alloy." *Corros. Sci.*, 52(5), 1603–1609.

Gräfen, H., Horn, E.M., Schlecker, H. and Schindler, H. (2000). "Corrosion" *Ullmanns Encycl. Ind. Chem.*, Wiley-VCH, Weinheim.

Greenblatt, J.H. (1956). "A mechanism for the anodic dissolution of magnesium." *J. Electrochem. Soc.*, 103(10), 539–543.

Gu, X.N. and Zheng, Y.F. (2010). "A review on magnesium alloys as biodegradable materials." *Front. Mater. Sci. China*, 4(2), 111–115.

Gulbrandsen, E. (1992). "Anodic behaviour of Mg in HCO_3^-/CO_3^{2-} buffer solutions. Quasi-steady measurements." *Electrochim. Acta*, 37(8), 1403–1412.

Gulbrandsen, E., Taftø, J. and Olsen, A. (1993). "The passive behaviour of Mg in alkaline fluoride solutions. Electrochemical and electron microscopical investigations." *Corros. Sci.*, 34(9), 1423–1440.

Guo, X.P., Song, G.L., Hu, J.Y. and Huang, D.B. (2013). "3 - Corrosion inhibition of magnesium (Mg) Alloys." *Corros. Prev. Magnes. Alloys*, Woodhead Publishing

Series in Metals and Surface Engineering, G. L. Song, ed., Woodhead Publishing, 61–84.

Guo, Y., Yang, S., Feng, W., Li, Y. and Cheng, Y. (2016). "Electrochemical study of inhibition effect of a Schiff base towards magnesium alloy corrosion." *Int. J. Electrochem. Sci.*, 11(7), 6043–6051.

Gupta, M. and Sharon, N.M.L. (2011). "Introduction to magnesium." *Magnesium, magnesium alloys and magnesium composites*, John Wiley & Sons, New Jersey, 1-11.

Ha, H.Y., Kang, J.Y., Yang, J., Yim, C.D. and You, B.S. (2013). "Limitations in the use of the potentiodynamic polarisation curves to investigate the effect of Zn on the corrosion behaviour of as-extruded Mg–Zn binary alloy." *Corros. Sci.*, 75, 426–433.

Hafiz, A.A., Keera, S.T. and Badawi, A.M. (2003). "Ethanolamine morpholine oleate as corrosion inhibitor for mild steel in acid solutions." *Corros. Eng. Sci. Technol.*, 38(1), 76–78.

Hall, H.K. (1957). "Correlation of the Base Strengths of Amines." *J. Am. Chem. Soc.*, 79(20), 5441–5444.

Heakal, F.E.T., Shehata, O.S. and Tantawy, N.S. (2012). "Enhanced corrosion resistance of magnesium alloy AM60 by cerium(III) in chloride solution." *Corros. Sci.*, 56, 86–95.

Hegazy, M.A. and Aiad, I. (2015). "1-Dodecyl-4-(((3-morpholinopropyl) imino) methyl) pyridin-1-ium bromide as a novel corrosion inhibitor for carbon steel during phosphoric acid production." *J. Ind. Eng. Chem.*, 31, 91–99.

Helal, N.H. and Badawy, W.A. (2011). "Environmentally safe corrosion inhibition of Mg–Al–Zn alloy in chloride free neutral solutions by amino acids." *Electrochim. Acta,*, 56(19), 6581–6587.

Hou, L., Dang, N., Yang, H., Liu, B., Li, Y., Wei, Y. and Chen, X.B. (2016). "A combined inhibiting effect of sodium alginate and sodium phosphate on the corrosion

of magnesium alloy AZ31 in NaCl solution." *J. Electrochem. Soc.*, 163(8), C486–C494.

Howlett, P.C., Neil, W., Khoo, T., Sun, J., Forsyth, M. and MacFarlane, D.R. (2008). "An electrochemical impedance study of ionic liquid film formation and aqueous corrosion of magnesium alloy ZE41." *Isr. J. Chem.*, 48, 313–318.

Hu, J., Huang, D., Song, G.L. and Guo, X. (2011). "The synergistic inhibition effect of organic silicate and inorganic Zn salt on corrosion of Mg-10Gd-3Y magnesium alloy." *Corros. Sci.*, 53(12), 4093–4101.

Hu, J., Huang, D., Zhang, G., Song, G.L. and Guo, X. (2012). "Research on the inhibition mechanism of tetraphenylporphyrin on AZ91D magnesium alloy." *Corros. Sci.*, 63, 367–378.

Hu, J.Y., Song, X.Q., Zhang, Z., Zeng, D.Z., Shi, T.H. and Gao, J.F. (2015). "The corrosion inhibition behaviors of 2′-hydroxy-acetophenone for AZ91D magnesium alloy." *Mater. Corros.*, 66(4), 396–404.

Hu, J., Zeng, D., Zhang, Z., Shi, T., Song, G.L. and Guo, X. (2013). "2-Hydroxy-4-methoxy-acetophenone as an environment-friendly corrosion inhibitor for AZ91D magnesium alloy." *Corros. Sci.*, 74, 35–43.

Hu, Z., Liu, R.L., Kairy, S.K., Li, X., Yan, H., and Birbilis, N. (2019). "Effect of Sm additions on the microstructure and corrosion behavior of magnesium alloy AZ91." *Corros. Sci.*, 149, 144–152.

Huang, D.B., Hu, J.Y., Song, G.L. and Guo, X.P. (2013a). "Self-corrosion, galvanic corrosion and inhibition of GW103 and AZ91D Mg alloys in ethylene glycol solution." *Corros. Eng. Sci. Technol.*, 48(2), 155–160.

Huang, D., Hu, J., Song, G.L. and Guo, X. (2011). "Inhibition effect of inorganic and organic inhibitors on the corrosion of Mg–10Gd–3Y–0.5Zr alloy in an ethylene glycol solution at ambient and elevated temperatures." *Electrochim. Acta*, 56(27), 10166–10178.

Huang, D., Hu, J., Song, G.L. and Guo, X. (2012). "Galvanic corrosion and inhibition of GW103 and AZ91D Mg alloys coupled to an Al alloy in an ethylene glycol solution at ambient and elevated temperatures." *Corrosion*, 68(6), 475–488.

Huang, D., Tu, Y., Song, G. and Guo, X. (2013b). "Inhibition effects of pyrazine and piperazine on the corrosion of Mg-10Gd-3Y-0.5Zr alloy in an ethylene glycol solution." *Am. J. Anal. Chem.*, 4(6), 36.

Jacobs, J.J., Gilbert, J.L. and Urban, R.M. (1998). "Corrosion of metal orthopaedic implants." *J. Bone Jt. Surg.* 80(2), 268–282.

Jafari, H. and Amiryavari, P. (2016). "The effects of zirconium and beryllium on microstructure evolution, mechanical properties and corrosion behaviour of as-cast AZ63 alloy." *Mater. Sci. Eng. A*, 654, 161–168.

Jafari, H. and Hassanizadeh, B.M. (2018). "Influence of Zr and Be on microstructure and electrochemical behavior of AZ63 anode." *Mater. Corros.*, 70, 633–641.

Jafarian, M., Gobal, F., Danaee, I., Biabani, R., and Mahjani, M.G. (2008). "Electrochemical studies of the pitting corrosion of tin in citric acid solution containing Cl." *Electrochim. Acta*, 53(13), 4528–4536.

Jamalian, M. and Field, D.P. (2019). "Effects of shot peening parameters on gradient microstructure and mechanical properties of TRC AZ31." *Mater. Charact.*, 148, 9–16.

Jamesh, M., Kumar, S. and Narayanan, T.S. (2011). "Corrosion behavior of commercially pure Mg and ZM21 Mg alloy in Ringer's solution–Long term evaluation by EIS." *Corros. Sci.*, 53(2), 645–654.

Jayanthi, K., Sivaraju, M. and Kannan, K. (2012). "Inhibiting properties of morpholine as corrosion Inhibitor for mild steel in 2N sulphuric acid and Phosphoric acid medium." *J. Chem.*, 9(4), 2213–2225.

Jeong, S.H., Kim, B.J., Lim, H.K., Kim, W.T., Kim, D.H. and Jeon, S.H. (2018). "Effect of Zr addition on the corrosion behavior of extruded Mg alloys in NaCl solution." *Mater. Trans.*, 59(3), 499–502.

John, S. and Joseph, A. (2013). "Quantum chemical and electrochemical studies on the corrosion inhibition of aluminium in 1 N HNO_3 using 1, 2, 4-triazine." *Mater. Corros.*, 64(7), 625–632.

Jones, D.A. (1996). *Principles and prevention of corrosion*, second edition, Prentice Hall, Upper Saddle River.

Jönsson, M., Persson, D. and Gubner, R. (2007). "The initial steps of atmospheric corrosion on magnesium alloy AZ91D." *J. Electrochem. Soc.*, 154(11), C684–C691.

Jüttner, K. (1990). "Electrochemical impedance spectroscopy (EIS) of corrosion processes on inhomogeneous surfaces." *Electrochim. Acta,*, 35(10), 1501–1508.

Kara, Y.S., Sagdinc, S.G. and Esme, A. (2012). "Theoretical study on the relationship between the molecular structure and corrosion inhibition efficiency of long alkyl side chain acetamide and isoxazolidine derivatives." *Prot. Met. Phys. Chem. Surf.*, 48(6), 710–721.

Karavai, O.V., Bastos, A.C., Zheludkevich, M.L., Taryba, M.G., Lamaka, S.V. and Ferreira, M.G.S. (2010). "Localized electrochemical study of corrosion inhibition in microdefects on coated AZ31 magnesium alloy." *Electrochim. Acta*, 55(19), 5401–5406.

Kartsonakis, I.A., Stanciu, S.G., Matei, A.A., Karaxi, E.K., Hristu, R., Karantonis, A. and Charitidis, C.A. (2015). "Evaluation of the protective ability of typical corrosion inhibitors for magnesium alloys towards the Mg ZK30 variant." *Corros. Sci.*, 100, 194–208.

Khaled, K.F. (2008). "Molecular simulation, quantum chemical calculations and electrochemical studies for inhibition of mild steel by triazoles." *Electrochim. Acta*, 53(9), 3484–3492.

Kumar, S.L.A., Gopiraman, M., Kumar, M.S. and Sreekanth, A. (2011). "2-Acetylpyridine-N (4)-morpholine thiosemicarbazone (HAcpMTSc) as a corrosion inhibitor on mild steel in HCl." *Ind. Eng. Chem. Res.*, 50(13), 7824–7832.

Lamaka, S.V., Höche, D., Petrauskas, R.P., Blawert, C. and Zheludkevich, M.L. (2016). "A new concept for corrosion inhibition of magnesium: Suppression of iron re-deposition." *Electrochem. Commun.*, 62, 5–8.

Lee, D.Y., Kim, W.C. and Kim, J.G. (2012). "Effect of nitrite concentration on the corrosion behaviour of carbon steel pipelines in synthetic tap water." *Corros. Sci.*, 64, 105–114.

Leleu, S., Rives, B., Bour, J., Causse, N. and Pébère, N. (2018). "On the stability of the oxides film formed on a magnesium alloy containing rare-earth elements." *Electrochim. Acta*, 290, 586–594.

Leleu, S., Rives, B., Causse, N. and Pébère, N. (2019). "Corrosion rate determination of rare-earth Mg alloys in a Na_2SO_4 solution by electrochemical measurements and inductive coupled plasma-optical emission spectroscopy." *J. Magnes. Alloys*, 7(1), 47–57.

Li, L., Pan, F. and Lei, J. (2011). "Environmental friendly corrosion inhibitors for magnesium alloys." *Magnesium Alloys-Corrosion and Surface Treatments*, Frank Czerwinski, eds., IntechOpen.

Li, T., Zhang, H., He, Y. and Wang, X. (2015). "Comparison of corrosion behavior of Mg-1.5Zn-0.6Zr and AZ91D alloys in a NaCl solution." *Mater. Corros.*, 66(1), 7–15.

Li, Y., Ba, Z.X., Li, Y.L., Ge, Y. and Zhu, X.C. (2017a). "Influence of sodium alginate inhibitor addition on the corrosion protection performance of AZ91D magnesium alloy in NaCl solution." *Anti-Corros. Methods Mater.*, 64(5), 486–491.

Li, Z., Chen, M., Li, W., Zheng, H., You, C., Liu, D. and Jin, F. (2017b). "The synergistic effect of trace Sr and Zr on the microstructure and properties of a biodegradable Mg-Zn-Zr-Sr alloy." *J. Alloys Compd.*, 702, 290–302.

Liao, J., Hotta, M. and Yamamoto, N. (2012). "Corrosion behavior of fine-grained AZ31B magnesium alloy." *Corros. Sci.*, 61, 208–214.

Liu, D., Song, Y., Shan, D. and Han, E.H. (2018). "Comparison of the inhibition effect of four inhibitors on the corrosion behaviour of AM60 magnesium alloy." *Int. J. Electrochem. Sci.*, 13(3), 2219–2235.

Liu, L., Yuan, F., Zhao, M., Gao, C., Feng, P., Yang, Y., Yang, S. and Shuai, C. (2017). "Rare earth element yttrium modified Mg-Al-Zn alloy: Microstructure, degradation properties and hardness." *Materials*, 10(5), 477.

Liu, Q., Cheng, W., Zhang, H., Xu, C. and Zhang, J. (2014). "The role of Ca on the microstructure and corrosion behavior of Mg–8Sn–1Al–1Zn–Ca alloys." *J. Alloys Compd.*, 590, 162–167.

Liu, W., Cao, F., Chang, L., Zhang, Z. and Zhang, J. (2009). "Effect of rare earth element Ce and La on corrosion behavior of AM60 magnesium alloy." *Corros. Sci.*, 51(6), 1334–1343.

Logan, S. (2007). "A lightweight automobile body concept featuring ultra-large, thin-wall structural magnesium castings." *Essent. Read. Magnes. Technol.*, Springer, 55–63.

Lu, X., Li, Y., Ju, P., Chen, Y., Yang, J., Qian, K., Zhang, T. and Wang, F. (2019). "Unveiling the inhibition mechanism of an effective inhibitor for AZ91 Mg alloy." *Corros. Sci.*, 148, 264–271.

Lukovits, I., Kalman, E. and Zucchi, F. (2001). "Corrosion inhibitors-correlation between electronic structure and efficiency." *Corrosion*, 57(1), 3–8.

Luo, A.A. (2002). "Magnesium: Current and potential automotive applications." *JOM*, 54(2), 42–48.

Lyndon, J.A., Gupta, R.K., Gibson, M.A. and Birbilis, N. (2013). "Electrochemical behaviour of the β-phase intermetallic (Mg_2Al_3) as a function of pH as relevant to corrosion of aluminium–magnesium alloys." *Corros. Sci.*, 70, 290–293.

Mahallawy, N.E., Hammouda, R., Shoeib, M. and Diaa, A.A. (2018). "Effect of solution treatment on the microstructure, tensile properties, and corrosion behavior of the Mg–5Sn–2Zn–0.1Mn alloy." *Mater. Res. Express*, 5(1), 16511.

Makar, G.L. and Kruger, J. (1990). "Corrosion studies of rapidly solidified magnesium alloys." *J. Electrochem. Soc.*, 137(2), 414–421.

Mandal, M., Moon, A.P., Deo, G., Mendis, C.L. and Mondal, K. (2014). "Corrosion behavior of Mg–2.4Zn alloy micro-alloyed with Ag and Ca." *Corros. Sci.*, 78, 172–182.

Mansfeld, F. (1990). "Electrochemical impedance spectroscopy (EIS) as a new tool for investigating methods of corrosion protection." *Electrochim. Acta*, 35(10), 1533–1544.

Martinez, S. and Stern, I. (2002). "Thermodynamic characterization of metal dissolution and inhibitor adsorption processes in the low carbon steel/mimosa tannin/sulfuric acid system." *Appl. Surf. Sci.*, 199(1–4), 83–89.

Masel, R.I. (1996). "Adsorption II: adsorption isotherms." *Principles of adsorption and reaction on solid surfaces*, Wiley Interscience, New York, 235-302.

Mathieu, S., Rapin, C., Hazan, J. and Steinmetz, P. (2002). "Corrosion behaviour of high pressure die-cast and semi-solid cast AZ91D alloys." *Corros. Sci.*, 44(12), 2737–2756.

Mathieu, S., Rapin, C., Steinmetz, J. and Steinmetz, P. (2003). "A corrosion study of the main constituent phases of AZ91 magnesium alloys." *Corros. Sci.*, 45(12), 2741–2755.

Matsubara, H., Ichige, Y., Fujita, K., Nishiyama, H. and Hodouchi, K. (2013). "Effect of impurity Fe on corrosion behavior of AM50 and AM60 magnesium alloys." *Corros. Sci.*, 66, 203–210.

McCafferty, E. (2010). *Introduction to corrosion science*, Springer, New York.

Mesbah, A., Juers, C., Lacouture, F., Mathieu, S., Rocca, E., François, M. and Steinmetz, J. (2007). "Inhibitors for magnesium corrosion: Metal organic frameworks." *Solid State Sci.*, 9(3), 322–328.

Metalnikov, P., Ben-Hamu, G., Eliezer, D. and Shin, K.S. (2019). "Role of Sn in microstructure and corrosion behavior of new wrought Mg-5Al alloy." *J. Alloys Compd.*, 777, 835–849.

Mingo, B., Arrabal, R., Mohedano, M., Mendis, C.L., Olmo, R.D., Matykina, E., Hort, N., Merino, M. C. and Pardo, A. (2017). "Corrosion of Mg-9Al alloy with minor alloying elements (Mn, Nd, Ca, Y and Sn)." *Mater. Des.*, 130, 48–58.

Mirzakhanzadeh, Z., Kosari, A., Moayed, M.H., Naderi, R., Taheri, P. and Mol, J.M.C. (2018). "Enhanced corrosion protection of mild steel by the synergetic effect of zinc aluminum polyphosphate and 2-mercaptobenzimidazole inhibitors incorporated in epoxy-polyamide coatings." *Corros. Sci.*, 138, 372–379.

Montemor, M.F. and Ferreira, M.G.S. (2007). "Electrochemical study of modified bis-[triethoxysilylpropyl] tetrasulfide silane films applied on the AZ31 Mg alloy." *Electrochim. Acta*, 52(27), 7486–7495.

NACE International. (2016), https://inspectioneering.com/news/2016-03-08/5202/nace-study-estimates-global-cost-of-corrosion-at-25-trillion-ann (March 8, 2016).

Nakatsugawa, I., Kamado, S., Kojima, Y., Ninomiya, R. and Kubota, K. (2011). "Corrosion of magnesium alloys containing rare earth elements." *Corros. Rev.*, 16(1–2), 139–158.

Nasrazadani, S., Diaz, J., Stevens, J. and Theimer, R. (2007). "Effects of DBU, morpholine, and DMA on corrosion of low carbon steel exposed to steam." *Corros. Sci.*, 49(7), 3024–3039.

Nasser, A.J.A. and Sathiq, M.A. (2016). "N-[Morpholin-4-yl (phenyl) methyl] acetamide as corrosion inhibitor for mild steel in hydrochloric acid medium." *Arab. J. Chem.*, 9, S691–S698.

Natta, M.G.L.B. (2001). "Evidence of two anodic processes in the polarization curves of magnesium in aqueous media." *Corrosion*, 57(8), 712–720.

Neil, W.C., Forsyth, M., Howlett, P.C., Hutchinson, C.R. and Hinton, B.R.W. (2009). "Corrosion of magnesium alloy ZE41–The role of microstructural features." *Corros. Sci.*, 51(2), 387–394.

Neil, W.C., Forsyth, M., Howlett, P.C., Hutchinson, C.R. and Hinton, B.R.W. (2011). "Corrosion of heat treated magnesium alloy ZE41." *Corros. Sci.*, 53(10), 3299–3308.

Niu, J., Chen, Q., Xu, N. and Wei, Z. (2008). "Effect of combinative addition of strontium and rare earth elements on corrosion resistance of AZ91D magnesium alloy." *Trans. Nonferrous Met. Soc. China*, 18(5), 1058–1064.

Nnaji, N.J., Ujam, O.T., Ibisi, N.E., Ani, J.U., Onuegbu, T.O., Olasunkanmi, L.O. and Ebenso, E.E. (2017). "Morpholine and piperazine based carboxamide derivatives as corrosion inhibitors of mild steel in HCl medium." *J. Mol. Liq.*, 230, 652–661.

Nordlien, J.H., Ono, S., Masuko, N. and Nisancioglu, K. (1997). "A TEM investigation of naturally formed oxide films on pure magnesium." *Corros. Sci.*, 39(8), 1397–1414.

Ortíz, M.R., Rodríguez, M.A., Carranza, R.M. and Rebak, R.B. (2013). "Oxyanions as inhibitors of chloride-induced crevice corrosion of alloy 22." *Corros. Sci.*, 68, 72–83.

Papavinasam, S. (2000). *Uhlig's corrosion handbook.* Wiley, New York.

Papavinasam, S. (2011). "Evaluation and selection of corrosion inhibitors." *Uhlig's corrosion handbook*, R.W. Revie, eds., John Wiley & Sons, New Jersey, 1169-1178.

Pardo, A., Feliu, S., Merino, M.C., Arrabal, R. and Matykina, E. (2010). "Electrochemical estimation of the corrosion rate of magnesium/aluminium alloys." *Int. J. Corros*., 2010, 1-8.

Pardo, A., Merino, M.C., Coy, A.E., Arrabal, R., Viejo, F. and Matykina, E. (2008a). "Corrosion behaviour of magnesium/aluminium alloys in 3.5 wt.% NaCl." *Corros. Sci.*, 50(3), 823–834.

Pardo, A., Merino, M.C., Coy, A.E., Viejo, F., Arrabal, R. and Feliú Jr, S. (2008b). "Influence of microstructure and composition on the corrosion behaviour of Mg/Al alloys in chloride media." *Electrochim. Acta*, 53(27), 7890–7902.

Pebere, N., Riera, C. and Dabosi, F. (1990). "Investigation of magnesium corrosion in aerated sodium sulfate solution by electrochemical impedance spectroscopy." *Electrochim. Acta,* 35(2), 555–561.

Peng, L.M., Chang, J.W., Guo, X.W., Atrens, A., Ding, W.J. and Peng, Y.H. (2009). "Influence of heat treatment and microstructure on the corrosion of magnesium alloy Mg-10Gd-3Y-0.4 Zr." *J. Appl. Electrochem.*, 39(6), 913–920.

Peng, Z.K., Zhang, X.M., Chen, J.M., Xiao, Y. and Jiang, H. (2005). "Grain refining mechanism in Mg–9Gd–4Y alloys by zirconium." *Mater. Sci. Technol.*, 21(6), 722–726.

Perez, N. (2004). *Electrochemistry and corrosion science.* First edition, Kluwer Academic, New York.

Perrault, G.G. (1970). "Potentiostatic study of the magnesium electrode in aqueous solution." *J. Electroanal. Chem. Interfacial Electrochem.*, 27(1), 47–58.

Pilling, N.B. and Bedworth, R.E. (1923). "The oxidation of metals at high temperatures." *J. Inst. Met*., 29, 529-591.

Pokhmurskii, V.I., Zin, I.M., Vynar, V.A. and Bily, L.M. (2011). "Contradictory effect of chromate inhibitor on corrosive wear of aluminium alloy." *Corros. Sci.*, 53(3), 904–908.

Polmear, I.J. (1992). "Physical metallurgy of magnesium alloys." *Magnes. Alloys Their Appl.*, 201–212.

Pourbaix, M. (1974). *Pourbaix diagram for the system of magnesium and water at 25 ^{o}C*. Atlas of electrochemical equilibria aqueous solutions, National Association of Corrosion Engineers, Houston, 139.

Prasad, A., Uggowitzer, P.J., Shi, Z. and Atrens, A. (2012). "Production of high purity magnesium alloys by melt purification with Zr." *Adv. Eng. Mater.*, 14(7), 477–490.

Qian, M., StJohn, D.H. and Frost, M.T. (2003). "Zirconium alloying and grain refinement of magnesium alloys." *Magnes. Technol.*, 2003, 209–214.

Qiang, Y., Zhang, S., Tan, B. and Chen, S. (2018). "Evaluation of Ginkgo leaf extract as an eco-friendly corrosion inhibitor of X70 steel in HCl solution." *Corros. Sci.*, 133, 6–16.

Qiao, Z., Shi, Z., Hort, N., Zainal Abidin, N.I. and Atrens, A. (2012). "Corrosion behaviour of a nominally high purity Mg ingot produced by permanent mould direct chill casting." *Corros. Sci.*, 61, 185–207.

Rammelt, U., Koehler, S. and Reinhard, G. (2008). "Synergistic effect of benzoate and benzotriazole on passivation of mild steel." *Corros. Sci.*, 50(6), 1659–1663.

Revie, R.W. (2011). *Uhlig's corrosion handbook*, third edition, John Wiley & Sons, New York.

Roberge, P.R. (2008). *Corrosion engineering: Principles and practice*. McGraw-Hill, New York.

Rokhlin, L.L. (2014). *Magnesium Alloys Containing Rare Earth Metals : Structure and Properties*. CRC Press, New York.

Rosalbino, F., Angelini, E., De Negri, S., Saccone, A. and Delfino, S. (2006). "Electrochemical behaviour assessment of novel Mg-rich Mg–Al–RE alloys (RE= Ce, Er)." *Intermetallics*, 14(12), 1487–1492.

Rosen, G.I., Segal, G. and Lubinsky, A. (2005). "Large profile magnesium alloy extrusions for automotive applications." *Magnesium technology 2005*, N.R. Neelameggham, H.I. Kaplan and B.R. Powell, eds., TMS, *California*, 61.

Sadeghi, A., Hasanpur, E., Bahmani, A. and Shin, K.S. (2018). "Corrosion behaviour of AZ31 magnesium alloy containing various levels of strontium." *Corros. Sci.*, 141, 117–126.

Sasaki, T.T., Oh-ishi, K., Ohkubo, T. and Hono, K. (2006). "Enhanced age hardening response by the addition of Zn in Mg–Sn alloys." *Scr. Mater.*, 55(3), 251–254.

Sastri, V.S. (1998). *Corrosion inhibitors: principles and applications*. Wiley, New York.

Sastri, V.S. (2012). *Green corrosion inhibitors: Theory and practice*. John Wiley & Sons, New York.

Sastri, V.S., Ghali, E. and Elboujdaini, M. (2007). *Corrosion prevention and protection: Practical solutions*, John Wiley & Sons, New York.

Sato, N. (2012). "Basics of corrosion chemistry." *Green Corrosion Chemistry and Engineering: Opportunities and Challenges*, First Edition, Wiley, 1–32.

Schorr, M. and Yahalom, J. (1972). "The significance of the energy of activation for the dissolution reaction of metal in acids." *Corros. Sci.*, 12(11), 867–868.

Schweitzer, P.A. (2009). *Fundamentals of corrosion: Mechanisms, causes, and preventative methods*. CRC press, New York.

Seifzadeh, D. and Basharnavaz, H. (2013). "Corrosion protection of AZ91 magnesium alloy in cooling systems." *Trans. Nonferrous Met. Soc. China*, 23(9), 2577–2584.

Seifzadeh, D., Basharnavaz, H. and Bezaatpour, A. (2013). "A Schiff base compound as effective corrosion inhibitor for magnesium in acidic media." *Mater. Chem. Phys.*, 138(2), 794–802.

Seifzadeh, D., Bezaatpour, A. and Joghani, R.A. (2014). "Corrosion inhibition effect of N, N'-bis (2-pyridylmethylidene)-1, 2-diiminoethane on AZ91D magnesium alloy in acidic media." *Trans. Nonferrous Met. Soc. China*, 24(11), 3441–3451.

Seifzadeh, D., Bezaatpour, A. and Joghani, R.A. (2016a). "Shot noise analysis to investigate the corrosion inhibition of AZ91D magnesium alloy in sulfuric acid solution." *Prot. Met. Phys. Chem. Surf.*, 52(2), 329–338.

Seifzadeh, D., Bezaatpour, A., Shamkhali, A.N. and Basharnavaz, H. (2016b). "Experimental and theoretical studies to examine the inhibition effect of a Schiff base against magnesium corrosion." *Trans. Indian Inst. Met.*, 69(8), 1545–1555.

Senthilkumar, A.N., Tharini, K. and Sethuraman, M.G. (2011). "Studies on a few substituted piperidin-4-one oximes as corrosion inhibitor for mild steel in HCl." *J. Mater. Eng. Perform.*, 20(6), 969–977.

Shang, W., He, C., Wen, Y., Wang, Y. and Zhang, Z. (2016). "Performance evaluation of triethanolamine as corrosion inhibitor for magnesium alloy in 3.5 wt% NaCl solution." *RSC Adv.*, 6(115), 113967–113980.

Sherif, E.M. and Almajid, A.A. (2011). "Corrosion of magnesium/manganese alloy in chloride solutions and its inhibition by 5-(3-Aminophenyl)-tetrazole." *Int. J. Electrochem. Sci*., 6, 2131–2148.

Sherif, E.S.M. (2011). "Effects of 5-(3-Aminophenyl)-tetrazole as a corrosion inhibitor on the corrosion of Mg/Mn alloy in Arabian Gulf water." *Int. J. Electrochem. Sci.*, 6, 5372–5387.

Shi, H., Han, E.H. and Liu, F. (2011). "Corrosion protection of aluminium alloy 2024-T3 in 0.05 M NaCl by cerium cinnamate." *Corros. Sci.*, 53(7), 2374–2384.

Shi, Z., Cao, F., Song, G.L., Liu, M. and Atrens, A. (2013). "Corrosion behaviour in salt spray and in 3.5% NaCl solution saturated with $Mg(OH)_2$ of as-cast and solution heat-treated binary Mg–RE alloys: RE=Ce, La, Nd, Y, Gd." *Corros. Sci.*, 76, 98–118.

Shi, Z., Jia, J. X. and Atrens, A. (2012). "Galvanostatic anodic polarisation curves and galvanic corrosion of high purity Mg in 3.5% NaCl saturated with $Mg(OH)_2$." *Corros. Sci.*, 60, 296–308.

Shrestha, N., Utgikar, V. and Raja, K. S. (2018). "The effect of grain size on the corrosion behavior of Mg-RE alloy ZE10A." *ECS Trans.*, 85(13), 671–682.

Shubo LI, W.D. and Shubo LI, W.D. (2018). "Effect of Zr addition on the grain refinement mechanism of Mg-Gd-Er alloys." *Acta Met. Sin*, 54(6), 911–917.

Simanjuntak, S., Cavanaugh, M.K., Gandel, D.S., Easton, M.A., Gibson, M.A. and Birbilis, N. (2014). "The influence of iron, manganese, and zirconium on the corrosion of magnesium: An artificial neural network approach." *Corrosion*, 71(2), 199–208.

Singh, A., Ansari, K.R., Haque, J., Dohare, P., Lgaz, H., Salghi, R. and Quraishi, M. A. (2018). "Effect of electron donating functional groups on corrosion inhibition of mild steel in hydrochloric acid: Experimental and quantum chemical study." *J. Taiwan Inst. Chem. Eng.*, 82, 233–251.

Slavcheva, E., Petkova, G. and Andreev, P. (2005). "Inhibition of corrosion of AZ91 magnesium alloy in ethylene glycol solution in presence of chloride anions." *Mater. Corros.*, 56(2), 83–87.

Slavcheva, E. and Schmitt, G. (2002). "Screening of new corrosion inhibitors via electrochemical noise analysis." *Mater. Corros.*, 53(9), 647–655.

Somasundaran, P. (2006). *Encyclopedia of Surface and Colloid Science*. CRC Press, New York.

Song, G.L. (2011). *Corrosion of Magnesium Alloys,* first edition, Woodhead Publishing, UK.

Song, G. (2005). "Recent progress in corrosion and protection of magnesium alloys." *Adv. Eng. Mater.*, 7(7), 563–586.

Song, G. and Atrens, A. (2003). "Understanding magnesium corrosion-A Framework for improved alloy performance." *Adv. Eng. Mater.*, 5(12), 837–858.

Song, G. and Atrens, A. (2007). "Recent insights into the mechanism of magnesium corrosion and research suggestions." *Adv. Eng. Mater.*, 9(3), 177–183.

Song, G., Atrens, A. and Dargusch, M. (1998a). "Influence of microstructure on the corrosion of diecast AZ91D." *Corros. Sci.*, 41(2), 249–273.

Song, G., Atrens, A., Li, Y. and Zhang, B. (1997a). "Negative difference effect of magnesium." *Proc. corrosion and prevention-97, Australasian Corrosion Association,* Inc., 38.

Song, G., Atrens, A., Stjohn, D., Nairn, J. and Li, Y. (1997b). "The electrochemical corrosion of pure magnesium in 1 N NaCl." *Corros. Sci.*, 39(5), 855–875.

Song, G., Atrens, A., Wu, X. and Zhang, B. (1998b). "Corrosion behaviour of AZ21, AZ501 and AZ91 in sodium chloride." *Corros. Sci.*, 40(10), 1769–1791.

Song, G., Bowles, A.L. and StJohn, D.H. (2004). "Corrosion resistance of aged die cast magnesium alloy AZ91D." *Mater. Sci. Eng. A*, 366(1), 74–86.

Song, G.L. and Atrens, A. (1999). "Corrosion mechanisms of magnesium alloys." *Adv. Eng. Mater.*, 1(1), 11–33.

Song, G. and StJohn, D. (2002). "The effect of zirconium grain refinement on the corrosion behaviour of magnesium-rare earth alloy MEZ." *J. Light Met.*, 2(1), 1–16.

Song, G. and StJohn, D. (2004). "Corrosion behaviour of magnesium in ethylene glycol." *Corros. Sci.*, 46(6), 1381–1399.

Song, G., StJohn, D., Bettles, C. and Dunlop, G. (2005). "The corrosion performance of magnesium alloy AM-SC1 in automotive engine block applications." *JOM*, 57(5), 54–56.

Song, G. and StJohn, D.H. (2005). "Corrosion of magnesium alloys in commercial engine coolants." *Mater. Corros.*, 56(1), 15–23.

Song, G.L. (2009). “Effect of tin modification on corrosion of AM70 magnesium alloy.” *Corros. Sci.*, 51(9), 2063–2070.

Song, G.L. and Xu, Z. (2010). “The surface, microstructure and corrosion of magnesium alloy AZ31 sheet.” *Electrochim. Acta*, 55(13), 4148–4161.

Song, G.L. and Xu, Z. (2012). “Crystal orientation and electrochemical corrosion of polycrystalline Mg.” *Corros. Sci.*, 63, 100–112.

Song, W., Martin, H.J., Hicks, A., Seely, D., Walton, C.A., Lawrimore II, W. B., Wang, P.T. and Horstemeyer, M.F. (2014). “Corrosion behaviour of extruded AM30 magnesium alloy under salt-spray and immersion environments.” *Corros. Sci.*, 78, 353–368.

Song, Y., Han, E.H., Shan, D., Yim, C.D. and You, B.S. (2012). “The effect of Zn concentration on the corrosion behavior of Mg–xZn alloys.” *Corros. Sci.*, 65, 322–330.

Song, Y.L., Liu, Y.H., Wang, S.H., Yu, S.R. and Zhu, X.Y. (2007). “Effect of cerium addition on microstructure and corrosion resistance of die cast AZ91 magnesium alloy.” *Mater. Corros.*, 58(3), 189–192.

Srinivasan, S. (2006). “Electrode/electrolyte interfaces: Structure and kinetics of charge transfer.” *Fuel Cells*, Springer, 27–92.

Stefenel, M.M., Vuano, B.M. and Mayer, C.E. (2001). “Corrosion inhibition of pure aluminum by morpholine-methylene-phosphonic acid in neutral chloride solution.” *Corrosion*, 57(10), 898–904.

Subramanian, A., Natesan, M., Muralidharan, V.S., Balakrishnan, K. and Vasudevan, T. (2000). “An overview: vapor phase corrosion inhibitors.” *Corrosion*, 56(2), 144–155.

Südholz, A.D., Birbilis, N., Bettles, C.J. and Gibson, M.A. (2009). “Corrosion behaviour of Mg-alloy AZ91E with atypical alloying additions.” *J. Alloys Compd.*, 471(1–2), 109–115.

Sudholz, A.D., Gusieva, K., Chen, X.B., Muddle, B.C., Gibson, M.A. and Birbilis, N. (2011). "Electrochemical behaviour and corrosion of Mg–Y alloys." *Corros. Sci.*, 53(6), 2277–2282.

Sun, M., Wu, G., Wang, W. and Ding, W. (2009). "Effect of Zr on the microstructure, mechanical properties and corrosion resistance of Mg–10Gd–3Y magnesium alloy." *Mater. Sci. Eng. A*, 523, 145–151.

Tait, W. S. (1994). *An introduction to electrochemical corrosion testing for practicing engineers and scientists*, PairODocs, Racine.

Takenaka, T., Ono, T., Narazaki, Y., Naka, Y. and Kawakami, M. (2007). "Improvement of corrosion resistance of magnesium metal by rare earth elements." *Electrochim. Acta*, 53(1), 117–121.

Tan, B., Zhang, S., Qiang, Y., Guo, L., Feng, L., Liao, C., Xu, Y. and Chen, S. (2018). "A combined experimental and theoretical study of the inhibition effect of three disulfide-based flavouring agents for copper corrosion in 0.5 M sulfuric acid." *J. Colloid. Interface. Sci.*, 526, 268–280.

Thirugnanaselvi, S., Kuttirani, S. and Emelda, A.R. (2014). "Effect of Schiff base as corrosion inhibitor on AZ31 magnesium alloy in hydrochloric acid solution." *Trans. Nonferrous Met. Soc. China*, 24(6), 1969–1977.

Thomaz, T.R., Weber, C.R., Pelegrini, T., Dick, L.F.P. and Knörnschild, G. (2010). "The negative difference effect of magnesium and of the AZ91 alloy in chloride and stannate-containing solutions." *Corros. Sci.*, 52(7), 2235–2243.

Thompson, N,G. and Payer, G.H. (1998). "DC electrochemical test methods." *Corrosion testing made easy*, National Association of Corrosion Engineers, Houston.

Torres, V.V., Amado, R.S., De Sá, C.F., Fernandez, T.L., Silva Riehl, C.A. da, Torres, A.G. and D'Elia, E. (2011). "Inhibitory action of aqueous coffee ground extracts on the corrosion of carbon steel in HCl solution." *Corros. Sci.*, 53(7), 2385–2392.

Tunold, R., Holtan, H., Berge, M.B.H., Lasson, A. and Steen-Hansen, R. (1977). "The corrosion of magnesium in aqueous solution containing chloride ions." *Corros. Sci.*, 17(4), 353–365.

Udhayan, R. and Bhatt, D.P. (1996). "On the corrosion behaviour of magnesium and its alloys using electrochemical techniques." *J. Power Sources*, 63(1), 103–107.

Uhlig, H.H. and Revie, R.W. (2008). *Corrosion and corrosion control : an introduction to corrosion science and engineering*, fourth edition, John Wiley & Sons, New York.

Valcarce, M.B. and Vázquez, M. (2010). "Phosphate ions used as green inhibitor against copper corrosion in tap water." *Corros. Sci.*, 52(4), 1413–1420.

Verissimo, N.C., Freitas, E.S., Cheung, N., Garcia, A. and Osório, W.R. (2017). "The effects of Zn segregation and microstructure length scale on the corrosion behavior of a directionally solidified Mg-25 wt.%Zn alloy." *J. Alloys Compd.*, 723, 649–660.

Vuorinen, E., Ngobeni, P., Van der Klashorst, G.H., Skinner, W., De Wet, E. and Ernst, W.S. (1994). "Derivatives of cyclobexylamine and morpholine as volatile corrosion inbibitors." *Br. Corros. J.*, 29(2), 120–121.

Wang, B.J., Xu, D.K., Wang, S.D., Sheng, L.Y., Zeng, R.C. and Han, E. (2019). "Influence of solution treatment on the corrosion fatigue behavior of an as-forged Mg-Zn-Y-Zr alloy." *Int. J. Fatigue*, 120, 46–55.

Wang, G., Huang, G., Chen, X., Deng, Q., Tang, A., Jiang, B. and Pan, F. (2017). "Effects of Zn addition on the mechanical properties and texture of extruded Mg-Zn-Ca-Ce magnesium alloy sheets." *Mater. Sci. Eng. A*, 705, 46–54.

Wang, J.L., Ke, C., Pohl, K., Birbilis, N. and Chen, X.B. (2015). "The unexpected role of benzotriazole in mitigating magnesium alloy corrosion: a nucleating agent for crystalline nanostructured magnesium hydroxide film." *J. Electrochem. Soc.*, 162(8), C403–C411.

Wang, L., Shinohara, T. and Zhang, B.P. (2010a). "Influence of chloride, sulfate and bicarbonate anions on the corrosion behavior of AZ31 magnesium alloy." *J. Alloys Compd.*, 496(1–2), 500–507.

Wang, L., Zhou, T. and Liang, J. (2012). "Corrosion and self-healing behaviour of AZ91D magnesium alloy in ethylene glycol/water solutions." *Mater. Corros.*, 63(8), 713–719.

Wang, M.F., Xiao, D.H., Zhou, P.F., Liu, W.S., Ma, Y.Z. and Sun, B.R. (2018). "Effects of rare earth yttrium on microstructure and properties of Mg-Al-Zn alloy." *J. Alloys Compd.*, 742, 232–239.

Wang, N.G., Wang, R.C., Peng, C.Q., Yan, F. and Zhang, X.Y. (2010b). "Corrosion behavior of Mg-Al-Pb and Mg-Al-Pb-Zn-Mn alloys in 3.5% NaCl solution." *Trans. Nonferrous Met. Soc. China*, 20(10), 1936–1943.

Wendt, A. (2005). "Magnesium castings in aeronautics applications – Special requirements." *Magnesium technology 2005*, N.R. Neelameggham, H.I. Kaplan and B.R. Powell, eds., TMS, *California*, 269-273.

Williams, G., Grace, R. and Woods, R.M. (2014). "Inhibition of the localized corrosion of Mg alloy AZ31 in chloride containing electrolyte." *Corrosion*, 71(2), 184–198.

Williams, G., McMurray, H.N., and Grace, R. (2010). "Inhibition of magnesium localised corrosion in chloride containing electrolyte." *Electrochim. Acta*, 55(27), 7824–7833.

Wu, G., Fan, Y., Gao, H., Zhai, C. and Zhu, Y.P. (2005). "The effect of Ca and rare earth elements on the microstructure, mechanical properties and corrosion behavior of AZ91D." *Mater. Sci. Eng. A*, 408(1), 255–263.

Wu, L., Wang, C., Pokharel, D.B., Etim, I.I.N., Zhao, L., Dong, J., Ke, W. and Chen, N. (2018). "Effect of applied potential on the microstructure, composition and

corrosion resistance evolution of fluoride conversion film on AZ31 magnesium alloy." *J. Mater. Sci. Technol.*, 34(11), 2084–2090.

Xia, X., Nie, J.F., Davies, C.H.J., Tang, W.N., Xu, S.W. and Birbilis, N. (2015). "The influence of low levels of zinc, calcium, gadolinium, strontium, and zirconium on the corrosion of magnesium for wrought applications." *Corrosion*, 71(11), 1370–1386.

Xu, J., Yang, Q., Sufyan Javed, M., Gong, Y., Kashif Aslam, M. and Chen, C. (2017). "The effects of NaF concentration on electrochemical and corrosion behavior of AZ31B magnesium alloy in a composite electrolyte." *RSC Adv.*, 7(10), 5880–5887.

Yamasaki, M., Hayashi, N., Izumi, S. and Kawamura, Y. (2007). "Corrosion behavior of rapidly solidified Mg–Zn–rare earth element alloys in NaCl solution." *Corros. Sci.*, 49(1), 255–262.

Yang, J., Blawert, C., Lamaka, S.V., Yasakau, K.A., Wang, L., Laipple, D., Schieda, M., Di, S. and Zheludkevich, M.L. (2018). "Corrosion inhibition of pure Mg containing a high level of iron impurity in pH neutral NaCl solution." *Corros. Sci.*, 142, 222–237.

Yang, J., Peng, J., Nyberg, E.A. and Pan, F. (2016). "Effect of Ca addition on the corrosion behavior of Mg–Al–Mn alloy." *Appl. Surf. Sci.*, 369, 92–100.

Yang, L., Li, Y., Qian, B. and Hou, B. (2015). "Polyaspartic acid as a corrosion inhibitor for WE43 magnesium alloy." *J. Magnes. Alloys*, 3(1), 47–51.

Yin, D., Zhang, E. and Zeng, S. (2008). "Effect of Zn on mechanical property and corrosion property of extruded Mg-Zn-Mn alloy." *Trans. Nonferrous Met. Soc. China*, 18(4), 763–768.

Yohai, L., Vázquez, M. and Valcarce, M.B. (2011). "Brass corrosion in tap water distribution systems inhibited by phosphate ions." *Corros. Sci.*, 53(3), 1130–1136.

Yuan, M. and Zheng, Z. (2014). "Effects of Zn on the microstructures and mechanical properties of Mg–3Sm–0.5Gd–xZn–0.5Zr (x= 0, 0.3 and 0.6) alloy." *J. Alloys Compd.*, 590, 355–361.

Zaharieva, J., Milanova, M., Mitov, M., Lutov, L., Manev, S. and Todorovsky, D. (2009). "Corrosion of aluminium and aluminium alloy in ethylene glycol–water mixtures." *J. Alloys Compd.*, 470(1–2), 397–403.

Zander, D. and Zumdick, N.A. (2015). "Influence of Ca and Zn on the microstructure and corrosion of biodegradable Mg–Ca–Zn alloys." *Corros. Sci.*, 93, 222–233.

Zeng, R.C., Sun, L., Zheng, Y.F., Cui, H.Z. and Han, E.H. (2014). "Corrosion and characterisation of dual phase Mg–Li–Ca alloy in Hank's solution: The influence of microstructural features." *Corros. Sci.*, 79, 69–82.

Zhang, D.Q., Gao, L.X. and Zhou, G.D. (2005). "Morpholinium oligomer as a novel vapor phase inhibitor on the corrosion of mild steel." *Corrosion*, 61(4), 392–396.

Zhang, D., Qi, Z., Wei, B. and Wang, Z. (2018a). "Effect of thermal oxidation on microstructure and corrosion behavior of the PVD Hf-coated Mg alloy." *Adv. Eng. Mater.*, 20(2), 1700556.

Zhang, E., He, W., Du, H. and Yang, K. (2008). "Microstructure, mechanical properties and corrosion properties of Mg–Zn–Y alloys with low Zn content." *Mater. Sci. Eng. A*, 488(1–2), 102–111.

Zhang, P., Li, Q., Li, L.Q., Zhang, X.X. and Wang, Z.W. (2015). "A study of environment-friendly synergistic inhibitors for AZ91D magnesium alloy." *Mater. Corros.*, 66(1), 31–34.

Zhang, S., Zhang, X., Zhao, C., Li, J., Song, Y., Xie, C., Tao, H., Zhang, Y., He, Y. and Jiang, Y. (2010). "Research on an Mg–Zn alloy as a degradable biomaterial." *Acta Biomater.*, 6(2), 626–640.

Zhang, T., Meng, G., Shao, Y., Cui, Z. and Wang, F. (2011a). "Corrosion of hot extrusion AZ91 magnesium alloy. Part II: Effect of rare earth element neodymium (Nd) on the corrosion behavior of extruded alloy." *Corros. Sci.*, 53(9), 2934–2942.

Zhang, T., Shao, Y., Meng, G., Cui, Z. and Wang, F. (2011b). "Corrosion of hot extrusion AZ91 magnesium alloy. Part I: Relation between the microstructure and corrosion behavior." *Corros. Sci.*, 53(5), 1960–1968.

Zhang, Y., Li, J. and Li, J. (2018b). "Effects of microstructure transformation on mechanical properties, corrosion behaviors of Mg-Zn-Mn-Ca alloys in simulated body fluid." *J. Mech. Behav. Biomed. Mater.*, 80, 246–257.

Zhang, T., Shao, Y., Meng, G., and Wang, F. (2007). "Electrochemical noise analysis of the corrosion of AZ91D magnesium alloy in alkaline chloride solution." *Electrochim. Acta,* 53(2), 561–568.

Zhao, J. and Chen, G. (2012). "The synergistic inhibition effect of oleic-based imidazoline and sodium benzoate on mild steel corrosion in a CO_2-saturated brine solution." *Electrochim. Acta*, 69, 247–255.

Zhao, M.C., Liu, M., Song, G. and Atrens, A. (2008a). "Influence of the β-phase morphology on the corrosion of the Mg alloy AZ91." *Corros. Sci.*, 50(7), 1939–1953.

Zhao, M.C., Liu, M., Song, G.L. and Atrens, A. (2008b). "Influence of pH and chloride ion concentration on the corrosion of Mg alloy ZE41." *Corros. Sci.*, 50(11), 3168–3178.

Zhao, S., Peng, Q., Li, H. and Liu, B. (2014). "Effects of super-high pressure on microstructures, nano-mechanical behaviors and corrosion properties of Mg-Al alloys." *J. Alloys Compd.*, 584, 56–62.

Zheludkevich, M.L., Shchukin, D.G., Yasakau, K.A., Möhwald, H. and Ferreira, M.G. (2007). "Anticorrosion coatings with self-healing effect based on nanocontainers impregnated with corrosion inhibitor." *Chem. Mater.*, 19(3), 402–411.

Zheng, Y., Peng, R., Jin, H., Luo, Y. and Ping, Y. (2017). "Film formation on magnesium alloy AZ31B in 1-butyl-3-methylimidazolium dibutylphosphate ionic liquid." *Surf. Coat. Technol.*, 325, 539–547.

Zucchi, F., Grassi, V., Frignani, A., Monticelli, C. and Trabanelli, G. (2006). "Electrochemical behaviour of a magnesium alloy containing rare earth elements." *J. Appl. Electrochem.*, 36(2), 195–204.

Zucchi, F., Grassi, V. and Zanotto, F. (2009). "Sodium monocarboxylates as inhibitors of AZ31 alloy corrosion in a synthetic cooling water." *Mater. Corros.*, 60(3), 199–205.

Zulfareen, N., Kannan, K., Venugopal, T. and Gnanavel, S. (2016). "Synthesis, characterization and corrosion inhibition efficiency of N-(4-(Morpholinomethyl Carbamoyl Phenyl) Furan-2-Carboxamide for brass in HCl medium." *Arab. J. Chem.*, 9(1), 121–135.

LIST OF PUBLICATIONS

a) In journals

1) Medhashree, H. and Shetty, A.N. (2015). "Studies on corrosion of Mg-Al-Zn alloy in 30% aqueous ethylene glycol." *Mater. Sci. Forum*, 830-831, 679-682.

2) Medhashree, H. and Shetty, A.N. (2017). "Electrochemical corrosion study of Mg-Al-Zn alloy in aqueous ethylene glycol containing chloride ions." *J. Mater. Res. Technol.*, 6, 40-49.

3) Medhashree, H. and Shetty, A.N. (2017). "Electrochemical investigation on the effects of sulfate ion concentration, temperature and medium pH on the corrosion behavior of Mg–Al–Zn–Mn alloy in aqueous ethylene glycol." *J. Magnes. Alloys*, 5, 64-73.

4) Medhashree, H. and Shetty, A.N. (2018). "Synergistic inhibition effect of trisodium phosphate and sodium benzoate with sodium dodecyl benzene sulphonate on the corrosion of Mg-Al-Zn-Mn alloy in 30% ethylene glycol containing chloride ions." *J. Adhes. Sci. Technol.*, 1–26.

b) In conferences

1) Medhashree, H. and Shetty, A.N. (2014). "Corrosion study of Mg-Al-Zn alloy in aqueous ethylene glycol solution containing chloride anions." in National Conference on Pure and Applied Chemistry (NACOPAC), held at Mysore, Karnataka on 29-12-2014.

2) Medhashree, H. and Shetty, A.N. (2015). "Studies on corrosion of Mg-Al-Zn alloy in 30% aqueous ethylene glycol." in International Conference on Advanced Materials and Manufacturing Processes for Strategic Sectors (ICAMPS-2015) held at Triruvanantapuram, Kerala on 13-05-2015.

3) Medhashree, H. and Shetty, A.N. (2015). “Effect of temperature and medium pH on the corrosion behavior of Mg-Al-Zn Alloy in 30% aqueous ethylene glycol containing chloride anions.” International Corrosion Prevention Symposium for Research Scholars (CORSYM-2015) held at Chennai, Tamilnadu on 31-07-2015.

4) Medhashree, H. and Shetty, A.N. (2018). “Synergistic inhibition study of organic and inorganic inhibitors on the corrosion of Mg-Al-Zn alloy in 30% aqueous ethylene glycol containing sulfate ions.” in International conference on Sustainable chemistry for health, environment and materials (SU-CHEM 2018) held at Hyderabad, Telangana state on 05-08-2018.

BIODATA

Name **:** Medhashree H

DOB **:** 15-december-1988

Place of birth **:** Sagar, Karnataka

Language known **:** English, Hindi, Kannada

Gender **:** Female

Material status **:** Married

Contact number **:** +919686922234

Email id **:** medhashreebhat@gmail.com

Address **:** T-C 72, RTPS colony

Shaktinagar, Raichur-584170

Education details:

Qualification	**Year**	**Institution**	**University**
PhD	Submitted the thesis in May 2019	NITK, Surathkal	NITK, Surathkal
NET	June-2013	CSIR, MHRD, India	
M Sc (Chemistry)	2010-2011	NITK, Surathkal	NITK, Surathkal
B Sc (Hon's)	2007-2009	Sahyadri Science College, Shimoga	Kuvempu University
PUC	2005-2006	Govt. Junior college, Sagar	-
SSLC	2003-2004	H. Shivalingappa High School, Sagar	-

RESEARCH POSITIONS

1) As a Project Assistant in Syngene, A Biocon company, Bangalore, from 7th June 2010 to 2nd July 2010.

2) As a Project Assistant in Solid State and Structural Chemistry unit, IISc, Bangalore from September 2013 to December 2013.

PROFESSIONAL EXPERIENCE

1) As a Research Associate in R&D, Apotex Pharmachem India Pvt. Ltd, Bangalore from July 2011 to July 2012.

2) As an Associate-I in R&D, Apotex Pharmachem India Pvt. Ltd., Bangalore from July 2012 to December 2012.

3) As Chemist in RTPS, Karnataka power corporation Ltd., Raichur from October 2015 to till date.

CONFERENCES & SEMINARS ATTENDED:

1) One day state level conference on "Space Science and Technology" held at Sahyadri Science College, Shimoga.

2) One day national level conference on "Nanochemistry-A Science of Diminished Dimensions", held at Sahyadri Science College, Shimoga.

3) Two days state level conference on "Emerging Trends in Medicinal Chemistry and Drug Designing", held at SDM College Ujire, Dakshina kannada.

4) Three days National level conference on "Recent Trends in Chemical Research (NCRTCR 2010)", held at NITK Surathkal, Mangalore.

5) Two days national conference on "National Conference on Pure and Applied Chemistry (NACOPAC)", held at Mysore University, Mysore.

6) Three days International Corrosion Prevention Symposium for Research Scholars (CORSYM-2015), held at IIT Madras, Chennai.

7) Three days international conference on "Advanced Materials and Manufacturing Processes for Strategic Sectors (ICAMPS-2015)", held at Trivendrum, Kerala.

8) Three days international conference on "Sustainable chemistry for health, environment and materials (SUCHEM-2018)", held at IICT, Hyderabad.

RESEARCH PUBLICATIONS

a) In journals

1) Medhashree, H. and Shetty, A.N. (2015). "Studies on corrosion of Mg-Al-Zn alloy in 30% aqueous ethylene glycol." *Mater. Sci. Forum.,* 830-831, 679-682.

2) Medhashree, H. and Shetty, A.N. (2017). "Electrochemical corrosion study of Mg-Al-Zn alloy in aqueous ethylene glycol containing chloride ions." *J. Mater. Res. Technol.,* 6, 40-49.

3) Medhashree, H. and Shetty, A.N. (2017). "Electrochemical investigation on the effects of sulfate ion concentration, temperature and medium pH on the corrosion behavior of Mg–Al–Zn–Mn alloy in aqueous ethylene glycol." *J. Magnes. Alloys*., 5, 64-73.

4) Medhashree, H. and Shetty, A.N. (2018). "Synergistic inhibition effect of trisodium phosphate and sodium benzoate with sodium dodecyl benzene sulphonate on the corrosion of Mg-Al-Zn-Mn alloy in 30% ethylene glycol containing chloride ions." *J. Adhes. Sci. Technol.,* 1–26.

b) In conferences

1) Medhashree, H. and Shetty, A.N. (2014). "Corrosion study of Mg-Al-Zn alloy in aqueous ethylene glycol solution containing chloride anions." in National Conference on Pure and Applied Chemistry (NACOPAC), held at Mysore on 29-12-2014.

2) Medhashree, H. and Shetty, A.N. (2015). "Studies on corrosion of Mg-Al-Zn alloy in 30% aqueous ethylene glycol." in International Conference on Advanced Materials and Manufacturing Processes for Strategic Sectors (ICAMPS-2015) held at Triruvanantapuram, Kerala on 13-05-2015.

3) Medhashree, H. and Shetty, A.N. (2015). "Effect of temperature and medium pH on the corrosion behavior of Mg-Al-Zn Alloy in 30% aqueous ethylene glycol containing chloride anions." International Corrosion Prevention Symposium for Research Scholars (CORSYM-2015) held at Chennai, Tamilnadu on 31-07-2015.

4) Medhashree, H. and Shetty, A.N. (2018). "Effect of temperature and medium pH on the corrosion behavior of Mg-Al-Zn Alloy in 30% aqueous ethylene glycol containing chloride anions." International conference for (SUCHEM-2018) held at IICT, Hyderabad on 06-08-2018.